Technical Report

TR-01-23

Copper corrosion under expected conditions in a deep geologic repository

F King
Integrity Corrosion Consulting Ltd, Calgary, Alberta, Canada

L Ahonen
Geological Survey of Finland, Espoo, Finland

C Taxén
Swedish Corrosion Institute, Stockholm, Sweden

U Vuorinen
VTT Chemical Technology, Espoo, Finland

L Werme
Svensk Kärnbränslehantering AB

Svensk Kärnbränslehantering AB
Swedish Nuclear Fuel
and Waste Management Co
Box 5864
SE-102 40 Stockholm Sweden
Tel 08-459 84 00
+46 8 459 84 00
Fax 08-661 57 19
+46 8 661 57 19

Copper corrosion under expected conditions in a deep geologic repository

F King
Integrity Corrosion Consulting Ltd, Calgary, Alberta, Canada

L Ahonen
Geological Survey of Finland, Espoo, Finland

C Taxén
Swedish Corrosion Institute, Stockholm, Sweden

U Vuorinen
VTT Chemical Technology, Espoo, Finland

L Werme
Svensk Kärnbränslehantering AB

Keywords: copper, corrosion, canister, nuclear waste, lifetime prediction, modelling, thermodynamics, kinetics, general corrosion, pitting, stress corrosion cracking, gamma radiation, repository environment, microbially influenced corrosion.

Abstract

Copper has been the corrosion barrier of choice for the canister in the Swedish and Finnish, nuclear waste disposal programmes for over 20 years. During that time many studies have been carried out on the corrosion behaviour of copper under conditions likely to exist in an underground nuclear disposal repository located in the Fenno-Scandian bedrock. This review is a summary of what has been learnt about the long-term behaviour of the corrosion barrier during this period and what the implications of this knowledge are for the predicted service life of the canisters.

The review is based on the existing knowledge from various nuclear waste management programs around the world and from the open literature. Various areas are considered: the expected evolution of the geochemical conditions in the groundwater and of the repository environment, the thermodynamics of copper corrosion, corrosion before and during saturation of the compacted bentonite buffer by groundwater, general and localized corrosion following saturation of the compacted bentonite buffer, stress corrosion cracking, radiation effects, the implications of corrosion on the service life of the canister, and areas for further study.

Much has been learnt about the long-term corrosion behaviour of copper canisters over the past 20 years. The majority of the information reviewed here is drawn from the Swedish/Finnish and Canadian programmes. Despite differences in scientific approach, and canister and repository design, the results of these two programmes both suggest that copper provides an excellent corrosion barrier in an underground repository.

The conclusion drawn from this review is that the original prediction made in 1978 of canister lifetimes exceeding 100,000 years remains valid.

Foreword

This report is a result of a joint collaborative SKB-Posiva study. Many people have contributed to the production of this report. The authors are grateful to the following for contributing various sections to the report: Ola Karnland, Arto Muurinen, Karsten Pedersen, Petteri Pitkänen, and Peter Wikberg (section 2), Bo Rosborg (section 7). The authors would also like to thank Margit Snellman and Jukka-Pekka Salo for reviewing the report and for providing their helpful comments.

Content

1 Introduction

The repository in Sweden and Finland is based on the Swedish KBS-3 design. The basic concept for the disposal of spent fuel is based on its encapsulation and emplacement in crystalline rock at a depth of about 500 m. The spent nuclear fuel is planned to be encapsulated in spheriodal graphite cast iron canisters that have an outer 50 mm thick shield made of copper. Once filled and sealed, the copper-iron canisters will be emplaced individually in vertical boreholes in the floors of deposition tunnels feeding off central tunnels. The space between the canisters and the wall of the borehole will be filled with compacted bentonite. The tunnels and shafts will be backfilled with a mixture of crushed rock and bentonite, and sealing plugs will be emplaced to block specific transport pathways for groundwater. The function of the canister is to isolate the spent fuel from the surrounding environment. The canister design, therefore, aims at providing with a high probability a corrosion lifetime of at least 100,000 years in the repository. In addition to the required chemical resistance, the canister must also have sufficient mechanical strength to withstand the loads caused by disposal at a depth of 400 to 700 m, i.e., an evenly distributed load of 7 MPa hydrostatic pressure from groundwater and a 7 MPa pressure from swelling of the bentonite. Additional design requirements concern limitations on heat and radiation dose to the near field and choice of materials that do not adversly affect the performance of the near field buffer. Therefore, the maximum allowed surface temperature has been set to 100°C and the maximum allowed surface dose rate to 1 Gy/h. The fuel in the canister should also remain subcritical even if water enters the canister.

In order to meet these requirements, the canister has been designed with an insert that provides mechanical strength and radiation shielding, and keeps the fuel assemblies in fixed positions. The outer copper shell provides the corrosion protection for the canister. This outer shell is made of oxygen free copper (Cu-OF). To improve the creep strength and the creep ductility of Cu-OF at higher temperatures (+175 to +300°C), 30 to 70 ppm phosphorus is added to the oxygen free high conductivity copper. Figure 1-1 shows an exploded view of the copper – cast iron canister in the version designed for

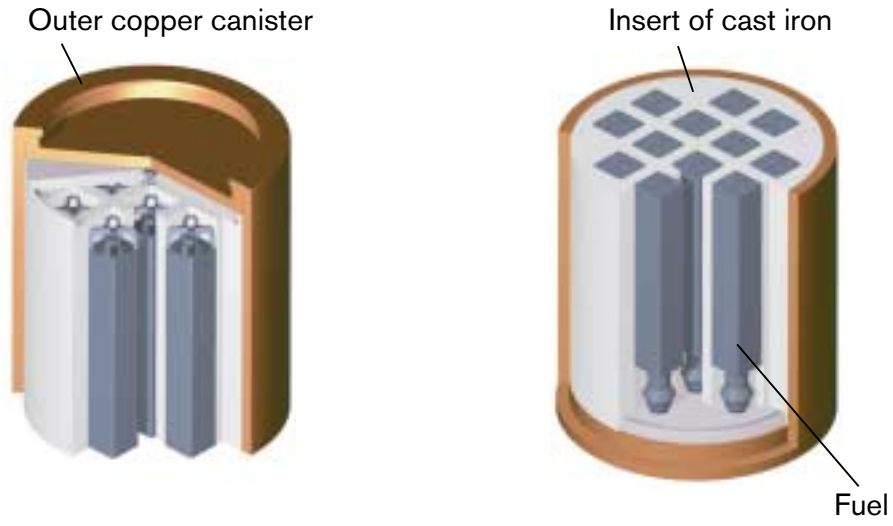

Figure 1-1. *Exploded view of spent BWR fuel disposal canister.*

BWR fuel. Figure 1-2 illustrates the emplacement of the copper canister in compacted bentonite buffer material and sealing of the tunnels with compacted crushed rock-bentonite backfill for an SKB-3 design repository.

The purpose of the present report is to present the state-of-the-art of knowledge of the corrosion of copper under the conditions expected in deep geological repositories in Sweden and Finland and to identify areas for further research. The report discusses the following topics:

- the chemical evolution of the repository and its surroundings;
- thermodynamic data relevant for copper corrosion;
- the corrosion modes and the extent of the corrosion of the copper canister before emplacement;
- corrosion after emplacement before and during water saturation of the compacted bentonite buffer;
- canister corrosion after water saturation of the compacted bentonite buffer;
- the potential for stress corrosion cracking;
- corrosion induced by radiation;
- the implications for the canister service life;
- areas for further research.

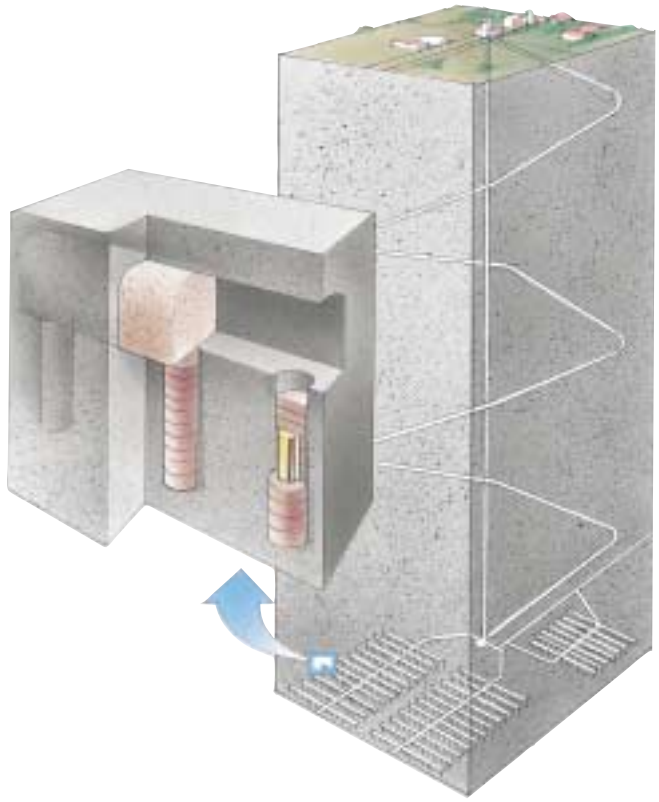

Figure 1-2. *Illustration of the emplacement of a copper canister in compacted bentonite buffer and sealing of the tunnels with bentonite-crushed rock backfill in an SKB-3 design repository.*

2 Estimated geochemical conditions at the repository depth

This section gives a brief discussion of the expected evolution of some groundwater constituents and the predicted concentrations in bentonite pore-water corresponding to those of the evolved groundwater. Microbial processes involved in the groundwater environment and the bentonite buffer are discussed separately in more detail, but their assumed effect has been taken into account in assessing the values presented for groundwater and bentonite pore-water. The effects of γ-radiation through radiolysis of the gases and the aqueous solutions that are present close to the canister surface are discussed in section 8.

2.1 Groundwater chemistry in the bedrock at repository depth in Finland and Sweden

The chemistry of the groundwater at the possible repository sites in Finland and Sweden is basically well known. Tables 2-1, 2-2 and 2-3 present the predicted values at closure of the repository, after resaturation, and up to 10,000 years into the future. The data in tables 2-1 and 2-2 for two Swedish sites were used in the SR 97 post closure safety assessment /SKB 1999a/. The data for Olkiluoto, Finland in table 2-3 (see section 2.1.2) are based on Pitkänen et al. /1996, 1999/.

Table 2-1. Predicted chemical composition of the groundwater at repository depth in the Simpevarp area in Oskarshamn. The concentrations are given both in mg/L and mol/L.

Constituent		At closure	After resaturation (<100 years after closure)	10,000 years into the future
pH		6–8	7.7	8–9
Eh	mV	0 to −400	−300	−200 to −300
Na^+	mg/L	1,000–3,000	2,100	100–2,000
	mol/L	$(4.4–13.1)\cdot10^{-2}$	$9.1\cdot10^{-2}$	$(0.4–8.7)\cdot10^{-2}$
K^+	mg/L	5–20	8	2–10
	mol/L	$(1.3–5.1)\cdot10^{-4}$	$2.0\cdot10^{-4}$	$(0.5–2.6)\cdot10^{-4}$
Ca^{2+}	mg/L	1,000–3,000	1,890	20–2,000
	mol/L	$(2.5–7.5)\cdot10^{-2}$	$4.7\cdot10^{-2}$	$(0.05–5.0)\cdot10^{-2}$
Mg^{2+}	mg/L	10–200	42	1–40
	mol/L	$(0.4–8.2)\cdot10^{-3}$	$1.7\cdot10^{-3}$	$(0.04–1.7)\cdot10^{-3}$
HCO_3^-	mg/L	10–1,000	10	10–20
	mol/L	$(0.2–16.4)\cdot10^{-3}$	$0.2\cdot10^{-3}$	$(0.2–0.4)\cdot10^{-3}$
Cl^-	mg/L	3,000–10,000	6,410	200–5,000
	mol/L	$(0.8–2.8)\cdot10^{-1}$	$1.8\cdot10^{-1}$	$(0.06–1.4)\cdot10^{-1}$
SO_4^{2-}	mg/L	100–600	560	1–400
	mol/L	$(1.0–6.3)\cdot10^{-3}$	$5.8\cdot10^{-3}$	$(0.01–4.2)\cdot10^{-3}$
HS^-	mg/L	0–10	0.15	0–1
	mol/L	$(0–0.3)\cdot10^{-3}$	$0.5\cdot10^{-5}$	$(0–0.3)\cdot10^{-4}$

Table 2-2. Predicted chemical composition of the groundwater at repository depth in the Forsmark-North Uppland area. A difference of the conditions after resaturation compared with table 2-1 is related to an at-coast/inland location. The concentrations are given both in mg/L and mol/L.

Constituent		At closure	After resaturation (<100y after closure)	10,000 years into the future
pH		6–8	7.0–7.9	7–9
Eh	mV	0 to –400	–200/–250	–200 to –300
Na^+	mg/L	300–2,000	1,700–275	100–1,000
	mol/L	$1.3–8.7)\cdot10^{-2}$	$(7.4–1.2)\cdot10^{-2}$	$(0.4–4.3)\cdot10^{-2}$
K^+	mg/L	2–13	13–2	2–10
	mol/L	$(0.5–3.3)\cdot10^{-4}$	$(3.3–0.5)\cdot10^{-4}$	$(0.5–2.6)\cdot10^{-4}$
Ca^{2+}	mg/L	150–1,650	1,650–142	20–1,000
	mol/L	$(0.4–4.1)\cdot10^{-2}$	$(4.1–0.4)\cdot10^{-2}$	$(0.05–2.5)\cdot10^{-2}$
Mg^{2+}	mg/L	17–110	110–17	4–100
	mol/L	$(0.7–4.5)\cdot10^{-3}$	$(4.5–0.7)\cdot10^{-3}$	$(0.2–4.1)\cdot10^{-3}$
HCO_3^-	mg/L	50–300	47–278	20–40
	mol/L	$(0.8–4.9)\cdot10^{-3}$	$(0.8–4.6)\cdot10^{-3}$	$(0.3–0.7)\cdot10^{-3}$
Cl^-	mg/L	500–5,000	5,500–555	200–5,000
	mol/L	$(0.1–1.4)\cdot10^{-1}$	$(1.6–0.2)\cdot10^{-1}$	$(0.06–1.4)\cdot10^{-1}$
SO_4^{2-}	mg/L	40–400	370–49	1–400
	mol/L	$(0.4–4.2)\cdot10^{-3}$	$(3.9–0.5)\cdot10^{-3}$	$(0.01–4.2)\cdot10^{-3}$
HS^-	mg/L	0–10	<0.01–0	0–1
	mol/L	$0–0.3\cdot10^{-3}$	$<0.3\cdot10^{-6}–0$	$0–0.3\cdot10^{-4}$

In the long term (i.e., over a glacial cycle of 150,000 years), major changes in chemical composition can be expected as a result of the climate changes. Based on the climate scenarios defined in SR 97 we might expect:

- **Temperate/boreal condition.** During the period when the climate is gradually changing shoreline displacement is expected to be the only process of any significant importance for the groundwater composition. This might change the chemistry by replacing the freshwater by brackish or saline water.

  The salinity of the seawater may vary from brackish to salt. During some periods, the Baltic may be a lake. Based on current knowledge, one must assume that for long periods of time (of the order of thousand years) the salinity at sites close to the current shoreline may correspond to that currently observed in the Atlantic. This gives an upper limit to the salinity of the water infiltrating into the rock of 35 g/L /Vieno 2000/.

- **During periods of permafrost** groundwater turnover is expected to be lower than under current conditions. Almost impermeable areas of frozen ground are expected to force groundwater movements to greater depth. Another important process related to freezing is that solutes are frozen out. Freezing-induced salt exclusion and the reduction in groundwater turnover are both top-down processes, and together they can contribute to a significant increase in salinity. The salinity is expected to reach slightly more than 35 g/L.

- **During glaciation** the ice sheet governs the boundary conditions for groundwater flow. In the melting zone and at the ice margin, high water pressures are expected to occur locally. Towards the ice margin and ice tunnels the head gradients may be high.

Table 2-3. Potential hydrogeochemical conditions at repository depth (400–700 m) in the Olkiluoto site. The concentrations are given both in mg/L and mol/L.

Constituent		Initial, indisturbed conditions	At closure, infiltration into unsaturated bentonite	After closure and saturation** (i.e. up to 100 years)	After closure up to 10,000 years
pH		7.8–8.3	6–8	7–8	7.5–8.3
Redox	mV	−230 to −280	Oxic to −250	−150 to −250	−200 to −280
DIC	mol/L	$(0.7–0.1)\cdot10^{-3}$	$(0.1–10)\cdot10^{-3}$	$(0.5–10)\cdot10^{-3}$	$(0.1–7)\cdot10^{-3}$
Cl^-	mg/L mol/L	7,500–15,000 $(2.1–4.2)\cdot10^{-1}$	1,000–22,000 $(0.3–6.2)\cdot10^{-1}$	1,000–5,000 $(0.3–1.4)\cdot10^{-1}$	200–15,000 $(0.06–4.2)\cdot10^{-1}$
Na^+	mg/L mol/L	2,500–5,000 $(1.1–2.2)\cdot10^{-1}$	500–6,500 $(0.2–2.8)\cdot10^{-1}$	500–2,000 $(0.2–0.9)\cdot10^{-1}$	300–5,000 $(0.1–2.2)\cdot10^{-1}$
Ca^{2+}	mg/L mol/L	1,500–4,000 $(0.4–1.0)\cdot10^{-1}$	100–6,000 $(0.03–1.5)\cdot10^{-1}$	100–1,000 $(0.03–0.2)\cdot10^{-1}$	20–4,000 $(0.005–1.0)\cdot10^{-1}$
Mg^{2+}	mg/L mol/L	30–70 $(1.2–2.9)\cdot10^{-3}$	10–250 $(0.04–1.0)\cdot10^{-2}$	10–250 $(0.04–1.0)\cdot10^{-2}$	10–250 $(0.04–1.0)\cdot10^{-2}$
K^+	mg/L mol/L	10–20 $(2.6–5.1)\cdot10^{-4}$	5–30 $(1.3–7.7)\cdot10^{-4}$	5–30 $(1.3–7.7)\cdot10^{-4}$	5–20 $(1.3–5.1)\cdot10^{-4}$
SO_4^{2-}	mg/L mol/L	0–20 $0–0.2\cdot10^{-3}$	0–500 $0–5.2\cdot10^{-3}$	10–500 $(0.1–5.2)\cdot10^{-3}$	0–500 $0–5.2\cdot10^{-3}$
HS^-	mg/L mol/L	0–3 $0.9\cdot10^{-4}–0$	0–3 $0–0.9\cdot10^{-4}$	0–10 $0–3.0\cdot10^{-4}$	0–3 $0–0.9\cdot10^{-4}$
NH_4^+	mg/L mol/L	<0.05 $<0.03\cdot10^{-4}$	<0.1, but if marine <3* $<5.5\cdot10^{-6}$, $<1.7\cdot10^{-4}$	0.05–3 $(0.03–1.7)\cdot10^{-4}$	<1 $<0.6\cdot10^{-4}$
$CH_4(g)$	ml/L mol/L	50–400 $(0.2–1.8)\cdot10^{-2}$	<0.1, but if saline <600 $<4.5\cdot10^{-6}$, $<2.7\cdot10^{-2}$	<100 $0.4\cdot10^{-2}$	0.1–400 $(0.004–17.9)\cdot10^{-3}$
$H_2(g)$	ml/L mol/L	<0.5 $<2.2\cdot10^{-5}$	<0.5, but if saline <20 $<2.2\cdot10^{-5}$, $<8.9\cdot10^{-4}$	<0.1 $<4.4\cdot10^{-6}$	<0.5 $<2.2\cdot10^{-5}$
DOC#	mgC/L mol/L	<2 $<1.7\cdot10^{-4}$	<2 $<1.7\cdot10^{-4}$	<10 $<8.3\cdot10^{-4}$	<2 $<1.7\cdot10^{-4}$
Microbes		SRB, methanogens	Aerobic bacteria, SRB, IRB methanogens	SRB, IRB,	IRB, SRB, methanogens

*) Based on Hästholmen results.
**) Probably marine water will dominate.
#) Most of current DOC data is unreliable. Mostly, samples with high pump rate have only a few mg/L.

This will drive glacial meltwater deep down to the subsurface. Results of calculations show that it is possible to transport oxidising meltwater to repository depth. No evidence of such conditions is found in the bedrock, which makes this scenario unlikely. The composition of the glacial meltwater, when it has reached repository depth, is 5–10 mg/L of sodium, calcium, magnesium, sulphate and chloride, 20–40 mg/L of bicarbonate and pH 8-9 /SKB 1999b/. The water is anoxic but does not contain any reducing compounds of iron, manganese or sulphide.

2.1.1 Hydrochemical conditions at Olkiluoto: initial state

Palaeo-hydrological stages with typical chemical and isotopic signatures have left clear imprints on current groundwater compositions /Pitkänen et al. 1999/. They have caused great variability, which is observable in the chemical data (figures 2-1 and 2-2) notably in salinity (fresh – brackish – saline), water types (dominance between Na^{+}–Ca^{2+} and HCO_3^{-}–SO_4^{2-}–Cl^{-}) and contents of conservative constituents (Cl^{-}, Br^{-}, $\delta^{2}H$ and $\delta^{18}O$). Hydrochemical data also reveal the extensive mixing phenomena of different end-member waters from each palaeo source.

The interpretation of chemical and isotopic data indicates five end-member water types affecting the current groundwater compositions at the site:

Modern
- carbonate-rich meteoric water infiltrated from the surface, and
- seawater from the Gulf of Bothnia (0–2,500 BP).

Relic
- SO_4^{2-}-rich Litorina Sea water (2,500–7,500 BP),
- fresh water prior to the Litorina Sea stage containing glacial melt water (7,500–10,000 BP), and
- saline water (Ca-Na-Cl brine) intruded and/or formed under the influence of hydrothermal activity (pre-Quaternary, probably early Phanerozoic to Precambrian in age).

A detailed description of the hydrochemical characteristics and history of the waters occurring presently at different depths in Olkiluoto is given by Pitkänen et al. /1999/.

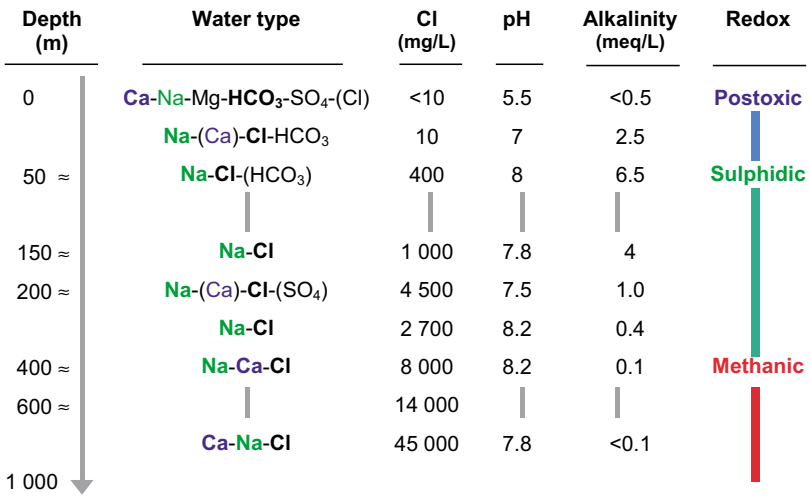

Figure 2-1. *Vertical variation of the main hydrochemical constituents at Olkiluoto. Vertical lines represent smooth changes in groundwater.*

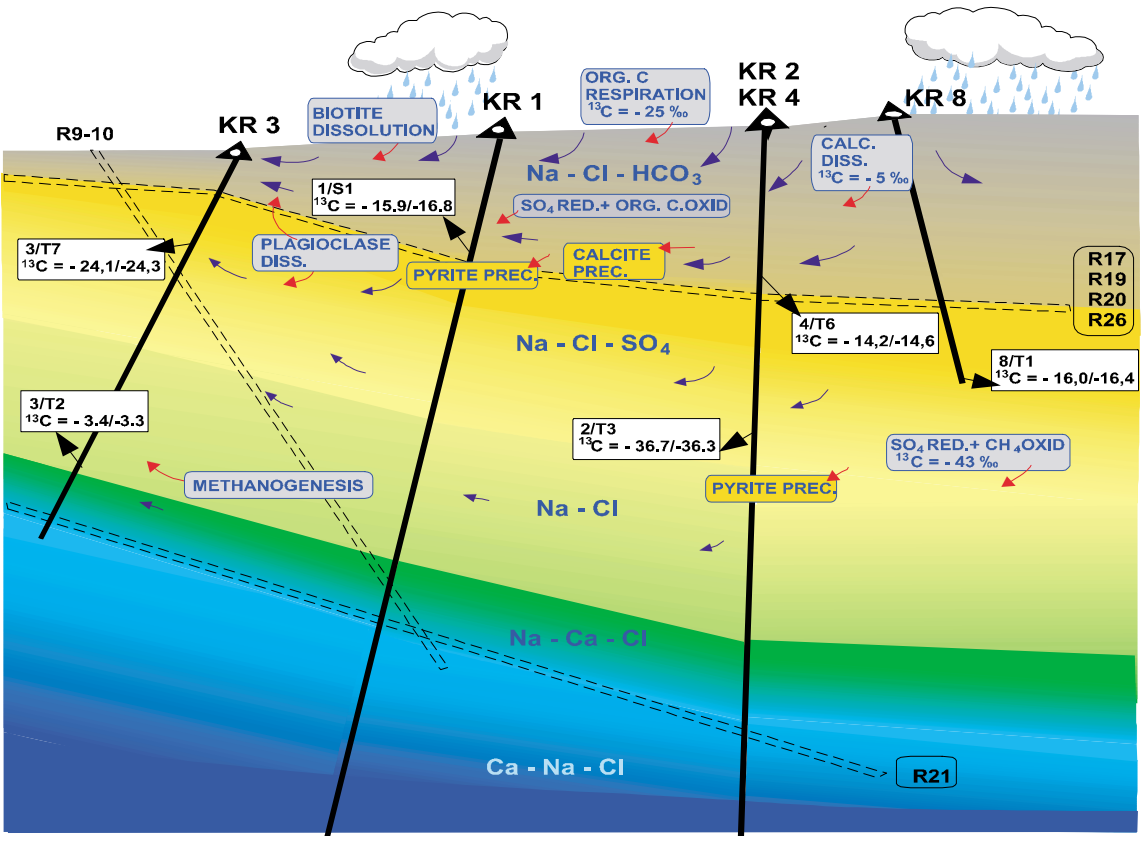

Figure 2-2. *Illustrated cross-section of hydrobiogeochemical and hydrogeological conditions in the bedrock of Olkiluoto based on interpretation of hydrogeochemistry. Changes in colour describe alteration in water type. Blue arrows represent flow directions. Rounded rectangles contain the main sources with estimated $\delta^{13}C$ data, and sinks affecting pH and redox conditions. Rectangles show measured/calculated $\delta^{13}C$(DIC). Generalised fracture zones are coded by R. Boreholes KR2 and KR4 are combined due to their similar hydrogeological character. Approximate scale of the figure is 1.5 km (horizontal) x 1 km (vertical).*

2.1.2 Assessment of temporal hydogeochemical evolution at Olkiluoto

The following assessesment of future hydrochemical estimates of potential groundwater infiltration into the repository system (table 2-3) is based on the present–day groundwater composition at Olkiluoto, interpreted hydrogeochemical evolution /Pitkänen et al. 1999/, numerical groundwater flow predictions /Löfman 1999, 2000/, and observations done for other sites in Finland and Äspö in Sweden. The ranges of constituents in the initial condition (i.e., the undisturbed state) are selected from the current database and geochemical modelling results, representing water analyses at the planned repository depth of about 500 m (400–700 m, Olkiluoto).

Salinity and Cl

During the repository operation, non-saline water and Baltic seawater are expected to be drawn into the repository from above, and saline water from below. It seems that infiltration of meteoric water will be, however, limited to fairly shallow depths and seawater intrusion may dominate the drawdown from the surface /e.g. Luukkonen 2001/. Therefore, the salinity of the groundwater is expected to remain mainly slightly brackish

around the repository after closure. However, locally more saline groundwater than the initial state may intrude from greater depths into the system during operation and be injected into the bentonite at the closure stage.

As a result of postglacial land uplift, the hydraulic gradient will increase at Olkiluoto and the infiltration of dilute meteoric water will penetrate deeper into the bedrock. The site scale flow model /Löfman 1999/ predicts that dilute infiltration will displace brackish and saline groundwater at repository depth during the next 10,000 years. However, complementary simulations involving, for example, the double porosity approach /Löfman 2000/ and groundwater flow in the last 7,000 years /Bath et al. 2000/, suggest that flow models exaggerate the vertical drawdown of meteoric recharge. Observations from other study sites in Finland located above sea level since glaciation, for example Palmottu /e.g. Blomqvist et al. 2000/, also support the slow descent of diluting recharge water to great depths.

In the far future, Olkiluoto and possible sites in Sweden will endure glacial cycles with a permafrost stage, glaciation, deglaciation, and another temperate climate. Hydrogeochemical interpretations concerning past cycles /Pitkänen et al. 1999/ indicate that during glaciation the salinity at Olkiluoto has not been significantly higher than is currently found at repository depth. The results of geochemical modelling suggest that the Cl^- concentration may not have been more than is currently found at 700–800 m depth, i.e. 22 g/L, corresponding 35 g/L TDS. The upper part of the bedrock has been filled with brackish groundwater in which the mean Cl^- concentration would have been about 3.5 g/L. During deglaciation, the salinity has decreased to a half by glacial melt in the upper part of the bedrock; therefore, dilution would have been less at the repository level. It can be hypothesised that the values interpreted for the glacial period have been generated by permafrost after previous interglacial (Eem), during which groundwater may have been diluted similarly as it is assumed for the next 10,000 years.

During the next temperate domain a marine stage is probable. It is also possible that the Baltic basin will be filled with oceanic water. The Cl^- concentration is about 20 g/L, but marine input is expected to be diluted before reaching the repository depth, like Litorina seawater, according to the results from the Olkiluoto and Hästholmen sites. Accordingly, the presumption is that the more saline water has mixed with the fresh water in the upper part of the bedrock and has become diluted before descending deeper in the bedrock.

Potassium is generally high in marine waters (up to 400 mg/L). However, in current groundwaters, K^+ has been strongly depleted by cation exchange and mixing, so that K^+ concentrations in Litorina-derived groundwaters are only 10–30% of the original concentration in Litorina seawater. This marine-derived water has not yet reached the repository level (figure 2-1), so the K^+ concentration will further decrease before the groundwater has descended to the 500 m level.

pH and redox conditions

In the long run, the pH and redox conditions will be buffered by the same processes as in the initial state, mainly resulting in similar pH and redox values. The stage just after the closure is an exception when the pH values can be slightly acidic and the redox clearly positive. However, oxygen trapped in the repository will react within a few years with organic matter /SKB 1999c/, and the anaerobic oxidation of organic matter with the reduction of iron (III) compounds (oxidised during the operation) and SO_4^{2-} will

decrease the redox potential to negative values. Biological oxidation of organic matter will be quite rapid after closure, producing carbonate, which will decrease the pH of the infiltrating groundwater. Fracture calcites are strong pH-buffers and equilibrium with calcite is considered to increase the pH above 7 quite soon after closure.

Total changes in pH conditions are strongly dependent on the calcium and carbonate content of the infiltrating groundwater, assuming calcite buffers the pH. Preliminary simulations by PHREEQC indicated that the input of 10 mmol/L bicarbonate (corresponding to the reduction of 5 mmol/L (480 mg/L) SO_4^{2-} with anaerobic oxidation of organic carbon) in saline water (Cl^-: 8 g/L, Ca^+: 2 g/L, HCO_3^-: 18 mg/L, pH:7.6) in equilibrium with calcite decreased the groundwater pH to a value of 6.4, whereas a similar increment in brackish bicarbonate-rich groundwater (Cl^-: 900 mg/L, Ca^{2+}: 100 mg/L, HCO_3^-: 250 mg/L, pH: 8.1) decreased the pH to only 7.1.

Sulphide

Sulphide concentrations will hardly deviate from the current values (maximum observed 3 mg/L) during the major part of the 10,000 years after closure. Increased levels of organic material during the early post closure phase, however, may lead to increased bacterial sulphate reduction. The amount of SO_4^{2-} is not considered to limit the extent of reduction due to the high SO_4^{2-} concentrations in marine-derived groundwaters that may infiltrate the repository level during the operational phase. The dissolved sulphide that is formed will be precipitated, among other things, as iron sulphide so that the sulphide concentrations will probably be limited to less than 10 mg/L.

Ammonium

Ammonium is produced by the decomposition of organic debris in the sea bottom sediments. It is easily removed from groundwater by an irreversible cation exchange process. Therefore, the concentration of ammonium will probably be at a very low level (below detection limit), except if seawater intrusion rapidly reaches the repository level. This will only be possible during the operational phase, but the flow through sediments is fairly fast during this period and ammonium will not reach high concentrations (a few mg/L).

Methane

Methane is connected to non-marine groundwater deep in the bedrock. The content of methane increases with salinity so that the current saline groundwaters between 400–600 m depth contain 200–400 mL/L at Olkiluoto, while the sulphate-poor brackish groundwater above contains about 50–100 mL/L. High methane contents are specifically found in the saline groundwater at Olkiluoto, the levels being much lower for Swedish sites and for the Hästholmen site. These amounts may be exceeded if more saline groundwater intrudes into the repository, which most probably would occur at the closure stage. However, methane will be oxidised quickly if oxygen is left in the system and methanotrophs are present. The methane content may increase once again during permafrost and glacial periods and reach the 500 mL/L level.

2.2 Bentonite pore-water chemistry in the repository

In order to avoid confusion, bentonite pore-water is defined in this discussion as being the free water in equilibrium with bentonite.

Bentonite materials normally consist of the clay mineral montmorillonite and accessory minerals, e.g., feldspars, quartz and calcite. The desired physical properties are mainly governed by the montmorillonite, which therefore normally dominates the bentonite material in commercial products. The type and amount of accessory minerals vary quite substantially between the different commercial products depending on the mining site. Montmorillonite has a relatively low solubility, and the actual accessory mineral composition in combination with the added water solution therefore determines the pore-water composition. In this work we consider Wyoming MX-80 bentonite only, which of course has natural variations in composition and in the amounts of accessory minerals, but the uncertainties in the contents are expected to be small /SKB 1999c/.

According to the current concept, the compacted bentonite blocks placed in the deposition hole will have an initial degree of saturation of 85% /SKB 1999c/. Following closure, the repository host rock and excavation damaged zone is expected to return to saturated conditions over a few years. The full saturation and subsequent homogenisation of bentonite in the deposition hole are expected to occur between 6 and 35 years /SKB 1999d/, but it could also extend over a longer time period, even some hundreds of years depending, e.g., on the access of water to the deposition hole. At full saturation, the target bentonite density is 2 Mg/m^3 and the hydraulic conductivity is very low, less than 10^{-12}m/s /SKB 1999d/. It has to be assumed that no contact between the bentonite pore-water and the copper canister is possible unless the bentonite is fully saturated.

All near-field materials will experience a period of heating and a subsequent period of cooling. Elevated temperatures will continue to persist for thousands of years, but the maximum temperature will be reached between 10 and 20 years after disposal (figure 2-3). The maximum canister surface temperature of 90°C is calculated assuming

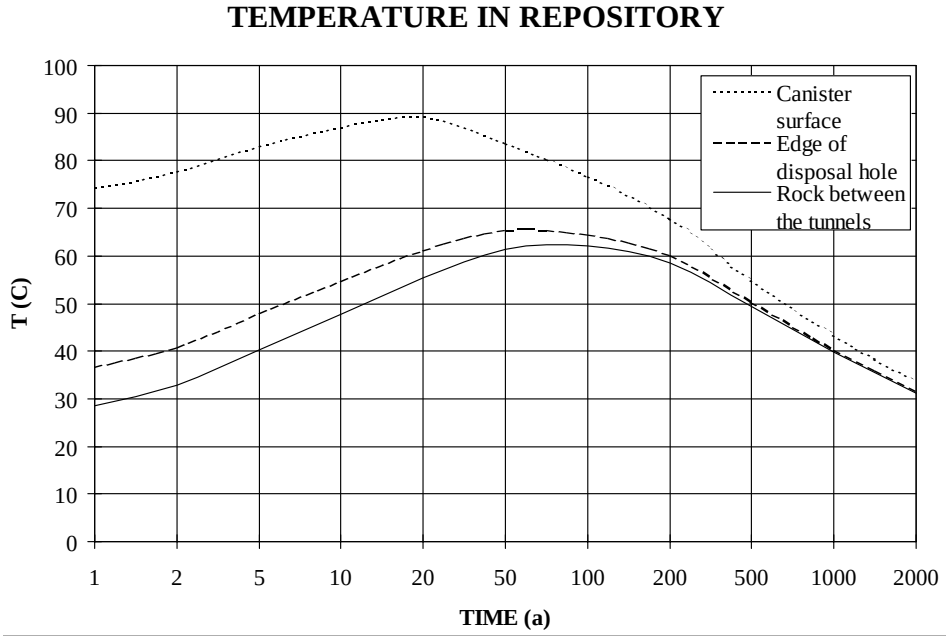

Figure 2-3. *Evaluated temperature changes in repository with elapsed time /Raiko and Salo 1999/.*

dry bentonite and 11°C for the initial temperature of the bedrock. However, saturation of the bentonite is likely to reduce this maximum canister temperature by up to 15°C /Raiko and Salo 1999; Ageskog and Jansson 1999/. The temperature rise in the near-field will not adversely affect the performance of the bentonite buffer. The mineralogical and chemical properties of the bentonite in the deposition hole will not be affected by temperatures below 130°C /Pusch et al. 1991; SKB 1995/. This has been verified by investigations on bentonite from a depth of 500 m at Hamra, Gotland in Sweden /SKB 1992/, which has been heated to temperatures of 110–120°C for at least 10 Ma during its geological history without any signs of cementation or significant deterioration /Crawford and Wilmot 1998/. The temperature conditions in the repository system will approach the natural state after 10,000 years when the decay heat has declined to less than one percent of its original value.

The general trends of temperature effects on the chemical processes are known (table 2-4), but no results on experimental or modelling studies are available for a more exact assessment. However, some results on laboratory experiments have shown a redistribution of the easily dissolving accessory minerals (e.g., gypsum and calcite) during water saturation of bentonite under a thermal gradient /Karnland 1995/. Calcium sulphate (gypsum, anhydrite) and calcium carbonate (calcite) have a decreasing solubility with increasing temperature, which was proposed as a possible cause for the precipitation.

Table 2-4. Groundwater constituents important in bentonite pore-water for corrosion of copper (in bold) and associated processes affecting the values of the constituents. Processes which are dominant are also given in bold.

Constituent	Cause of possible changes in the constituent values	Direction of change	
pH	calcite dissolution precipitation	increase	buffering of pH
	pyrite dissolution	decrease	
	temperature increase	decrease	
	decrease in redox	decrease	
	partial pressure of CO_2	increase	
Alkalinity	calcite dissolution precipitation	increase	
		decrease	
Redox, O_2	active microbial processes	decrease	buffering of Eh
	oxidation of pyrite	decrease	
	oxidation of other Fe(II) accessory minerals	decrease	
Cl^-	halite dissolution	increase	
Ca^{2+}	$CaSO_4$ (anhydrite or gypsum) dissolution	increase	
	calcite dissolution	increase	
	calcite precipitation	decrease	
	ion exchange with Na^+	decrease	
SO_4^{2-}	oxidation of pyrite	increase	
	$CaSO_4$ (anhydrite or gypsum) dissolution	increase	
HS^-	microbially mediated sulphate reduction	increase	
	pyrite precipitation	decrease	
NH_4^+	ion exchange with Na^+	decrease	
CH_4(g)	increased temperature	decrease CH_4(aq)	
	increased pressure	increase CH_4(aq)	
Microbes	water activities comparable to saturated compacted bentonite => microbes not viable	no effect	

Another possible cause may be evaporation of water at the interface between the bentonite and the central tubes. The latter process has been observed to also precipitate other easily dissolved substances derived from groundwater, e.g., sodium chloride (halite). Precipitation of gypsum has been also confirmed in the LOT field experiments at Äspö /Karnland et al. 2000/.

The processes affecting the bentonite pore-water constituents of importance in the corrosion of the copper canister are given in table 2-4. Processes that have an effect on the other constituents are also included. Some of the processes have fast kinetics, some are reversible, some irreversible, and for some reactions to occur microbial activity is a prerequisite. The processes given in bold are the decisive processes in causing notable changes in the corresponding constituents.

The assessment of long-term pore-water evolution presented here is based on modelling exercises /Bruno et al. 1999; Wersin et al. 1994; Wieland et al. 1994/. Experimental results on interaction of aqueous solutions with bentonite are available from short-term batch experiments /Snellman et al. 1987/ and experiments with compacted bentonite /Muurinen and Lehikoinen 1999/, giving some information about the pore-water chemistry at saturation. Long-term experimental results on the bentonite pore-water will be obtained from the LOT experiment after its completion in 2001 /SKB 2000/. Table 2-5 gives the estimated values for the constituents of interest for bentonite pore-water in the case of the Olkiluoto site. These estimates are also considered valid for the Swedish sites except for the chloride and methane contents, which are expected to be lower. The assessment is based on the assumption that bentonite becomes fully saturated within the first 100 years by which time the infiltrating groundwater has become anoxic again.

Table 2-5. Estimated constituent values in bentonite pore-water at Olkiluoto during the evolutionary periods considered.

Constituent		Infiltrating groundwater at closure	Pore-water in saturated bentonite (up to 100 years)	Pore-water after closure up to 10,000 years
pH		6–8	7–9	7–9
Redox	mV	Oxic to −250	−150 to −250	−200 to −280
DIC[a)]	mol/L	$(0.02\text{-}1.6)\cdot10^{-4}$	–[b)]	–[b)]
Cl^-	mol/L	$(0.3\text{-}6.2)\cdot10^{-1}$	$(0.3\text{-}6.2)\cdot10^{-1}$	$(0.06\text{-}4.2)\cdot10^{-1}$
Na^+	mol/L	$(0.2\text{-}2.8)\cdot10^{-1}$	$(3\text{-}5)\cdot10^{-1}$	$(3\text{-}4)\cdot10^{-1}$
Ca^{2+}	mol/L	$(0.3\text{-}1.5)\cdot10^{-1}$	$(4\text{-}40)\cdot10^{-3}$	$(4\text{-}40)\cdot10^{-3}$
SO_4^{2-}	mol/L	$(0\text{-}5.2)\cdot10^{-3}$	$1.4\cdot10^{-1}$	$1.4\cdot10^{-1}$
HS^-	mol/L	$(0–0.9)\cdot10^{-4}$	$(0\text{-}0.3)\cdot10^{-3}$	$(0\text{-}0.9)\cdot10^{-4}$
NH_4^+	mol/L	$<5.5\cdot10^{-6}$ $<1.7\cdot10^{-4}$*	$(0.03–1.7)\cdot10^{-4}$	$<5.5\cdot10^{-5}$
CH_4(g)	mL/L	$<4.5\cdot10^{-6}$ $<2.7\cdot10^{-2}$**	$<4.5\cdot10^{-3}$	$(0.004–17.9)\cdot10^{-3}$

* constituent value in the case of marine water
** constituent value in the case of saline water
a) dissolved inorganic carbon
b) no estimate

Bruno et al. /1999/ have modelled the interaction of bentonite and groundwater by applying instantaneous equilibrium and a number of exchange cycles with incoming groundwater. In the modelling exercise, the expected porewater/bentonite ratio (0.41cm^3 water/cm^3 bentonite) in the repository was used, the amounts of accessory minerals (calcite and pyrite) were included, as well as ion exchange processes. The interaction with three Swedish groundwaters (Äspö, Finnsjön, Gideå) was modelled. A general conclusion from the results of bentonite-groundwater equilibrium modelling was that the three reacting groundwaters do not have a marked effect on the actual bentonite pore-water composition, only some depletion of the accessory minerals (e.g. pyrite). Exceptions were anhydrite and halite, which were completely washed out.

The composition of Äspö groundwater is closest to Olkiluoto groundwater. Accordingly the evaluated values for Olkiluoto given in table 2-5 are based on the modelling results for Äspö /Bruno et al. 1999/, but the saturation values are also based on the few experimental results /Snellman et al. 1987; Muurinen and Lehikoinen 1999/. Major differences between Äspö and Olkiluoto groundwater are in pH and salinity (Na^+, Ca^{2+}, Cl^-), but the ranges considered at different time periods cover a large domain.

Based on a hydraulic conductivity of 10^{-11} m/s and a hydraulic gradient of 0.1 in bentonite (thickness of 0.35 m), Wanner et al. /1992/ and Wieland et al. /1994/ estimated a period of 13,800 years for the total pore-water replacement. According to this estimation, the bentonite pore-water would not be fully replaced after 10,000 years, i.e., by the time of the second evolutionary period considered here. Another estimation based on a hypothetical water flow leaving the near field (SITE 94, 1996) implies total replacement of the bentonite pore-water after 10,000 years.

pH

Wieland et al. /1994/ have modelled (mixing tank) the evolution of pH in the near-field contacting bentonite with simplified Allard and Äspö groundwaters. In the case of Allard groundwater, the pH remained fixed at 8.4 while calcite was present in the system (up to about 90 exchange cycles), but after complete removal of calcite the pH gradually decreased to about 6.8. The pH value of 8.4 is comparable with the experimentally obtained value of 8.6 /Muurinen and Lehikoinen 1999/. However, the modelling results /Wieland et al. 1994/ in the case of Äspö groundwater and experimental results with simplified Olkiluoto groundwater /Muurinen and Lehikoinen 1999/ are not correspondingly comparable. The modelling results indicated lower pH (about 6) than the experimental measurement gave (8.1). It has to be noted that the tested saline solutions differed in contents, especially in the initial pH values and alkalinity (5 times higher in the modelling exercise).

According to modelling by Bruno et al. /1999/, the alkalinity buffering capacity is not largely affected by the replacement of pore-water with granitic groundwater, either from Äspö, Gideå or Finnsjön. The large input of Ca^{2+} with groundwater (e.g., Äspö and Olkiluoto) induces precipitation of calcite and buffers the alkalinity keeping the pH levels above 8. This agrees well with the measured bentonite pore-water pH of 8.1 obtained in short-term experiments /Muurinen and Lehikoinen 1999/ when the contacting solution was simulated Olkiluoto groundwater.

In the determination of the pH value of a system, there are limitations, both in experiments and modelling exercises. The major limitation in modelling exercises is the lack of knowledge of the partial pressure of carbon dioxide (pCO_2) in the systems considered, and whether the systems should be modelled as open or closed. In experiments, control of the gaseous phase is also difficult and often not adequate. Muurinen and Lehikoinen

/1999/ modelled the bentonite pore-water chemistry of their experiments applying both closed and open system approaches. In the closed system the pH value obtained was 1 to 2 pH units higher than in the open system, with an assumed log pCO_2 of –3.36. The experimental values agreed with those of the open system.

Oxygen and redox

The uptake of oxygen by micro-organisms and geologic media has been demonstrated and the results summarised by Puigdomenech et al. /2001/. In the conclusions it was stated that, once anoxic conditions have been reached, the return towards reducing conditions proceeds in several months, for which different reaction paths were identified. The paths are probably catalysed by bacterial activity and controlled by reaction of the solution with magnetite, pyrite and Fe(III) oxyhydroxides.

However, in saturated bentonite the microbial processes cease (see section 2.3) and the only processes remaining are solution-mineral processes. Wersin et al. /1994/ have calculated the evolution of oxygen in the near-field taking into account the important processes affecting oxygen migration, diffusion, and oxidation of pyrite and dissolved Fe(II). The effect of increased temperature (60ºC) and hydrostatic pressure were allowed to dissolve all the available O_2 in the pore-water. The time estimated for the O_2 concentration to decrease to 1% of the initial value ranged between 7 and 290 years, with the elapsed time at which transition to anoxic conditions occurred was estimated to be within the same time range. Thus, the oxidation potential of –100 to –400 mV was estimated to prevail after 10–300 years of emplacement. Modelling estimates from Canadian studies /Johnson et al. 1996/ predict that the initially trapped oxygen could persist for hundreds of years.

The simulations by Bruno et al. /1999/ indicated that the reduction capacity of the bentonite system would only be exhausted after 300,000 years if a continuous flow of Äspö groundwater equilibrated with the atmosphere reacted with bentonite with the lowest pyrite content (0.01 wt.%).

Chloride

The chloride content in bentonite pore-water is determined by the concentration of Cl^- in the saline groundwater. The small amount of halite present as an accessory mineral in bentonite did not increase the Cl^- concentration in experiments with saline contacting solutions (TDS=24 g/L), but an increased Cl^- concentration was observed in the case of a fresh contacting solution (TDS=0.25 g/L) /Muurinen and Lehikoinen 1999/. After the bentonite has become saturated, diffusion is the only mechanism by which the compositions of the bentonite pore-water and the contacting groundwater will equilibrate.

Sulphate and Sulphide

The sulphate concentration increases substantially in bentonite pore-water when compared to the content in the contacting solutions, both saline and fresh. This has been observed in experiments /Muurinen and Lehikoinen 1999/ and in modelling studies /Bruno et al. 1999/, and results from the dissolution of gypsum (or anhydrite). Microbes are not expected to be viable in saturated bentonite and consequently sulphate is not expected to become converted to sulphide by microbial processes. The sulphide content in bentonite pore-water is foreseen to remain at the levels of the diffusing groundwater.

Ammonium

Ammonium present in groundwater and diffusing into bentonite will probably be re-moved by an irreversible cation exchange process /Appelo and Postma 1993/, but as no experimentally verified data are available the values given in table 2-5 are those estimated for the groundwater.

Methane

The concentration of methane in the bentonite pore-water will reflect the concentration in the contacting groundwater.

2.3 Microorganisms

2.3.1 Groundwater microbiology

The presence and activity of microorganisms in Fennoscandian groundwater have been studied extensively. They occur abundantly and show significant activity at most sites investigated. The total numbers of bacteria have been measured in more than 100 samples from different sites at different depths (figure 2-4), and the molecular and physiological diversity of those microbes are extensive, representing most major groups of microorganisms and all main physiological groups. The growing pool of knowledge about intraterrestrial microbiology significant to Finnish and Swedish repository conditions has been published in a series of scientific papers over the last 10 years. Those scientific contributions have recently been reviewed by Pedersen /2000, 2001/. Results and interpretations of importance for evaluation of geochemical conditions at repository depth are introduced below with references in detail to the underlying research results.

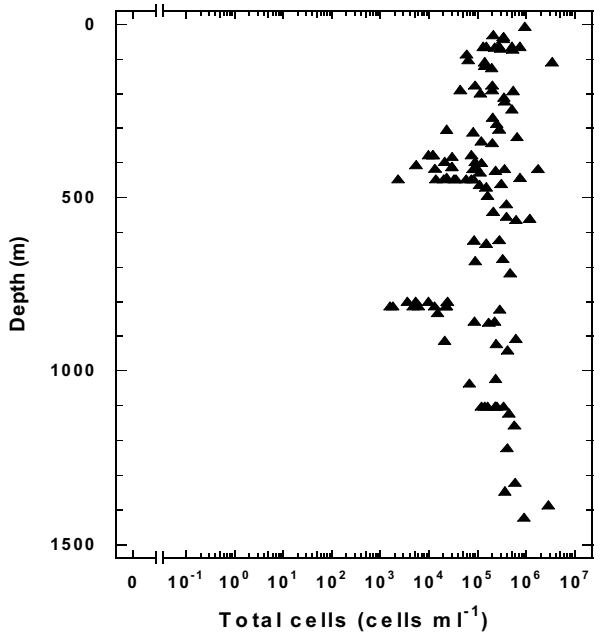

Figure 2-4. *Total number of cells observed at various sites. At least one determination was done on each level in each borehole. The number of observations depicted in the figure is 112.*

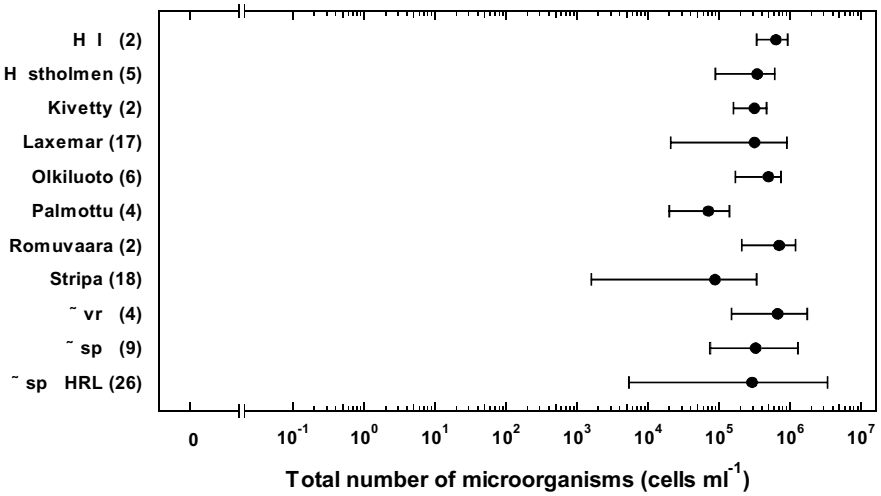

Figure 2-5. *The total number of microorganisms observed at the eleven sites investigated. The figure shows the average total number of microorganisms per site; the bar gives the range of data used to calculate the average number. The number in parenthesis following the site name gives the sum of observations for the site and sums of observations are sets of mean values based on between two and six repetitions.*

Total numbers of microorganisms

Total numbers of subsurface microorganisms vary greatly, depending on the site studied. Values in the range of 10^3–10^8 cells mL^{-1} of groundwater or gram of sediment have been reported for underground environments /Pedersen 1993; Fredrickson and Onstott 1996; Herbert 1990/. Generally, the average total number of cells commonly found in the Fennoscandian igneous rock aquifers is in the range of 10^5–10^6 cells mL^{-1}, although the range of single observations is from 1×10^3 to 5×10^6 cells mL^{-1} (figure 2-5).

The total number of cells in specific boreholes was studied extensively at Stripa and Äspö and the variability was found to be remarkably small /Pedersen and Ekendahl 1992; Ekendahl and Pedersen 1994; Pedersen et al. 1997; Pedersen et al. 1996/. The variation in total numbers between boreholes and the non-variability in total numbers within specific boreholes is indicative of stable environments with little, or no, changes in the conditions for microbial life. These conditions may, however, vary considerably between sites and boreholes intersecting the Fennoscandian Shield igneous rock aquifers. This observation compares well with data on the groundwater chemistry in boreholes, which may vary significantly between boreholes, depths and sites, but is often non-variable within specific boreholes over the time-span of samplings /Nilsson 1995/.

Physiological groups of culturable bacteria

Culturing methods were applied to study bacteria in groundwater from the Äspö HRL tunnel and from five sites in Finland /Kotelnikova and Pedersen 1998; Haveman et al. 1999/. Figure 2-6 summarizes the most probable number (MPN) results of iron reducing (IRB) and sulphate reducing bacteria (SRB), heterotrophic and autotrophic acetogens, and heterotrophic and autotrophic methanogens.

Iron-reducing bacteria and SRB in the range of 10^0–10^4 cells mL^{-1} were detected at many of the depths investigated (figure 2-6). The presence or absence of pyrite as a fracture mineral correlated well with the presence or absence of SRB at the Finnish Hästholmen and Olkiluoto sites /Haveman et al. 1999/. Pyrite formation on fractures

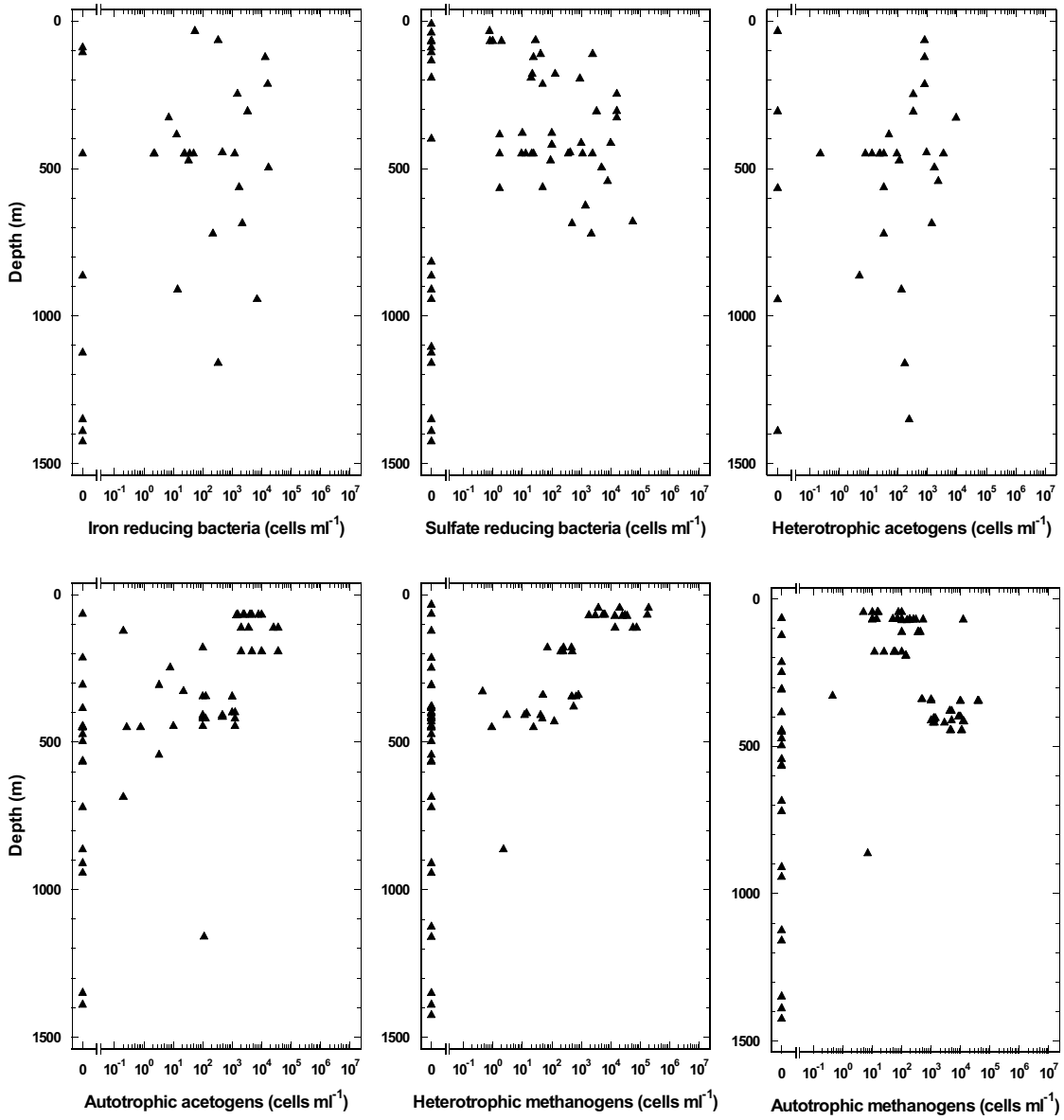

Figure 2-6. *MPN of different physiological groups of microorganisms observed at the 11 sites investigated. Each observation consists of a MPN determination, with three or five parallel tubes in the dilution series.*

in these cold aquifers may reflect long-term SRB activity, which may not always be apparent from groundwater chemistry data; however, in Olkiluoto the groundwater chemistry data indicated earlier occurrences or ongoing sulphate reduction /Pitkänen et al. 1999/. No correlation could be found between sulphate or sulphide concentrations and MPN of SRB. In the Äspö HRL tunnel it was found that the MPN of SRB correlated well with geological, hydrological, and groundwater isotope data, indicative of ongoing sulphate reduction /Laaksoharju et al. 1995; Pedersen 1997/.

Some of the largest numbers of SRB were found in boreholes with both very low and very high sulphate and generally low sulphide concentrations. Under steady-state conditions, the time frames of various processes in hard rock may span millions of years and thus even the slowest transport rate may replenish sulphate to SRB within this time frame resulting in a steady-state concentration of sulphate and a build-up of pyrite precipitates.

In most hydrothermally oxidized fractures, IRB have access to an almost unlimited source of ferric iron, provided they can reach it. Humic and fulvic acids in deep groundwaters have been demonstrated to act as electron shuttles between ferric iron sources and IRB /Coates et al. 1998/. The molecular size of these compounds is small enough to allow penetration of the rock matrix, which then enables iron reduction in parts of the rock that are not directly accessible to the IRB. Attempts to correlate numbers of IRB with amounts of ferric and ferrous iron have not been successful because, much more so than the sulphur redox couples, the iron redox couple is sensitive to inorganic processes, at least where reduction is concerned. Therefore, it is not possible to discriminate between biological and chemical iron redox reactions. Adaptation of mixing models has been demonstrated to be more fruitful /Banwart et al. 1996/. The effect of IRB on carbon dioxide and ferrous iron production was demonstrated for a shallow groundwater intrusion system at the Äspö HRL tunnel.

Äspö HRL groundwater has indicated that the physiological group of acetogenic bacteria is important in the subterranean environment /Pedersen et al. 1996/. Later applications of MPN media for heterotrophic and autotrophic acetogens have lent support to this hypothesis. Heterotrophic acetogens have, with five exceptions, been found at all depths studied; autotrophic acetogens have also been shown to occur frequently, and the numbers of autotrophic acetate-producing bacteria correlate well with the numbers of heterotrophic methanogens (figure 2-6), including acetoclastic ones /Kotelnikova and Pedersen 1998/. A wide range of bacteria, including methanogens, SRB and IRB may use acetate as an energy source.

The presence of hydrogen and carbon dioxide in most deep groundwaters examined (table 2-3) indicates that autotrophic methanogenesis should be possible and the MPN analyses indeed report significant numbers of organisms responsible for this process at Hålö, Äspö HRL, and Olkiluoto, altough in most samples from Finland no positive indications of methanogens was observed /Haveman et al. 1999; Kotelnikova and Pedersen 1998/. However, the possibility cannot yet be excluded that the MPN determinations were inaccurate.

Microbial oxygen reducing activity

The possibility that microorganisms may be able to buffer against an oxidising disturbance in bentonite, backfill and the deep host rock environment has previously been overlooked. During the past decade, a series of different projects have been launched, aimed at understanding the fate of oxygen in a repository, as well as the redox buffer capacity of rock and groundwater. The general conclusion from these projects is that microbes will dominate the oxygen removal and redox control processes /Banwart 1995; Kotelnikova and Pedersen 1999, 2000; Puigdomenech et al. 2001/.

Microbial decomposition and the production of organic material depend on the sources of energy and on the electron acceptors present. Hydrogen, organic carbon, methane and reduced inorganic molecules are possible energy sources in subterranean environments. The major oxygen buffers that can be used are methane and organic carbon. Hydrogen, sulphide and ferrous iron can also contribute but these compounds generally appear in much lower concentrations than do methane and organic carbon (e.g., table 2-3). However, locally, they may have a significant effect.

A variety of bacteria, the methanotrophs, readily oxidise methane with oxygen. Methanotrophs are found wherever stable sources of methane are present. There is some evidence that although methane oxidisers are obligate aerobes, they are sensitive to oxygen and prefer microaerophilic habitats for development. Recently published data, however,

indicate that methane oxidation can occur in some anaerobic environments /Hindrichs et al. 1999/. The methane oxidisers are often concentrated in a narrow band between anaerobic and aerobic zones where methane meets an oxygenated system. Such environments will be common in future repositories during the open phase and for some time after closure. Once established, this group of bacteria will be active for as long as oxygen is present for the oxidation of methane. After closure, they will most probably react all available methane with the remaining oxygen.

A deep repository will rapidly become anoxic after closure if methane is in excess. The concentration of methane in many deep groundwaters is so high (table 2-3) that for microbial removal of all oxygen, all that is needed is one to five volumes of methane-containing groundwater to mix with one volume of oxygen-containing groundwater. The time required for this process depends on the bacterial activity, but it is expected to be a fast process, as most microbes work very fast when given the chance to proliferate. A significant microbial oxygen reduction with the organic carbon naturally present in groundwater (table 2-3) was documented in the REX project at the Äspö HRL. The aerobic microbes were demonstrated to have a dominating role in the reduction of oxygen /Puigdomenech et al. 2001; Kotelnikova and Pedersen 2000/.

A time related model for microbial activity in the host rock

The oxygen reduction projects /Kotelnikova and Pedersen 1999, 2000; Puigdomenech et al. 2001/ all conclude that microbes in hard rock aquifers and tunnels are capable of reducing oxygen. The results indicate that a large benefit of geosphere microbes for repository performance is their massive capacity to protect the host rock and repository from oxygen, and their production of groundwater components that lower the redox potential. Figure 2-7 illustrates a possible geosphere scenario over different climatic

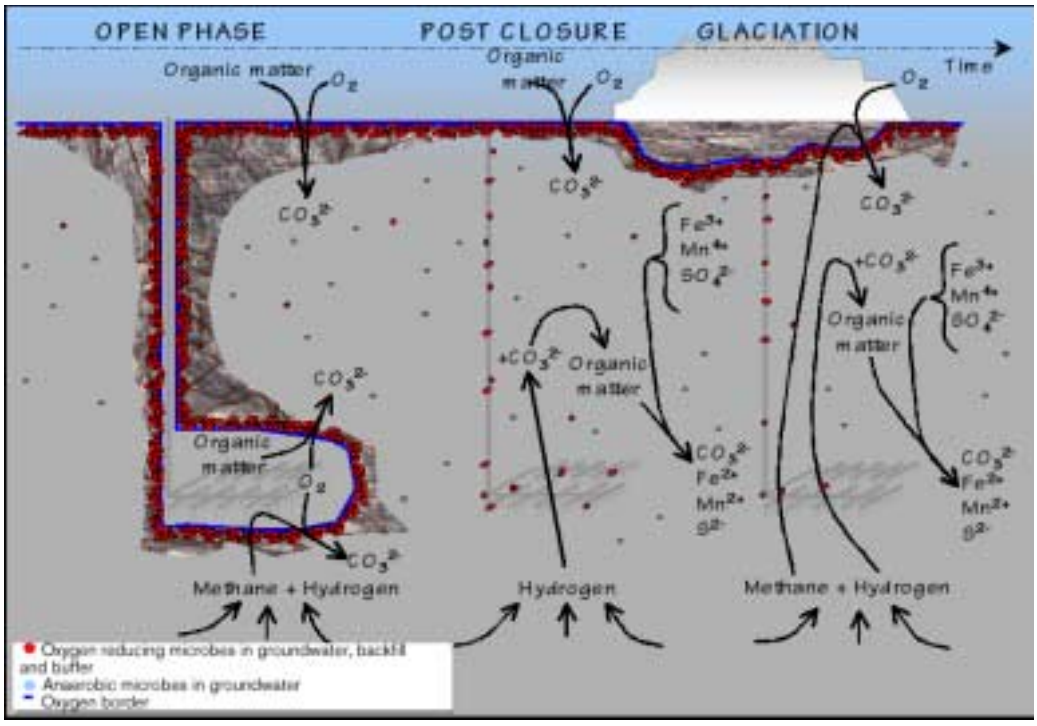

Figure 2-7. *A schematic model of how microbes in the geosphere would stop oxygen from reaching a HLW repository and keep the groundwater redox potential at low levels. See text for an explanation.*

conditions, starting with the open phase. Oxygen will move with recharging groundwater into the basement rock and will diffuse from the tunnel air into the rock matrix. However, the recharging groundwater will contain organic matter and microbes will continuously reduce this oxygen by oxidising organic carbon. Anaerobic microbes in the hard rock aquifers in the host rock are known to reduce ferric iron, manganese(IV) and sulphate to ferrous iron, manganese(II) and sulphide with organic carbon. These metals and the sulphur will react with oxygen when the water reaches a tunnel. Mats of microbes develop on the tunnel walls where groundwater seeps out and produce organic carbon with the energy derived from these groundwater components. Other microbes can later use the organic matter for additional oxygen reduction. Thus the microbes close biogeochemical cycles /Pedersen and Karlsson 1995/.

Periods of glaciation present a special case (figure 2-7). During such events, the input of organic carbon with recharging groundwater will be low because, during a glaciation, photosynthetic production of organic carbon will cease. The REX projects demonstrated a significant activity of methane-oxidising bacteria. Methane is produced in deep magmatic rocks and migrates upwards /Apps and van de Kamp 1993/. The continuous flow of methane from deep mantle rocks will not depend on glaciation events. Hydrogen is an even better oxygen reducer for microbes than is methane, but this gas appears in lower concentrations (table 2-3). In conclusion, the microbial oxygen reduction effect will most probably be sustainable over the lifetime of a repository.

2.3.2 Survival and activity of microorganisms in the buffer

The worst case scenario for corrosion of the copper canister would be if sulphate reducing bacteria formed biofilms on the canisters or grew intensively in the buffer close to the canister. The corrosion process would be controlled by the transport of sulphate to the canister, if enough hydrogen or degradable organic carbon were available for such growth. This could lead to considerably accelerated corrosion since the transport of sulphate is expected to be much faster than the transport of sulphide, due to the fact that the sulphate concentrations in the bentonite can be up to tens of mmol/L /Bruno et al. 1999; Muurinen and Lehikoinen 1999/.

During the initial phase, the temperature in the repository will be elevated, with a maximum canister surface temperature of 90°C. This is, however, not an absolute constraint for micro-organisms. Sulphate-reducing bacteria may survive. The γ-radiation field at the canister surface (an intact canister is considered) will not be high and thus will not have any marked effect on the survival of microbes. The low availability of water in the buffer (i.e., the water content relative to groundwater) will, however, add a constraint on the likelihood of long-term survival. Altogether, conditions for survival will be very difficult for microbes existing close to the canister. This has been investigated with techniques in microbial ecology and several extensive investigations have been performed;

- A long-term test (LOT) of buffer material at the Äspö Hard Rock Laboratory (HRL) in Sweden provided the opportunity of exposing strains of bacteria to conditions realistic to a high-level radioactive waste repository (HLWR). The conditions were similar to those expected in a repository, except for the absence of radioactivity and the difference in scale. The main focus was on sulphide-producing bacteria and their ability to survive. Bacteria were chosen for different relevant characteristics and were exposed to low (20–30°C) and high (50–70°C) temperatures. The major outcome was elimination below the detection limits for all except the spore-forming bacteria, which survived at the lower temperature, although the numbers remaining were

much lower than initially introduced. At the higher temperature, only two bacteria survived most probably as spores, which are metabolically inactive and do not produce sulphide. A slow but significant death rate of viable cells and spores would eventually lead to the complete eradication of life in the buffer. Extrapolation of the results obtained suggests that this would occur well before the first 10,000 years of the repository life /Pedersen et al. 2000a/.

- In follow-up oedometer experiments in the laboratory, bacteria were introduced into bentonite clay under optimal conditions /Pedersen et al. 2000b/. All species studied could be cultivated from the surface layer, mostly in high numbers, which implies at least initially favourable conditions for survival in the top layer of clay. Only three of the nine bacteria tested could be cultivated from the deepest layer (3–6 mm), indicating a species selection at depth. The maximum depth conclusively reached was at least 3 mm.

The bentonite is not sterile at the start, since up to 3.4×10^4 cells gdw^{-1} (cells per gram of dry weight of clay) have been cultivated from the clay at 30°C. Some microorganisms will, therefore, be present in the clay before its contact with the groundwater.

When compacted bentonite with a low water content comes in contact with water, it starts to swell. The surface of the clay block will form a gel that slowly transforms to a compacted bentonite, the water content of which is dependent on how much the clay can swell. The rock walls in a HLW deposition hole will restrict the swelling process, and therefore, the water content, to about 26% v/w. A suitable measure of the availability of water, or water content, is the thermodynamic water activity (a_w) of a system in equilibrium. Microorganisms can grow over a large range of a_w (0.75–0.999), but most favour an a_w of (0.98) or above (for a salinity of the water of about 3.6%). Bentonite that has been compacted to 2 $Mg \cdot m^{-3}$, and which is water-saturated (approximately 26% v/w), has an a_w of 0.96. This number illustrates that the water content will decrease during swelling in a deposition hole.

The microorganisms present in the groundwater will successively encounter a decreasing a_w which, according to earlier results, would result in a significant decrease in cultivability /Motamedi et al. 1996; Pedersen et al. 2000a/.

If sulphate reducing bacteria are present in the groundwater, they will be embedded in the clay close to the rock wall and close to the canister wall. Their survival and their possible sulphate-reducing activity become an important process to study with respect to the integrity of the waste canisters and the safe performance of a future HLW repository.

- Autoradiography results have shown that sulphide production will occur in the clay very close to the copper surface at the lowest clay density studied, viz. 1.5 $Mg \cdot m^{-3}$, but it could not be observed at higher densities. This is in accordance with the cultivation results obtained showing that the cultivability of introduced sulphate reducing bacteria is high at a density of 1.5 $Mg \cdot m^{-3}$, but rapidly decreases when the density increases /Motamedi et al. 1996; Pedersen et al. 2000a,b/.

A model for survival and activity of microorganisms in bentonite

The importance of the results on the survival and activity of microorganisms in compacted bentonite for a HLW repository can be summarised in a hypothetical model, as outlined in figure 2-8. At the time of deposition, there will be a canister, bentonite blocks and a hole in the rock. The next step will be to allow water to fill up all the void

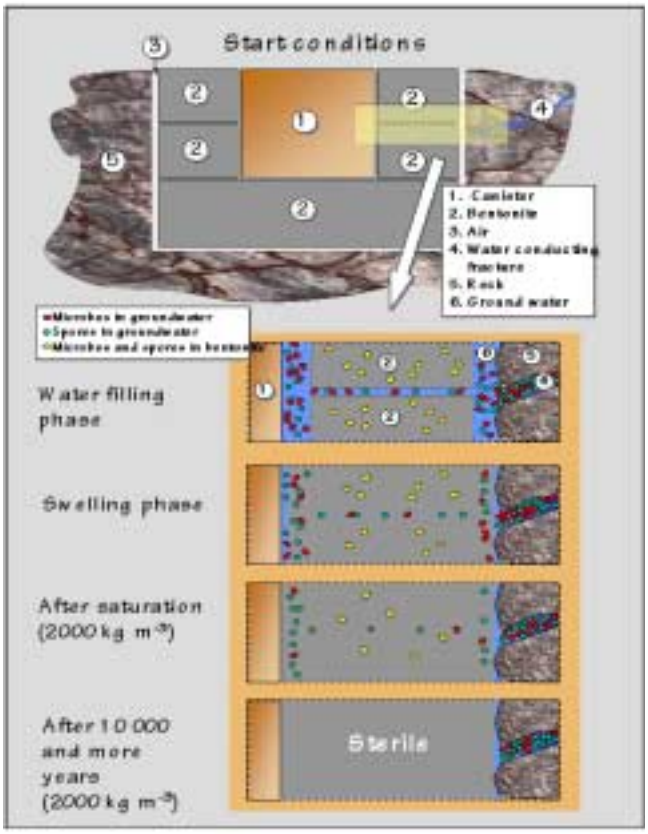

Figure 2-8. *A schematic model of how microbial populations will alter their presence in the buffer. See text for an explanation.*

volume. This water may either be groundwater from the rock or, possibly, groundwater or surface water added from above at deposition. Irrespective of the source, the water will contain microorganisms and these will mix with the buffer during swelling. The swelling of the clay will seed groundwater microorganisms in the buffer to depths possibly reaching a couple of centimetres from the canister and rock surfaces. The microorganisms indigenous to the bentonite will be present inside the bentonite and, also, in the mixing zone.

The results on the survival of non-spore-forming microorganisms in bentonite, reported above, imply that the number of viable microorganisms will decrease rapidly during swelling and that very few viable cells will be present at full compaction. Spore-forming species appear to have a better prospect of staying viable and cultivable over time, compared to non-spore-forming ones. This model is based on current data, obtained with laboratory cultures. It can be argued that naturally occurring microorganisms in the bentonite and groundwater will probably be more resistant, although the working hypothesis will remain as a total eradication of all life in the buffer. More research is presently being performed, using in situ conditions with naturally occurring microorganisms, to test this assumption (section 10).

2.4 Expected corrosion environment for the canisters

In section 2.1, three groundwater conditions were considered at various evolutionary stages up to 10,000 years into the future and even after the next glacial period. It was concluded that predictions further than 10,000 years into the future can be made only very qualitatively based on presumed climatic stages. The assessments are only valid for the base scenario where it is assumed that the spent fuel canister is initially intact and is successfully placed in the deposition hole with compacted bentonite blocks.

Groundwaters infiltrating into a repository in the three cases considered, the Simpevarp and Forsmark areas in Sweden and Olkiluoto in Finland, range from brackish to saline. In the case of Olkiluoto the values are assessed for all the constituents considered important to the corrosion of copper: pH, Eh, Cl^-, and HS^-, as well as NH_4^+ and methane, of which the two latter are lacking in the case of the Swedish sites. Nevertheless, the ranges in NH_4^+ and methane contents determined at Olkiluoto and Hästholmen probably represent the variability that can be expected to be encountered in deep groundwater at coastal sites in crystalline bedrock of the Fennoscandian shield.

A summary of the ranges of groundwater constituents estimated for different times is presented in table 2-6 and the table for bentonite pore-water in the case of Olkiluoto in table 2-7.

Table 2-6. Ranges of groundwater constituents estimated at different times.

Constituent		At closure, infiltration into unsaturated bentonite	After closure and saturation (up to 100 years)	After closure up to 10,000 years
pH		6–8	7–8	7–9
Redox	mV	Oxic to –400	–150 to –308	–200 to –300
DIC[a)]	mol/L	$(0.1–16.4)\cdot10^{-3}$	$(0.5–10)\cdot10^{-3}$	$(0.1–7)\cdot10^{-3}$
Cl^-	mol/L	$(0.1–6.2)\cdot10^{-1}$	$(0.2–1.6)\cdot10^{-1}$	$(0.06–4.2)\cdot10^{-1}$
Na^+	mol/L	$(0.1–2.8)\cdot10^{-1}$	$(0.02–9.1)\cdot10^{-2}$	$(0.04–2.2)\cdot10^{-1}$
Ca^{2+}	mol/L	$(0.03–1.5)\cdot10^{-1}$	$(0.03–0.2)\cdot10^{-1}$	$(0.005–1.0)\cdot10^{-1}$
Mg^{2+}	mol/L	$(0.4–1.0)\cdot10^{-2}$	$(0.4–1.0)\cdot10^{-2}$	$(0.004–1.0)\cdot10^{-2}$
K^+	mol/L	$(1.3–7.7)\cdot10^{-4}$	$(1.3–7.7)\cdot10^{-4}$	$(0.5–5.1)\cdot10^{-4}$
SO_4^{2-}	mol/L	$0–6.3\cdot10^{-3}$	$(0–5.8)\cdot10^{-3}$	$0–5.2\cdot10^{-3}$
HS^-	mol/L	$0–3.0\cdot10^{-4}$	$0–3.0\cdot10^{-4}$	$0–0.9\cdot10^{-4}$
NH_4^+	mol/L	$< 5.5\cdot10^{-6}$, if marine $< 1.7\cdot10^{-4}$	$(0.03–1.7)\cdot10^{-4}$	$< 0.6\cdot10^{-4}$
$CH_4(g)$	mol/L	$< 4.5\cdot10^{-6}$, if saline $< 2.7\cdot10^{-2}$	$0.4\cdot10^{-2}$	$(0.004–17.9)\cdot10^{-3}$
$H_2(g)$	mol/L	$< 2.2\cdot10^{-5}$, if saline $< 8.9\cdot10^{-4}$	$< 4.4\cdot10^{-6}$	$< 2.2\cdot10^{-5}$
DOC[b)]	mol/L of C	$< 1.7\cdot10^{-4}$	$< 8.3\cdot10^{-4}$	$< 1.7\cdot10^{-4}$

a) dissolved inorganic carbon
b) dissolved organic carbon

Table 2-7. Estimated constituent ranges at different times in bentonite pore-water in the case of Olkiluoto.

Constituent		Infiltrating groundwater at closure	Pore-water in saturated bentonite (up to100 years)	Por-water after closure up to 10,000 years
pH		6–8	7–9	7–9
Redox	mV	Oxic to –250	–150 to –250	–200 to –280
DIC	mol/L	$(0.02–1.6)\cdot10^{-4}$	no estimate	no estimate
Cl^-	mol/L	$(0.3–6.2)\cdot10^{-1}$	$(0.3–6.2)\cdot10^{-1}$	$(0.06–4.2)\cdot10^{-1}$
Na^+	mol/L	$(0.2–2.8)\cdot10^{-1}$	$(3-5)\cdot10^{-1}$	$(3–4)\cdot10^{-1}$
Ca^{2+}	mol/L	$(0.3–1.5)\cdot10^{-1}$	$(0.4–4.0)\cdot10^{-2}$	$(0.4–4.0)\cdot10^{-2}$
SO_4^{2-}	mol/L	$(0–5.2)\cdot10^{-3}$	$1.4\cdot10^{-1}$	$1.4\cdot10^{-1}$
HS^-	mol/L	$(0–0.9)\cdot10^{-4}$	$(0–3)\cdot10^{-4}$	$(0–0.9)\cdot10^{-4}$
NH_4^+	mol/L	$<5.5\cdot10^{-6}$ $<1.7\cdot10^{-4}$*	$(0.03–1.7)\cdot10^{-4}$	$<5.5\cdot10^{-5}$
$CH_4(g)$	mL/L	$<4.5\cdot10^{-6}$ $<2.7\cdot10^{-2}$**	$<4.5\cdot10^{-3}$	$(0.004–17.9)\cdot10^{-3}$

*) constituent value in the case of marine water
**) constituent value in the case of saline water

At closure

The redox conditions of the **infiltrating groundwater** are oxic initially, and oxygen is present in the repository atmosphere, but will return to anoxic conditions due to microbial oxygen reduction processes. Later, microbial reduction processes (e.g., IRB, SRB) will produce negative reducing conditions. The change to anoxic conditions is expected to occur rather fast, especially if methane is in excess, as in Olkiluoto groundwaters. The sulphide content will also be limited to less than $3\cdot10^{-4}$ mol/L. The Eh level is estimated to be able to reach as low as –400 mV, except in Olkiluoto where the lower estimate is about –250 mV.

The behaviour of the pH in all three groundwaters is expected to follow similar trends. After the expected initial decrease in pH due to the microbial processes, fracture calcites will buffer the pH to higher values and the expected range of the pH values will be between 6 and 8. The expected variation in chloride content is great, between 0.01 mol/L and 0.62 mol/L, the highest value representing Olkiluoto. The large estimated range results from the possible local variations, which depend on the exact flowpaths into the repository.

As for methane and ammonium, in the case of high concentrations the origin of the infiltrating groundwater is decisive, saline or marine. The methane content is estimated to remain below $5.5\cdot10^{-6}$ mol/L except in the case of saline groundwater when the value could be much higher, in the order of 10^{-2} mol/L. The estimate for ammonium content is below $0.6\cdot10^{-5}$ mol/L, but in the case of marine groundwaters a higher concentration is presumed, about 10^{-4} mol/L.

After the closure of the repository

After the closure of the repository, groundwater with the above-assessed constituent variations is expected to contact the compacted bentonite. It is assumed that the gaps between the compacted bentonite and the canister and between the compacted bentonite and the host rock are not initially filled with water at closure but the groundwater will infiltrate only via the tunnel or fractures in the deposition hole. As a result of the diffusing groundwater, the bentonite is expected to swell and induce sealing of the available free space. Rapid chemical changes occur due to cation exchange and dissolution of some easily dissolved mineral phases. Initially, the bentonite is not sterile but some microorganisms will be present and during the swelling phase the microbial population present in the groundwater will eventually become embedded in the clay, but not deeper than a couple of centimetres from the clay surface.

At this stage the canister is assumed to have contact only with the unsaturated compacted bentonite at the bottom of the canister.

Up to 100 years

This is the most complex evolutionary period to consider, during which several simultaneous thermal, mechanical, hydraulic, chemical and biological processes occur, the net effect of which on the disposal system is not yet well understood. However, in the near future important results from large-scale field experiments will improve our understanding of the system behaviour (e.g., LOT, FEBEX (Full-scale engineered barriers experiment in crystalline host rock /Huertas et al. 2000/)). In this work the different processes and their effects have been treated more or less separately, as those effects are better known. It is also assumed that during this phase the bentonite will become fully saturated and reach the required density and the bentonite pore-water will contact the canister.

As the diffusing groundwater advances in the bentonite buffer, oxygen trapped inside the bentonite and radiation-induced oxidants will be consumed in possible oxidation reactions, e.g., oxidation of sulphides or of the copper canister. The γ-radiation field from the decay of ^{137}Cs ($t_{1/2}$ = 30 years) will not last long and will cause only minor production of oxidants at very low levels throughout this evolutionary period, dropping to insignificant levels after some hundreds of years (see section 8 for more details). Regardless of this, the Eh values in the bentonite pore-water are estimated to stay between –150 mV and –250 mV, due to the large reducing capacity of, e.g., pyrite. In the case of the Simpevarp area, the Eh value could be as low as –300 mV.

The long-term survival of microbes in bentonite is primarily impacted by the low water activity and elevated temperature, while the radiation effects are quite marginal. The number of surviving microorganisms will decrease rapidly during swelling of the bentonite and very few viable microbes will be present at full saturation. Consequently, even if the sulphate content in the pore water is high because of dissolution of sulphate minerals in the bentonite, the estimated level of HS^- is that in the local groundwater (tables 2-6 and 2-7).

The pH of the bentonite pore-water will be buffered to values ranging from 7 to 9 due to interaction of calcite present in bentonite. The chloride content of the pore-water still reflects that of the infiltrating groundwater at closure (table 2-6), as it has not yet been diluted by the local groundwater by diffusion. The ammonium and methane contents are also estimated to be the same as in the local groundwater (table 2-7).

The net effect of the increased temperature and temperature gradient (some 30°C around 20 years after deposition) in the buffer may bring about consequences not foreseen in this work. However, the effects of temperature on several individual constituents of importance are known in general, e.g., an increase in temperature will cause a decrease in pH as will the precipitation of calcite and gypsum. An increase in pH may be caused by calcite dissolution due to the presence of dissolved CO_2. More detailed evaluation of such effects, or rather an estimation of the overall consequences for the bentonite pore-water chemistry in an elevated temperature field can be made only after the long term experiment (LOT) at Äspö /SKB, 2000/ is finished and the results evaluated.

10,000 years into the future

By this time the effect of temperature induced by the canister has levelled off and the chemical conditions in the bentonite pore-water are presumed to reflect those of the bedrock groundwater. The deep saline groundwaters are expected to have approached brackish or non-saline due to land uplift at the present coastal areas of Olkiluoto and Simpevarp. The estimates for the constituents of interest, pH, redox, chloride, sulphide, ammonium and methane are shown in table 2-7. The sulphate content in the pore-water is the only constituent which is still presumed to be at a higher level than in the local groundwater.

Temporal evolution to the far future

Beyond 10,000 years the bentonite pore-water is presumed to reflect the regional groundwater changes as a result of climate changes. The sites will experience a glacial cycle of 150,000 years, with stages of permafrost, glaciation, and deglaciation, before returning to a more temperate climate. During the periods of permafrost the salinity and consequently the chloride content can be high, up to 0.62 mol/L. During glaciation, deglaciation and the next temperate period, when the Baltic basin may also be filled with oceanic water, the chloride content will remain below this high value. High methane contents may be encountered once again during the permafrost period, of the order of 0.022 mol/L.

3 Review of thermodynamic data for copper of relevance to copper corrosion

3.1 General

Thermodynamic data allow the stable states within a multi-component system to be predicted. With the approach used here and in all the references cited, free energies of formation, and the enthalpies and entropies for aqueous species are given for the reference state of infinite dilution. Entropies and heat capacities allow equilibrium constants to be calculated for any temperature within the intended range (0–100°C). In order to give acceptable estimates of the stability of the aqueous species, the departure from infinite dilution must be recognised; activity coefficients must be estimated, particularly for charged species.

3.2 Thermodynamic parameters

Fundamental functions of thermodynamics of aqueous systems at constant pressure (P) and constant temperature (T) are defined by the Gibbs free energy (G), enthalpy (H) and entropy (S):

$$G = H - TS \qquad 3\text{-}1$$

The Gibbs free energy is the measure of the available energy in a system, if pressure and volume (V) of the system are constant (i.e., there is no 'PV' work). The term TS may be defined as unavailable energy, or bound energy. Entropy may be defined as a measure of the system disorder and randomness, while (at constant P) enthalpy describes the heat content. Absolute values of G and H cannot be determined, but the change in their values can be measured when a system shifts from one state to another (i.e., a chemical reaction takes place):

$$\Delta G = \Delta H - T\Delta S \qquad 3\text{-}2$$

In phases containing numerous components, as for example (natural) waters, the term chemical potential (μ) is used to define the partial Gibbs free energies of each component:

$$\mu_i = \left(\frac{\partial G}{\partial n_i} \right)_{P,T,n_i} \qquad 3\text{-}3$$

Differences in chemical potentials between species determine the thermodynamic driving force which allow reactions to take place. There is a linear thermodynamic relationship between chemical potential and activity (a) of each species ($\mu_i = \mu_i^o + RT\ln a_i$). The activity scale is fixed by means of a standard state (denoted by superscript ^{o}) and by a reference state. The reference state for a dissolved component in water is infinite dilution,

in which the activity of the component equals its molal concentration, thus approaching zero. The standard state is the hypothetical ideal solution, in which the component has unit concentration and unit activity.

Recent compilations of thermodynamic data for copper have been published by Puigdomenech and Taxén /2000, 2001/ and by Ahonen /2001/. The work by Puigdomenech and Taxén also contains thermodynamic data for a large number of auxiliary species in the system chlorine-fluorine-oxygen-sulphur-nitrogen-phosphorous-carbon-hydrogen-sodium-calcium. The basic data include the free energy of formation from the elements (ΔG_f), entropy (S^0) and heat capacity (C_p) for each chemical compound. An alternative approach is used by Ahonen, who lists the free energies of reaction (ΔG^0_r), the reaction entropy (ΔS^0) and the change in heat capacity (ΔC_p).

3.3 Equilibrium constants

The most frequently used thermodynamic parameter in solution chemistry and in aqueous geochemistry is the thermodynamic stability constant, which is defined as the quotient of the activities of the reaction products and reactants.

Equilibrium constants are calculated from thermodynamic data according to

$$\ln K^\circ = -\frac{1}{RT}\sum_i \nu_i \, \Delta G_f^o(i) \qquad 3\text{-}4$$

where K° is the standard equilibrium constant, R is the gas constant, T is the absolute temperature, $\Delta G^\circ_f(i)$ is the Gibbs energy of formation for a reactant (or product) i, and n_i is the corresponding stoichiometric coefficient.

For a general equilibrium reaction

n A + m B = p C + q D

the relationship between the standard equilibrium constant and the value for a given ionic medium is

$$\begin{aligned} K^\circ_{eq} &= a_C^{\,p}\, a_D^{\,q}\, a_A^{\,-n}\, a_B^{\,-m} \\ &= \gamma_C^{\,p}\,[C]^p\,\gamma_D^{\,q}\,[D]^q\,\gamma_A^{\,-n}\,[A]^{-n}\,\gamma_B^{\,-m}\,[B]^{-m} \qquad 3\text{-}5 \\ &= \gamma_C^{\,p}\,\gamma_D^{\,q}\,\gamma_A^{\,-n}\,\gamma_B^{\,-m}\,K_{eq} \end{aligned}$$

where the square brackets [ ] indicate concentration, a_i and γ_i are the activity and the activity coefficient of species i respectively, and K°_{eq} and K_{eq} are the equilibrium constant for standard and non-standard conditions, respectively. The two sets of thermodynamic data referenced here allow K°_{eq} to be calculated. The more useful conditional equilibrium constant (K_{eq}) can only be estimated through activity coefficients.

3.4 Effect of temperature

Temperature effects for solids and gaseous compounds can been obtained from the integrals of the heat capacity temperature functions:

$$\Delta G^{\circ}(T) = \Delta G^{\circ}(T_0) - (T - T_0)\Delta S^{\circ}(T_0) + \int_{T_0}^{T} \Delta C_p^{\circ}\, dT - T\int_{T_0}^{T} \frac{\Delta C_p^{\circ}}{T}\, dT \qquad 3\text{-}6$$

This procedure is described in many references, for example in Kubaschewski et al. /1993/ and Puigdomenech et al. /1997/. The equilibrium constant at temperature T is then calculated from equation 3-4.

Using the listed ΔH_r compiled by Ahonen in appendix II the expression for the equilibrium constant takes a slightly different form /Langmuir 1997/:

$$\ln \frac{K(T)}{K(T_o)} = \frac{-\Delta H_r^o}{R}\left[\frac{1}{T} - \frac{1}{T_0}\right] + \frac{\Delta C_p^o}{R}\left[\frac{T_0}{T} - 1 - \ln \frac{T_0}{T}\right] \qquad 3\text{-}7$$

Equation 3-7 is valid for cases where ΔC_p (the change in heat capacity) is independent of temperature.

3.5 Effect of salinity

Available thermodynamic data are valid at infinite dilution. The effects of finite salt concentrations are in general large and some kind of estimate of this effect is required. In principle, there are two methods. One can use conditional equilibrium constants and enter concentrations instead of activities in the equilibrium expressions or one can use activity coefficients and enter the product concentration times activity coefficient in the equilibrium expressions. In practice, the value of a conditional equilibrium constant can be estimated only through activity coefficients with application of equation 3-5.

3.5.1 Activity coefficients

Thermodynamic equilibrium constants give the relationship between the activities of species. Usually the concentration of a given species is of greater interest than the chemical activity. The chemical activity, a_i, of an aqueous species, i, is related to its concentration, C_i, through the activity coefficient, γ_i:

$$a_i = \gamma_i C_i \qquad 3\text{-}8$$

The activity coefficients are as equally thermodynamic in nature as the equilibrium constants. The standard state for the aqueous species is infinite dilution. That is, in extremely dilute solutions the value of the activity coefficient approaches unity. At higher concentrations, the dependence of the activity coefficient on the concentration is complicated. The deviations from unity are significant and some kind of estimate is usually required.

Single ion activity coefficients cannot be independently measured, only their total effect on the thermodynamic stability constants and on osmotic pressure. The mean activity coefficient ($\gamma\pm$) of an electrolyte solution is the geometric mean of the individual activity coefficients /e.g. Langmuir 1997/:

$$\gamma_{\pm} = \left[\left(\gamma_{+}^{n+}\right)\left(\gamma_{-}^{n-}\right)\right]^{1/n} \qquad 3\text{-}9$$

where $n+$ and $n-$ refer to the charges of the anionic and cationic components, respectively. In pure water, electrolyte mean activity coefficients and single-ion activity coefficients approach unity. With increasing salinity electrostatic interactions between dissolved ions decrease their chemical potentials (i.e., they become 'less active'). Formation of aqueous complexes or ion-pairing also have the effect of decreasing the value of the mean activity coefficient. The mean activity coefficients of various pure electrolytes can be measured experimentally, and are available in compilations of thermodynamic data /e.g. Lobo 1989; Robinson and Stokes 1959/.

In dilute solutions, single ion activity coefficients may be approximated by Debye-Hückel or Davies approximations:

$$\log \gamma_i = \frac{-z_i^2 A\sqrt{I}}{1 + B\mathring{a}\sqrt{I}} \qquad \text{I < 0.1 M} \qquad 3\text{-}10$$

$$\log \gamma_i = -z_i^2 \, A \left(\frac{\sqrt{I}}{1+\sqrt{I}} - b\, I \right) \qquad \text{I < 0.5 M} \qquad 3\text{-}11$$

where z_i is the charge of species i, I is the ionic strength of the solution, and A is a temperature dependent constant (A ~0.509 at 25°C). A common value for b in equation 3-11 is 0.2 although Davies originally proposed a value of 0.3. The ranges of applicability are those suggested by Stumm and Morgan /1995/.

The experimental determination of the thermodynamic data is frequently made in solutions of relatively high concentrations through addition of inert ions. The Specific Interaction Theory, or SIT-model (Brönsted-Guggenheim-Scatchard model) has been found suitable for extrapolation of experimental data. The SIT-model includes one electrostatic term and additional terms that describe the crosswise influence of each ion of the opposite charge.

$$\log \gamma_i = \frac{-A_z i^2 \sqrt{I_m}}{1 + B\sqrt{I_m}} + \sum_k \varepsilon_{(i,k,I_m)} m_k \qquad 3\text{-}12$$

where i denotes the species considered, k and m_k denote the counter-ion and its concentration, respectively, and I_m is the ionic strength in molal units. The first term of the equation is the conventional extended Debye-Hückel equation describing the long-range electrostatic interactions between ions having opposite charges. The second term describes the short-range interactions of an ion with other ions of opposite charge. The SIT approach has been adopted as the standard procedure in the NEA Thermochemical data base review for the extrapolation from high ionic strengths to the reference state of infinite dilution /Grenthe et al. 2000/. Examination of the SIT interaction coefficients of

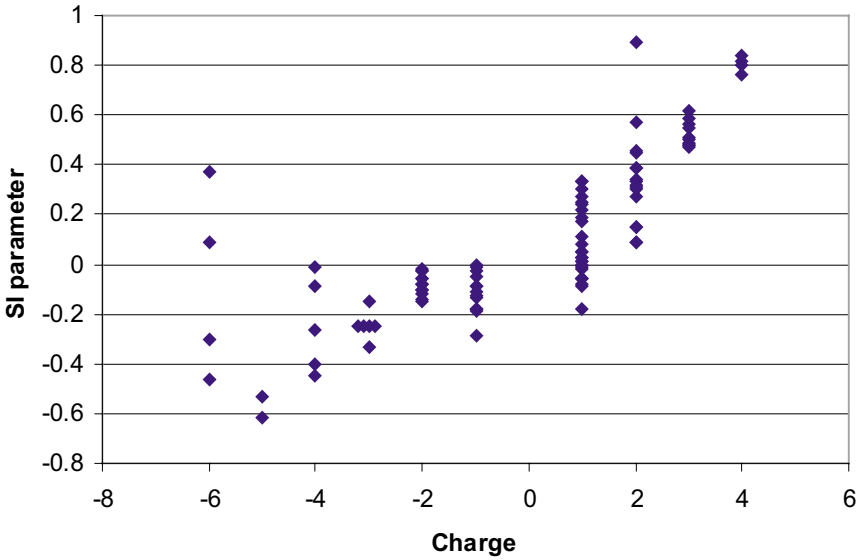

Figure 3-1. *Single-ion SIT-parameter data from Grenthe et al. /2000/.*

various ion pairs reveals some systematic dependence on the charge of the ions involved. Figure 3-1 shows a plot of SIT interaction coefficients versus the charge of the ion.

Pitzer has derived a system of equations that can describe the behaviour of mixed as well as single electrolytes with high accuracy /Pitzer 1991; Pitzer 1995/. The Pitzer equations are useful as a framework for describing the properties of a chemical system. Single electrolyte parameters are determined from activity coefficients determined in solutions of one salt at a time. Mixing terms can be determined from osmotic effects in binary mixtures of salts using the previously determined single electrolyte parameters. In Pitzer's approach to solution chemistry, complex formation plays a very small role. Almost all solutions are treated as fully dissociated but with pairwise interaction coefficients for ions of opposite sign as well as for ions of the same sign. Even Pitzer is forced to recognise HSO_4^-, as an aqueous complex and treat sulphuric acid more as a 1:1 electrolyte than as a 2:1 electrolyte although it is fully dissociated at low concentrations.

Natural groundwaters are complicated in composition. The application of the SIT (and Pitzer) approaches requires specific data for the ions in various hydrogeochemical environments. Because that is not possible in most cases, simplifications must be used. Most useful of these simplifications are those in which the coefficient in the second term is dependent only on the species under consideration or the coefficient is a constant. An example of this model is the "b-dot" (also known as the 'Truesdell-Jones' (T-J) model or the 'WATEQ Debye-Hückel' model) /Langmuir 1997/:

$$\log \gamma_i = -z_i^2 A \frac{\sqrt{I}}{1 + B\mathring{a}\sqrt{I}} + b\,I \qquad 3\text{-}13$$

For this model, values of b are presented in the literature for some major components. Examples are shown in tables 3-1 and 3-2. Another similar model, the "modified Helgeson model" /Puigdomenech and Taxén 2000/, includes an additional logarithmic term intended to account for dilution of the solution in terms of the mole fraction of the salt:

$$\log\gamma_i = -z_i^2 A\frac{\sqrt{I}}{1+B\mathring{a}\sqrt{I}} - \log(1+0.018015I) + bI \qquad 3\text{-}14$$

Parameter values for B, $\mathring{a}$ and b in equation 3-14, at different temperatures, are given in Puigdomenech and Taxén /2000/. It is suggested that, in the absence of sufficient data (ionic radii parameter $\mathring{a}$ for all the species involved), values for NaCl be used throughout.

Note: The equation, which applies to predominantly NaCl solutions, may be generally reliable up to ionic strength of about 2 mol·dm^{-3}.

Table 3-1. Non-zero 'b-dot' values in the Nagra/PSI thermodynamic database.

ion	Al^{3+}	Ba^{2+}	Ca^{2+}	Cl^-	F^-	Fe^{2+}	K^+	Li^+	Mg^{2+}	Mn^{2+}	Na^+	SO_4^{2-}	Sr^{2+}
b	0.19	0.09	0.15	0.01	0.08	0.16	0.01	0.2	0.22	0.22	0.06	−0.07	0.11

Table 3-2. Ion size (a_i=å) and b values for the Truesdell-Jones (b-dot) equation for individual ion activity coefficients /Langmuir 1997/.

	a_i	b		a_i	b
H^+	4.78	0.24	Fe^{2+}	5.08	0.16
Li^+	4.76	0.20	Co^{2+}	6.17	0.22
Na^+	4.0	0.075	Ni^{2+}	5.51	0.22
	4.32	0.06	Zn^{2+}	4.87	0.24
K^+	3.5	0.015	Cd^{2+}	5.80	0.10
	3.71	0.01	Pb^{2+}	4.80	0.01
Cs^+	1.81	0.01	OH^-	10.65	0.21
Mg^{2+}	5.5	0.20	F^-	3.46	0.08
	5.46	0.22	Cl^-	3.71	0.01
Ca^{2+}	5.0	0.165	ClO_4^-	5.30	0.08
	4.86	0.15	HCO_3^-	5.4	0
Sr^{2+}	5.48	0.11	SO_4^{2-}	5.0	−0.04
Ba^{2+}	4.55	0.09		5.31	−0.07
Al^{3+}	6.65	0.19			
Mn^{2+}	7.04	0.22			

3.5.2 Choice of method for estimation of the effects of salinity

The departures of the activity coefficients for charged species from unity in non-dilute solutions are, as a rule, large and some kind of estimate is required. Figure 3-2 shows approximate applicable ranges for the methods discussed here. The limits are those suggested by Langmuir /1997/. The figure also shows the mean activity coefficient of NaCl as function of concentration at 25°C. The different methods are applied with the parameter values suggested. Results can be compared to the experimentally determined values. It should be realised that, beyond the limiting form of the Debye-Hückel equation, none of the methods described here is based on an understanding of the nature of the interaction between ion-ion and ion-solvent.

The choice of method must be based on the following considerations:

- Available data.
- Consistency between complexation constants and interaction coefficients.
- Concentration and main components of the electrolyte, ground water or ionic medium.
- Temperature.
- Required/desired accuracy.

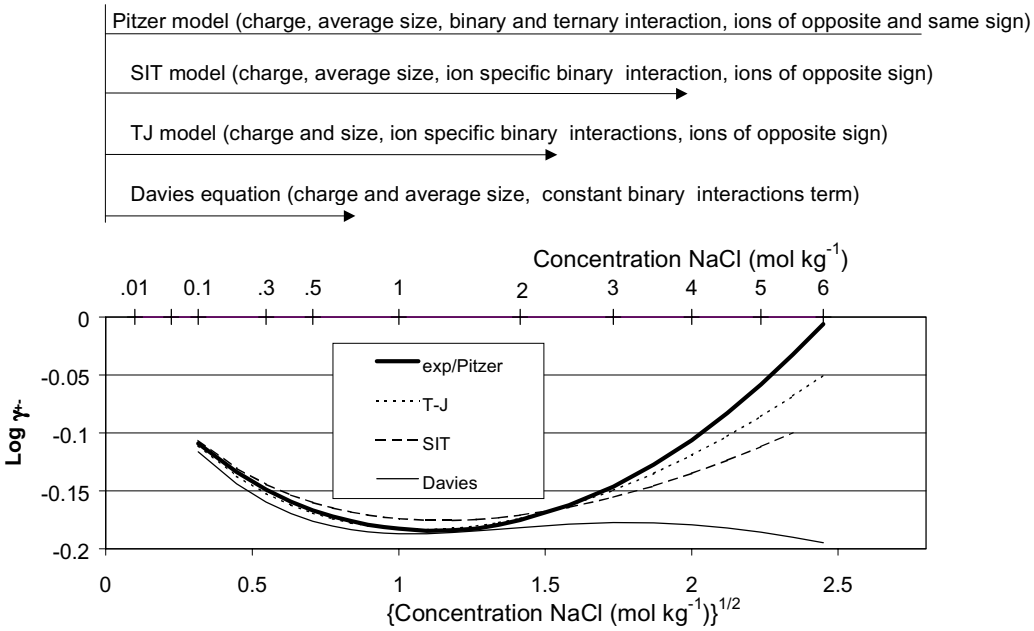

Figure 3-2. *Approximate applicable ranges for some different methods of estimating activity coefficients. Adapted from Langmuir /1997/. Example using the mean activity coefficient for NaCl at 25°C. Experimental data from Robinson and Stokes /1959/. Pitzer equations using* $\beta^{(0)} = 0.0765$, $\beta^{(1)} = 0.2664$, $C^{\Phi} = 0.00127$. *Truesdell-Jones method using* $B = 0.328$, $å = 4.0$, $b = 0.075$ *for* Na^+, $å = 3.71$, $b = 0.01$ *for* Cl^-. *SIT equation using* $\varepsilon(Na^+, Cl^-) = 0.03$. *Davies equation using* $b = 0.2$. *The ionic strength expressed in mol* kg^{-1} *was applied to all equations. [NaCl]aq was calculated using log k = –0.78 for Davies equation. [NaCl]aq was not considered for other methods, for which the inclusion of [NaCl]aq would be detrimental to their performance. The "true" ionic strength was used for the Davies equation. For the other methods the "true" ionic strength is equal to the stoichiometric ionic strength since [NaCl]aq is considered to be non-existent. See section 3.8.*

3.6 Effect of pressure

The effect of pressure on equilibrium constants may be estimated from /Langmuir 1997; Stumm and Morgan 1995/:

$$\log \frac{K^{\circ}_{p}}{K^{\circ}_{p^{\circ}}} = -\frac{\Delta V^{\circ}_{r}(p - p^{\circ})}{\ln(10)\,RT} \qquad 3\text{-}15$$

where p° is the standard pressure (1 bar), and ΔV°_{r} is the standard molar volume change for the reaction. The expected hydrostatic pressure at the planned repository depth of 500 m is estimated to be of the order of 50 bars. Puigdomenech and Taxén with reference to Langmuir /1997/ state that it is experimentally found that for dissociation reactions $\Delta V^{\circ}_{r} \geq -50$ cm^3/mol. Molar volumes for many minerals may be found in Robie and Hemingway /1995/. The "maximum" value of $\Delta V^{\circ}_{r} = -50$ cm^3/mol, corresponds to an increase of 0.26 log-units in the equilibrium constant at 300 bars.

3.7 Evaluation and selection of thermodynamic data

Appendix I contains the selection of thermodynamic data from SKB TR-00-13 /Puigdomenech and Taxén 2000/. Sources used and discussion of the selection can be found there. Appendix II contains a previously unpublished selection of thermodynamic data and discussion by Ahonen. These are two more-or-less independent selections of data. As will be shown by an application of these in chapter 6, the difference between the two sets, in terms of equilibrium concentrations of Cu(I), is not significant.

3.8 Consistency

There are a number of important questions of consistency of the data. The thermodynamic database must, of course, be internally consistent so that the stability of a compound can be calculated unambiguously. Additions of a chemical compound to the database must be made with regard to the thermodynamic parameters of the components already in the database and with regard to the thermodynamic parameters of the components used in the source. It must also be realised that old experimental data are subject to reinterpretation /Baes and Mesmer 1976/. It is possible that two different interpretations of the same data or very similar data appear in the literature. If the two interpretations result in chemical species with different composition, inclusion of both sets of species will of course introduce errors since the two interpretations may be alternative and not complementary.

Consistency is also important in the selection of the method and parameters for the estimation of activity coefficients. A deviation to lower values than predicted from the Debye-Hückel theory may be interpreted as the presence of a complex aqueous species or it may be interpreted as an interaction coefficient. Nuclear Energy Agency Thermochemical Data Base /Grenthe et al. 2000/ contains values for the interaction coefficient between CO_3^{2-} and Na^+ and between Cu^{2+} and Cl^-. SKB TR-00-13 /Puigdomenech and Taxén 2000/ contains equilibrium constants for $NaCO_3^-$ and $CuCl^+$.

Another example where care must be taken to maintain consistency is shown below. The success of a description using specific interaction coefficients may be determined by comparison with experimentally determined mean activity coefficients $\gamma_{\pm}$. Related, but not identical, is the single ion activity coefficient or specific ion activity coefficient γ_i. The difference between the concepts is shown below for a NaCl solution which is assumed to be partly associated.

$$\gamma_{\pm} = \frac{a_{Na+}}{[Na^+]_{tot}} = \frac{a_{Cl+}}{[Cl^+]_{tot}} \qquad 3\text{-}16$$

$$\gamma_{Cl^-} = \frac{a_{Cl+}}{[Cl^+]_{free}} \qquad \gamma_{Na^+} = \frac{a_{Na+}}{[Na^+]_{free}} \qquad 3\text{-}17$$

$$[Cl^-]_{free} = [Cl^-]_{tot} - [NaCl]_{aq}$$
$$[Na^+]_{free} = [Na^+]_{tot} - [NaCl]_{aq} \qquad 3\text{-}18$$

There is some confusion about these two definitions of activity coefficient. It is obvious that for electrolyte solutions where complex formation or ion-pairing is significant, ion specific activity coefficients cannot be determined from mean activity coefficients without considering the equilibrium constants for aqueous complex species. A related issue is the definition of ionic strength *I*. The ionic strength is in principle defined as:

$$I = \frac{1}{2}\sum z_i^2 C_i \qquad 3\text{-}19$$

where the sum is taken over all charged species in the solution. So what is the ionic strength of 1.0 mole NaCl per kg water? From the definition above it would be slightly less than 1.0 m because a fraction of the salt is bound in the neutral complex. Parallel to the definition above, which is sometimes referred to as the 'true' ionic strength /Helgeson et al. 1981/, is the stoichiometric ionic strength. The stoichiometric ionic strength has the value of 1.0 m in a 1.0 m NaCl solution because it assumes full dissociation of the salt.

To minimise confusion, any estimate of ion specific activity coefficients should be accompanied by a list of the values of the equilibrium constants used and an explicit definition of the ionic strength, including the concentration scale used (molar or molal). For reactions where water occurs in the reaction formula, it is useful to know whether the activity of water was considered explicitly or included in the activity coefficients of the other reactants and products.

3.9 Uncertainties

Neither SKB TR-00-13 /Puigdomenech and Taxén 2000/ nor the compilation by Ahonen /2001/ contain systematic estimates of the uncertainties in the thermodynamic parameters. The assignment of uncertainties to thermodynamic parameters calls for a critical review of all the relevant literature /Wanner and Östhols 2000/ and is beyond the scope of the present chapter. Some general remarks can nevertheless be made.

The thermodynamic parameters are generally determined at 25°C and estimates of the values at other temperatures are frequently associated with an extrapolation error. The extrapolation in terms of concentration of the electrolyte introduces further errors. The combination of elevated temperatures and high concentrations seems to give rise to the widest error limits. Grenthe et al. /2000/ predict that, assuming that the relevant interaction coefficients for the SIT-method are known for 25°C, the uncertainty in $\log_{10} \gamma_j$ will be up to 0.13**Im* (*Im* is the ionic strength in moles kg^{-1}) within the temperature

range 0 to 50°C. Worst case estimates of the uncertainties, from this source alone, for the reactions:

$Cu(s) + 2\ Cl^- + H_2O = CuCl_2^- + OH^- + ½\ H_2(aq)$

$Cu(s) + 3\ Cl^- + H_2O = CuCl_3^{2-} + OH^- + ½\ H_2(aq)$

is that at 50°C, the equilibrium concentrations of $CuCl_2^-$ and $CuCl_3^{2-}$ cannot be calculated to better precision than ±4*0.13 = ±0.52 and ±5*0.13 = ±0.65 logarithmic units respectively, at *Im*=1.0.

We do not know the value of the SIT-interaction coefficients for $CuCl_2^-$ and $CuCl_3^{2-}$, with the relevant cations in a groundwater, even at 25°C. SI-theory predicts an activity coefficient of unity for neutral species such as $H_2(aq)$. Other models and sources predict $(d\log \gamma / d\ I) \cong 0.1$ for neutral species /Harned and Owen 1958/. There is also uncertainty in the thermodynamic parameters at infinite dilution at 25°C. A tentative conclusion is that the equilibrium concentration of copper, arising from corrosion of metallic copper, during evolution of dissolved hydrogen, at 1.0 m ionic strength and 50°C, should not be quoted to better precision than ±1 logarithmic unit.

4 Corrosion prior to water saturation

After the fuel has been encapsulated, the copper canisters will be transported without unnecessary delay to the geologic repository and deposited. The expected time between encapsulation and deposition will normally be several weeks. In extreme cases, however, a delay between encapsulation and disposal of up to two years may occur. During that period, the canisters will be exposed to indoor air either at the encapsulation plant or at the repository site and to the atmosphere inside the vessel that will be used for transporting the canister to the repository site. The indoor air is expected to have a temperature of about 20°C. Due to the heat generated by the spent nuclear fuel, the canister itself will have a temperature higher than the surrounding air. The expected maximum surface temperature for a canister with a heat generation of 1.7 kW is somewhat less than 50°C when the canister is exposed to freely circulating air. When inside a radiation shield, the temperature may approach 100°C.

After sealing, the canisters are assumed to be stored in a facility with levels of air pollution comparable to those in an urban atmosphere. The environment at the repository site is rural, with no other additional sources of pollutants than what operating the repository creates. Also here, the levels are assumed to be equivalent to an urban atmosphere or better. In both cases, the canisters will be stored in well-ventilated areas and, in the case of a coastal site, protected from salt spay. The maximum levels per m^3 of pollutants detrimental to copper are estimated to be:

SO_2	100 µg
NO_2	75 µg
NH_3	<20 µg
H_2S	< 3 µg

4.1 Theoretical background

Leygraf /1995/ has recently reviewed the mechanisms and kinetics of atmospheric corrosion; Mattsson /1997/ and King and Kolář /1997a/ have subsequently reviewed the consequences of atmospheric corrosion of copper canisters for spent fuel disposal. The following is a summary of the state-of-the-art as presented by Leygraf, Mattsson and King and Kolář.

The formation of a water film on the metal surface is of fundamental importance to atmospheric corrosion. The thickness of this water film varies from a few monolayers at low relative humidity to thousands of monolayers at 100% relative humidity. When the relative humidity exceeds the “critical relative humidity”, the corrosion rate increases markedly with increasing humidity. This critical relative humidity depends on the surface conditions of the metal but is generally in the range 50–70%. Below this critical level, the corrosion rate is for all practical purposes negligible.

When the thickness of the water film exceeds about three monolayers, its properties become similar to those of bulk water. This occurs approximately at the critical relative humidity. At this film thickens, water-soluble pollutants will dissolve in the moisture film in equilibrium with the gaseous phase. The SO_2 present in the air will dissolve forming HSO_3^- and can be oxidised to sulphate by oxidants in the air. The NO_2 is assumed to be absorbed in the moisture film as HNO_3.

The aqueous phase acts as an electrolyte for electrochemical reactions where the cathodic reaction is the reduction of an oxidant from the atmosphere. The corrosion products that are formed may precipitate and form a protective layer, resulting in a decrease in the corrosion rate with time. For copper, this layer consists mainly of copper oxide with cuprous oxide closest to the metal surface, copper hydroxide and/or copper hydroxides containing other anions.

4.2 Corrosion prior to disposal

The indoor relative humidity in Scandinavia depends on geographic location. Coastal areas have higher relative humidity than inland locations. The relative humidity also has seasonal variations with higher relative humidity during the summer months. The actual indoor humidity will depend on the ventilation of the facility, but will be below the critical humidity at least during the winter months.

The elevated surface temperature (50°C) of the copper canister will ensure a relative humidity considerably lower than the critical humidity close to the canister surface. The corrosion rate can, therefore, be assumed to be very low. Rice et al. /1981/ have reported corrosion rates for copper exposed at ambient temperature in different atmospheres. The exposure times were 1 to 1.5 years. For city atmospheres, they reported corrosion rates of 6 to 27 nm per year. These data are in agreement with corrosion of copper in dry air as described by Miley and Evans /1948/. They found that a layer of predominantly copper oxide was formed on the surface and that this layer inhibited further corrosion when it had reached a thickness of 9–10 nm. These data refer to room temperature. There are, as far as we know, limited data available for the relevant canister temperature (see below). If the conclusion that the corrosion rate decreases to very low values after a layer of corrosion products of a certain thickness has been formed is correct, the corrosion rates at 50°C should not differ much from what is measured at room temperature. Alternatively, if there is a temperature dependence, it is not unreasonable to assume a doubling of the reaction rate for each 10°C. This would mean that the corrosion rate would be approximately 10 times higher at 50°C than at 20°C, i.e., the expected corrosion rates would be 60 to 270 nm per year.

King and Kolář /1997a/ discuss in their review two studies of atmospheric copper corrosion at elevated temperatures /Roy and Sircar 1981; Pinnel et al. 1979/. Roy and Sircar report logarithmic oxidation kinetics in dry air at temperatures between 75°C and 150°C, while Pinnel et al. report parabolic kinetics. Both studies were performed in dry air and, although the rate laws they propose give quite different kinetics for the growth of the oxide layer at 100°C, they predict a total oxide thickness after a few years exposure in the range 30 to 70 nm. Pinnel et al. found that pollutants in the air increased the oxidation rate by a factor of between 3 and 8.

The spent nuclear fuel inside the canisters will generate heat. The expected heat load per canister will be about 1.7 kW. This will result in a canister surface temperature several tens of degrees higher than the air temperature. Storing the copper canisters for extended periods of time before disposal for these conditions will have a negligible effect on their service life after disposal. The total corrosion attack even after two years storage will be less that 1 mm. The most likely corrosion product will be copper oxide.

4.3 Corrosion after disposal

After emplacement in the disposal holes, it will no longer be possible to actively control the composition of the atmosphere to which the canister is exposed. The relative humidity in the repository is expected to be very high. At the Äspö laboratory, the relative humidity is about 80% and the humidity in the repository should be similar.

The heat generated by the waste will lead to a redistribution of the moisture in the bentonite. The bentonite blocks will initially have a water ratio of 17%, corresponding to equilibrium with air with a relative humidity of 75% (85% water saturation for the bentonite blocks with the highest density, see section 2.2). The canister wall is expected to reach a temperature of up to 90°C. The temperature gradient in the bentonite created by the elevated canister temperature redistributes the water and lowers the water ratio closest to the canister to about 10%. This corresponds to a relative humidity of about 50%. Even though this is considerably lower than the ambient repository relative humidity, it is still high enough to be above the critical relative humidity. Corrosion is, therefore, expected to proceed with electrochemical reactions similar to those considered in aqueous solutions (see section 4.1).

Based on literature data for copper exposed outdoors to an atmosphere with similar levels of contaminants as the ones expected in the repository, Mattsson /1997/ estimates the corrosion rate to be 100 to 300 μm per year if the supply of oxygen is unlimited. The dominant surface species will most probably be Cu_2O. The corrosion attack is expected to be evenly distributed over the copper surface since pitting corrosion will not be possible under these conditions.

The maximum possible corrosion attack can be estimated from mass balance considerations. The total volume of buffer and backfill in the deposition tunnel and the disposition hole is 56.5 m^3 per canister. The porosity in the bentonite and the backfill material can be conservatively estimated to be 40%. If all of this porosity consisted of air, the amount of O_2 per canister would be 4.5 m^3, or approximately 200 mol. Assuming that Cu_2O is formed as the corrosion product, 800 mol of copper or 50 kg could be oxidised. This corresponds to a maximum depth of corrosion of 300 μm evenly distributed over the canister surface. In reality the corrosion will be considerably smaller since the transport of oxygen to the canister will be limiting and the residual oxygen will also be consumed through reaction with accessory minerals in the buffer and backfill and through microbial activity. These processes, which have been found to be very rapid, will also consume the oxygen in the groundwater that has been in contact with air during the construction and operation phase of the repository /Puigdomenech et al. 2001/. Wersin et al. /1994b/ have modelled the corrosion of copper taking into account transport by diffusion in addition to flow, equilibrium reactions and kinetic processes at the bentonite-canister interface. The results indicate a conservative corrosion rate of 7 μm/year for oxic conditions. A sensitivity analysis indicates that the main uncertainties arise from the diffusion properties of the clay.

King and Kolář /1997a/ quote results from long-term exposure tests performed in the U.S. The tests were performed for up to 20 years and the mean penetration was found to be given by $d = 2.5 \cdot t^{2/3}$, where t is the exposure time in years. The decrease of the corrosion rate with time indicates the formation of an, at least partially, protective film. The corrosion products consisted of a compact layer of Cu_2O covered by basic Cu(II) salts. King and Kolář also performed bounding calculations of the corrosion during the unsaturated phase in the repository as a result of uniform attack. The assessments relate to a proposed Canadian repository concept with in-room emplacement rather than the

in-floor emplacement that is considered by SKB and Posiva. Predicted corrosion depths ranged from less than 90 nm in the case of oxidation (see section 4.2) to about 90 μm in the case of thin-film corrosion.

Damage of the canister surface caused by handling during emplacement is unlikely to significantly affect the corrosion behaviour. Unlike some passive materials, copper is not susceptible to galvanic corrosion due to embedded iron particles resulting from the use of steel handling equipment. In fact, iron particles would temporarily galvanically protect the canister surface. Scratches and other defects in the surface oxide caused by handling would rapidly oxidize when exposed to the repository environment until the protective oxide layer had been reformed. Neither would handling introduce stress raising defects of sufficient size to cause cracking in the absence of a suitable environment for stress corrosion cracking (see section 7). Plastically deformed material might preferentially dissolve, but this localized dissolution would stop once the deformed material had been corroded.

In summary, the literature surveys that have been performed all suggest that the corrosion attack during the unsaturated phase will most probably be uniform in nature and the extent of corrosion attack will have a negligible effect on the canister lifetime. Some further study of this period may be warranted (section 10).

5 Corrosion during water saturation

The canisters will be deposited in 8 m deep holes surrounded by 0.35 m of highly compacted bentonite with low hydraulic permeability. The tunnels will be backfilled with a mixture of bentonite and crushed rock. The buffer and backfill are not saturated with water during the installation. About 25% of the total amount of water in the buffer must be provided by the host rock. This wetting process, leading to the final water saturated conditions around the waste canisters, the form of its progress, and its duration will influence the form and the extent of the corrosion during this phase in the canister service life.

As was discussed in section 4, the bentonite blocks initially have a water ratio of 17%. The surface temperature of the canister wall may reach 90°C and the temperature gradient this creates in the bentonite redistributes the water and lowers the water ratio close to the canister to about 10%. Water from the rock will eventually saturate the backfill and buffer and create saturated conditions at the canister surface.

The progress of the wetting process is incompletely understood. Börgesson and Hernelind /1999/ have tried to model the wetting of the bentonite. The overall results are rather inconclusive; the influence of the rock properties and the boundary conditions are quite large. Börgesson and Hernelind give, however, a typical example of the water saturation process. In their example, they assume that the water is supplied to the deposition hole at a rate of 0.044 L/h through two fractures and through the rock matrix with a permeability of 10^{-13} m/s. The water pressure reached its full value of 5 MPa a distance of 10 m from the deposition hole. In the model, there was no gap between the bentonite blocks and the canister surface. As a consequence, no definite conclusions can be made concerning how and when the bentonite contacts the canister. The calculations showed a quite uneven increase in the degree of water saturation around the canister during the first 5–8 years. Full water saturation was achieved after about 12 years.

This inhomogeneous increase in water content in the bentonite will also most probably result in an uneven swelling of the buffer. As a consequence of this, the gap may close in some areas while it remains open in others. Sites where the bentonite first contacts the copper canisters are latent sites for corrosion pits. It is to be expected that the electrochemical reduction of oxygen is faster at sites where there is a good supply of oxygen, there is an electrolyte present and where there is a short distance to a site where electrochemical corrosion of copper can take place. Locally increased corrosion rates may therefore be expected at the three phase boundary; copper/moist bentonite/air. However, since the gaps close gradually as the bentonite swells, the location of these sites will not be constant. Once the bentonite has reached full saturation, the whole canister surface will have been exposed to this condition. The fact that some sites have been exposed to conditions that enable electrochemical corrosion longer than others may cause slightly uneven corrosion. Apart from that, the gradual closing of the gaps is not likely to result in any significant localised effects. Because of the locally aggressive conditions, the minimum potential for initiation of localised corrosion may be exceeded and corrosion pits may develop. The presence of these pits may have the effect that the minimum potential for initiation of localised corrosion no longer is exceeded and no new pits can start. The potential for propagation of pitting may still be exceeded and the existing pits may continue to grow. The resulting pit depth is determined by the ratio between

the rate of the general corrosion close to the cathodic sites and the rate of growth of the remote corrosion pits. Averaged over the whole canister surface, the corrosion can still not exceed the 300 μm limit determined by the amount of available oxidant.

Work sponsored by Ontario Power Generation in Canada is addressing the issue of under-deposit corrosion as a result of different rates of access of O_2 to the canister surface /A. Brennenstuhl, private communication, 2001/. Preliminary results suggest that although areas in contact with fully swollen bentonite may corrode faster than areas in contact with partially swollen material, the extent of localization diminishes with time as the oxygen concentration falls. No discrete pitting was observed in any of the tests. Coupled with the gradual swelling of the bentonite over the entire canister surface, the degree of localization of the attack due to this phenomenon is expected to be small. These results are expected to be published in 2001.

The temperature gradient through the bentonite may affect the buffer function by different enrichment processes of dissolved substances. One such process is ion transport parallel to water uptake from the outer cooler parts of the bentonite, or from the surrounding groundwater, to the wetting front in the originally unsaturated bentonite. The transport is assumed to take place by a cyclic evaporation/condensation process in which water is sucked in from cooler parts, evaporates at the wetting front, and is partly redistributed in the form of steam. Dissolved salts will thereby be deposited at the wetting front.

A second possible process is precipitation of species, which have lower solubility at higher temperature, such as calcium sulphate (gypsum) and calcium carbonate (calcite). Both these minerals may be present in the bentonite as impurities.

Karnland /1995/ has shown in laboratory experiments that the enrichment of easily dissolved minerals in a bentonite buffer can be reduced by:

- High buffer density.
- Low content of accessory minerals in the buffer.
- Low electrolyte content in the surrounding water.
- High water pressure.

The use of increased water content in bentonite blocks, supply of low electrolyte water in open slots, and a fast restoration of the hydrostatic pressure are, consequently, considered in a KBS-3 repository in order to reduce mineral redistribution and enrichment.

Very few long-term experiments have been performed under conditions that simulate in a realistic way the early stages of the development of the repository. Recently, however, the results from the pilot phase of a "Long Term Test of Buffer Material" at Äspö Hard Rock Laboratory have been published /Karnland and Sandén 2000; Karnland et al. 2000/. In these experiments, heaters in copper tubes were buried in bentonite clay in deposition holes drilled into the rock. The clay also contained copper coupons for corrosion testing. The analyses of the clay at the copper clay interface showed enrichment in both calcium sulphate and calcium carbonate. The mean corrosion attack on the copper was found to be 3 μm per year. This is in quite good agreement with the modelling results of Wersin et al. /1994b/. The corrosion attack was somewhat uneven, but both optical microscopy and SEM revealed no signs of pitting. Several types of corrosion products were present, among them Cu_2O and $Cu_2CO_3(OH)_2$ (malachite). These corrosion products have obviously been formed under oxidising conditions.

King et al. /1992/ have reported laboratory experiments of copper corrosion in compacted bentonite/sand mixtures using a saline synthetic groundwater (0.97 M Cl^-). Under those conditions, a basic cupric chloride ($CuCl_2 \cdot 3Cu(OH)_2$) was found as discrete crystals on top of an oxide layer that that they reported as possibly Cu_2O. The corrosion rates were in the range 30–50 μm per year. It is reasonable to assume that the copper chlorides/hydroxy chlorides may also form as an initial corrosion product in saline groundwaters during the water saturation phase on compacted pure bentonite.

Aaltonen and Varis /1993/ have performed long-term laboratory corrosion tests of copper in contact with bentonite and groundwater. The tests were carried out in bentonite compacted to a dry density of 1.8–1.9 g/cm^3 placed inside small copper canisters with perforated lids. The canisters were submerged in three different types of water: one with about 60 mg/L sulphate and chloride, one with the sulphate content increased to 6,200 mg/L and one with the chloride content increased to 7,600 mg/L. The bicarbonate contents of all three waters were in the range 570–600 mg/L. The test temperature was 80°C. The test cells were analysed after 3, 6, 9, 12, 24, 36, and 72 months. After only 3 months, the measured E_H was below –300 mV and continued to drop until about 9 months after the start of the experiments. Towards the end of the experiments, the E_H increased but always stayed below –300 mV. The E_H drop at the beginning of the experiments was accompanied by an increase in pH. The corrosion products were identified using ESCA on the samples from 12 months exposure. On the inside of the canisters, they were found to contain cuprous oxide, cupric oxide and copper carbonate. The interpretation was that the copper carbonate was produced in the initially air saturated water and as the E_H dropped and pH increased, cupric and cuprous oxides were formed. The oxide layers were adherent on both sides of the copper canisters. No indication of pitting corrosion could be seen. The conclusion was that the corrosion potential had dropped to levels where pitting corrosion could not be sustained. Another observation was that although initially increased concentrations of copper could be observed close to the copper surface, this disappeared for longer exposure times. An explanation for this could be that dissolution of copper took place initially when there was oxygen present in the system. Once the system had gone anaerobic, the corrosion virtually stopped and a redistribution of the copper occurred in the bentonite. Aaltonen and Varis give no estimates of the corrosion rates.

As was also mentioned in section 4, the residual oxygen in the system will be capable of a total corrosion attack of 300 μm from the time the deposition hole is sealed and the tunnel backfilled. Once the oxygen has been consumed, only anaerobic corrosion will be possible.

6 Corrosion after water saturation

6.1 Introduction

Following saturation of the repository, the environment surrounding the canister will continue to evolve. As a consequence, the corrosion behaviour of the canister will also change with time. Eventually, however, the environment and the corrosion behaviour will attain a steady state. In general, the evolution in conditions will lead to less aggressive forms of corrosion and the corrosion behaviour of the canister will evolve from an initial period of relatively fast general corrosion accompanied by possible localized corrosion, to a long-term steady-state condition of a low rate of general corrosion with no, or little, localized attack.

The evolution of geochemical conditions inside the repository has been discussed in detail in section 2. For the purposes of this section, the following conditions are assumed. The compacted bentonite is assumed to be saturated with groundwater, so that the mass transport of species to and from the canister surface is by diffusion through water-filled pores, so that the more-rapid transport of species such as O_2 through vapour-filled pores need not be considered /King and Kolář 1997a/. In addition, it is assumed that the bentonite adjacent to the canister surface is always saturated, so that the supply of H_2O does not limit the extent of corrosion. As groundwater saturates the buffer, the pore-water Cl^- concentration will gradually increase. Initially, trapped atmospheric O_2 will create oxidizing conditions, but as this O_2 is consumed by (i) corrosion of the canister, (ii) reaction with oxidizable mineral impurities and sulphide in the clay, and (iii) microbial activity, the conditions will become anoxic and remain so indefinitely. The canister surface temperature will be raised by the decay heat from the spent fuel, which will result in a temperature gradient away from the canister. The canister, and repository, will slowly cool over a period of several thousand years (see section 2). Thus, during the period considered here, the environmental conditions will evolve from initially warm and oxic, to eventually cool and anoxic.

At the time that the repository saturates, the canister surface will be covered by corrosion products formed during the saturation phase (section 5). It is assumed here that, upon saturation, the canister surface will be covered by a duplex corrosion product layer comprising an inner layer of Cu_2O and an outer layer of basic Cu(II) salts, most likely either malachite ($Cu_2CO_3(OH)_2$) or atacamite ($CuCl_2 \cdot 3Cu(OH)_2$), depending upon the relative concentrations of CO_3^{2-} and Cl^- in the pore water.

Given this evolution of environmental conditions, the following general statements can be made regarding the expected general and localized corrosion behaviour of the canister. Initially, general corrosion will be supported by the reduction of the atmospheric O_2 trapped in the bentonite. Redox conditions will be relatively oxidizing and the corrosion potential (E_{CORR}) of the canister surface will be relatively positive. Localized corrosion is possible during this period, in the form of either distinct pitting or under-deposit corrosion, leading to a general roughening of the surface. As the initially trapped O_2 is consumed, the rate of corrosion will become limited by the diffusion of O_2 to the canister surface. Eventually, conditions will become anoxic and corrosion will be supported by the reduction of H_2O in the presence of sulphide in the clay and groundwater. The rate

of corrosion is expected to be limited by the rate of supply of sulphide to the canister surface, and to fall to very low levels indefinitely. Even in the absence of sulphide, thermodynamic calculations suggest that there is the possibility of corrosion supported by the reduction of H_2O in the presence of high Cl^- concentrations. Only general corrosion is expected under anoxic conditions.

The evidence for the evolution in the corrosion behaviour described above is detailed in this section. The available experimental and theoretical evidence is discussed from both a kinetic and thermodynamic viewpoint.

6.2 General corrosion

6.2.1 Kinetic studies of the effects of oxygen and chloride

6.2.1.1 Influence of oxygen

Various aspects of the effect of O_2 on the corrosion of Cu will be considered here. Thermodynamically, the presence of O_2 affects the redox potential in the repository, from which the stable dissolved and solid Cu species can be predicted (as a function of pH). Kinetically, a significant number of studies have been conducted on (i) the mechanism of O_2 reduction on Cu, (ii) the effect of O_2 on the corrosion potential (E_{CORR}) and the corrosion rate (or corrosion current density i_{CORR}), (iii) the homogeneous oxidation of Cu(I) to Cu(II), and (iv) the corrosion behaviour of Cu in compacted clay-based materials.

Initially, the redox conditions in the saturated repository are expected to be determined by the presence of trapped atmospheric O_2 in the pores of the buffer material. Theoretically, even trace amounts of O_2 result in oxidizing redox potentials. For example, for a dissolved $[O_2]$ of 8 ppb (i.e., 0.1% of the value for aerated H_2O at room temperature), the redox potential predicted for the couple:

$$O_2 + 2H_2O + 4e^- = 4OH^- \qquad 6\text{-}1$$

is +0.76 V_{SHE} (+0.52 V_{SCE}) at pH 7 at 25°C. Comparison with the E_H-pH diagram for Cu in 1 mol·dm^{-3} Cl^- solution (figure 6-1) shows that the thermodynamically stable dissolved species is $CuCl^+$ and the stable solid species is either CuO or $CuCl_2 \cdot 3Cu(OH)_2$, depending upon the activity of Cl^-. As the trapped O_2 is consumed, redox conditions will become more reducing. At some stage in the evolution of repository conditions, some process other than reaction 6-1 will control the redox conditions. Ultimately, the redox potential could lie close to the H_2/H_2O equilibrium line (–0.41 V_{SHE} (–0.65 V_{SCE}) at pH 7 in the presence of 1 atm H_2), especially in the presence of sulphide. During this evolution in E_H, first Cu_2O and then Cu will become the thermodynamically stable solids and $CuCl_2^-$ (and higher complexes) will become the predominant dissolved species.

From a kinetic viewpoint, E_{CORR} and not E_H determines the corrosion behaviour. The E_H value represents the maximum value of E_{CORR}, but because reaction 6-1 is highly irreversible (and, therefore, not at equilibrium), E_{CORR} is invariably significantly more negative than the E_H in O_2-containing solutions. Figure 6-2 shows the predicted range of E_{CORR} values for Cu in compacted clay for dissolved O_2 concentrations between 8 ppm (aerated water) and 8 ppb and for Cl^- concentrations between 0.001 mol·dm^{-3} and 1 mol·dm^{-3}. This figure was constructed using a steady-state E_{CORR} model for the corrosion of Cu in O_2-containing Cl^- solutions /King et al. 1995a/, under mass-transport conditions similar to those for a Cu canister surrounded by compacted clay (1-cm-thick

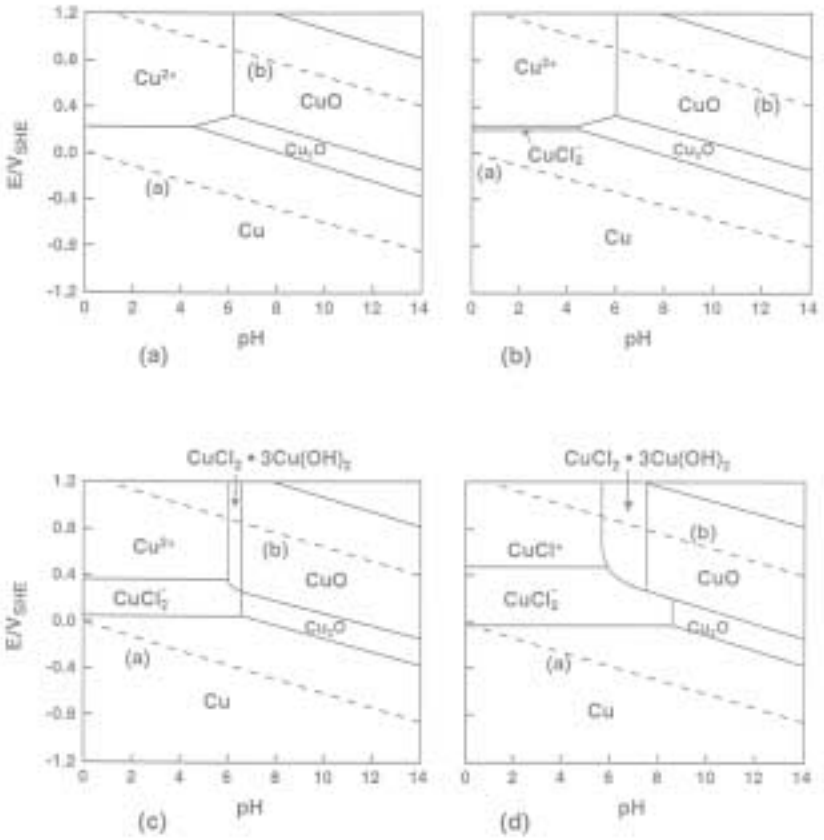

Figure 6-1. *Potential/pH (Pourbaix) diagrams for the system Cu/Cl$^-$/H$_2$O at 25°C for various chloride concentrations. (a) 10^{-3} mol·dm^{-3}, (b) 10^{-2} mol·dm^{-3}, (c) 0.1 mol·dm^{-3}, (d) 1.0 mol·dm^{-3}. Figures constructed for a total dissolved Cu activity of 10^{-6} mol·dm^{-3}.*

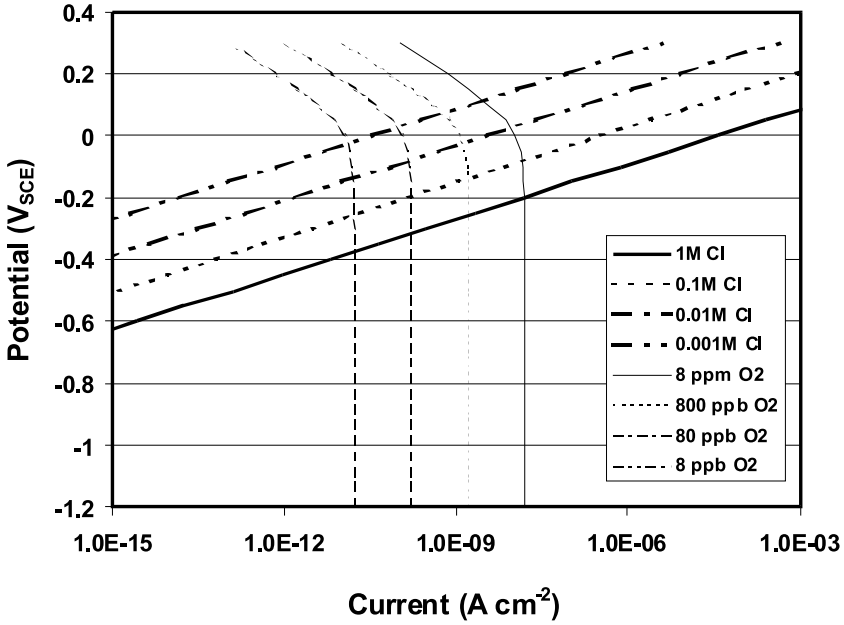

Figure 6-2. *Evans' diagram showing the dependence of the corrosion potential of copper on dissolved oxygen and chloride ion concentrations in the presence of compacted clay. Based on the steady-state model of King et al. /1995a/ with a clay-layer thickness of 1 cm and O_2 and $CuCl_2^-$ diffusion coefficients a factor of 100 smaller than in bulk solution.*

clay layer, O_2 and $CuCl_2^-$ diffusion coefficients a factor of 100 lower than in solution). Thus, in comparison to the E_H value of +0.52 V_{SCE} in solution containing 8 ppb O_2, the predicted E_{CORR} varies between –0.027 V_{SCE} and –0.376 V_{SCE}, depending upon the Cl^- concentration (see section 6.2.1.2).

The mechanism of the reduction of O_2 on Cu has been studied in detail under well-defined mass-transport conditions /King et al. 1995b,c; Vazquez et al. 1994a,b/. The reaction is highly irreversible, and occurs at measurable rates at potentials more negative than approximately –0.3 V_{SCE}. The predominant reaction pathway involves the reduction of O_2 to OH^- ions via four sequential 1-electron transfer steps, according to the overall reaction:

$$O_2 + 2H_2O + 4e^- \rightarrow 4OH^- \qquad 6\text{-}2$$

where the arrow indicates the irreversibility of the reaction and distinguishes reaction 6-2 from the equilibrium reaction 6-1. The reaction is catalyzed by different Cu surface states. King et al. /1995b,c/ suggest catalysis by a Cu(0)/Cu(I) redox couple, whereas Vazquez et al. /1994a,b/ propose a sequence of chemical and electrochemical processes involving Cu_2O and CuO surface species.

In general, however, the two groups of investigators are in agreement on the overall mechanism, for the reduction of O_2 on Cu. In addition to the overall 4-electron reduction process described above, the reaction is characterized by:

1. slower rates of O_2 reduction on oxide-covered surfaces than on film-free Cu,
2. minimal amounts of H_2O_2 produced as a stable intermediate species,
3. transport-limited currents given by the 4-electron reaction 6-2,
4. first-order kinetics with respect to the concentration of O_2,
5. Tafel slopes more negative than –120 mV in neutral and slightly alkaline solutions.

The latter observation is explained by the dependence of the number of surface catalytic sites on the potential. The observed Tafel slope is a consequence of the combined effects of potential on the rate of O_2 reduction and on the number of surface sites /King et al. 1995c/. In neutral solutions, the reduction of O_2 leads to an increase in the interfacial pH due to the formation of OH^- ions. Interfacial pH values as high as pH 10–11 are observed in bulk solution in oxygenated solution. In general, the increase in the interfacial pH depends on the relative rates of O_2 reduction and of the diffusion of OH^- away from the Cu surface. The number of surface sites for O_2 reduction increases with increasing pH /King et al. 1995c/.

The nature of the surface film on the canister surface will affect the rate of O_2 reduction during the saturated phase. The outer layer of the duplex film comprises electrically insulating basic Cu(II) salts. If a continuous layer of these species is formed, the rate of interfacial O_2 reduction will be reduced significantly /Kato et al. 1980a/. Generally, however, the outer layer will be porous and non-continuous, so that O_2 reduction can proceed on the inner Cu_2O layer. The rate of the interfacial reaction will depend on the electronic properties of the defected, semi-conducting Cu_2O layer. Although the rate of the interfacial reaction will be slower than on a "bare" Cu surface, the overall rate of O_2 reduction on the canister surface is likely to be controlled by the rate of supply of O_2, as discussed below, rather than by the rate of the surface reaction. A consequence of the presence of electrically insulating basic Cu(II) salts is the possible spatial separation of anodic and cathodic surface reactions, possibly leading to localized corrosion (see section 6.3.1).

Mechanistic studies of O_2 reduction on Cu are invariably performed in bulk solution involving rapid rates of mass transport to and from the surface. The presence of compacted bentonite will increase the likelihood that the rate of O_2 reduction on the canister surface will be determined by the rate of supply. From figure 6-2, the O_2 reduction reaction is predicted to be limited by the rate of (steady-state) diffusion across the 1-cm clay layer at potentials more negative than approximately 0 to –0.1 V_{SCE}. Thus, in 1 mol·dm^{-3} Cl^-, the O_2 reduction reaction is transport limited at E_{CORR} at all $[O_2]$. In 0.001 mol·dm^{-3} Cl^- solution, the O_2 reduction reaction becomes transport limited under freely corroding conditions only at low $[O_2]$ (<~8 ppb).

Figure 6-2 also shows the effect of O_2 concentration on E_{CORR} and i_{CORR}. As would be expected, both E_{CORR} and i_{CORR} decrease with decreasing $[O_2]$ (figure 6-3). The dependence of E_{CORR} and i_{CORR} on log $[O_2]$ in 1 mol·dm^{-3} Cl^- is consistent with transport control of both the anodic (Cu dissolution) and cathodic (O_2 reduction) reactions. Thus, E_{CORR} decreases by 2.3RT/F V for each factor of ten decrease in $[O_2]$ (i.e., by 59 mV/decade) /Power and Ritchie 1981/ and the rate of corrosion is first order with respect to $[O_2]$ (i.e., $d\log i_{CORR}/d\log[O_2] = 1$). The dependence of i_{CORR} on $[O_2]$ does not necessarily indicate that the rate of corrosion is O_2-transport limited, however, since the rate of the anodic transport step (the diffusion of $CuCl_2^-$ away from the Cu surface) also decreases with $[O_2]$ (due to the decrease of the interfacial $[CuCl_2^-]$ with decreasing E_{CORR}). The extent of transport control of both reactions diminishes with decreasing $[Cl^-]$. In 0.001 mol·dm^{-3} Cl^-, for example, E_{CORR} decreases by only 47 mV per decade decrease in $[O_2]$ (figure 6-3(a)) and $d\log i_{CORR}/d\log[O_2] = 0.80$ (figure 6-3(b)), both indications that the O_2 reduction reaction is partially controlled by the rate of the interfacial reaction (reaction 6-2).

In general, the rate of mass transport to and from the canister has a significant effect on E_{CORR}, i_{CORR}, and the nature of the rate-controlling processes for the anodic, cathodic, and overall corrosion reactions. For the equivalent $[O_2]$ and $[Cl^-]$, the steady-state E_{CORR} value in bulk solution (assumed diffusion layer thickness 0.01 cm) is 77 mV more negative than in the presence of clay and the corrosion rate is a factor of ~500 times higher /King et al. 1995a/. Unlike the situation in compacted clay, the O_2 reduction reaction is not transport limited at E_{CORR} in bulk solution, but is instead under joint kinetic-transport control. Factors that lead to higher rates of mass transport to and from the canister, therefore, will tend to result in more negative E_{CORR} but higher corrosion rates. Such factors could include lower compaction density and a smaller thickness of bentonite. (Although not considered in this section, partial desiccation of the bentonite would have a complex effect on E_{CORR} and i_{CORR}, since the rate of O_2 diffusion to the canister would increase greatly due to vapour-phase diffusion through partially air-filled pores, but the rate of diffusion of $CuCl_2^-$ would be slowed for the same reason).

An effect of O_2 not included in the mixed-potential model of King et al. /1995a/ described above, is the homogeneous oxidation of Cu(I) to Cu(II). As described in the next section, Cu dissolves as Cu(I) at E_{CORR} in Cl^- solutions, yet precipitated Cu(II) salts are invariably observed on the surface of corrosion coupons exposed to compacted bentonite (or bentonite-sand mixtures) /King et al. 1992, 1997a/. Cupric species are formed from the homogeneous irreversible oxidation of Cu(I) by O_2, according to /Sharma and Millero 1988/

$$4Cu(I) + O_2 + 2H_2O \rightarrow 4Cu(II) + 4OH^- \qquad 6\text{-}3$$

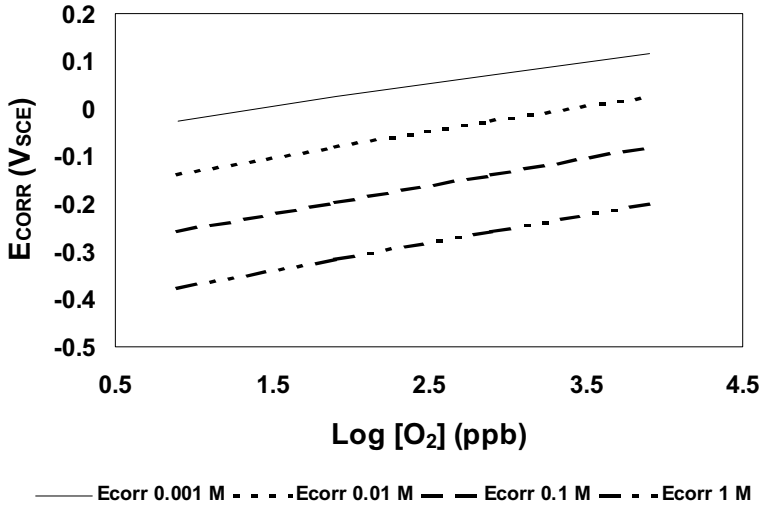

Figure 6-3(a). *Predicted dependence of E_{CORR} on $[O_2]$.*

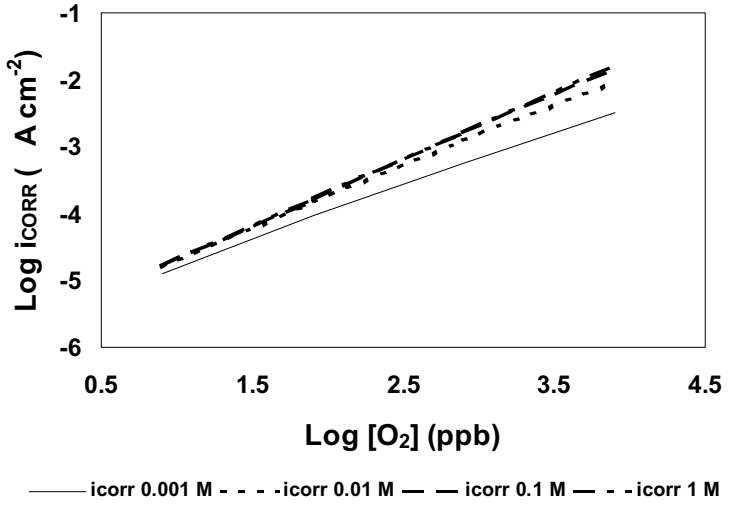

Figure 6-3(b). *Predicted dependence of i_{CORR} on $[O_2]$.*

Figure 6-3. *Predicted dependencies of the corrosion potential (E_{CORR}) and corrosion current density (i_{CORR}) on oxygen concentration based on the data in figure 6-2. Data shown for various $[Cl^-]$.*

The overall rate of Cu(I) oxidation is second order, being first order with respect to both [Cu(I)] and [O_2] /Sharma and Millero 1988/. The rate constant is a function of pH, temperature and solution composition. The precise speciation of the Cu(I) and Cu(II) species will depend on the composition of the pore water. A significant fraction of the Cu(II) formed by reaction 6-3 will adsorb on the bentonite clay buffer. Other Cu(II) species will precipitate on the canister surface, resulting in a thickening of the outer layer of the duplex Cu_2O/basic Cu(II) salt film formed on the canister surface during the unsaturated phase.

Cupric species can also be reduced on the canister surface, according to

$$Cu(II) + 2Cl^- \rightarrow CuCl_2^- + e^- \qquad 6\text{-}4$$

Chloride stabilizes Cu(I) to such a degree that the reaction is irreversible, and the disproportionation of Cu (i.e., 2Cu(I) = Cu(II) + Cu) is not thermodynamically favoured /Peters and Cruser 1965/. Like the O_2 reduction reaction, the interfacial reduction of Cu(II) will proceed on the Cu_2O-covered canister surface, but will not occur on the fraction of the surface covered by the insulating basic Cu(II) salts.

A number of workers have studied the corrosion behaviour of Cu in O_2-containing compacted clay environments. Aaltonen and Varis /1993/ exposed OFHC and a Cu-0.1%Ag alloy to compacted bentonite saturated with synthetic Finnish groundwaters for periods of up to 2 years. Redox conditions within the open cells were first found to become more reducing as O_2 was rapidly consumed by the corrosion reaction, but then became more oxidizing later in the experiment, possibly because of the ingress of atmospheric O_2. The Cu coupons were covered by Cu_2O, CuO and $CuCO_3$ corrosion products (the latter presumably as $CuCO_3 \cdot Cu(OH)_2$), the carbonate salt being favoured over the corresponding basic Cu(II) chloride salt because of the high bicarbonate content of the groundwaters (~600 ppm). Copper concentration profiles were observed in the bentonite at short times, with the Cu diffusing evenly throughout the clay after 2 years. No difference was observed in the corrosion behaviour of the two alloys, although no corrosion rates were given. No evidence for localized corrosion was observed.

More recently, Karnland et al. /2000/ have reported the results of the examination of coupons from long-term corrosion tests in compacted bentonite at the Äspö Hard Rock Laboratory. The estimated mean corrosion rate after 1-year exposure was 3 $\mu m \cdot a^{-1}$. As observed by Aaltonen and Varis /1993/, Cu diffused into the surrounding bentonite. No indications of pitting attack were observed.

An extensive series of corrosion experiments has been performed as a function of $[O_2]$ and $[Cl^-]$ in compacted bentonite-sand buffer material (to simulate conditions in a Canadian repository) /King et al. 1992, 1997a; Litke et al. 1992/. These tests were performed under well-defined 1-D mass-transport conditions, so that the effect of the diffusion of reactants and products to and from the Cu surface could be determined. The rate of consumption of O_2 in the head-space above the experiments was found to decrease with $t^{1/2}$, suggesting that the reduction of O_2 was transport limited. However, the corrosion rate was not proportional to the initial $[O_2]$, suggesting the overall rate of corrosion was not cathodically limited. Instead, under the relatively oxidizing conditions employed in these tests, the corrosion rate was found to be determined by the diffusion of Cu away from the coupon surface.

As discussed in more detail in the next section, the corrosion behaviour was determined by the speciation of dissolved Cu. Adsorption of Cu(II) by the bentonite clay (or precipitation of $CuCl_2 \cdot 3Cu(OH)_2$ on the coupon surface) lowered the interfacial [Cu(II)] concentration, driving further dissolution of the coupon. As a result, corrosion rates were higher under conditions that favoured the formation of Cu(II), such as higher $[O_2]$. In addition, higher total interfacial [Cu] (i.e., the sum of adsorbed, precipitated and pore-water Cu) and steeper Cu concentration gradients were observed when Cu(II) was formed. Figure 6-4 shows the measured total [Cu] profiles in the compacted bentonite following 30-d corrosion experiments at 95°C with a synthetic groundwater containing ~1 $mol \cdot dm^{-3}$ Cl^- for different initial $[O_2]$. High interfacial [Cu] and steep concentration gradients were observed in aerated buffer, whereas much lower interfacial [Cu] and shallower Cu profiles were observed with 0.25 vol.% O_2. At the lower $[O_2]$, a greater fraction of the dissolved Cu was in the form of weakly adsorbed $CuCl_2^-$, resulting in lower total [Cu] and a smaller driving force for dissolution.

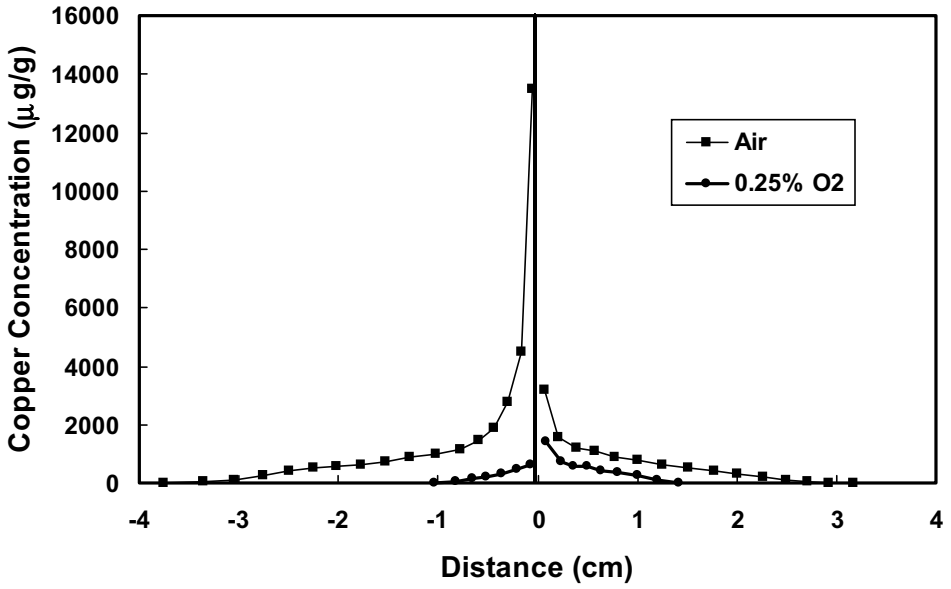

Figure 6-4. *Measured total copper concentration profiles in groundwater-saturated compacted bentonite in contact with a copper coupon following 30 days exposure at 95°C for two initial oxygen concentrations /King et al. 1997a/. The Cu coupon was placed in the centre of the clay (dry density 1.2 Mg·m^{-3}). Groundwater Cl^- concentration ~1 mol·dm^{-3}. The clay contained 0.5 wt.% Fe filings added as an O_2 scavenger.*

The dependence of the corrosion rate on $[O_2]$ was lower than that predicted using the steady-state model of King et al. /1995a/ described above (figure 6-3(b)). On average, the corrosion rate was proportional to $[O_2]^{0.47}$, as opposed to the linear dependence predicted by the steady-state electrochemical model. There are two reasons for the difference between the predicted and observed reaction order. First, it is likely that the rate of O_2 diffusion was higher in the compacted bentonite than assumed in the steady-state prediction both because diffusion would have occurred under transient as opposed to steady-state conditions and, possibly, because the bentonite was not totally saturated. Second, a fraction of the O_2 was consumed by the homogeneous oxidation of Cu(I) (reaction 6-3), a reaction not included in the steady-state model. Oxygen consumption by reaction 6-3 was not significant in the room-temperature tests on which the model was based, since the rate of oxidation is 20 times slower at 25°C compared with the experimental temperature of 95°C used in the corrosion tests.

Copper concentration profiles similar to those found experimentally have been observed in seabed clay sediments surrounding a buried bronze cannon /Hallberg et al. 1988; King 1995/. Figure 6-5 shows a comparison between the clay sediment [Cu] profiles and a profile measured experimentally /King 1995/. In both cases, the interfacial [Cu] is of the order of 10 mg·g^{-1} and the Cu has diffused a maximum distance of ~5 cm. The exposure temperature (7±5°C for thebronze cannon and 100°C for the experimental profile) and exposure period (310 years versus 180 days) were quite different, but the activation energy for the diffusion coefficient derived from the data in figure 6-5 is very similar to that determined experimentally (~50 kJ·mol^{-1} /King 1995/).

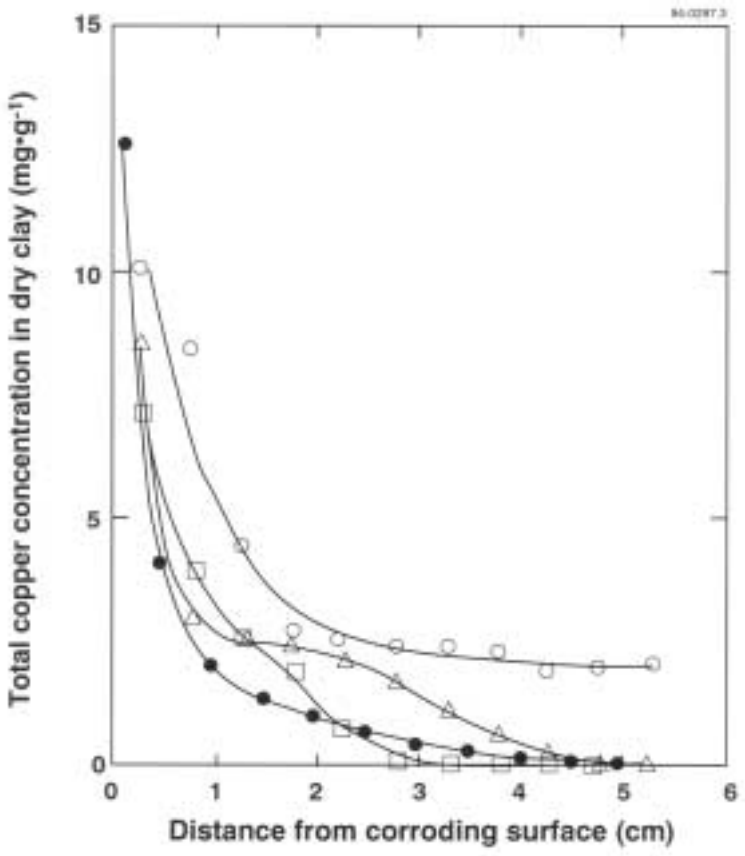

Figure 6-5. *Comparison of copper concentration profiles in sea sediments adjacent to a submerged bronze cannon and a profile observed experimentally in compacted bentonite-sand buffer material in contact with a copper coupon. The sea-sediment profiles (O□Δ) developed over a period of 310 years at a mean ambient temperature of 7±5°C compared with an exposure period of 180 d at 100°C for the buffer material profile (•) (King 1995).*

6.2.1.2 Influence of chloride

A great deal of evidence is available concerning the effect of Cl^- on the corrosion of Cu. The two areas considered in this section are: (i) the electrochemistry of Cu in Cl^- environments, and (ii) the effect of groundwater salinity on the corrosion of Cu in compacted bentonite. The thermodynamic aspects of Cu corrosion in Cl^- solutions are discussed in section 6.2.2.

Figure 6-1 shows the effect of Cl^- concentration on the relative thermodynamic stability of various solid and dissolved species. Chloride ions stabilize dissolved Cu(I) in the form of complex anions, such as $CuCl_2^-$ and $CuCl_3^{2-}$ (see section 3). At sufficiently low pH, Cu corrosion is accompanied by the evolution of H_2 in Cl^- solutions, with the critical pH for H^+/H_2O reduction at E_{CORR} increasing with increasing $[Cl^-]$ and temperature. At the same time, the stability of $CuCl_2 \cdot 3Cu(OH)_2$ with respect to Cu_2O and CuO increases, as indicated by the growth in the size of the stability field of the former at the expense of those of the latter species in figure 6-1.

The electrochemical behaviour of Cu in Cl^- solutions has been extensively studied, in large part because of the widespread use of Cu alloys in sea water and other saline solutions. The mechanism for the interfacial dissolution reaction has been determined from studies under controlled mass transport conditions. The most appropriate description of the various chemical and electrochemical steps in the anodic dissolution of Cu is

$$Cu + Cl^- = CuCl_{ADS} + e^- \qquad 6\text{-}5(a)$$

$$CuCl_{ADS} + Cl^- = CuCl_2^- \text{ (surface)} \qquad 6\text{-}5(b)$$

$$CuCl_2^- \text{ (surface)} \xrightarrow{\text{diffusion}} CuCl_2^- \text{ (bulk)} \qquad \text{rds} \qquad 6\text{-}5(c)$$

The adsorbed $CuCl_{ADS}$ species is formed at a potential more negative than that predicted on the basis of the thermodynamic properties of bulk CuCl. Despite earlier assumptions to the contrary, reaction 6-5(a) is not at equilibrium. The rate-determining step (rds) in the overall dissolution reaction is the mass transport of dissolved $CuCl_2^-$ from the surface to the bulk environment (reaction 6-5(c)). Equations 6-5 describe the mechanism of the dissolution of Cu in Cl^- solutions in the so-called "apparent Tafel region," which extends to potentials of ~0 V_{SCE} depending on the $[Cl^-]$ /Lee and Nobe 1986/. Within the apparent Tafel region, this mechanism is valid over a wide range of Cl^- concentrations, ranging from ~0.01 mol·dm^{-3} /Kiss et al. 1971/ to >5 mol·dm^{-3} /Brossard 1983/. (At $[Cl^-]$ of 1 mol·dm^{-3} and higher, the higher Cl^- complexes, such as $CuCl_3^{2-}$, become predominant and the stoichiometry of reactions 6-5 change accordingly). King et al. /1995a/ used this reaction mechanism to account for the corrosion behaviour of Cu in O_2-containing Cl^- solutions over a wide range of mass-transport conditions, $[Cl^-]$ and $[O_2]$.

The rate of dissolution of Cu in Cl^- solutions is a function of both the rate of mass transport and of potential. The dependence on the rate of mass transport is a simple consequence of the mass-transport step (reaction 6-5(c)) being rate-determining. As shown in figure 6-2, the rate of dissolution also increases with increasing potential, as a result of the increase in the interfacial $[CuCl_2^-]$, which increases the driving force for the mass transport of dissolved Cu away from the corroding surface.

The steady-state model of King et al. /1995a/ can be used to predict the dependence of E_{CORR} and i_{CORR} on $[Cl^-]$ in compacted clay. Figure 6-6 shows the dependencies on $[Cl^-]$ derived from the Evans' diagram in figure 6-2. The dependence of E_{CORR} on $[Cl^-]$ varies from –105 mV/dec in environments containing 8 ppm O_2 to –116 mV/dec in the presence of 8 ppb O_2 (figure 6-6(a)). For complete transport control of both anodic and cathodic reactions, the predicted dependence would be –118 mv/dec at 25°C, i.e., $dE_{CORR}/d\log[Cl^-] = 2(2.3RT/F)$, where the factor of 2 corresponds to the complexation of Cu(I) by two Cl^- ions. (Here, Cl^- concentrations have been used instead of the more-correct Cl^- activities, section 3). The change in $[Cl^-]$ dependence of E_{CORR} with decreasing $[O_2]$ reflects the increasing transport-limitation of the O_2 reduction reaction. The corrosion current density is only weakly dependent on $[Cl^-]$, varying from $[Cl^-]^{0.033}$ for 8 ppb O_2 to $[Cl^-]^{0.23}$ in 8 ppm O_2 (figure 6-6(b)). The relative independence of i_{CORR} on $[Cl^-]$ suggests that the overall corrosion rate is largely mass-transport limited by the supply of O_2 to the Cu surface. Mass-transport limitation by the diffusion of $CuCl_2^-$ **away** from, or of Cl^- **to**, the Cu surface would result in i_{CORR} being proportional to $[Cl^-]^2$. The much smaller predicted dependence of i_{CORR} on $[Cl^-]$ is consistent with rate control largely by the supply of O_2, especially at lower $[O_2]$.

Chloride ions play an important role in the formation and properties of surface films on Cu. Cuprous oxide may form via a number of processes in Cl^--containing environments.

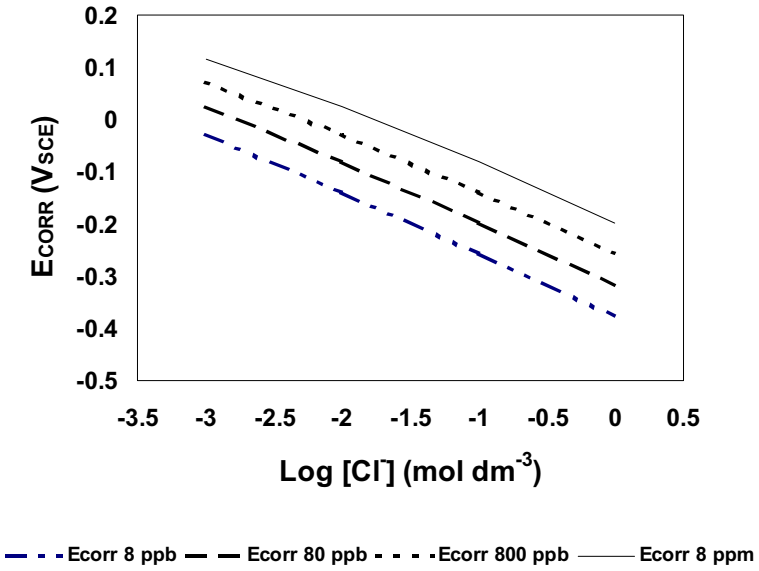

Figure 6-6(a). *Predicted dependence of E_{CORR} on [Cl^-].*

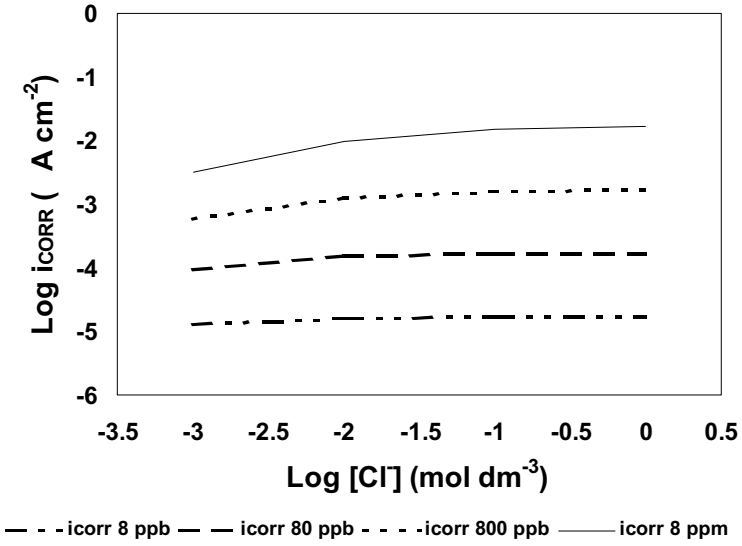

Figure 6-6(b). *Predicted dependence of i_{CORR} on [Cl^-].*

Figure 6-6. *Predicted dependencies of the corrosion potential (E_{CORR}) and corrosion current density (i_{CORR}) on chloride concentration based on the data in figure 6-2. Data shown for various [O_2].*

The initial stages of film formation involve a competition between Cl^- and OH^- for surface sites, followed by the loss of H_2O

$$CuCl_{ADS} + OH^- = Cu(OH)_{ADS} + Cl^- \qquad 6\text{-}6(a)$$

$$2Cu(OH)_{ADS} \rightarrow Cu_2O + H_2O \qquad 6\text{-}6(b)$$

The extent of Cu_2O formation depends on the relative [Cl^-] and [OH^-] (i.e., pH) and the rate of mass transport, with higher [Cl^-] and rates of mass transport favouring the forma-

tion of, and higher pH favouring Cu_2O formation. Although these processes relate only to the formation of the first few monolayers of Cu_2O, they are nevertheless important in determining the properties of the passivating interfacial Cu_2O layer. The incorporation of CuCl "islands" in the surface Cu_2O film creates defects which are believed to be initiation points for pitting (see section 6.3).

Beyond the first several tens of monolayers (i.e., for films of the order of 1–10 nm in thickness), thicker Cu_2O layers probably form by a dissolution/precipitation process. Copper continues to dissolve through the thin surface layer, especially via defects and cracks in the film. Hydrolysis of dissolved $CuCl_2^-$, or of CuCl produced by the precipitation of dissolved Cu(I), results in further Cu_2O growth

$$2CuCl_2^- + H_2O \rightarrow Cu_2O + 2H^+ + 4Cl^- \qquad 6\text{-}7(a)$$

or

$$2CuCl + H_2O \rightarrow Cu_2O + 2H^+ + 2Cl^- \qquad 6\text{-}7(b)$$

In the presence of O_2 in Cl^--containing environments, an outer layer of precipitated $CuCl_2{\cdot}3Cu(OH)_2$ forms on the Cu_2O film. This layer forms by the precipitation of dissolved Cu(II), formed by the homogeneous oxidation of Cu(I) by O_2 (reaction 6-3), once local super-saturation of the environment by Cu(II) is achieved. Evidence for this mechanism comes from the observation of discrete $CuCl_2{\cdot}3Cu(OH)_2$ crystals aligned along linear defects (formed above polishing lines on the Cu surface) on an underlying Cu_2O layer (figure 6-7(a)). It is believed that Cu dissolved as $CuCl_2^-$ through the defected oxide, with local super-saturation by Cu(II) occurring upon oxidation of the Cu(I) species by O_2. Other authors suggest that the $CuCl_2{\cdot}3Cu(OH)_2$ layer forms through the oxidation of the underlying Cu_2O film /Bianchi et al. 1978; Mansfeld et al. 1994/, via the overall reaction

$$2Cu_2O + O_2 + 2Cl^- + 4H_2O \rightarrow CuCl_2{\cdot}3Cu(OH)_2 + 2OH^- \qquad 6\text{-}8$$

Reaction 6-8 infers that the outer $CuCl_2{\cdot}3Cu(OH)_2$ layer grows at the expense of the inner Cu_2O film, although no evidence has been presented to support this mechanism.

Chloride ions will also affect the properties and stability of the precipitated films. The substitution of monovalent Cl^- ions for divalent O^{2-} ions in the Cu_2O lattice creates defects and enhances the semi-conducting properties of the surface film. Thus, Cu_2O films formed in Cl^- solutions may support electrochemical processes, such as the O_2 reduction reaction and the anodic dissolution of Cu, and be less protective, compared with the more-strongly passivating Cu_2O films formed in the absence of Cl^- and/or at higher pH. Depending upon the $[Cl^-]$, however, Cu_2O films formed in Cl^- solutions may be more susceptible to localized breakdown and pitting attack. At sufficiently high $[Cl^-]$, the surface layer may become so defected that it no longer protects the surface and Cu dissolves actively.

In contrast to the complex semi-conducting properties of Cu_2O films, $CuCl_2{\cdot}3Cu(OH)_2$ appears to form an electrically insulating layer. Using electrodes prepared from geological atacamite ($CuCl_2{\cdot}3Cu(OH)_2$) samples, King and Strandlund (unpublished work) were unable to measure an E_{CORR} value, suggesting the surface did not support electrochemical processes. In laboratory studies in compacted clay, the surface $CuCl_2{\cdot}3Cu(OH)_2$ layer is discontinuous, exposing the underlying Cu_2O film to the environment (figure 6-7(b)). Complete coverage by $CuCl_2{\cdot}3Cu(OH)_2$ would passivate the surface /Kato et al. 1980a,b/, although usually the interfacial electrochemical processes proceed on the underlying Cu_2O surface /Kato et al. 1980a,b; Schüssler and Exner 1993/.

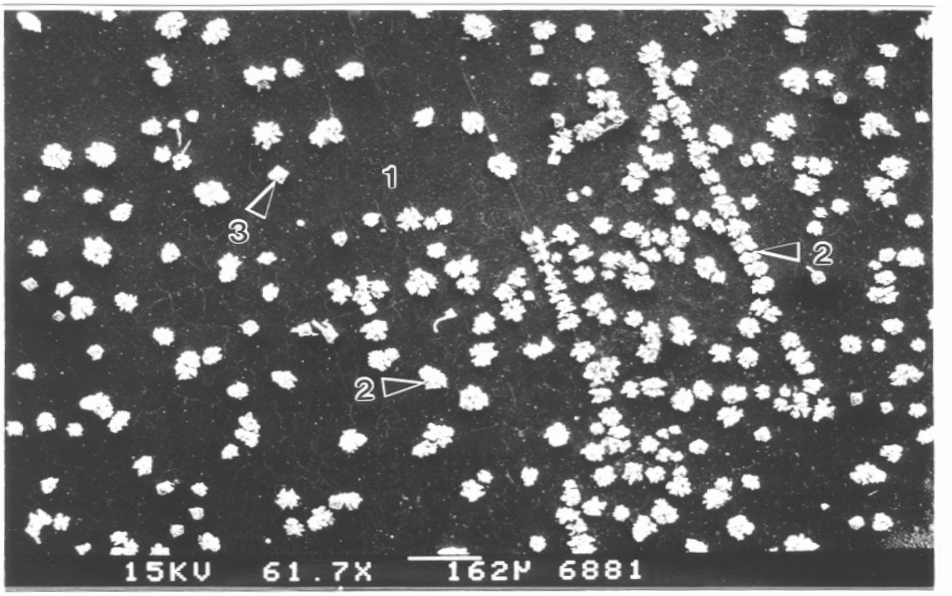

Figure 6-7(a). *Secondary electron image of precipitated $CuCl_2 \cdot 3Cu(OH)_2$ crystals (2) aligned along linear defects in the underlying Cu_2O film (1). Also shown are discrete CuO crystals (3).*

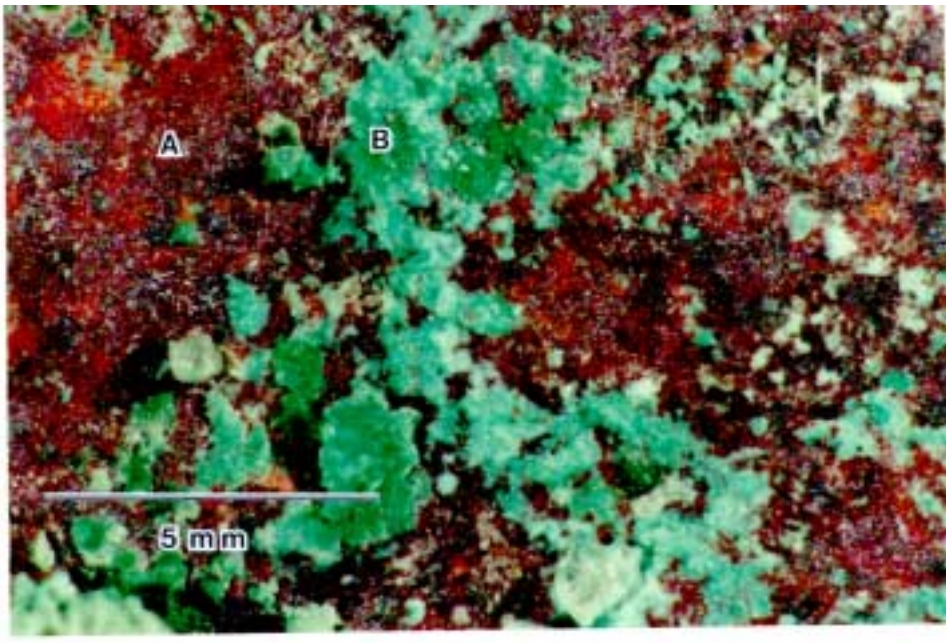

Figure 6-7(b). *Photograph of the duplex corrosion product typical of that formed on copper in groundwater saturated compacted bentonite consisting of an underlying layer of Cu_2O (A) and an upper layer (B) of precipitated basic cupric salts ($CuCl_2 \cdot 3Cu(OH)_2$).*

Figure 6-7. *The development of surface films on copper surfaces exposed to saline groundwater and compacted clay material /Litke et al. 1992/.*

Relatively few studies have been carried out on the dissolution of Cu_2O and $CuCl_2 \cdot 3Cu(OH)_2$ in Cl^- solutions. In unpublished preliminary studies, King and co-workers /King and Légère and King and Strandlund, unpublished work/, found the dissolution of both Cu_2O and $CuCl_2 \cdot 3Cu(OH)_2$ to be dependent on pH, but independent of $[Cl^-]$. The apparent activation energy for the dissolution of Cu_2O was 40 $kJ \cdot mol^{-1}$ at pH 5 /King and Légère, unpublished work/. There is no evidence that $CuCl_2 \cdot 3Cu(OH)_2$ dissolved reductively (i.e., by coupling the reduction of Cu(II) to the oxidation of Cu) as occurs for some Fe oxides, presumably because of the electrically insulating nature of the precipitate. Therefore, both Cu_2O and $CuCl_2 \cdot 3Cu(OH)_2$ are expected to dissolve chemically in Cl^- solutions, although there is a lack of information regarding the mechanisms and rates of the dissolution processes.

Although Cl^- may be the predominant groundwater species, the pore water will contain other anions, especially at short times prior to the influx of Cl^-. A major pore-water constituent will be sulphate ions. All the available evidence indicates that the dissolution behaviour of Cu in Cl^-/SO_4^{2-} mixtures will follow the same mechanism as in Cl^- solutions (i.e., reaction 6-5). Kiss et al. /1971/ studied the dissolution behaviour of Cu in 0.5 $mol \cdot dm^{-3}$ H_2SO_4 containing 0.007–0.09 $mol \cdot dm^{-3}$ Cl^-, but explained all of their observations in terms of the $CuCl_2^-$ species. King and co-workers /King and Tang 1998; King et al. 1995d/ simultaneously determined the fluxes of Cu(I) and Cu(II) produced during the dissolution of a Cu electrode in a 0.1 $mol \cdot dm^{-3}$ Cl^-/0.1 $mol \cdot dm^{-3}$ SO_4^{2-} mixture. Although the addition of SO_4^{2-} shifted the potential at which Cu(II) was produced directly at the surface by ~100 mV in the negative direction, only Cu(I) was detected in the apparent Tafel region, extending to 100–200 mV positive of E. Therefore, there is no evidence that Cu will dissolve directly as Cu(II) in the SO_4^{2-}-enriched pore water in compacted bentonite.

Another abundant anion in the pore water will be HCO_3^-/CO_3^{2-}. Carbonate does not form strong complexes with Cu(I) and Cu(II) and is not directly involved in the dissolution mechanism. The primary role of carbonate will be in the formation of surface films. The basic Cu(II) carbonate salt, $CuCO_3 \cdot Cu(OH)_2$, tends to be more stable than $CuCl_2 \cdot 3Cu(OH)_2$ and forms preferentially in sea water. Both Aaltonen and Varis /1993/ and Karnland et al. /2000/ observed $CuCO_3 \cdot Cu(OH)_2$, rather than $CuCl_2 \cdot 3Cu(OH)_2$, in laboratory and pilot scale corrosion tests under repository conditions. Another effect of carbonate is to render the surface more passive than in HCO_3^-/CO_3^{2-}-free environments. This could increase the probability of localized corrosion, as discussed in section 6-3.

A species that may be present in the repository in small amounts is ammonia, introduced either during vault construction, by microbial activity in the groundwater, or by gas-phase radiolysis of atmospheric N_2. Ammonia is important for the stress corrosion cracking of Cu. Ammonia also forms strong complexes with Cu(I) and Cu(II). Electrochemical studies in Cl^-/NH_3 solutions, however, show that dissolution as $CuCl_2^-$ predominates in 0.1 $mol \cdot dm^{-3}$ Cl^- at pH 7 with total ammonia additions of up to 10^{-2} $mol \cdot dm^{-3}$ /King et al. 1997b/. Thus, despite the fact that the Cu(I)-NH_3 complexes are stronger than the equivalent Cu(I)-Cl^- complexes, the latter dominate because of the low $[NH_3]$ in neutral and slightly alkaline solutions. (The pK_a for the NH_3/NH_4^+ reaction is 9.3 at 25°C, so that NH_4^+ is the predominant form at pH <9.3).

Chloride ions also have an effect on the homogeneous oxidation of Cu(I) to Cu(II) by O_2 because the rate constant for reaction 6-3 is a function of salinity /Sharma and Millero 1988/. In NaCl solution, the second-order rate constant for the oxidation of Cu(I) is ~100 times larger in 0.1 $mol \cdot dm^{-3}$ Cl^- solution compared with 1 $mol \cdot dm^{-3}$ Cl^-. The effect of Cl^- is a result of the stabilizing effect of Cu(I)-Cl^- complex formation.

The effect of groundwater salinity on the corrosion behaviour of Cu in compacted bentonite has been reported by King et al. /1997a/. Copper coupons were sandwiched between plugs of Na-bentonite compacted to a dry density of 1.2 $Mg \cdot m^{-3}$ and saturated with synthetic groundwaters of three different salinities and at two different $[O_2]$. The experiment was designed such that well-defined 1-D mass-transport conditions were maintained throughout. Tests were conducted at a temperature of 95°C for periods between 10 days and 6 months. The three groundwaters used were representative of those possible in a Canadian repository, with $[Cl^-]$ of 0.17 $mol \cdot dm^{-3}$, 0.97 $mol \cdot dm^{-3}$, and 2.5 $mol \cdot dm^{-3}$. A reservoir of groundwater was maintained at the exit side of the compacted clay plugs. These solutions were initially saturated with either air or a nominally 0.2 vol.% O_2/N_2 mixture. At the end of the experiments, the clay plugs were sectioned into slices between 1- and 3-mm thick and the total Cu content in each slice determined. The Cu thus determined comprises Cu dissolved in the pore-water, precipitated Cu and Cu adsorbed on the clay. Following visual examination, the precipitated corrosion products were removed and the corrosion rate was determined from the weight loss of the coupon.

The results of the tests suggested an effect of groundwater salinity and $[O_2]$ on the speciation of corroded Cu and a consequent effect on the corrosion behaviour. The tests were divided into those in which Cu(I) appeared to be the predominant oxidation state and those in which there was evidence for Cu(II) species. This classification was based on the visual appearance of the corrosion products (assisted by the bright green colouration of Cu(II) precipitates) and on the shape of the Cu concentration profiles in the clay. Concentration profiles characteristic of Cu(II) species tend to be short and steep with high interfacial [Cu] /King et al. 1992; Litke et al. 1992/, similar to that for the aerated solution profile in figure 6-4. The steep profiles are a consequence of the strong adsorption of Cu(II) by the bentonite clay /Ryan and King 1994/. Concentration profiles characteristic of Cu(I) species, on the other hand, are shallow and extended with low interfacial [Cu]. These characteristics can be rationalized if the predominant species is $CuCl_2^-$, which is mobile and weakly adsorbed (leading to extended [Cu] profiles and low interfacial concentrations).

For the various conditions studied, Cu(II) tended to predominate the lower the groundwater salinity and the higher the $[O_2]$. Thus, for the lowest groundwater salinity ($[Cl^-]$ = 0.17 $mol \cdot dm^{-3}$), the [Cu] profiles and corrosion products exhibited evidence for Cu(II) species for both $[O_2]$. In the highest salinity groundwater ($[Cl^-]$ = 2.5 $mol \cdot dm^{-3}$), on the other hand, there was no evidence for Cu(II) species in either aerated or 0.2 vol.% O_2/N_2 environments. At the intermediate salinity ($[Cl^-]$ = 0.97 $mol \cdot dm^{-3}$), Cu(II) predominated in aerated environments, but concentration profiles and corrosion products characteristic of Cu(I) predominated in 0.2 vol.% O_2/N_2.

The relative amounts of Cu(I) and Cu(II) in the various tests can be rationalized based on the stability of Cu(I) in the different environments. The first-order rate constant for the oxidation of Cu(I) (obtained from the product of the second-order rate constant given by Sharma and Millero /1988/ and the respective dissolved $[O_2]$) varies by ~5 orders of magnitude over the range of experimental conditions studied. Thus, the rate of oxidation of Cu(I) in the aerated 0.17 $mol \cdot dm^{-3}$ Cl^- groundwater is ~80,000 times faster than in the high salinity groundwater saturated with 0.2 vol.% O_2/N_2. The respective Cu(I) half-lives are 0.15 s and 12,000 s, respectively. As a general guide, tests in which the calculated Cu(I) half life was <100 s were characterized by Cu(II) corrosion products and [Cu] profiles, whereas those with half-lives >100 s suggested the predominance of Cu(I) species. The calculated Cu(I) half-lives were estimated based on studies in bulk solution, and the actual half-lives in compacted buffer could be substantially longer

because of the effect of the spatial restrictions of the pore network on the collision frequency of O_2 and Cu(I).

Of more interest than the effect of salinity on the Cu concentration profiles and corrosion products is the effect on the corrosion rate. Figure 6-8 shows the results of the three sets of conditions for which tests were performed in all three groundwaters. The results suggest that the corrosion rate **decreases** with increasing salinity. This conclusion can be rationalized on the basis of a Cu-transport rate-determining step /King et al. 1992/. If the interfacial dissolution processes are fast with respect to the rate of mass transport **and** are reversible, any process that removes dissolved Cu from the corroding interface will result in a higher corrosion rate. In the case of Cu(I), the only processes removing dissolved Cu from the interface are the relatively slow diffusion through the compacted clay and the precipitation of Cu_2O. For Cu(II), however, dissolved Cu is removed from the interface by adsorption on the bentonite clay, in addition to diffusion and precipitation processes. The bentonite has a large capacity to adsorb Cu(II), with the slices of clay nearest the corroding coupon containing as much as 12 $mg \cdot g^{-1}$ Cu, equivalent to adsorption of Cu(II) on 50% of the total exchange sites on the clay. It is interesting to note that the experimental corrosion rates in figure 6-8, especially at the lower $[O_2]$, are similar to those observed by Karnland et al. /2000/ in the long-term pilot scale corrosion tests at Aspo (~3 $\mu m \cdot a^{-1}$).

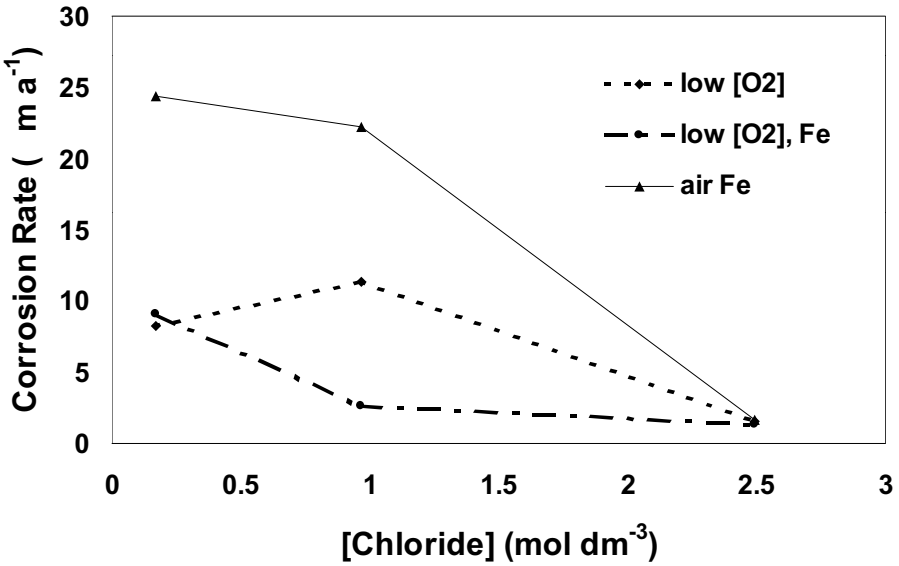

Figure 6-8. *Dependence of the corrosion rate of copper in compacted clay on the salinity of the groundwater. Tests conducted at 95°C for 90 days in groundwater-saturated bentonite clay (dry density 1.2 $Mg \cdot m^{-3}$). The groundwaters were either initially aerated or equilibrated with a 0.2 vol.% O_2/N_2 (low $[O_2]$). In some tests, 0.5 wt.% Fe powder was added to the dry clay prior to compaction.*

Figure 6-9 shows the proposed mechanism for the corrosion of Cu in compacted bentonite saturated with saline, O_2-containing groundwaters. Copper dissolves reversibly in the form of $CuCl_2^-$ species. If this species is stable, i.e., at high $[Cl^-]$ and/or low $[O_2]$, $CuCl_2^-$ slowly diffuses away from the Cu surface as the rate-controlling process. In low-salinity groundwaters and/or at high $[O_2]$, Cu(I) is irreversibly oxidized to Cu(II). Cupric species are removed from solution by adsorption and (to a greater extent than Cu(I)) by precipitation. These processes drive further dissolution by slowing down the rate of reduction of Cu(II) to Cu(I). Otherwise, the subsequent increase in the interfacial $[CuCl_2^-]$ would inhibit further Cu dissolution because the dissolution of Cu as Cu(I) is reversible. Thus, reactions involving Cu(II) are effectively reversible by virtue of the two coupled **irreversible** reactions, Cu(I) oxidation to Cu(II) by O_2 and Cu(II) reduction to Cu(I) on the Cu surface. Both of these reactions must participate in the mechanism, because otherwise the reactions involving Cu(II) would not be reversible and removing dissolved Cu(II) from the interfacial region would not affect the corrosion rate.

The experimental evidence is not consistent with an O_2 mass-transport limited corrosion reaction. Although O_2 was consumed during the course of the tests proportional to $t^{1/2}$ (consistent with a diffusion-limited O_2 reduction reaction), the dependence of corrosion rate on $[Cl^-]$ is too large to be explained by the effect of salinity on O_2 solubility /King et al. 1992, 1997a; Litke et al. 1992/. Thus, there is no evidence for O_2-transport control of the corrosion of Cu in compacted clay, at least not at the clay density and over the range of $[O_2]$ used in the tests. Theoretically, at some stage in the evolution of repository conditions, the corrosion rate should become limited by the rate of O_2 supply to the canister surface. Based on the results of the experiments discussed here, however, O_2-transport control can only be expected at dissolved $[O_2] < \sim 2 \times 10^{-6}$ mol·dm^{-3}, the concentration in 1 mol·dm^{-3} Cl^- solutions saturated with 0.2 vol.% O_2/N_2 at room temperature.

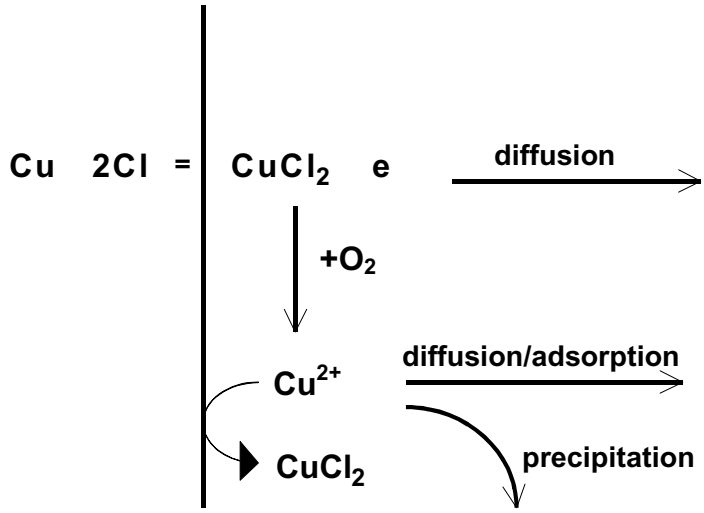

Figure 6-9. *Proposed mechanism for the corrosion of copper in compacted buffer material saturated with saline, O_2-containing groundwater.*

Contrary to the observed experimental data, the steady-state corrosion model of /King et al. 1995a/ predicts that the corrosion rate marginally increases with [Cl^-] in aerated solution and is impendent of salinity at lower [O_2]. As discussed in the previous section, the oxidation of Cu(I) to Cu(II) does not appear to have been a significant process in the experiments on which the steady-state model was based. The most likely reason for the difference in observed behaviour at room temperature in NaCl solutions and at 95°C in synthetic groundwater solutions is the effect of temperature on the rate of Cu(I) oxidation by O_2.

6.2.2 Influence of chloride in the absence of oxygen

According to thermodynamic considerations a combination of high chloride content, low pH (pH <5–6), high temperature (80–100°C) and oxygen-free conditions could be unfavorable for the general corrosion of Cu /Beverskog and Puigdomenech 1998; Ahonen 1999; Puigdomenech and Taxén 2000/. In the reports by Ahonen /1999/ and Puigdomenech and Taxén /2000/ it was, however, stated that the presence of other electron acceptors than protons is needed for corrosion to occur. Also large uncertainties in the models for the thermodynamic calculations for high ionic strengths and high temperatures was notified and the lack of mass transport estimates of oxidants and corrosion products. Experimental data of copper corrosion in highly saline high temperature waters in totally oxygen-free conditions are not available.

The corrosion of copper to aqueous species with water or protons as the only electron acceptor can be written /SKB 1983; Swedish Corrosion Institute 1978/ as

$$Cu(s) + n\ Cl^- + m\ H_2O = CuCl_n(OH)_m^{1-n-m} + (m-1)\ H^+ + \tfrac{1}{2}\ H_2(aq) \qquad 6\text{-}9$$

Other electron acceptors and mass-transport limitations are discussed in section 6.2.4.1. Appendices I and II in section 3 give thermodynamic data from which the concentrations of dissolved species $CuCl_n(OH)_m^{1-n-m}$ can be estimated for various combinations of *n* and *m*. The two sets of data were developed by different authors and differ in the method used to estimate the activity coefficients.

Reaction 6-9 and the two sets of thermodynamic data can be used to predict the concentration of dissolved Cu species in equilibrium with metallic Cu as a function of pH, [Cl^-], and temperature. Calculations were performed for a temperature of 100°C, and for [Cl^-] up to 2 mol/kg at pH 4–11. The activity of water was set to unity although the available data suggest that the correct value at 100°C in 2 mol/kg NaCl is close to 0.93 /Lobo 1989/. The ionic strength was set equal to the free chloride concentration without conversion from mol/kg water to mol/L. The values of the parameters in the model for calculation of the activity coefficients were selected to be reasonable and to allow a sensitivity analysis. The values of the activity coefficients are therefore not necessarily exactly those preferred by the original author (see appendices I and II, section 3).

Figure 6-10 shows the isoconcentration curves for the total dissolved copper in a pH-[Cl^-]-diagram. The two sets of thermodynamic data used, combined with the different methods for estimation of activity coefficients, give quite similar results. The results only differ markedly for a total concentration of dissolved copper of lower than 10^{-6} mol/kg. Based on these thermodynamic calculations the equilibrium concentration of Cu, at 100°C for Cl <1.5 mol/kg and pH >6, is $<10^{-6}$ mol/kg. For higher Cl-contents and lower pH:s copper could corrode to the extent that Cu_{tot} exceeds 10^{-6} mol/kg.

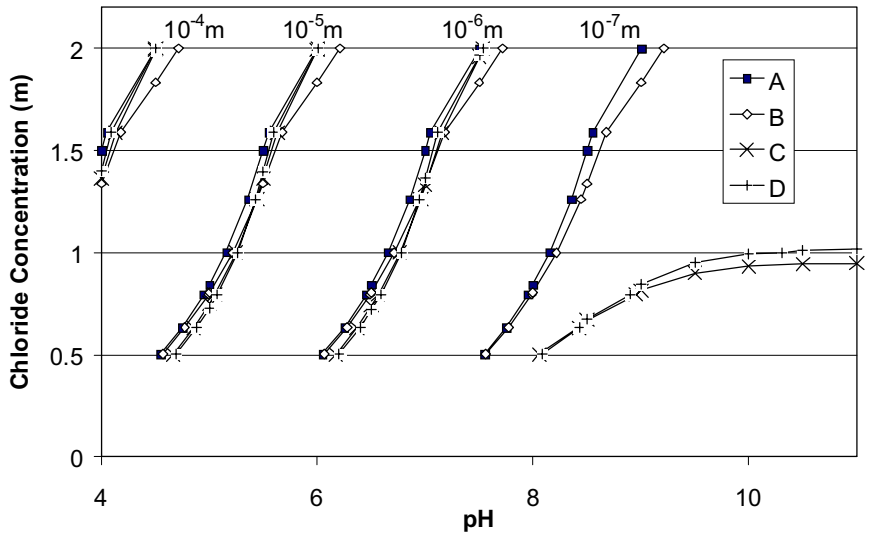

Figure 6-10. *Isoconcentration curves for the total concentration of dissolved copper in equilibrium with metallic copper and stoichiometric concentrations of dissolved hydrogen gas at 100°C. Thermodynamic data for $H_2(aq)$ from NBS 82 (HSC Chemistry ver. 3.0) was used in all cases. [NaCl]aq was calculated using log k=-0.45 ($\gamma_{NaCl(aq)}$=1) for all cases.*
A: Data from appendix I, section 3, activity coefficients from Davies equation using b=0.2.
B: Data from appendix II, section 3, activity coefficients from the modified Helgeson equation.
*C: Data from appendix I, activity coefficients from Davies equation using b=0.1, lg $\gamma(H_2(aq))=0.094$*Im.
*D: Data from appendix II, activity coefficients from Davies equation using b=0.3, $\gamma(H_2(aq))=0.094$*Im.

A copper canister in a repository will be subjected to elevated pressures. Tables 6-1 and 6-2 give the partial molal volumes for the individual reactants in reaction 6-9 and for the overall reaction for various combinations of *n* and *m*, respectively. For a change in pressure from 0.1 MPa to 5 MPa (equivalent to the hydrostatic head at a depth of 500 m), the equilibrium constant for reaction 6-9 increases by only ~10%, with the change in the equilibrium dissolved Cu concentration being <10%. Therefore, the change in pressure in the repository will have little effect on the predicted dissolved Cu concentration.

Table 6-1. Partial molal volumes of the reactants and products.

Reactant /product	Partial molal volumes cm³/mol
Cu(s)	7.1
H+	0
Cu+	−10.5
Cl−	17.9
$CuCl_n(OH)_m^{1-n-m}$	>0
H2(aq)	~0
H2O	18

Table 6-2. Partial molal volumes of reaction.

ΔVr max cm^3/mol n (Cl^-)	m (OH^-) 0	1	2
0	−17.6	−35.6	−53.6
1	−25.0	−43.0	
2	−42.9		
3	−60.8		

6.2.3 Influence of sulphide

The behaviour of Cu in sulphide-containing environments is important because of the potential for the corrosion of Cu to be supported by the reduction of H_2O. Cuprous sulphide (Cu_2S) is thermodynamically stable at potentials below the H_2/H_2O equilibrium line /Pourbaix and Pourbaix 1992/. Because of this thermodynamic stability and because of the presence of sulphide minerals in many types of bentonite and in deep Fenno-Scandian Shield groundwaters (section 2), Cu canisters may be subject to corrosion in the presence of sulphide under the long-term reducing conditions expected to develop in the repository.

Various workers have studied the electrochemical and corrosion behaviour of Cu alloys in sulphide environments. The majority of these studies are associated with corrosion of Cu alloys in polluted seawater. Care should be taken in applying the results of these studies to the corrosion of Cu canisters, however, because most of them involved Cu-Ni alloys (commonly used in marine heat exchangers) and because the particularly aggressive forms of corrosion observed in these applications are associated with **alternating** oxidizing and reducing conditions.

Several electrochemical studies of the early stages of film formation on Cu in sulphide environments have been published. As commonly observed in other environments, Cu forms a duplex bilayer corrosion product film in sulphide solutions, comprising an inner layer of Cu_2S (variously reported to be between 0.4 nm /de Chialvo and Arvia 1985/ and 25–50 nm thick /Vasquez Moll et al. 1985/ and a thicker outer layer of CuS. Non-stoichiometric sulphides ($Cu_{2-x}S$, with x = 0.08, 0.23, 0.40 and 0.69) may form during the conversion of Cu_2S to CuS. The rate of growth of the CuS layer is believed to be controlled by the rate of transport of sulphide to the surface, which would be a particularly slow process in the compacted bentonite to be used in a repository.

A number of corrosion studies have also examined the role of sulphide on the behaviour of Cu and Cu alloys. Macdonald et al. /1979/ also observed a duplex sulphide film on Cu-Ni alloys in deaerated sea water, but suggested the formation of an inner Cu-Ni sulphide and an outer Cu_2S layer. The Cu_2S layer was found to have a lower electrical resistance than the corresponding Cu_2O film formed in the absence of sulphide. Syrett /1981/ reported a duplex film comprising an inner layer of Cu_2O, whose growth was hindered at grain boundaries in the underlying Cu-Ni alloy. The presence of sulphide resulted in the formation of an outer Cu_2S and $Cu_{2-x}S$ film due to the precipitation of Cu(I) diffusing through defects in the underlying Cu_2O layer. The reduction of H_2O was thought to occur at the Cu_2O/Cu_2S interface, with the accompanying local increase in pH resulting in growth of the Cu_2O layer. This duplex Cu_2O/Cu_2S layer might be expected to form in a repository once the initially trapped atmospheric O_2 has been consumed and the environmental conditions become more reducing.

A number of studies have been performed under freely corroding conditions, with various explanations for the processes determining E_{CORR}. Based on the close correlation between the E_{CORR} of Cu electrodes in deaerated sulphide solutions and the equilibrium potential for the precipitated Cu sulphide covering the electrode, de Chialvo and Arvia /1985/ suggested that E_{CORR} was determined by the redox potential between the Cu sulphide and dissolved sulphide in solution. Thus, for Cu_2S-covered surfaces, E_{CORR} was determined by the redox potential for the reaction

$$2Cu + S^{2-} = Cu_2S + 2e^- \qquad 6\text{-}10$$

namely, $E_{CORR} = -1.13 - 0.030 \log[S^{2-}]\ V_{SCE}$. For CuS-covered electrodes, E_{CORR} was determined by the redox potential for the reaction

$$Cu + S^{2-} = CuS + 2e^- \qquad 6\text{-}11$$

namely, $E_{CORR} = -0.94 - 0.030 \log[S^{2-}]\ V_{SCE}$. Implicit in reaction 6-11 is the assumption that CuS is a Cu(II) sulphide, but there is strong spectroscopic evidence /Perry and Taylor 1986/ that CuS is a Cu(I) solid, with sulphide present in the form of a polysulphide.

Macdonald et al. /1979/ reported some data showing an E_{CORR} dependence on $[HS^-]$ of –29 mV/dec, supporting the mechanism of de Chialvo and Arvia /1985/. However, they showed other E_{CORR} data exhibiting different dependences on $[HS^-]$, and themselves suggested that E_{CORR} was a mixed-potential determined by the relative rates of the anodic reaction and the cathodic reduction of H_2O. Mor and Beccaria /1975/ also observed a dependence of E_{CORR} on sulphide of ca. –30 mV/dec in artificial sea water for short exposures, but the dependence increased to –40 to –60 mV/dec upon ageing of the surface. This latter dependence is more consistent with a mixed-potential between the anodic reaction and the cathodic reduction of H_2O or HS^- than the redox control suggested by de Chialvo and Arvia /1985/. Escobar et al. /1999/ also observed a –60 mV/dec dependence of E_{CORR} on $[HS^-]$ at temperatures of 15°C, 25°C and 90°C. Alhajji and Reda /1994/ suggested HS^-, rather than H_2O, was the oxidant, with a two-stage cathodic reaction involving

$$HS^- + e^- \rightarrow H_{ads} + S^{2-} \qquad 6\text{-}12(a)$$

followed by

$$S^{2-} + H_2O \rightarrow HS^- + OH^- \qquad 6\text{-}12(b)$$

although the overall reaction is stoichiometrically identical to the reduction of H_2O

$$H_2O + e^- \rightarrow H_{ads} + OH^- \qquad 6\text{-}13$$

A simulation of the evolution of redox conditions in a Swedish/Finnish repository was performed by King and Stroes-Gascoyne /1995/, although the experiment was actually performed to determine the effect of sulphate-reducing bacteria on the corrosion of a Cu canister in a Canadian repository. Copper electrodes were exposed to a 1 $mol \cdot dm^{-3}$ NaCl solution under well-controlled mass-transport conditions, either by rotating the electrode in bulk solution or by placing a 0.1-cm-thick layer of compacted bentonite (clay dry density 1.2 $Mg \cdot m^{-3}$) between the electrode and the bulk solution. The E_{CORR} of the electrode was measured as the purge gas was changed or as sulphide ions were added to the bulk electrolyte. The solution was initially aerated, but the purge gas was sequentially changed to 2 vol.% O_2/N_2, 0.2 vol.% O_2/N_2, and 100% Ar (nominally deaerated). In two experiments, sufficient Na_2S was added to the solution to give a bulk $[HS^-]$ of either 10 $\mu g \cdot g^{-1}$ or 100 $\mu g \cdot g^{-1}$.

Figure 6-11 shows the time dependence of E_{CORR} for three experiments, one in bulk solution and two with the compacted clay electrode. The E_{CORR} of the rotating electrode in bulk solution responded quickly to changes in the purge gas, decreasing with decreasing $[O_2]$ (curve (a)). Under these rapid mass-transport conditions, the anodic reaction is mass-transport controlled and the cathodic reaction is limited by the rate of the interfacial reduction of O_2 at E_{CORR} /King et al. 1995a/. Upon the addition of 10 $\mu g \cdot g^{-1}$ HS^-, E_{CORR} drops immediately by ~500 mV to a value of ca. –0.90 V_{SCE}. Increasing the $[HS^-]$ to 100 $\mu g \cdot g^{-1}$ resulted in a further 60 mV drop in E_{CORR}. The precipitous drop in E_{CORR} upon the first addition of HS^- was explained in terms of a switch in the anodic reaction from dissolution as $CuCl_2^-$ to the formation of a Cu_2S or CuS surface film, and a switch in the cathodic reaction from the reduction of residual O_2 to the reduction of H_2O (or HS^-). The –60 mV/dec decrease in E_{CORR} with $[HS^-]$ suggests E_{CORR} is determined by the relative rates of Cu dissolution and H_2O reduction, rather than by either of the redox couples in reactions 6-10 and 6-11 (which would give a –30 mV/dec dependence).

In the presence of compacted clay, a similar decrease in E_{CORR} is observed upon the addition of HS^-, but more slowly as a consequence of the restricted mass-transport conditions. The E_{CORR} of the compacted clay electrode also decreases as the $[O_2]$ is decreased (curves (b) and (c), figure 6-11). The magnitude of the decrease suggests complete transport control of the anodic and cathodic reactions (see figure 6-2). Upon the addition of 10 $\mu g \cdot g^{-1}$ HS^- (point D, curve (c)), E_{CORR} decreases by 10–20 mV but then stabilizes for the next 75 hrs. The addition of 100 $\mu g \cdot g^{-1}$ HS^- (point E, curve (c)) causes a further decrease in E_{CORR} by 50–60 mV followed by a second plateau of ~40 hrs. These small decreases in E_{CORR} were thought to be due to the consumption of residual

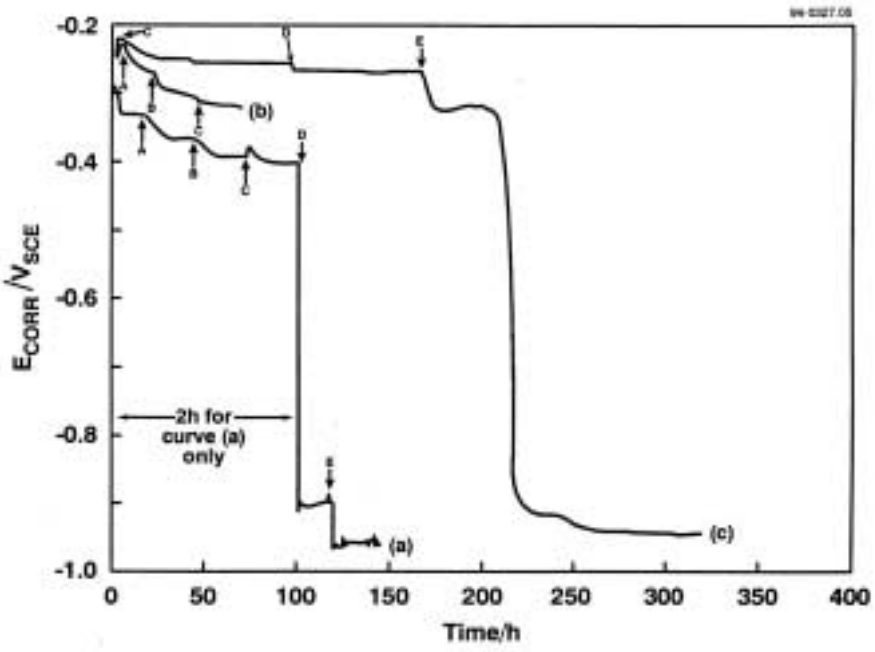

Figure 6-11. *Variation of the corrosion potential of a copper/compacted clay electrode and of a copper rotating disc electrode in 1 mol·dm^{-3} NaCl solution as a function of oxygen and sulphide concentration /King and Stroes-Gascoyne 1995/. (a) Rotating disc electrode in bulk solution (the time axis for the first 2 h of this experiment has been expanded by a factor of 50 for clarity); (b) copper/compacted clay electrode in O_2-containing solution only; (c) copper/compacted clay electrode with various $[O_2]$ and sulphide additions. The arrows represent the times at which either the overpurge atmosphere was changed or sulphide additions were made according to: (A) 2 vol.% O_2/N_2; (B) 0.2 vol.% O_2/N_2; (C) Ar; (D) 10 $\mu g \cdot g^{-1}$ sulphide; (E) 100 $\mu g \cdot g^{-1}$ sulphide.*

O_2 in the clay layer by reaction with HS^-. After the second plateau period, however, E_{CORR} drops precipitously by ~0.6 V_{SCE} to a final steady-state value virtually identical to that observed in bulk solution at that [HS^-].

Figure 6-12 shows a semi-schematic Evans' diagram for the compacted clay experiments in figure 6-11. In O_2-containing environments, both anodic and cathodic reactions are transport limited at E_{CORR}. Upon the addition of HS^-, the cathodic and anodic reactions change and E_{CORR} shifts to a more negative value as a result. Unlike the changes in [O_2], which cause an immediate change in E_{CORR}, the addition of HS^- to the system only has an effect on E_{CORR} after a delay period. In the case of the transport-limited reduction of O_2, a change in the bulk [O_2] has an immediate effect on the flux of O_2 to the electrode surface, and a consequent immediate effect on E_{CORR}. In the case of HS^-, however, the sulphide must first diffuse to the Cu surface before it can affect a change in E_{CORR}. Thus, sulphide only has an effect because of the formation of Cu_2S or CuS corrosion products, which are stable at sufficiently negative redox potentials that corrosion can be supported by hydrogen evolution. Although not conclusive proof, this evidence suggests that the rate of Cu corrosion is controlled by the rate of supply of HS^-. The delay period of 40 hrs between adding 100 $\mu g \cdot g^{-1}$ HS^- and the precipitous drop in E_{CORR} can be used to estimate the effective diffusion coefficient of HS^-. Based on a simple $\sqrt{Dt}$ calculation

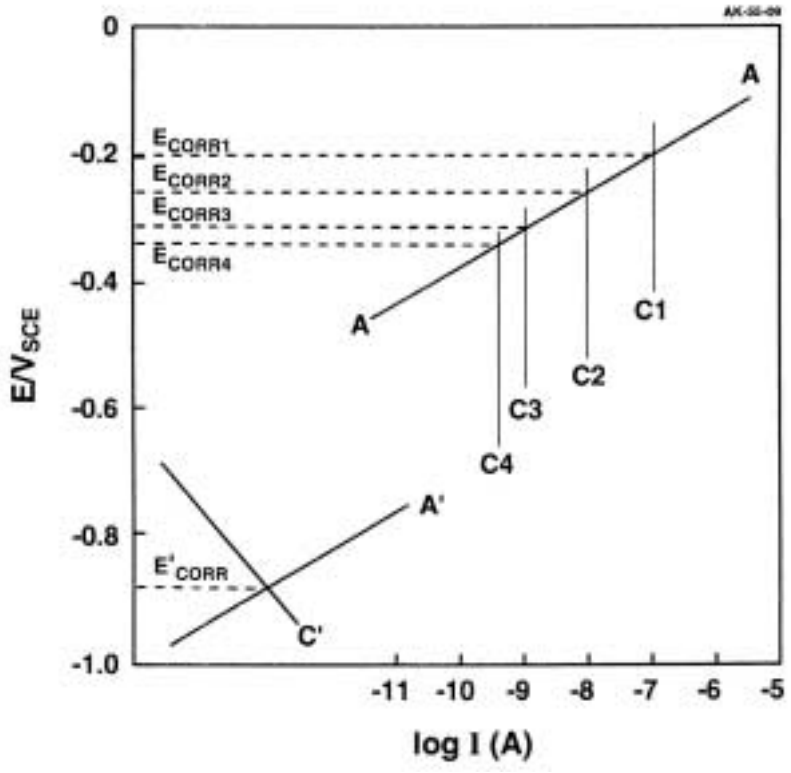

Figure 6-12. *Evans diagram illustrating the variation of E_{CORR} for a clay-covered copper electrode in O_2-containing 1.0 mol·dm^{-3} NaCl and in HS^--containing solution. Line A and lines C1 to C4 are the anodic and cathodic I/E curves predicted from experimental data for an anodic reaction limited by $CuCl_2^-$ diffusion through the clay layer (line A) and for the transport-limited reduction of O_2 for aerated solution (line C1), and for solutions purged with 2 vol.% O_2/N_2 (line C2), 0.2 vol.% O_2/N_2 (line C3) and in nominally deaerated solution (line C4). The various E_{CORR} values marked on the potential axis are the respective corrosion potentials. Lines A' and C' represent the I/E curves for unspecified anodic and cathodic reactions in HS^--containing solution, assumed to have Tafel slopes of 60 mV and –120 mV, respectively. Clay-layer thickness 0.1 cm, electrode surface area 1.0 cm^2.*

for the 0.1-cm clay layer, the estimated diffusion coefficient is of the order of 7×10^{-8} $cm^{-2} \cdot s^{-1}$, a reasonable value for anionic diffusion in compacted clay.

The variation of E_{CORR} for the clay-covered electrode in figure 6-11 may be similar to that expected for a canister in a Swedish/Finnish repository, albeit on a much shorter timescale. Initially, E_{CORR} will be determined by the relative kinetics of the anodic dissolution of Cu as and of the reduction of O_2. As the trapped O_2 is consumed, E_{CORR} will decrease. At some stage during the evolution of the repository environment, the nature of the reactions on the Cu surface will change. In the presence of sulphide, the anodic and cathodic reactions will change to the formation of Cu sulphide films and the evolution of hydrogen. A relatively rapid decrease in E_{CORR} by several hundred mV can be expected, with an ultimate E_{CORR} value in the range of -0.80 V_{SCE} to -1.0 V_{SCE}, depending upon the concentration of HS^- at the canister surface.

As briefly mentioned above, the most serious corrosion in sulphide-polluted sea water arises from alternating aerated and deaerated environments /King 1996a/. These alternating conditions may have one of two effects. First, exposure to sulphide environments after initial exposure to an aerated environment (or vice versa) can result in alteration of the corrosion products and spalling of otherwise protective surface films due to volume changes associated with the growth of the altered layer. Thus, truly protective surface films are not stabilized under alternating oxidizing and reducing conditions. Second, Cu sulphide films are more catalytic towards the reduction of O_2 than Cu_2O films, due to their more-defected structure. Thus, following the growth of a Cu sulphide film under reducing conditions, the introduction of dissolved O_2 would cause a rapid increase in corrosion rate. In either case, such effects should not occur in a repository, since the environment is expected to evolve from initially aerated to reducing in the long term, and to remain so indefinitely.

6.2.4 Modelling of general corrosion

Just as there are both thermodynamic and kinetic approaches to describing the effects of O_2, Cl^- and HS^- on the corrosion of Cu, there are various approaches to predicting the long-term general corrosion behaviour of the canisters in a repository. Canister lifetime predictions based on a thermodynamic description of the corrosion process(es) generally involve an assumption of rapid interfacial kinetics and rate control by the rate of (diffusive) mass transport. Kinetically based lifetime-prediction models combine the finite kinetics of interfacial reactions with possible limitation by mass transport to and from the corroding surface. Thermodynamic models represent a "worst-case" assessment because of the assumption of infinite interfacial kinetics, and produce a conservative estimate of the corrosion rate. Both thermodynamic and kinetic models have been used to predict the lifetimes of Cu canisters in deep geologic repositories.

6.2.4.1 Thermodynamic and mass-transport limited approach

Werme et al. /1992/ describe a mass-transport limited model for predicting the extent of corrosion of copper canisters in a Swedish repository due to sulphide. In a previous assessment /SKB 1983/, it had been conservatively assumed that all of the sulphide in the bentonite surrounding the canister, plus that formed by microbial activity in the deposition hole, was consumed in the first 1,000 years. Thereafter, sulphide was assumed to diffuse to the canister from the tunnel and from the groundwater. The sources of sulphide in the tunnel were (i) the sulphide impurities in the bentonite and sulphide produced by microbial activity. In the groundwater, the maximum sulphide concentration was assumed to be 1 mg/L, corresponding to that present naturally in the groundwater

Table 6-3. Predicted time dependence of the depth of corrosion (in mm) due to sulphide from various sources /SKB 1983, modified from Werme et al. 1992/.

Source of sulphide	Exposure time (yr)			
	10^3	10^4	10^5	10^6
Deposition hole:				
1. from bentonite	0.032	0.032	0.032	0.032
2. from microbial activity in bentonite	0.023	0.023	0.023	0.023
Tunnel:				
1. from bentonite	3.6×10^{-5}	3.2×10^{-4}	0.0032	0.032
2. from microbial activity in tunnel	9.0×10^{-6}	5.5×10^{-5}	5.5×10^{-4}	0.0055
Groundwater:				
1. present naturally in groundwater	9.1×10^{-5}	8.6×10^{-4}	0.0086	0.086
2. from microbial activity in groundwater	9.1×10^{-5}	8.6×10^{-4}	0.0086	0.086

plus that produced by microbial activity. Table 6-3 gives the predicted depth of corrosion as a function of time due to sulphide from these various sources /SKB 1983/.

Werme et al. /1992/ re-considered the conservative assumption that all of the sulphide in the deposition hole was consumed within 1,000 years. Using a 1-dimensional sulphide consumption model assuming instantaneous consumption of sulphide on the canister surface, they estimated that the sulphide in the deposition hole would be consumed in 850,000 years. The amount of sulphide estimated to be present in the deposition hole (both as an impurity in the bentonite and produced from microbial activity) was higher than that assumed in SKB /1983/, and gave a maximum depth of corrosion after 850,000 years of just over 1 mm. Until the sulphide in the deposition hole is consumed, there can be no diffusion of sulphide from the tunnel or from the groundwater, since the bentonite pore-water [HS^-] exceeds that in the tunnel or groundwater.

In appendix III in this report a new model for the general corrosion of Cu in the presence of Cl under oxygen-free conditions is presented. The following reaction is considered:

$$Cu(s) + H^+ + n\ Cl^- \leftrightarrow \tfrac{1}{2}\ H_2(aq) + CuCl_n^{(1-n)} \qquad 6\text{-}14$$

and the mass-transport-limited rate of corrosion of copper in anoxic groundwater with high [Cl^-] is estimated. If the interfacial reaction kinetics are fast, the rate of corrosion is limited by the diffusion of both $CuCl_n^{(1-n)}$ and H_2 away from the canister surface. In the absence of other effects, the corrosion rate would be expected to decrease with time as the respective concentration gradients at the canister surface decrease as the two species diffuse through the bentonite.

Any process that maintains a high concentration gradient at the canister surface, however, will maintain a high corrosion rate. Two such processes are the precipitation of $CuCl_n^{(1-n)}$ by solid sulphides and the oxidation of H_2 by reaction with Fe(III):

$$2CuCl_n^{(1-n)} + MeS(s) \rightarrow Cu_2S(s) + Me(II) + 2nCl^- \qquad 6\text{-}15$$

and

$$\tfrac{1}{2}H_2(aq) + Fe(III)(bentonite) \rightarrow H^+ + Fe(II)(bentonite) \qquad 6\text{-}16$$

respectively, where Me(II) is a divalent metal ion. Bentonite (MX-80) may contain up to 0.1 wt.% sulphide, mostly as pyrite (FeS_2). The total Fe content is ~4 wt.%, predominantly as substituted Fe(III) in the montmorillonite lattice and as Fe_3O_4 particles.

A mass-transport-reaction model with cylindrical geometry was developed to calculate the diffusive flux of $CuCl_n^{(1-n)}$ and H_2 away from the canister and, hence, the corrosion rate. The interfacial fluxes of $CuCl_n^{(1-n)}$ and H_2 (J_{Cu} and J_{H2}, respectively) were coupled according to reaction 6-14, such that

$$J_{Cu} = 2J_{H2} \qquad \text{[mol/cm, s]} \qquad 6\text{-}17$$

The fluxes are expressed in moles per secund and unit length of the cylinder. The respective concentrations of dissolved Cu and H_2 (C_{Cu} and C_{H2}, respectively) at the copper surface, are also linked through electrochemical equilibria (k)

$$C_{Cu} \cdot \sqrt{C_{H2}} = k \qquad 6\text{-}18$$

where $k = 1.2 \cdot 10^{-11}$ in 1.0 mol/kg Cl^- at pH7 and 50°C. This value is obtained using thermodynamic data for $CuCl_2^-$, Cu(s), Cl^-, H^+ from SKB TR-00-13 /Puigdomenech and Taxén 2000/, also in appendix I in this report, and thermodynamic data for H_2(aq) from NBS 82 (HSC Chemistry ver 3.0). The transition from activities to concentrations was made using Davies' approximation for the charged species. The activity of the dissolved molecular hydrogen was assumed to be equal to its concentration (γ=1). Copper metal was assumed to be present at unit activity. Reactions between $CuCl_n^{(1-n)}$ and MeS (FeS_2) and between H_2 and Fe(III) were assumed to be instantaneous. The coupled mass-transport-reaction equations were solved using Runge-Kutta techniques.

The bentonite in the deposition hole was simulated by a series of 70 nested cylinders. The canister surface temperature was assumed to be a constant 50°C, with the bentonite at a temperature of 25°C. Only the dichloro Cu(I) complex $CuCl_2^-$ was considered. An initial [Cl^-] of 0.1 mol/kg was assumed in the bentonite, with a constant [Cl^-] of 1.0 mol/kg maintained at the simulated bentonite/rock interface. Diffusion coefficients in bentonite were assumed to be 10^{-11} m^2/s for all dissolved species except for H_2(aq), $4.5 \cdot 10^{-11}$ m^2/s.

Figure 6-13 shows the predicted corrosion rate and depth of corrosion as a function of time for 1.0 mg reactive sulphide and 3 mg reactive Fe(III) per kilogram bentonite. The corrosion rate increases with time initially as the Cl^- diffuses to the canister surface from the rock (a process that takes of the order of 300–400 years). After this time, the corrosion rate is predicted to decrease with time as the concentration gradients of the dissolved $CuCl_2^-$ and H_2 become less steep. The sulphide and Fe(III) content of the bentonite nearest the canister are reduced by reaction with $CuCl_2^-$ and H_2, respectively, although only a relatively small fraction of the total inventory is consumed within the first 6,000 years shown in figure 6-13. The total depth of corrosion is negligible, amounting to only ~0.06 μm after 6,000 years in bentonite at pH 7 with 1.0 m NaCl.

Higher sulphide and/or Fe(III) concentrations would lead to higher predicted corrosion rates, since reaction between these species and $CuCl_2^-$ and H_2, respectively, would maintain the initially high gradients at the canister surface, for a longer time. However, even with a 3,000-fold increase in Fe(III) content and a 100–1,000-fold increase in sulphide content, the maximum depth of corrosion due to reaction 6-14 is predicted to be <6 μm after 50,000 years in bentonite at pH 7 with 1.0 m NaCl. In contrast, the direct sulphidation of the surface by

$$2Cu + HS^- + H^+ = Cu_2S + H_2 \qquad 6\text{-}19$$

results in ~5 times more corrosion after the same period of time /Werme et al. 1992/.

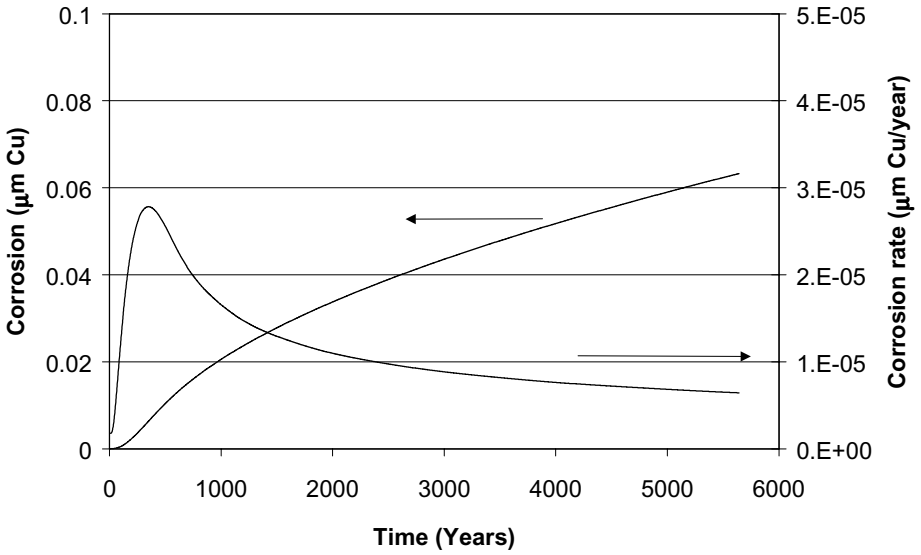

Figure 6-13. *Corrosion and corrosion rate as function of time. pH 7.0 50°C, 1.0 mg reactive sulphide and 3 mg reactive Fe(III) per kilogram bentonite.*

The sensitivity of the depth of corrosion, according to reaction 6-14, to changes in pH and chloride concentration is discussed in appendix III.

6.2.4.2 Kinetic approach

In contrast to the thermodynamically based models used in the Swedish and Finnish programmes, the assessment of the rate of general corrosion in the Canadian programme has been based on both thermodynamic (mass-transport limited) and kinetic models. Three different models have been proposed, each having their particular strengths and weaknesses. The three models are: (i) the Cu(II) mass-transport limited model for oxidizing conditions /King and LeNeveu 1992; King et al. 1994/, (ii) the steady-state kinetic model of King et al. /1995a/, described above, and (iii) the transient kinetic Copper Corrosion Model (CCM) /King and Kolář 1995, 1996a, 2000/.

The **Cu(II) mass-transport limited model** was developed based on the results of corrosion experiments in compacted buffer material under oxidizing conditions /King et al. 1992/. Under these conditions, the diffusion of Cu(II) away from the Cu surface limited the rate of corrosion, which is given by

$$\text{Rate} = \frac{2A_{Cu}\rho_d m_0}{\rho_{Cu}(\pi t)^{1/2}}\left(\frac{\varepsilon_e \tau_f D_0}{r}\right)^{1/2} \qquad 6\text{-}20$$

where A_{Cu} and ρ_{Cu} are the atomic mass and density of Cu, ρ_d is the dry density of the buffer material, m_0 is the total concentration of Cu in the buffer immediately adjacent to the canister surface, t is the time, ε_e and τ_f are the effective porosity for mass transport and the tortuosity factor of the buffer, D_0 is the bulk-solution diffusion coefficient of Cu(II), and r is the buffer capacity factor for Cu(II), which is related to the extent of adsorption on the clay. Good agreement was found between corrosion rates predicted from equation 6-20 and the observed corrosion rate of Cu in compacted buffer material

for various temperatures (50–150°C), buffer dry densities (1.45–1.79 $Mg \cdot m^{-3}$), and exposure times (1 month – 2 years) /King et al. 1992)/

Equation 6-20 was used as the basis for a model to predict the lifetime of Cu canisters in a Canadian repository /King and LeNeveu 1992; King et al. 1994/. Implicit in the use of this expression is the assumption that the mechanism does not change over time, i.e., the corrosion rate does not become limited by the supply of O_2 to the canister surface. This is clearly a conservative assumption for a sealed repository and, together with the assumption of infinitely fast interfacial kinetics, this model results in an extremely conservative assessment of the canister lifetimes. Nevertheless, the minimum predicted lifetime for a 25-mm-thick Cu canister (only 16 mm of which was used as the corrosion allowance) in a Canadian repository was of the order of 30,000 yrs. Predictions based on a more-realistic interfacial Cu concentration produced lifetimes of ~10^6 yrs, **even for the conservative assumption of an infinite supply of O_2**. The model was also used to predict the corrosion rate for the bronze cannon natural analogue /King 1995/, Cu concentrations profiles for which are shown in figure 6-5. The predicted rate was within a factor of six of the rate estimated for the cannon.

The Cu(II) transport model has a number of advantages and disadvantages. The advantages of the model include: (i) its computational simplicity and the ease with which it can be incorporated into performance assessment models for the entire repository, which generally include a detailed description of the mass-transport conditions, (ii) the limited number of required input parameters, (iii) the experimental basis for the rate equation, and (iv) the conservatism inherent in the model. The disadvantages of the model are: (i) the over-conservatism in the model because of the failure to take into account the limitation by the amount of available O_2, and (ii) the limited amount of output data, comprising only the corrosion rate as a function of time and the total depth of corrosion. To avoid overly conservative lifetime predictions, this model should only be applied to permanently aerobic systems, or to the early stages in the evolution of a sealed repository.

The **steady-state kinetic model** was developed to interpret the results of short-term laboratory electrochemical experiments /King et al. 1995a,b,c/. Data from separate electrochemical studies on the anodic dissolution of Cu in Cl^- solutions /King et al. 1995a/ and on the reduction of O_2 on Cu /King et al. 1995b,c/ were combined with steady-state mass-transport expressions to produce a mixed-potential model capable of predicting E_{CORR} and i_{CORR} for a wide range of mass transport and environmental conditions. Good agreement between predicted and measured E_{CORR} values was demonstrated for $[O_2]$ between $<10^{-6}$ $mol \cdot dm^{-3}$ and 2×10^{-4} $mol \cdot dm^{-3}$ and for steady-state mass-transfer coefficients between 10^{-7} $cm \cdot s^{-1}$ and 10^{-2} $cm \cdot s^{-1}$. Of particular relevance for the corrosion of Cu canisters was the application of the model to predict the steady-state E_{CORR} of a Cu electrode separated from a bulk Cl^- solution (simulating saline groundwater) by a 1-cm-thick layer of compacted bentonite clay. In 0.1 $mol \cdot dm^{-3}$ NaCl solution, variously purged with air, 2% O_2/N_2, 0.2% O_2/N_2, and nominally deaerated, the maximum deviation between the predicted and measured steady-state E_{CORR} was only 17 mV.

The steady-state model has never been used to predict canister lifetimes, but has instead been used to interpret the results of experimental studies, some of which were described above. As such, the model has certain limitations, the most major being the exclusion of processes involving Cu(II). For example, the steady-state model predicts little dependence of the corrosion rate on $[Cl^-]$ (figure 6-6(b)), whereas the rate is actually observed to decrease with increasing salinity in tests at elevated temperature (figure 6-8). The experimental observations have been explained in terms of the effect of Cl^- and O_2 on the Cu(I)/Cu(II) speciation, an effect not included in the steady-state model.

Notwithstanding these limitations, the steady-state model is a useful tool for a number of applications. In addition to the interpretation of the results from short-term laboratory studies at room temperature, the model may also be applicable to the later stages in the evolution of the repository environment, during which processes involving Cu(II) will be less important than they are in the early, oxidizing period. As such, the steady-state model complements the Cu(II) transport-limited model described above. A distinct advantage of the steady-state model over the previous model, however, is its ability to predict the E_{CORR}, in addition to i_{CORR}. As will be shown later, comparison of the (predicted) E_{CORR} to critical potentials for localized corrosion is a powerful method for predicting the long-term localized corrosion behaviour of the canister.

The most advanced general corrosion model developed in the Canadian programme, and consequently the one that has proven most useful, is the **transient kinetic Cu corrosion model** (CCM) /King and Kolář 1995, 1996a, 2000/. The CCM is based on the experimentally determined reaction scheme for the corrosion of Cu in compacted buffer with O_2-containing saline groundwater shown in figure 6-14. This reaction scheme was derived on the basis of (i) corrosion studies in compacted bentonite /King et al. 1992, 1997a; Litke et al. 1992/, (ii) electrochemical studies of the anodic dissolution of Cu in Cl^- and Cl^-/SO_4^{2-} solutions /King and Tang 1998; King et al. 1995a,d/ and the reduction of O_2 on Cu /King et al. 1995b,c/, (iii) the homogeneous oxidation of Cu(I) by O_2 in Cl^- solutions /Sharma and Millero 1988/, (iv) the consumption of O_2 by reaction with Fe(II) /Wehrli 1990/, and (v) the adsorption of Cu(II) on bentonite and the diffusion of dissolved Cu through compacted buffer /King 1995; Ryan and King 1994/. Thus, there is a very substantial experimental database underlying the model.

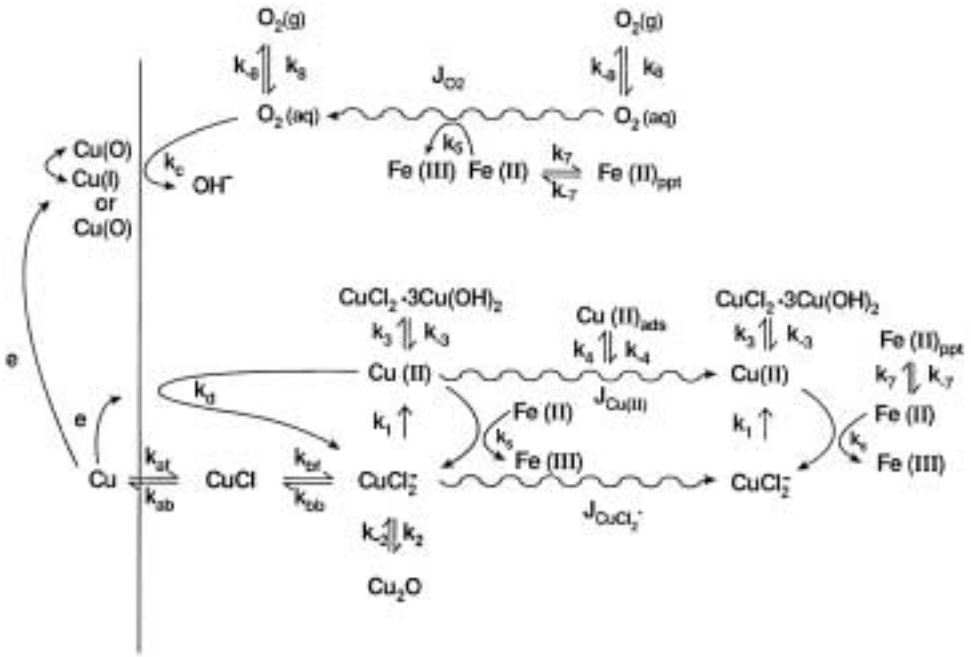

Figure 6-14. *Mechanism for the general corrosion of copper in compacted buffer material with O_2-containing saline groundwater /King 1996b/.*

The mathematical model itself is based on a 1-D description of the various mass-transport barriers in the repository and a series of mass-balance equations, one for each of the chemical species in the model. A total of 10 species are considered in the current version of the model: dissolved O_2, gaseous O_2, Cl^-, $CuCl_2^-$, dissolved Cu(II), Cu(II) adsorbed on clay surfaces, Cu_2O, $CuCl_2 \cdot 3Cu(OH)_2$, dissolved Fe(II) and precipitated Fe(II). The mass-balance equations are of the form

$$\varepsilon_a \frac{\partial c}{\partial t} = \frac{\partial}{\partial x}\left(\varepsilon_e \tau D_0 \frac{\partial c}{\partial x} \right) + \varepsilon_a \sum_i R_i + \sum_i R_i \text{'} \qquad 6\text{-}21$$

where c is the pore-water concentration, ε_a is the accessible porosity, and the ΣR_i and ΣR_i' terms represent the sums of the rates of formation and loss of the species in question. These latter terms account for the various adsorption/desorption, precipitation/dissolution and redox reactions illustrated in figure 6-14. Certain species are assumed not to diffuse (i.e., Cu_2O, $CuCl_2 \cdot 3Cu(OH)_2$, adsorbed Cu(II) and Fe(II)(ppt)), so that the respective mass-balance equations contain no diffusive flux term. The spatial and temporal variation of temperature is also included in the model, for which an analogous 1-dimensional heat-conduction equation is written.

The reactions shown in figure 6-14 are assumed to occur in a spatial grid, bounded on the left-hand boundary by the canister surface and on the right-hand boundary by, generally, a major water-bearing fracture. In between the two boundaries the spatial grid is divided into layers that, for a Canadian repository, describe the layers of compacted buffer and backfill materials, a layer of excavation-disturbed rock and a layer of "intact" rock that act as mass-transport barriers.

The series of ten mass-balance equations (and the heat-conduction equation) are solved subject to various initial and boundary conditions. Of these, the most important from a corrosion viewpoint are the boundary conditions at the canister surface for the species involved in the corrosion reactions, i.e., O_2, Cl^-, $CuCl_2^-$, and dissolved Cu(II). For these species, the electrochemical kinetic expressions describing the rates of reactions 6-2, 6-5 (for both Cl^- and $CuCl_2^-$), and 6-4 are used as flux boundary conditions. These reactions constitute an electrochemical mixed-potential model, enabling the time dependence of the E_{CORR} and i_{CORR} of the canister to be calculated. In this way, the interfacial electrochemical reactions are coupled to the mass-transport, adsorption/desorption, precipitation/dissolution, chemical and redox processes occurring in the repository. The right-hand boundary conditions are generally defined by the groundwater properties, which enables the effects of, for example, variations in groundwater salinity or of the influx of aerated meteoric water to be determined. It is this coupling of interfacial and near-field processes that makes this form of modelling so flexible.

One of the useful features of the CCM is the wide range of output data that are produced. In addition to predicting the time dependence of the E_{CORR} and corrosion rate of the canister, the model also predicts the spatial and time dependence of the concentration of each of the ten chemical species, and of the rate and extent of each of the individual reactions. These latter data can be used, for example, to predict the time dependence of the increase in salinity in the repository, or of the consumption of O_2.

As an example of the predictions from the CCM, figure 6-15 shows the predicted time dependence of the E_{CORR} and i_{CORR} of a Cu canister in a Canadian repository. For this particular simulation, the trapped O_2 in the buffer and backfill was predicted to be

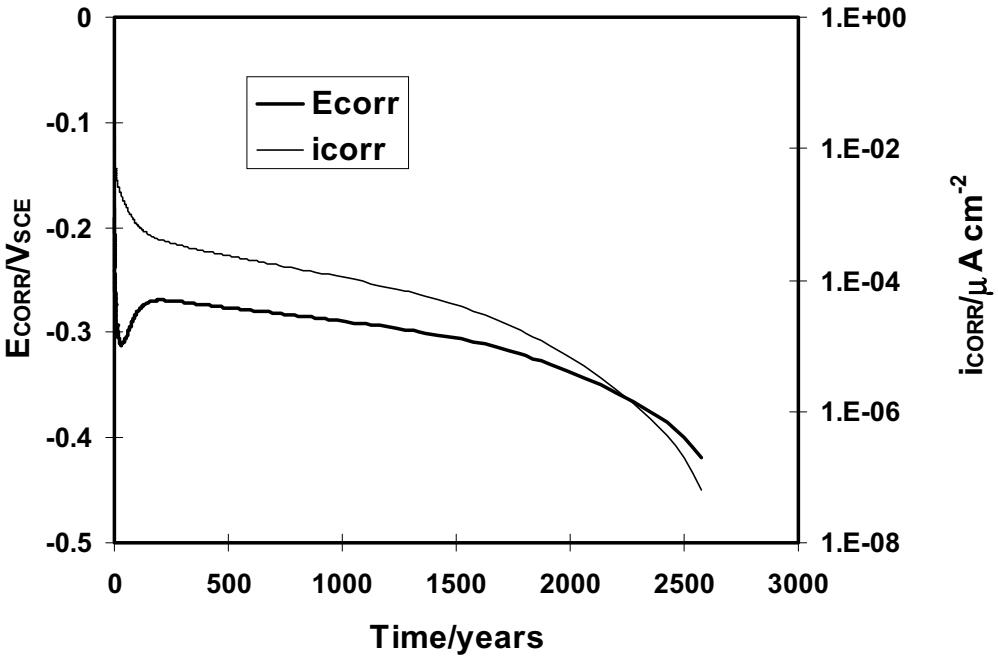

Figure 6-15. *Predicted time dependence of the corrosion potential (E_{CORR}) and corrosion current density (i_{CORR}) of a copper canister in a Canadian repository /King 1996b/.*

consumed in ~2,600 years. (Note: the consumption of trapped O_2 would be expected to be faster with a high-sulphide content bentonite in the deposition holes. The current reference bentonite in Sweden and Finland, MX-80, has a typical sulphide content of 0.1 wt.%). In addition, the consumption of O_2 by reaction with Fe minerals and organics in the bentonite was not considered in the calculation above). Both E_{CORR} and i_{CORR} decrease during this initial period as the trapped O_2 is consumed. The mean predicted corrosion rate over the first year is ~0.3 $\mu m \cdot a^{-1}$, which is an order of magnitude lower than that observed by Karnland et al. /2000/ at Äspö. In the simulation, however, the buffer is assumed to be completely saturated, whereas the buffer in the pilot scale test may have been partially unsaturated, which drastically increases the rate of O_2 diffusion /Collin and Rasmuson 1988; King and Kolář 1997a/.

Figure 6-16 shows the predicted concentration profiles for dissolved O_2 in the repository as a function of time. The O_2 in the vapour-filled pores in the initially unsaturated buffer was assumed to instantaneously dissolve in the pore water, hence producing a dissolved $[O_2]$ equivalent to an O_2 partial pressure of 9–10 atm. In this simulation, the trapped O_2 in the buffer and backfill is consumed by reaction on the canister surface, by reaction with Fe(II) minerals in the backfill, and by diffusion out of the repository, where it is consumed by reaction with Fe(II) minerals in the excavation-disturbed zone (EDZ), and intact rock. The $[O_2]$ at the canister surface drops to ~1% of its initial value after 1 month, suggesting the reduction of O_2 is transport limited. Oxygen is consumed most rapidly in the EDZ and backfill, because of the abundance of Fe(II) minerals in these layers. The O_2 in the buffer layer is the last to be consumed, after ~2,600 years.

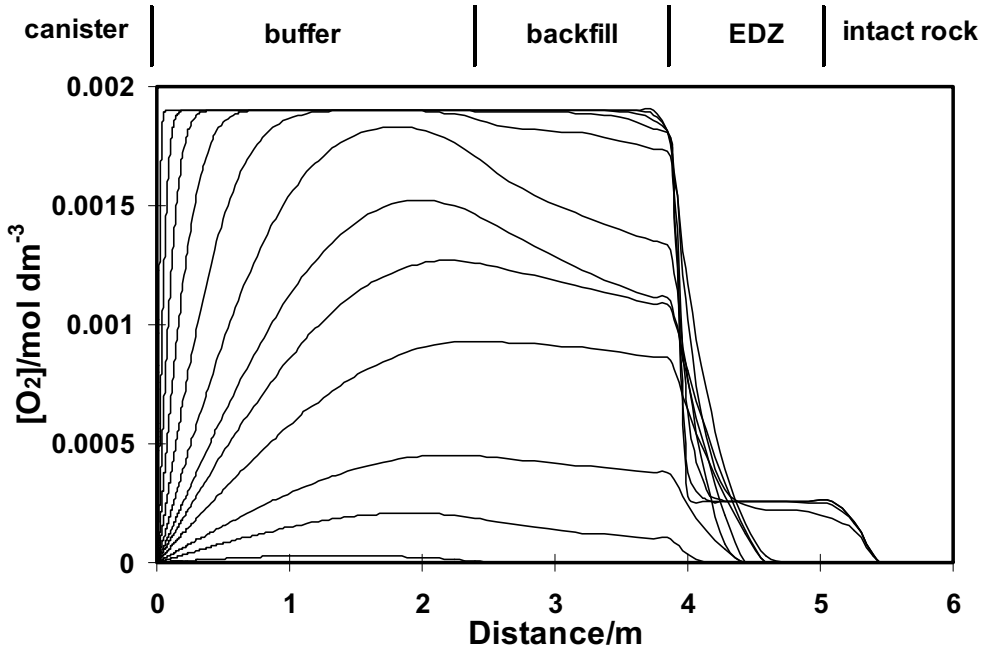

Figure 6-16. *Predicted variation of the concentration of dissolved oxygen as a function of time and position in a Canadian repository. The uppermost profile is for a time of 1 month, with the $[O_2]$ decreasing gradually with time until the final profile illustrated at a time of 1,840 years. For the purpose of these calculations it was assumed that all the O_2 in the vapour-filled pores was instantaneously dissolved in the pore water.*

Figure 6-17 shows that the general corrosion of the canister ceases once all of the initially trapped O_2 is consumed. The maximum depth of corrosion is ~11 μm. Of the total amount of atmospheric O_2 trapped in the vault initially, only ~17% causes corrosion of the canister, afurther 17% is consumed by the oxidation of Cu(I) to Cu(II), ~16% is consumed by reactions with Fe(II) minerals, and the remaining 50% is assumed to reside in inaccessible pores in the buffer and backfill materials. Although the Cu(II) produced by oxidation of Cu(I) can support corrosion (reaction 6-4), the rate is slow due to the strong adsorption of Cu(II). Even if all of the Cu(II) were reduced on the canister surface, the maximum additional corrosion would only amount to a further 11 μm.

In addition to predictions of the general corrosion of Cu /King 1996b; King and Kolář 1995, 1996a, 2000/, the CCM has been used to predict (i) the evolution of vault redox conditions /Kolář and King 1996/, (ii) the extent of SCC controlled by the flux of oxidant to the canister surface /King et al. 1999a,b,c/, (iii) corrosion prior to saturation of the disposal vault /King and Kolář 1997a/, (iv) the effect of geosphere conditions on the corrosion of Cu canisters /King and Kolář 1997b/, (v) the results of Cu corrosion experiments under simulated disposal conditions and of observations from a bronze cannon natural analogue /King and Kolář 1996b/, and (vi) the probability of pitting of Cu canisters /King and Kolář 2000/.

There are a number of major advantages to the CCM over the other two models described above. First, the CCM is based on an extensive experimental database, lending credibility to the predictions made using the model. Second, unlike the Cu(II) transport model and the steady-state E_{CORR} model, the CCM includes all relevant interfacial, homogenous kinetic, and mass transport processes. Third, the use of electrochemical expressions for the interfacial boundary conditions enables both E_{CORR} and i_{CORR} to be calculated directly, the former being particularly useful for predicting the probability

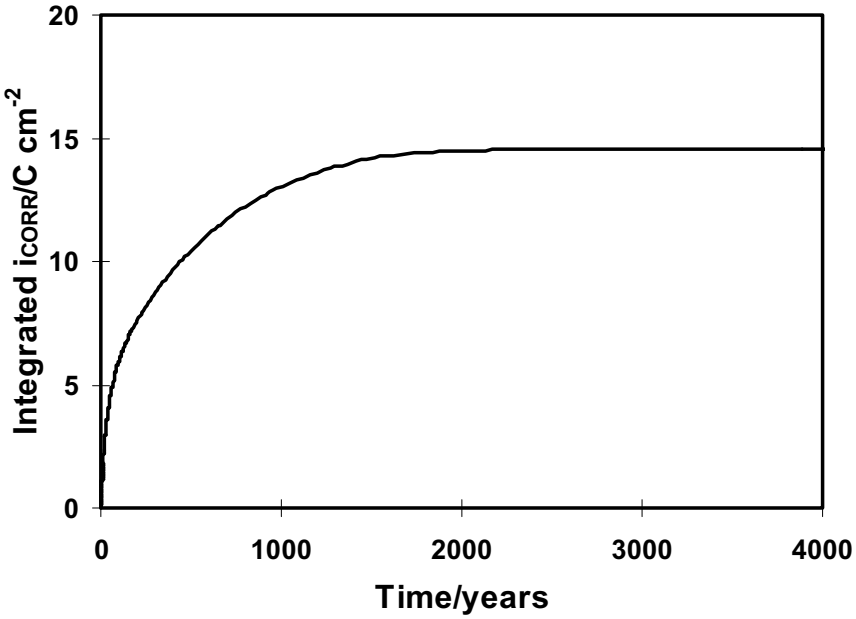

Figure 6-17. *Predicted time dependence on the extent of corrosion of a copper canister in a Canadian repository. A charge density of 15 C·cm^{-2} is equivalent to 11 μm of corrosion.*

of localized attack and stress corrosion cracking. Finally, the flexibility offered by the coupling of interfacial reactions and processes in the near-field enables many more processes other than the general corrosion of the canisters to be simulated.

The only disadvantages to the CCM are its computational complexity, which precludes its use in probabilistic performance assessment calculations and the large number of required input data. However, most of these parameters are available from the various experimental Cu corrosion studies described above, or from the literature.

No kinetic modelling has been performed for the corrosion of Cu in sulphide environments. However, the principles behind such a model have been demonstrated experimentally (figure 6-11), and the requisite interfacial kinetic data are available (section 6.2.3).

6.2.5 Miscellaneous corrosion processes

A number of other factors have been raised as possible issues for the long-term corrosion behaviour of copper canisters. Of these, the most important is the effect of welding on the corrosion properties. The growth of grains during welding can concentrate impurities at the grain boundary due to a decrease in the relative volumes of the grain body and the grain boundaries /Fennell et al. 2001/. Fennell et al. /2001/ found no effect of welding on the degree of intergranular corrosion of Cu-OF in bentonite-equilibrated Äspö groundwater with [Cl^-] of 20 mg/L and 20,000 mg/L. Experiments were carried out at room temperature in aerated solution, and used highly sensitive atomic force microscope measurements in an attempt to detect the smallest degree of grain boundary etching. Ryan et al. /1994/ found no preferential attack at the weld region of electron-beam welded copper samples exposed to compacted buffer material at 100°C for periods of up to 5 years. Therefore, there is no evidence to suggest that the weld region should suffer higher corrosion rates than the rest of the canister shell.

A second factor that may affect the rate of corrosion is the increased pressure at repository depth. However, as discussed in section 6.2.2, an increase in pressure from 0.1 MPa to 5 MPa will result in a <10% change in the equilibrium [$CuCl_2^-$], and a correspondingly small change in the corrosion rate. Mor and Beccaria /1979/ also observed a small effect of pressure on the anodic and, especially, the cathodic reactions involved in the corrosion of copper in seawater. The effect of pressure on the cathodic reaction is partially due to an increase in the concentration of dissolved O_2 with increasing O_2 partial pressure. Although this might also occur in a repository, due to the increase in pressure due to the development of the hydrostatic head, this effect neither increases the overall amount of O_2 nor the maximum extent of corrosion.

The presence of high concentrations of methane in deep Finnish groundwaters (up to 600 mL/L (0.027 mol·dm^{-3}), table 2-3) is expected to have no effect on the corrosion of the canisters. (Similar methane levels have not been reported in Swedish groundwaters (tables 2-1 and 2-2), but must be considered possible since both Swedish and Finnish repositories would be constructed in the same type of geological formation). Although copper alloys are generally not used in applications involving natural gas, this is because of impurities in the gas, rather than due to the methane itself. Lyle /1993/ showed that the corrosion rate of copper in natural gas depends primarily on the H_2S, O_2, and H_2O contents. The sulphur content of natural gas was also correlated with erosion in high-temperature methane-fueled combustion chambers /Walter et al. 1989/. Mercaptans, added to impart odour to the gas, may also pose integrity concerns for copper alloys in natural gas facilities. Acidic natural gas combustion products have also been shown to cause corrosion of copper heat exchangers /Buhler 1993/. However, in none of these studies is there any evidence that methane itself is deleterious towards copper alloys.

6.2.6 State-of-knowledge of the general corrosion of copper canisters

Much is known about the general corrosion behaviour of Cu under repository conditions. Detailed thermodynamic analyses on possible corrosion reactions have been performed, particularly in the Swedish and Finnish programmes. In Canada, more emphasis has been placed on kinetic studies under well-controlled mass-transport conditions. Combined, these complementary approaches provide a detailed understanding of the general corrosion behaviour of Cu canisters under the evolving conditions expected in a repository.

The most important parameters controlling the rate of general corrosion are: the rates of mass transport of species to and from the canister surface, the availability of O_2, the influx of Cl^- ions from the groundwater, and the supply of sulphide ions to the canister.

In a sealed repository, the extent of general corrosion is limited by the general lack of oxidants. Trapped atmospheric O_2 will support corrosion in the initial stages of the evolution of vault conditions, but the amount of available O_2 is limited and will be partially consumed by reaction with oxidizable minerals (principally sulphide minerals) in the repository. Under reducing conditions, corrosion will be supported by the slow supply of sulphide to the canister surface.

Because of the limited amount of available oxidant, general corrosion will not limit the canister lifetime.

Although much is known about the general corrosion of copper canisters, there are a number of areas where further work may be beneficial. These areas are discussed in more detail in section 10, but include the following: measurement and prediction of the evolution of redox conditions in the repository, the measurement and prediction of corrosion potentials in highly compacted bentonite, and further studies of the possibility of corrosion in highly saline groundwaters in the absence of oxygen

6.3 Localized corrosion

Localized corrosion refers to a range of corrosion phenomena that result in localized, as opposed to general, attack and which do not fall under the category of environmentally assisted cracking. For pure Cu alloys, which do not undergo dealloying, the most important form of localized corrosion is pitting. Before considering pitting in some detail, two other forms of localized corrosion of Cu will be briefly discussed: crevice corrosion and "ants-nest" corrosion.

Crevice corrosion is of significant concern for many alloy systems, especially passive materials containing alloying elements which strongly hydrolyze and can form locally acidified environments in occluded regions. The hydrolysis of Cu(I), especially when complexed by Cl^-, is weak /Baes and Mesmer 1976/, and local acidification in crevices is unlikely to occur. Cupric species hydrolyze more strongly, but, as argued above, the formation of Cu(II) requires the presence of O_2, and is unlikely to occur in occluded regions, such as crevices, where O_2 access is restricted. As a consequence, the crevice corrosion of pure Cu is uncommon, and when it is observed occurs via a differential Cu-ion concentration cell mechanism, with areas exposed to a high Cu-ion concentration acting as cathodic sites supporting the dissolution of areas in contact with a low concentration of dissolved Cu. This form of localized corrosion, however, is inherently self-limiting, because the differential [Cu] cell driving localized corrosion is destroyed by the dissolution itself. In long-term irradiated corrosion tests under simulated conditions of a Canadian repository, no crevice corrosion was observed on either creviced U–bend of creviced planar samples /Ryan et al. 1994/.

Ants-nest corrosion is a peculiar form of corrosion specific to Cu /Corbett and Elliot 2000/. It is associated with the presence of formic acid and results in localized dissolution of the material to produce a honeycomb-like ants-nest appearance. The phenomenon appears to be restricted to Cu alloy components in air-conditioning equipment. Ants-nest corrosion can be simulated in the laboratory in the presence of moist air and an organic acid, conditions unlikely to prevail in the repository.

6.3.1 Experimental studies of the pitting corrosion of copper

Pitting of Cu has been investigated in relation to a number of different applications of Cu alloys and for various environments. The most well-known phenomenon is the pitting of Cu water-distribution pipes. These studies are of limited use for predicting the pitting behaviour of Cu canisters, however, because of the difference in salinity between fresh potable waters and saline pore waters. However, a number of Cu pitting studies have also been reported in Cl^- solutions, with and without the addition of HCO_3^-. In addition, a number of corrosion studies have been performed under conditions that simulate those expected in a repository and provide direct evidence for the pitting behaviour of Cu canisters.

Pitting of Cu water pipes has been studied extensively since the 1960's. At least three types of pitting have been recognized; Types I and II pitting /Mattsson 1980/ and a type of pitting apparently induced by microbial activity /Fischer et al. 1988/ (not discussed further here because of the absence of microbial activity in highly compacted bentonite). Types I and II pitting occur under distinctly different conditions, Type I pitting being associated with cold, hard and moderately hard waters free of naturally occurring inhibitors, but containing HCO_3^-, SO_4^{2-}, Cl^- and O_2, and on Cu pipes with a residual surface carbon film remaining from the manufacturing process /Mattsson 1980/. Pit initiation involves the formation of a CuCl "pocket" in an otherwise protective Cu_2O film. Dissolution of Cu as $CuCl_2^-$ occurs at the defect produced by the CuCl pocket. The dissolved Cu(I) is oxidized to Cu(II) by O_2 and precipitates forming a crust of $CuCO_3 \cdot Cu(OH)_2$ and $CaCO_3$. The crust forms an occluded region in which localized dissolution continues. There is some question regarding the location of the cathode, with some favouring a classic mechanism involving the cathodic reduction of O_2 on exposed surfaces outside the pit, and others suggesting that both anodic and cathodic reactions are located within the occluded region formed by the $CuCO_3 \cdot Cu(OH)_2/CaCO_3$ cap /Campbell 1974; Lucey 1967/. A threshold potential for pit propagation has been defined (in terms of the potential of the exposed surface), with a value of between 0.06 V_{SCE} and 0.17 V_{SCE} /Campbell 1974/.

Type II pitting is associated with hot potable waters (>60°C) with a pH <7.4 and a $[HCO_3^-]:[SO_4^{2-}]$ ratio <1, and tends to produce pits with a larger depth:width ratio than the approximately hemispherical pits characteristic of Type I pitting. A specific form of Type II pitting has occurred in Japan, in which residual Cl_2 from sterilization procedures was sufficient to increase the E_{CORR} above the pitting potential of 0.115 V_{SCE} to 0.16 V_{SCE} /Fujii et al. 1984; Kasahara and Komukai 1987; Kasahara et al. 1988; Suzuki et al. 1983/.

Although pitting studies in potable waters may not be directly relevant to the pitting of Cu canisters in saline pore waters, the proposed mechanisms provide some insight into the possibility of localized corrosion in a repository. It is useful to consider three phases in the life of a pit; birth, propagation, and death. The initiation of Type I pits is associated with the formation of CuCl underneath a porous Cu_2O layer. The higher $[Cl^-]$ encountered in deep groundwaters may either make pit initiation more likely, or may induce so many defects in the Cu_2O layer that the surfaces dissolves generally (active dissolution) as opposed to locally as pits (passive behaviour).

Oxygen is a pre-requisite for pit propagation. In Type I pitting, O_2 either serves directly as the oxidant supporting pit growth, or oxidizes Cu(I) to Cu(II), with the latter species then acting as the oxidant. The reduction of O_2 to OH^- also produces local alkalinity, which supports and maintains the crust over the pit, which in turn maintains local acidity within the pit and sustains pit growth. A decrease in $[O_2]$ would result in less Cu dissolution and an increase in the pit pH, both of which would eventually cause the pit to stop propagating. Pitting of Cu water pipes is only sustained because of the high $[O_2]$ in fresh water and because it is continually replenished by the movement of water in the pipe. This would not be the case for pits on Cu canisters, both because of the limited amount of O_2 available and because of the restricted mass-transport conditions which will limit the supply of O_2 to the corrosion sites. Therefore, pits on Cu canisters will be far more likely to die than those on Cu water pipes.

Studies of the pitting of Cu in concentrated Cl^- and Cl^-/HCO_3^- solutions have been concerned with initiation events and the determination of breakdown potentials (E_b). These experiments are generally performed electrochemically under potential control and, therefore, provide information about film breakdown and pit growth under conditions where the cathodic reaction is not rate limiting. The results have been used to

interpret the behaviour of Cu in fresh waters, since concentration of the low levels of Cl^- and HCO_3^- in fresh waters may be a precursor to pit initiation. They are also of use in predicting the possibility of localized corrosion of Cu canisters in more saline conditions.

Figure 6-18 shows the variation of E_b with log [Cl^-] for Cu in Cl^- and Cl^-/HCO_3^- mixtures from a number of literature studies. There is a wide variation in the data, partly because of the use of different [HCO_3^-] in some of the studies, but also because E_b is a distributed, stochastic parameter. (Excluded from figure 6-18 are the E_b data from Drogowska et al. /1992/ in HCO_3^--free Cl^- solutions. These authors appear to have misinterpreted the active dissolution of Cu in Cl^- solutions as being due to the breakdown of a protective film /King and Kolář 2000/).

Despite the wide spread in the E_b data in figure 6-18, the trends observed by various workers are reasonably consistent. In Cl^-/HCO_3^- mixtures, HCO_3^- promotes passivation, whereas Cl^-promotes pitting. At a constant [HCO_3^-], therefore, E_b decreases with increasing [Cl^-] (see, for example, the data of Imai et al. /1996/ at [Cl^-] of 0.005, 0.016 and 0.049 mol·dm^{-3} in figure 6-18). Bicarbonate ions promote passivity more strongly than Cl^- ions promote film breakdown. This can be seen from the results of Drogowska et al. /1992/, in which E_b was determined in solutions with equal concentrations of HCO_3^- and Cl^- (the fitted line 3 in figure 6-18). Thus, E_b increases with increasing concentration (of both Cl^- and HCO_3^-), as opposed to the decrease in E_b with increasing [Cl^-] at constant [HCO_3^-]. For pore-waters containing between 0.001 mol·dm^{-3} and 0.1 mol·dm^{-3} Cl^- and with up to 0.02 mol·dm^{-3} HCO_3^-, E_b will be in the range from approximately –0.1 V_{SCE} to +0.3 V_{SCE}. Higher [HCO_3^-] will lead to more-positive E_b values, especially at lower [Cl^-]. In HCO_3^--free Cl^- solutions, E_b is quite positive, consistent with the trend towards active dissolution in Cl^-solutions.

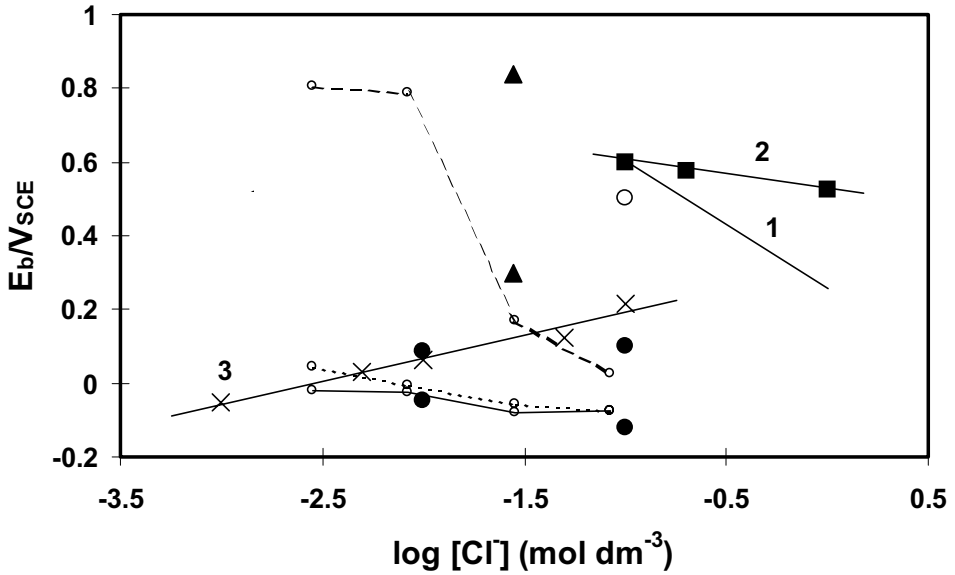

Figure 6-18. *Dependence of pitting (breakdown) potential E_b on chloride concentration in Cl^- solutions and in Cl^-/HCO_3^- mixtures at 25°C.The data were recorded potentiodynamically but have been corrected to zero scan rate to aid inter-comparison. No correction has been made for the variation of E_b with pH. Data from references (O) Qafsaoui et al. /1993/, (▲) Sridhar and Cragnolino /1993/, (●) Thomas and Tiller /1972a,b/, (■) Nishikata et al. /1990/, (×) Cl^-/HCO_3^- mixtures of Drogowska et al. /1992/, (-O-) Imai et al. /1996/. Lines fitted to (1) de Chialvo et al. /1985/, (2) Nishikata et al. /1990/, (3) Drogowska et al. /1992/ Cl^-/HCO_3^- data.*

There have been relatively few systematic studies of the effect of pH on E_b. The E_b values shown in figure 6-18 were determined in the pH range 7–9. Laz et al. /1992/ report a linear dependence of E_b on pH in the range pH 7–11 in 1 mol·dm^{-3} $NaClO_4$, with E_b increasing with pH (dE_b/dpH = 27 mV) presumably because of the greater stability of the passive layer with increasing pH. In alkaline solutions (pH > 12), the passive layer comprises an inner layer of Cu_2O and an outer passivating layer of either $Cu(OH)_2$ (at temperatures less than 35°C) or CuO (T > 35°C) /Shoesmith and Lee 1977/. However, Cl^- ions will compete with OH^- ions for surface adsorption sites and for complexation of dissolved Cu ions, thus interfering with the film formation process. Chloride will stabilize Cu(I) species, possibly preventing the formation of the passive Cu(II) outer layer (or dissolving it if it is already present). Thus, the structure of the film in alkaline saline environments, and the propensity for localized corrosion, will depend on whether the surface is exposed to alkaline environments prior to being exposed to Cl^- ions, or vice versa. One area in which this could be important for Cu canisters is if large amounts of concrete or cement are used and if the bentonite cannot buffer the high-pH pore water leaching from the concrete. Then, the effect on the canister will depend upon whether the alkaline plume from the concrete reaches the canister prior to the buffer material saturating with saline groundwater.

There are relatively few studies of the effect of temperature on E_b. Thomas and Tiller (1972b) report a linear decrease in E_b with increasing temperature, of approximately –0.8 V/°C. Of more importance than the absolute value of E_b is the difference between E_b and E_{CORR}, which Thomas and Tiller reported was constant because of the corresponding decrease of E_{CORR} with increasing temperature. Conversely, Drogowska et al. /1994/ reported a substantial increase in E_b with increasing temperature, amounting to +7.2 mV/°C. Sridhar and Cragnolino /1993/ reported a tendency away from localized corrosion to general corrosion with increasing temperature, which would imply an increasing value of ($E_b - E_{CORR}$) with increasing temperature.

A related parameter to E_b is the repassivation potential E_{rp}. Whereas E_b is the potential at which pits initiate, E_{rp} can be viewed as the potential at which propagating pits cease to grow. Widely used as a criterion for localized corrosion by regulatory bodies in the U.S., the use of E_{rp} is proposed as a more conservative measure of pitting susceptibility than E_b since E_{rp} is invariably more negative than E_b and should be subject to less scatter compared with the potential for the stochastic pit breakdown process. Relatively few values of E_{rp} have been reported for Cu in relevant conditions. Sridhar and Cragnolino /1993/ report E_{rp} values of 0.37 V_{SCE} and 0.07 V_{SCE} for Cu in solutions containing 0.14 mol·dm^{-3} HCO_3^-, 0.028 mol·dm^{-3} Cl^-, and either 2 x 10^{-4} mol·dm^{-3} or 0.01 mol·dm^{-3}, respectively.

There have been a number of studies of the passivation of Cu in HCO_3^- solutions. In Cl^--free solutions, passivation proceeds via the formation of a thin interfacial layer of $CuCO_3$ (formed from either Cu_2O or $Cu(OH)_{ADS}$ precursors), with the eventual precipitation of basic Cu(II) carbonate ($CuCO_3 \cdot Cu(OH)_2$) /Pérez Sánchez et al. 1990, 1993/. These processes will be hindered in Cl^--containing solutions because of the competition between Cl^- and HCO_3^- for the interfacial $Cu(OH)_{ADS}$ species. Sirkiä et al. /1999/ have identified a bilayer film structure on Cu in neutral HCO_3^- solutions, comprising an inner layer of semi-conducting Cu_2O and an outer layer of Cu(II) species. At relatively modest potentials (at which Cu(I) is the stable species), the rate of the anodic reaction is limited by the transport of ionic defects through the interfacial Cu_2O film. With increasing potential, and presumably also in the presence of Cl^- (although this was not investigated in this study), the number of charge carriers in the Cu_2O film increases, and the rate of oxidation becomes partially controlled by the rate of charge transfer reactions on the defected Cu_2O layer. Based on electrochemical studies, Imai et al. /1996/ have classified

the behaviour of Cu in Cl^-/HCO_3^- mixtures as being either active, passive, or active-passive (the latter characterized by a limited passive range). In HCO_3^- solutions, passive behaviour was observed for concentrations ≥0.016 mol·dm^{-3} (1,000 mg/L), with either active or active-passive behaviour at lower [HCO_3^-]. The addition of Cl^- promoted active-passive behaviour, especially for [Cl^-] ≥0.01 mol·dm^{-3} (~300 mg/L). Sulphate ions were also found to promote the breakdown of passive films formed in HCO_3^- solutions, although SO_4^{2-} was less aggressive than Cl^-.

Localized corrosion of Cu has been reported in sea water polluted by sulphide, but only under conditions of alternating aerated and deaerated conditions. As discussed above, cyclic redox conditions can disrupt the otherwise protective surface film (either Cu_2O or Cu_2S/CuS). In marine applications, disruption of the surface film is exacerbated by flow effects, which further destabilize the protective layer. Such alternating redox conditions are not expected in a repository.

Vasquez Moll et al. /1985/ considered the breakdown of sulphide films on Cu and the onset of localized dissolution. An E_b value of –0.74 V_{SCE} was reported in 0.01 mol·dm^{-3} HS^-, which shifted to more-positive values with decreasing HS^- concentration. Thus, E_{CORR} is ~200 mV more negative than E_b in sulphide solutions, based on the E_{CORR} values in sulphide solutions in figure 6-11. Escobar et al. /1999) observed pitting on Cu-OF samples in sulphide solutions at a potential of –0.218 V_{SCE}. Pitting was observed in 0.001 mol·dm^{-3} sulphide, but to a smaller degree if passivating species such as HCO_3^- ions were also present. This lead Escobar et al. /1999/ to suggest that a threshold sulphide concentration might exist below which pitting does not occur. In addition, the potentials at which these studies were performed are many hundreds of mV more positive than those likely in a repository, also making pitting of copper canisters unlikely. Provided conditions within the repository remain reducing, therefore, localized corrosion due to the breakdown of the protective Cu_2S/CuS film seems unlikely.

A number of corrosion studies have been performed under conditions that simulate the canister near-field environment. Copper coupons have been exposed to compacted buffer material wetted by (initially) aerated saline pore waters, and exposed for extended periods of time (up to 2 years) usually at elevated temperature /Aaltonen and Varis 1993; Karnland et al. 2000; King et al. 1992, 1997a; Litke et al. 1992/. These experiments simulate the likely environmental conditions soon after emplacement of the canisters and saturation of the buffer material. It is during this period in the evolution of vault conditions that localized corrosion is most likely, since the environment will be oxidizing (required for Types I and II pitting of Cu water pipes and for the ennoblement of E_{CORR} to values more-positive than E_b). Furthermore, the pore-water [HCO_3^-] may be significant because of the dissolution of carbonate minerals and the [Cl^-] may be sufficient to cause film breakdown, but not so high as to cause general dissolution of the surface. Thus, short-term lab and field tests can be used to study the period of most aggressive localized corrosion.

Despite the relative aggressiveness of the conditions in such tests, no evidence for pitting has been observed. Thus, both Aaltonen and Varis /1993/ and Karnland et al. /2000/ report no localized corrosion of Cu exposed to compacted clay over periods of up to 2 years. The only instance of non-uniform corrosion reported under such conditions is the so-called under-deposit corrosion reported by Litke et al. /1992/. An example of the surface roughness observed is shown in figure 6-19. The most important observation from figure 6-19 is that the entire surface has corroded, albeit to different extents. This, therefore, is not an example of pitting corrosion in the classical sense of permanently separated anodic and cathodic sites. Because the entire surface has corroded, the anodic

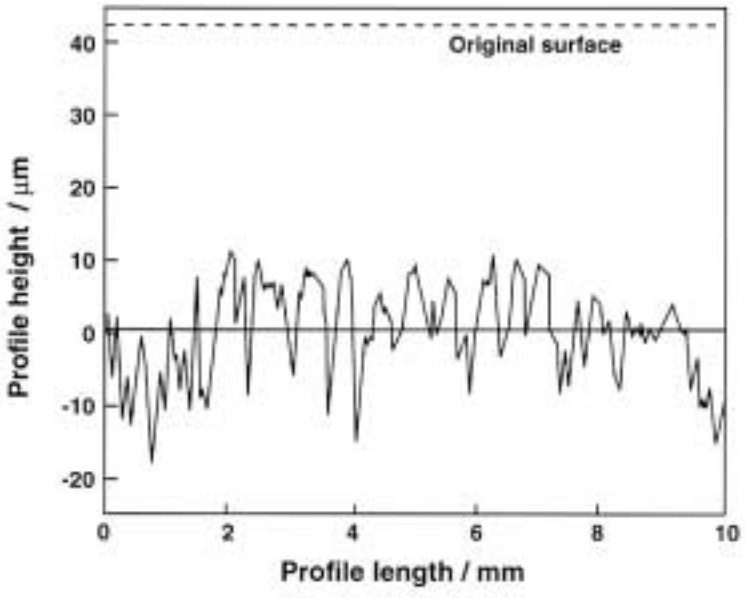

Figure 6-19. *Typical surface profile of stripped copper coupon following exposure to groundwater-saturated compacted buffer material at 50°C for 733 d /Litke et al. 1992/.*

reaction must have been located over the entire surface. The non-uniform nature of the attack suggests that either the rate of the anodic reaction was not uniform over the surface or that anodic and cathodic sites were temporarily spatially separated.

The extent of surface roughening by under-deposit corrosion is currently being studied in Canada in work sponsored by Ontario Power Generation. The electrochemical noise between coupled electrodes, one immersed in bulk solution and the other exposed to a freely swollen 1:1 bentonite:sand mixture, is being measured as a function of various factors /A. Brennenstuhl, private communication 2001/. Of the various factors studies, temperature, $[O_2]$ and pH have the greatest effect on the extent of localized corrosion. Preliminary results suggest that the degree of localization of corrosion in a repository should decrease with time as the canister temperature and the $[O_2]$ decrease.

6.3.2 Modelling approaches for the pitting corrosion of copper

The approach taken to model the long-term localized corrosion behaviour of the canister depends on the nature of the available data. If the pitting mechanism is known then detailed mechanistic models can be developed. Such models can provide information about either the initiation or growth of pits. Alternatively, if E_b and E_{CORR} data are available, the probability of pit initiation can be predicted. Finally, measured pit depths can be statistically or otherwise analyzed and predictions of pit growth on canisters made based on the depths of pits from shorter exposure periods.

Taxén /1996, 2000/ has described a model for the growth of pits based on mass transport and chemical equilibrium principles. Continued growth of the pit is contingent on the transport of reactants to the base of the pit where the anodic reaction is located and the transport of dissolved Cu out of the pit (figure 6-20). Both solid and dissolved corrosion products are assumed to form within the pit. If sufficient Cu is not transported out of the pit, the corrosion products in the pit become so dense and non-porous that growth is stifled and the pit dies.

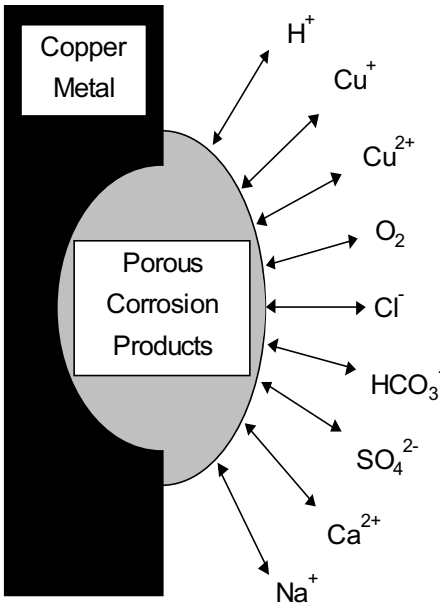

Figure 6-20. *Schematic illustration of the site of a corrosion pit in copper with aqueous species diffusing and migrating.*

Mass transport into and out of the pit is by a combination of diffusion and migration and is simulated by a 1-D mass-balance equation of the form

$$j_i = -\frac{c_i D_i}{RT} \cdot \frac{\partial \mu_i}{\partial x} \qquad 6\text{-}22$$

where j_i, c_i and D_i are the flux, concentration and diffusion coefficient of species i, and μ_i is the chemical potential, given by

$$\mu_i = \mu_i^0 + RT \ln a_i + z_i F \Phi \qquad 6\text{-}23$$

where a is the activity, z is the charge, F is Faradays constant and Φ is the electrical potential. The pit geometry is simulated by a series of hemispherical shells (with a constant surface area:thickness ratio) describing both the pit in the metal and the cap of porous corrosion products (figure 6-21). Chemical reactions between various species is assumed to be fast relative to the rate of mass transport, so that equilibrium chemical conditions can be used.

The fraction of corrosion products precipitating as a solid compared with the fraction that are transported out of the pit is decisive in determining whether the pit can continue to grow. Based on the relative molar volumes of Cu and of either Cu_2O or CuCl, a certain fraction of the corrosion products must be transported out of the pit to avoid starvation of the pit. If Cu_2O is precipitated within the pit, ≥40% of the corroded Cu must be transported out of the pit for continued pit propagation. If CuCl forms within the pit, this fraction is even larger (≥70%).

If ≥40% of the corrosion products are to be transported out of the pit, local acidification within the pit is necessary to avoid precipitation of the corrosion products. Acidification results from the formation of Cu_2O

$$2Cu + H_2O = Cu_2O + 2H^+ + 2e^- \qquad 6\text{-}24$$

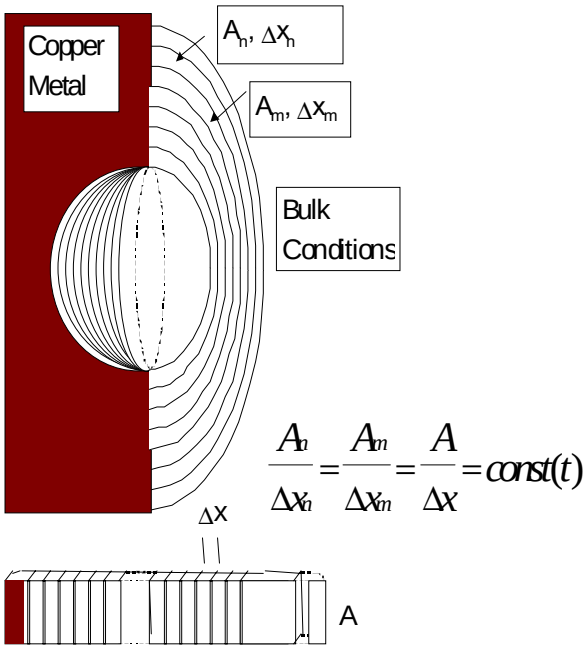

Figure 6-21. *Description of the site of a corrosion pit as consisting of thin shells.*

The equilibrium expression for reaction 6-24 defines a combination of potential and pH for the formation of Cu_2O, the lower the pH the higher the potential, and vice versa. The potential at which the transported fraction of the corroded copper is equal to 40% is termed the minimum potential for pit propagation. Potential drops in the solution caused by diffusion potentials and the passage of current were added. Activity coefficients were calculated as a function of ionic strength using the Davies' method.

Figure 6-22 shows the predicted conditions of potential and [Cl^-] for pit propagation. A number of conclusions about the role of various components in the water in the pitting process were drawn from the calculations:

- The pH of the bulk water outside the corrosion pit has a small influence on the minimum potential for pit propagation. The stability of the cuprous oxide against oxidation decreases with increasing pH. The potential window where reduction at a cuprous oxide surface can drive the anodic dissolution in a corrosion pit decreases with increasing pH. Pitting of copper is less likely to occur at high pH values.
- Expressing the difference between the minimum potential for propagation of a corrosion pit and the upper potential for stability of cuprous oxide as a margin against pitting, it is found that for a given pore-water composition, the value of this margin increases with temperature. Pitting is less likely to occur at higher temperatures.
- Of the common anions, chloride is the most aggressive species towards copper. Strong complex formation of chloride with monovalent copper allows high copper concentrations in contact with corroding copper metal. The chloride concentration is decisive for the value of the minimum pitting potential of copper. Using the margin against pitting as a criterion, it is found that the value of this margin decreases with increasing chloride concentration. Pitting is, according to this criterion, more likely to occur in waters with high chloride concentrations.

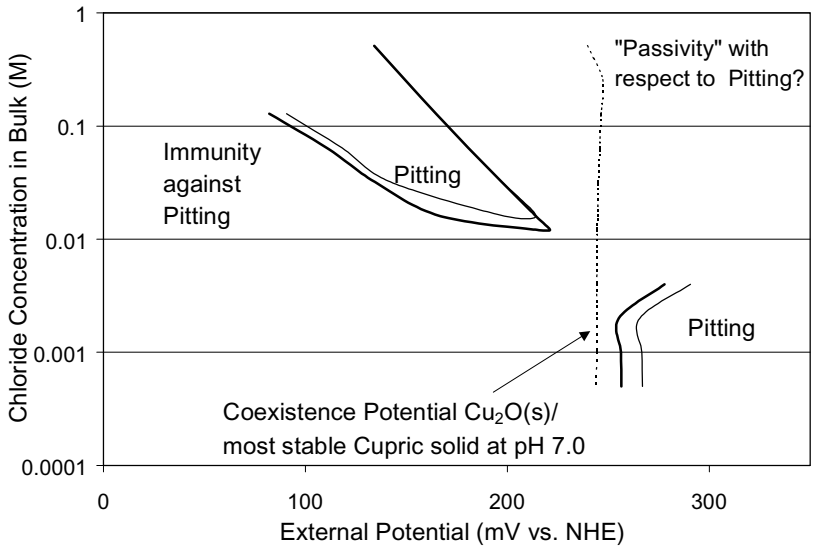

Figure 6-22. *Potential – chloride concentration diagram identifying conditions for pit propagation. The thick line indicates that the fraction of the oxidised copper which is transported away from the site of the oxidation as aqueous species is equal to 0.4, the thin line indicates conditions corresponding to the transported fraction equal to 0.5.*

- Carbonate forms strong complexes with divalent copper. Carbonate is more aggressive at the higher pH of the bulk than at the lower pH in a corrosion pit. A high carbonate concentration may facilitate the anodic reactions in general corrosion. The buffering capacity of bicarbonate at moderately low pH values facilitates the transport of acidity out of the pit. An increased transport rate for protons, in the form of carbonic acid, favours the formation of cuprous oxide in the pit rather than the competing formation of aqueous copper species. A high carbonate concentration may increase the value of the minimum pitting potential and decrease the value of the upper stability potential for cuprous oxide. Pitting is less likely to occur in water with high carbonate concentrations.
- Sulphate forms a complex with divalent copper. Sulphate is aggressive towards copper in a corrosion pit and almost inert with respect to the general corrosion. Pitting is more likely to occur in waters with high sulphate concentrations.
- Calcium may have an indirect beneficial effect. For a water with a high sulphate concentration, pitting is less likely to occur if the calcium concentration is of the same magnitude or higher.
- Oxygen at low concentrations can also give potentials higher than the minimum pitting potential. The influence at the site of the pit of the direct oxidation of monovalent copper to divalent has a small influence on the minimum pitting potential.
- Corrosion pits where the transport of copper is dominated by monovalent copper may lead to precipitation of large amounts of porous cuprous oxide in and outside the cavity. Where the transport is dominated by divalent copper, precipitation, in the form of basic salts, occurs at higher pH values and outside the cavity.
- Precipitation in the cavity decreases the aqueous cross sectional area available for diffusion and migration to a higher extent than precipitation outside the cavity. Pits where the precipitation occurs mainly outside the cavity have higher growth rates.

- Factors favouring the type of pits dominated by monovalent copper are high chloride contents in the bulk water and high temperature. Factors favouring the type of pits dominated by divalent copper are a high sulphate concentration, low concentrations of other salts and a high potential.
- Pitting of copper has been observed in waters with a composition and temperature such that the minimum pitting potential is in a range where cuprous oxide is not stable at the pH of the bulk water.
- Pitting of copper is possible in a wide range of solution compositions. In some waters a corrosion pit will not propagate unless the cuprous oxide at the external surface is stabilised or if there is electronic contact with a conducting, more noble phase.
- Limits of the propagation rates for corrosion pits in copper can be given only as conditional depending on the corrosion potential.
- In waters with chloride contents approaching that of sea water, pitting is possible with high propagation rates and at high pH values.

Many of these conclusions are consistent with the experimental observations described above.

For saline solutions with a Cl^- concentration >0.02 mol·dm^{-3}, the model can be simplified and analytical expressions used to define the minimum pitting potential and the fraction of Cu transported out of the pit (tf) as a function of pit pH, bulk [Cl^-] and total carbonate concentration. Figure 6-23 shows the predicted fraction of transported Cu as a function of pit pH for two different bulk [Cl^-]. For pit propagation, the pH inside the pit must be less than ~pH 5, with a corresponding minimum pitting potential of 0.17–0.19 V_{SHE} (–0.07 to –0.05 V_{SCE}, respectively) (bulk total carbonate concentration of 0.064 mol·dm^{-3}). Figure 6-24 shows the distribution of predicted minimum pitting potentials as a function of [Cl^-] and total carbonate concentration (to convert the NHE scale in figure 6-24 to the SCE scale used in figure 6-18, subtract 0.24 V from the NHE scale). The predicted minimum pitting potentials are 100–200 mV lower than the observed E_b values in figure 6-18. The predicted temperature dependence of the minimum pitting potential is similar to that observed by Thomas and Tiller /1972b/, amounting to –1.4 mV/°C.

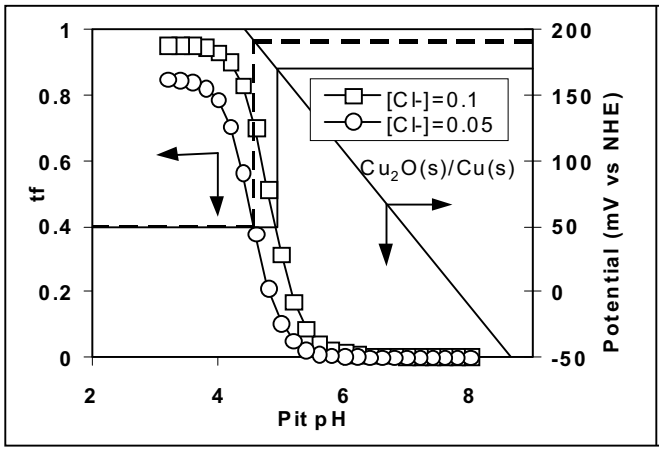

Figure 6-23. *Calculated values of tf as a function of the local pH at 25°C and bulk* $[CO_2]_{tot}$ *= 0.064 mol·dm*$^{-3}$.

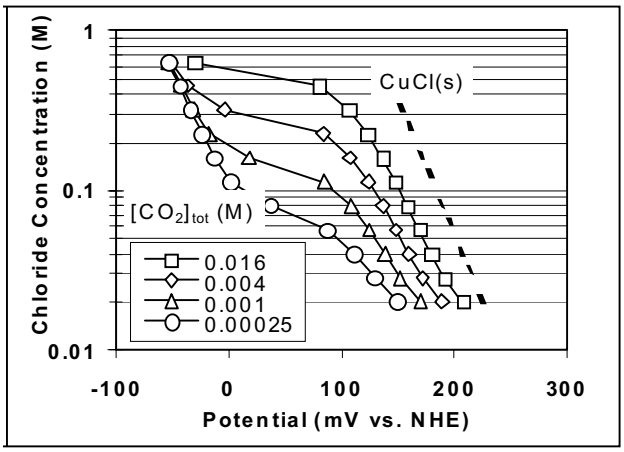

Figure 6-24. *Predicted minimum pitting potential as function of the bulk chloride concentration at 25°C for various bulk total carbonate concentrations.*

Taxén /1991/ has also developed a pit propagation model for Cu in reducing conditions in the presence of sulphide. The pit growth rate was assumed to be limited by the rate of supply of HS^- to the base of the pit by diffusion through either the buffer material or through a porous deposit of precipitated Cu_2S in the pit /Taxén 1991/. Two pit geometries were considered: a cylindrical pit of radius r_p, in which the sides of the pit are passive and dissolution only occurs at the pit bottom, and a hemispherical pit. In both cases, diffusion within the pit and within a hemispherical region of buffer adjacent to the pit mouth was assumed to be at steady state. Under these conditions, the pit growth rate was limited by the slower of the two diffusion processes (diffusion through the buffer or diffusion within the pit), which, given that the pit was assumed to be coupled to a semi-infinite hemisphere of buffer, is likely to be the supply of HS^- to the pit mouth. The assumption of steady-state concentration profiles underestimates the flux of H_2S during the transient period when $[HS^-]$ will be much steeper. To overcome this problem, the steady-state concentration profiles were assumed to be established at an undefined time t_0, at which time the pit depth was p_0. The analyses performed predicted the growth of the pit during the subsequent steady-state period. For a bulk $[HS^-]$ of 1 $\mu g \cdot g^{-1}$ and a pre-existing pit depth of 0.5 cm, the pit was predicted to grow by a further 0.5 to 1.1 cm in the subsequent 10^5 a.

King and Kolář /2000/ have proposed a conceptual model to account for the type of under-deposit corrosion observed on Cu exposed to compacted buffer material (figure 6-19). In this model, pits initiate stochastically over the surface and grow at a rate inversely proportional to the pit size, based on the assumption that the area of the cathode supporting pit growth is constant. Pit death, as a result of the accumulation of corrosion product on either the anodic or cathodic sites would also be simulated by a stochastically distributed pit death parameter. A series of such randomly distributed pit initiation, growth and death processes would result in the type of roughened surface observed experimentally. Some information on pit initiation rates is available /Qafsaoui et al. 1993/, but no data currently exists on the distribution of pit growth and death rates under repository conditions.

An alternative approach to modelling the localized corrosion behaviour of the canister is to predict the probability of pit initiation based on observed E_b values. This approach requires a knowledge of the variation of E_b with environmental conditions and of the time dependence of E_{CORR} for a canister. Based on the data in figure 6-18, the minimum

observed E_b value is –0.12 V_{SCE}. Although no predictions are available for the time dependence of E_{CORR} of a Cu canister in a Swedish or Finnish repository, the data in figure 6-15 can be used as a conservative estimate of E_{CORR} (E_{CORR} in a Swedish/Finnish repository is likely to be more negative than in a Canadian repository because of more rapid consumption of the trapped atmospheric O_2 by reaction with sulphide minerals that are expected to be present in the clay).

Comparison of the observed E_b with the predicted E_{CORR} suggests that pitting will not initiate on Cu canisters in a repository, consistent with the recent observations of Karnland et al. /2000/. Although not apparent from the scale used in figure 6-15, the predicted E_{CORR} is a minimum of 60 mV more negative than the minimum E_b. The maximum predicted value of E_{CORR} is –0.18 V_{SCE} after 3 days, which then decreases to –0.22 V_{SCE} (i.e., 100 mV below the minimum E_b) after ~5 months. During the subsequent ~2,600-yr-long aerated phase, E_{CORR} is substantially lower. Even if pits do initiate on the canister, comparison of E_{CORR} with the limited available E_{rp} data suggests that pit growth will not be sustained.

The final approach to predicting the extent of localized corrosion on Cu canisters is to make projections based on observed pit depths. Because pitting has not been observed on Cu exposed to simulated repository conditions, pit depth data has been taken for this purpose from literature studies of the long-term burial of Cu alloys /Romanoff 1989/ and from an analysis of pit depths on archaeological artifacts /Bresle et al. 1983/. Whilst the environmental conditions and Cu alloys are different from those in a repository, these studies offer the great advantage of having been "conducted" over long periods of time. Thus, the long-term soil corrosivity measurements of Romanoff /1989/ were conducted for times up to 14 years. The Bronze Age artifacts studied by Bresle et al. /1983/ had been exposed to the environment for an estimated period of 3,000 years.

In the Swedish and Finnish programmes, these pit depth data have been used to estimate a pitting factor /Mattsson 1980; SKB 1983; Swedish Corrosion Institute 1978, 1983; Werme et al. 1992/. The pitting factor (PF) is the ratio of the maximum pit depth (as measured from the original surface) to the depth of general corrosion and has a value >1 (PF = 1 corresponds to general corrosion). The maximum pit depth on a canister is then estimated by multiplying the depth of general corrosion, determined by some other means, by the PF. For the earliest predictions of canister lifetimes /Mattsson 1980; Swedish Corrosion Institute 1978/, a conservative PF value of 25 was used, based on the most severe case of pitting reported in the literature /Romanoff 1989/. Subsequent analysis of the archaeological artifacts /Bresle et al. 1983/, supported by the modelling studies of Taxén described above, have lead to the adoption of a more realistic PF of 5 /SKB 1983; Werme et al. 1992; Wersin et al. 1994b/. The use of PF in estimating canister lifetimes is summarized in section 9.

An alternative use of the same pit depth data has been developed in the Canadian programme /King and Kolář 2000; King and LeNeveu 1992/. The data were analysed using extreme-value statistics, in which the deepest pits on a collection of samples (or within a given area of the surface of one or more samples) of the same exposure time is fitted to an extreme-value distribution of the form

$$F(x) = \exp[-\exp(-ax + b)] \qquad 6\text{-}25$$

where F(x) is the cumulative probability that the depth of the deepest pit is less than or equal to a depth x, a is the scale (or shape) parameter, and b/a is the location parameter of the distribution. The fitting procedure produces vales for a and b for a given set of data for a given exposure period. Fitting several sets of data with different exposure

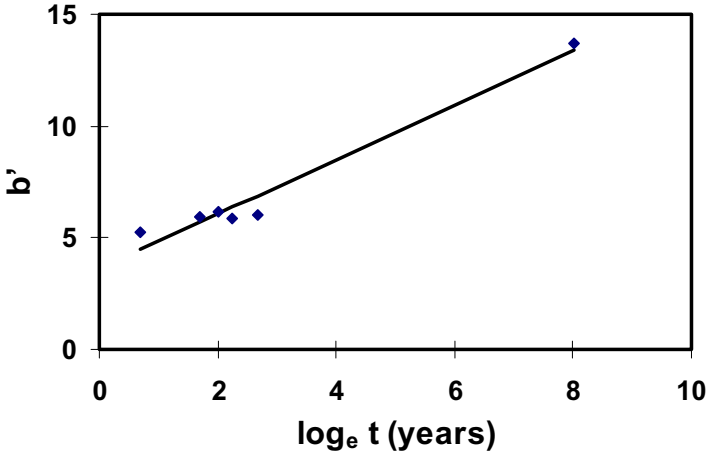

Figure 6-25. *Predicted time dependence of the pit depth extreme value distribution fitting parameter b (b' is the value of b normalized to a surface area of 5.8 m^2).*

periods gives the time dependence of the scale and location parameters. Then, the cumulative probability of a pit of a given depth on a canister as a function of time can be determined from equation 6-25 and the time dependences of a and b/a.

Fitting of the Romanoff /1989/ and Bresle et al. /1983/ data to equation 6-25 indicated that whilst the scale parameter was relatively independent of exposure time, the location parameter increased with time. Figure 6-25 shows the predicted time dependence of b' (the value of b normalized to an area of 5.76 m^2, the surface area of a Canadian dual-wall canister /Johnson et al. 1996; King 1996b/). Based on this time dependence, the maximum pit depth on a canister can be predicted. Figure 6-26 shows the maximum pit depth as a function of time, based on a probability of 10^{-11} that the pit will be deeper than the given depth (i.e., a probability of $<10^{-6}$ for any of the $\sim 10^5$ canisters in the Canadian repository considered in the analysis). Thus, after a period of 10^6 years, the maximum pit depth on any of the canisters is 7.6 mm, for the assumed probability.

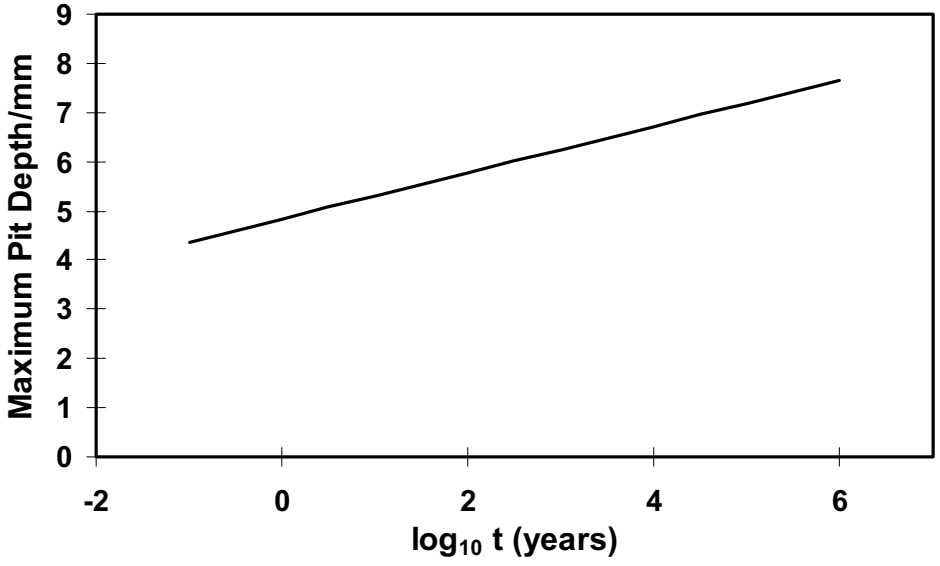

Figure 6-26. *Predicted maximum pit depth on a copper canister as a function of time (assumed canister surface area 5.76 m^2).*

Unlike the critical potential approach to pitting, neither the pitting factor nor the extreme-value analysis approach allows for pit death. Propagation is assumed to continue indefinitely regardless of the evolution in the repository environment, albeit at a diminishing rate in the extreme-value approach. The slope of figure 6-26 suggests the pit growth rate follows a $t^{0.47}$ time dependence.

The surface condition of the canister is not explicitly accounted for in any of the modelling studies discussed above. Near-surface defects (e.g., sub-surface weld porosity) could act as potential occluded regions on the canister surface if corrosion in the repository exposes the defect to the environment. However, although such sites might be preferential locations for localized corrosion, they are no more likely to lead to through-wall pitting than pits initiated at any other location because of the general lack of oxidant in the repository. Thus, even though local occluded chemistry could develop in a surface-breaking pore (just as it does under the cap of corrosion products formed during the pitting of copper water pipes), the aggressive local chemistry can only be maintained by a sufficient supply of O_2. In the Lucey /1967/ model for Type I pitting, for example, the acidification of the pit solution is a result of the hydrolysis of Cu(II), which in turn is formed from the homogeneous oxidation of Cu(I) by O_2. With a sufficient supply of O_2 (as occurs for copper water pipes, but which will not occur for a canister surrounded by highly compacted bentonite) this locally aggressive environment can be sustained. For the O_2-limited conditions within a repository, however, the occluded chemistry cannot be maintained, and the pit solution would eventually equilibrate with the bulk environment, as argued by King and Kolář /2000/.

6.3.3 State-of-knowledge of the pitting corrosion of copper canisters

Various experimental and modelling approaches have been developed to study the pitting of Cu. Although the extensive database on the pitting of Cu water pipes provides some useful mechanistic information, the results of corrosion experiments under simulated repository conditions suggests that canisters will not undergo classical pitting, but rather a form of under-deposit corrosion, in which there is no permanent separation of anodic and cathodic sites.

The mechanistic Cu pitting studies indicate that an oxidant (either O_2 or Cu(II)) is a pre-requisite for pit propagation. Since the near-field environment in the repository will evolve from initially oxidizing to ultimately reducing, this implies that pitting will only be possible (if at all) in the early stages of the repository life. Thus, the environment within the repository is evolving to one in which only general corrosion will occur. In addition, the difficult problem of predicting localized corrosion is made easier by the fact that predictions only have to be made for the early oxidizing period.

Given this evolution in localized corrosion behaviour with repository conditions, the most suitable pitting models are those that include the possibility of pit death. Of the currently available models, only those based on a critical potential (either for pit initiation or pit propagation) are capable of predicting when pitting may cease to be an active degradation mechanism in the repository. For analyses based on literature pit depth data (either the pitting factor or extreme-value approaches) it is implicitly assumed that pits propagate indefinitely. Predictions of pit depth based on these latter two approaches must be considered conservative.

Section 10 includes a number of areas of further study relating to localized corrosion. These areas include: the effect of near-surface-breaking defects, the properties of Cu_2O films, the effect of differential bentonite swelling pressure on localized corrosion, and the possible effect of elevated pH in the repository due to the use of concrete.

7 Stress corrosion cracking

The stress corrosion cracking (SCC) of Cu alloys is the oldest form of environmentally assisted cracking known, dating from the "season-cracking" of brass munitions in the mid-late 19th Century. Apart from the SCC of stainless steel in chloride solutions, the cracking behaviour of Cu and Cu alloys has probably been studied more than any other form of SCC. A number of reviews of the likely SCC behaviour of Cu canisters have been written /Farmer et al. 1988; King 1996; King and Litke 1997; Ikeda and King 2001; Saario et al. 1999/, on which this section has been based.

The three pre-requisites for SCC are a susceptible material, a tensile stress, and a suitably aggressive environment. The proposed canister material cannot be claimed to be immune to SCC, since pure coppers, especially those containing phosphorus, have been shown to be susceptible. Tensile stresses on the canister surface are likely during various stages in the evolution of the repository environment, either due to external loads or from residual manufacturing stresses. Finally, it is not possible to exclude the possibility that known SCC agents, such as ammonia or acetate, may be present in the repository. Therefore, the possibility of SCC of Cu canisters must be considered.

Of all corrosion processes, SCC is probably the most complex and the most difficult to predict. The extensive database on the SCC of pure coppers is summarized in the first section, followed by a discussion of various approaches for predicting the long-term SCC behaviour of Cu canisters in a deep underground repository.

7.1 Literature studies of the SCC of pure coppers

The SCC of pure coppers has been reported to be caused by three different species: ammonia, acetate and nitrite ions. Table 7-1 summarizes the various literature studies on the SCC of pure coppers in these three different environments, with an emphasis on studies associated with the SCC of Cu canisters.

7.1.1 Mechanisms proposed for the SCC of pure coppers

Various mechanisms have been proposed to account for SCC in general, some of which have been specifically proposed for the SCC of Cu /King 1996; Ikeda and King 2001/. Determining the mechanism(s) controlling crack initiation and/or growth is not simply of academic interest, but is necessary for developing predictive models for Cu canisters and for justifying long-term predictions of SCC behaviour.

The four mechanisms proposed to account for the SCC of Cu in various environments are /table 7-1, King 1996/: (a) the film-rupture/anodic-dissolution (FRAD) mechanism, (b) the tarnish-rupture (TR) mechanism, (c) film-induced cleavage (FIC), and (d) the surface-mobility (SM) model.

Table 7-1. Literature studies of the stress corrosion cracking of copper.

Table 7-1(a). Stress corrosion cracking in ammonia environments.

Environment	Solution	Proposed Mechanism[1)]	Comments[2)]	Reference
Tarnishing ammonia	Moist ammonia atmosphere	FRAD	IGSCC following rupture of Cu_2O film. Increasing susceptibility with increasing P content, as well as of other alloying elements (Zn, As, Sb, Si, Ni and Al).	Thompson and Tracy /1949/
Non-tarnishing ammonia	15 mol·dm^{-3} ammonia, pH ~13, 0.04 mol·dm^{-3} Cu(II)	FRAD	IGSCC following rupture of Cu_2O film.	Pugh et al. /1966/, Pugh /1979/
Ammonia	Flowing moist air containing ammonia, 0.5–108 mg/L ammonia	–	OFP Cu (0–1,500 ppm P), various stress levels, various grain sizes. Evidence for threshold P content of 50–80 ppm, evidence for threshold ammonia concentration, susceptibility increases with grain size.	Sato and Nagata /1978/
Tarnishing ammonia	0.05 mol·dm^{-3} ammonia	TR	Crack advance by rupture of adherent Cu_2O layer. Cracking only observed at ammonia concentrations ≤ 0.05 molin·dm^{-3}. TGSCC.	Suzuki and Hisamatsu /1981/
Non-tarnishing ammonia	15 mol·dm^{-3} ammonia, pH 12.5–13, 0.008–0.03 mol·dm^{-3} Cu(II)	FIC	TGSCC induced by nanoporous Cu layer produced by the rapid nucleation of etch pits. Nanoporous layer only produced under limited range of conditions of strain rate and high dissolution rates.	Sieradzki and Kim /1992/
Ammonia	Mattsson's solution containing various Cu^{2+} concentrations	–	OFE (UNS C10100) and OFP Cu. Constant displacement experiments in compacted buffer material. No cracking observed.	King et al. /1999a/
Ammonia	Deaerated synthetic brackish and saline Olkiluoto groundwater plus 1–100 mg/L ammonia, 100°C, pH 7	–	OFP Cu (45 ppm P), base and electron-beam welded material. SSRT, 10^{-6} s^{-1}. No cracking observed.	Arilahti et al. /2000/
Ammonia	Aerated 0.06 mol·dm^{-3} ammonia, room temperature	–	OFP Cu (35–45 ppm P), 20% cold worked. Constant load, $K_I = 32$ MPa$\sqrt{m}$. No cracking observed, general dissolution.	Pettersson and Oskarsson /2000/
Ammonia	Bentonite equilibrated synthetic groundwater containing 0.5 mg/L ammonia	–	OF and OFP Cu (40 ppm Cu). SSRT, $4 \cdot 10^{-7}$ s^{-1}. No cracking observed at potentials between −0.10 and −0.25 V_{SCE}.	Rosborg /1998), Rosborg and Werme /2001/

[1)] FRAD, FIC, TR and SM refer to film-rupture/anodic-dissolution, film-induced cleavage, tarnish-rupture and surface-mobility mechanisms, respectively.

[2)] IGSCC and TGSCC denote intergranular and transgranular stress corrosion cracking, respectively.

Table 7-1(b). Stress corrosion cracking in acetate solutions.

Environment	Solution	Proposed Mechanism[1)]	Comments[2)]	Reference
Cupric acetate	0.025 mol·dm^{-3} Cu(II) acetate	TR	IGSCC due to rupture of Cu_2O film. Illumination inhibits tarnish growth and cracking.	Escalante and Kruger /1971/
Sodium acetate	0.1 mol·dm^{-3} acetate and conditions of pH and E under which oxide formed	FIC	TGSCC cleavage-like cracking believed to be induced by the rupture of a thin Cu_2O layer.	Cassagne et al. /1990/

[1)] FRAD, FIC, TR and SM refer to film-rupture/anodic-dissolution, film-induced cleavage, tarnish-rupture and surface-mobility mechanisms, respectively.

[2)] IGSCC and TGSCC denote intergranular and transgranular stress corrosion cracking, respectively.

Table 7-1(c). Stress corrosion cracking in nitrite solutions.

Environment	Solution	Proposed Mechanism[1)]	Comments[2)]	Reference
$NaNO_2$	Aerated 1.0 mol·dm^{-3} NO_2^- at E_{CORR}	FRAD	TGSCC during slow-strain experiments. Film rupture caused by deformation at slip steps.	Pednekar et al. /1979/
$NaNO_2$	Aerated 1.0 mol·dm^{-3} NO_2^- E = 0 V_{SCE}, 25–40°C	FIC	Sustained TGSCC only under conditions of dynamic strain. Cracking stopped within 10–20 μm under constant load conditions.	Sieradzki et al. /1984/
$NaNO_2$	Aerated 0.3 mol·dm^{-3} NO_2^- at 80°C, E_{CORR} (–0.05 V_{SCE}) and +0.10 V_{SCE}, OFHC Cu	–	TGSCC following initiation at grain boundaries. Fracture surfaces cleavage-like with evidence for crack arrest markings.	Aaltonen et al. /1984/
$NaNO_2$	Various NO_2^- concentrations (pH 9), E and T	FRAD or FIC	TGSCC following initiation at grain boundaries. Evidence for threshold E and NO_2^- concentration below which cracking does not occur. Activation energy for crack growth 21 kJ·mol^{-1}. Cleavage-like fracture surfaces with crack arrest markings.	Yu and Parkins /1987/
$NaNO_2$	0.001–1.0 mol·dm^{-3} NO_2^- concentration room temperature and 80°C and various E. OFHC and phosphorus-deoxidized Cu	FRAD or FIC	TGSCC. Evidence for threshold E and NO_2^- concentration, possibly associated with a minimum crack-tip current density of 0.1 mA·cm^{-2}. Lower susceptibility at 80°C. OFHC and PDO Cu behaved identically.	Benjamin et al. /1988/
$NaNO_2$	1.0 mol·dm^{-3} NO_2^-, pH 9, E between E_{CORR} (–0.07 V_{SCE}) and +0.05 V_{SCE}	FIC	TGSCC cleavage-like cracking believed to be induced by the rupture of a thin Cu_2O layer.	Cassagne et al. /1990/

continued …..

Table 7-1(c). Stress corrosion cracking in nitrite solutions (continued).

Environment	Solution	Proposed Mechanism[1)]	Comments[2)]	Reference
$NaNO_2$	1 mol·dm^{-3} NO_2^-, ~pH 7.5, 0 to +0.10 V_{SCE}	FRAD or TR	TGSCC. Maximum susceptibility at E corresponding to formation of Cu_2O film.	Uchida et al. /1991/
$NaNO_2$	Various NO_2^- concentrations, E and T	–	TGSCC of OF Cu (UNS C10200). Cracking observed at E_{CORR} at 23°C, but not at 90°C. Anodic polarization induced cracking at both temperatures.	Beavers and Durr /1992/
$NaNO_2$	0.3 mol·dm^{-3} $NaNO_2$, synthetic saline groundwater, pH 9.3, room temperature and 80°C, various E	–	OFP Cu, SSRT, $1.5 \cdot 10^{-8}$–$5 \cdot 10^{-6}$ s^{-1}, TG initiation and IG propagation, aim of study to demonstrate use of potential threshold approach to canister modelling.	Rosberg and Svensson /1994/
$NaNO_2$	Various NO_2^- concentrations at E_{CORR} in aerated pH 9.0 solution	–	TGSCC of OFE Cu using constant extension rate technique. Evidence for crack coalescence and discontinuous crack growth.	King and Litke /1997/
$NaNO_2$	0.1 mol·dm^{-3} $NaNO_2$ (pH 9.0), various oxidant fluxes	–	TGSCC of OFE and OFP Cu as a function of oxidant supply. Constant extension rate tests. Modelling of canister lifetimes based on oxidant supply to canister.	King et al. /1999b,c/
$NaNO_2$	Various NO_2^- concentrations (pH 9.0), various Cl^- concentrations	–	TGSCC of OFE Cu. Inhibitive effect of Cl^- at certain Cl^- concentration and NO_2^-:Cl^- concentration ratios. Constant extension rate technique.	King et al. /1999a/
$NaNO_2$	0.15–0.3 mol·dm^{-3}, aerated, room temperature and 80°C	–	OFP Cu (35–55 ppm P), annealed and 10–20% cold work, pre-cracked compact-tension specimens, constant load, various K_I, determined crack growth rate as a function of K_I, Cu_2O identified in crack, K_{ISCC} ~30 MPa$\sqrt{m}$	Pettersson and Oskarsson /2000/
$NaNO_2$	Deaerated 0.1 mol·dm^{-3}, pH 9, room temperature, galvanostatic control, Cl^- ion additions	FRAD	OFP Cu, base and electron-beam welded material, SSRT and constant load, pre-cracked compact-tension specimens. SCC susceptibility decreased with decreasing nitrite or increasing Cl^- concentrations, data consistent with threshold potential.	Ikeda and Litke /2000/
$NaNO_2$	0.3 mol·dm^{-3}, room temperature, potentiostatic control	–	OF and OFP Cu, SSRT, $4 \cdot 10^{-7}$ s^{-1}. Mixture of IGSCC and TGSCC observed. Reduction in ductility potential dependent. Evidence for threshold potential of –0.10 V_{SCE}.	Rosborg /1998/, Rosborg and Werme /2001/

[1)] FRAD, FIC, TR and SM refer to film-rupture/anodic-dissolution, film-induced cleavage, tarnish-rupture and surface-mobility mechanisms, respectively.

[2)] IGSCC and TGSCC denote intergranular and transgranular stress corrosion cracking, respectively.

a) Film-rupture/anodic–dissolution model

There are a number of variants of the film-rupture/anodic-dissolution model (e.g., the slip dissolution model), but in each one crack advance occurs by dissolution following the rupture of a protective film at the crack tip. Anodic dissolution at the crack tip is supported by cathodic reactions on the crack walls or on surfaces outside the crack. An important implication for the SCC of Cu canisters is that, if cracking occurs, it will stop once all the oxidant in the repository has been consumed. Thus, the probability of SCC is highest during the early oxidizing period in the evolution of vault conditions, gradually becoming less likely as conditions become more anoxic.

The FRAD mechanism has been proposed to account for the SCC of Cu in ammonia and nitrite solutions (tables 1(a) and 1(c)).

Theoretical expressions have been derived to predict the crack growth rate for the FRAD mechanism. Under rapid straining conditions the crack tip is maintained oxide-free at all times, and the crack grows continuously with a velocity (v) determined by the crack-tip anodic current density (i_{CT})

$$v = i_{CT} \frac{M}{zF\rho} \qquad 7\text{-}1$$

where M is the atomic mass of Cu, z is the valency of dissolved metal, F is the Faraday constant, and ρ is the density of Cu. If the crack-tip strain rate ($\dot{\varepsilon}_{CT}$) is slow, the crack tip periodically repassivates and the crack advances discontinuously at a rate given by

$$v = \frac{Q_F}{\varepsilon_C} \dot{\varepsilon}_{CT} \frac{M}{zF\rho} \qquad 7\text{-}2$$

where Q_F is the charge density corresponding to crack advance and ε_C is the critical strain for film rupture.

The impact of evolving repository conditions will be to either diminish the crack-tip current density (under high strain rate conditions and continuous crack growth) or to decrease the charge density at the crack tip between repassivation events (under slow strain rate conditions and discontinuous crack growth). Although the overall amount of oxygen in the repository may be limited (amounting to only 33 μm of corrosion, if distributed uniformly over the canister surface /Werme et al. 1992/), the crack-tip current density can be high because of the small surface area of the crack tip compared with the potentially large cathodic surface area.

b) Tarnish-rupture mechanism

The tarnish-rupture mechanism has long been associated with the SCC of Cu alloys because of the observation of SCC of Cu and brasses in so-called tarnishing ammonia solutions. The TR mechanism is slightly different from the FRAD mechanism in that crack advance occurs by rupture of the oxide, rather than by dissolution following oxide rupture. By inference, therefore, cracking is discontinuous and the rate of crack growth is limited to the rate of film growth. The TR mechanism has been proposed for all three SCC agents (table 7-1).

The crack velocity is given by

$$v = C\left(\frac{\dot{\varepsilon}_{CT}}{\varepsilon_C}\right)^{1/n} \qquad 7\text{-}3$$

where C and n are constants describing the kinetics of tarnish growth, with n = 2 for parabolic kinetics and n = 3 for a cubic growth law.

Crack growth requires oxidation of the Cu to form the oxide, and a corresponding supply of oxidant to support corrosion. Implicitly, therefore, the rate of crack growth for a Cu canister will decrease with time as the rate of oxide growth decreases with the evolution of the repository environment.

c) Film-induced cleavage model

In the FIC model, a crack initiates in a surface film and is projected into the underlying ductile metal, inducing a cleavage-like crack. Formation of the surface layer in which the crack initiates requires oxidation of the surface, but the overall size of each crack event is typically ~10 times the thickness of the initiating film. Thus, a relatively small amount of corrosion can lead to a relatively long crack. The FIC mechanism has been proposed for the SCC of Cu in ammonia and acetate environments (tables 1(a) and 1(b)), for which the initiating layers were either a nanoporous Cu layer or a thin Cu_2O film, respectively.

The crack velocity for a FIC mechanism is given by

$$v = (j + L)\left(\frac{\dot{\varepsilon}_{CT}}{\varepsilon_C}\right) \qquad 7\text{-}4$$

where j is the length of the cleavage crack and L is the thickness of the initiating film.

Whilst crack growth by an FIC mechanism also requires a supply of oxidant, and therefore should be limited as the repository becomes anoxic, relatively deep cracks could be produced from a small amount of corrosion because ~90% of the crack advance is not supported by a corresponding cathodic reaction.

For the FIC mechanism, as for the discontinuous FRAD (equation 7-2) and TR (equation 7-3) models, cracking may also cease if the crack-tip strain rate is negligible. This may occur on a canister after the outer Cu shell has deformed onto the inner cast-iron insert.

d) Surface-mobility model

The SM model is a relatively new mechanism, primarily proposed by one school of workers /Galvele 1987/. It has not gained wide acceptance, although it has been proposed for the SCC of brass.

Crack advance is a result of the removal of atoms (or the introduction of vacancies) at the crack tip due to surface diffusion. The crack velocity is given by

$$v = \frac{D_S}{L'}\left[\exp\left(\frac{\sigma \cdot b^3}{kT}\right) - 1\right] \qquad 7\text{-}5$$

where D_S is the surface self-diffusion coefficient, L' is the diffusion distance of the atoms (or vacancies), s is the elastic surface stress at the crack tip, b is the atomic size, k is Boltzmann's constant and T is the absolute temperature.

According to the SM model, the crack velocity is never zero, since D_S is always finite. This poses some problems for Cu canisters, since even small crack velocities could produce significant cracks over the timescales of interest. Surface oxidation (corrosion) increases the crack velocity by producing adatoms with higher surface diffusivities than that of the pure metal. There is no explicit relationship between the rate of oxidation and the crack velocity.

7.1.2 SCC of pure coppers

7.1.2.1 Environmental effects

There are a number of ways in which the repository environment will impact the SCC behaviour of the canisters. The four main influences of the environment are: (i) the presence of an SCC agent, (ii) redox conditions, (iii) the influx of Cl^- ions, and (iv) temperature.

SCC agents and redox conditions

The only three species known to cause the SCC of Cu are ammonia, acetate (OAc^-), and nitrite NO_2^- ions. Of these three species, SCC in ammonia has been known for the longest period of time. From a practical viewpoint, the SCC of Cu in ammonia most often occurs in thin moisture films formed on Cu surfaces in humid air containing ammonia vapour. One relevant example of the SCC of Cu in moist air occurred during the excavation of an underground nuclear waste research facility in Hungary, when SCC of Cu pipes carrying cooling water underwent SCC due to ammonia fumes produced from blasting operations /King and Litke, unpublished results, 1995/. Nitrite ions are not expected to be present in deep groundwaters and therefore, since there is no other means by which nitrite can be formed in a Swedish/Finnish repository, SCC of copper canisters by nitrite can be considered highly unlikely.

Various mechanisms have been proposed for the SCC of Cu in ammonia (table 7-1(a)). The FRAD mechanism has been proposed in both tarnishing and non-tarnishing environments, the only difference being that a **visible** oxide is formed in tarnishing solutions, since a Cu_2O oxide is undoubtedly formed at the crack tip in both environments. The actual oxidant in these systems is believed to be Cu(II)-NH_3 complexes (e.g., $Cu(NH_3)_5^{2+}$), rather than O_2. However, the presence of O_2 is a pre-requisite for SCC, since in practical examples Cu(II) is produced by the homogeneous oxidation of Cu(I) by O_2. Suzuki and Hisamatsu /1981/ proposed a tarnish-rupture mechanism to explain their observations. Under rapid dissolution conditions, Sieradzki and Kim /1992/ were able to generate a nanoporous etch-pitted layer, which they suggested induced cracking via an FIC mechanism.

The effect of ammonia concentration has been reported in a number of studies. Many studies have been conducted in concentrated (15 mol·dm^{-3}) ammonia solutions, since such concentrated electrolytes could be formed by the absorption of ammonia vapour in thin surface water films. Others have used the standard Mattsson's solution, comprising 1 mol·dm^{-3} ammonia at various pH values and using added Cu(II) as the oxidant. Sato and Nagata /1978/ report a systematic study of the effect of ammonia concentration, but failed to define an absolute threshold concentration, although the incidence of SCC at ammonia concentrations of 0.5 mg/L (3 x 10^{-5} mol·dm^{-3}) was much less than at higher concentrations. Suzuki and Hisamatsu /1981/ report that SCC only occurred at concentrations **below** 0.05 mol·dm^{-3}, but do not report a lower concentration limit. Pettersson and Oskarsson /2000/ did not observe SCC of OFP Cu during constant load tests on pre-cracked specimens in 0.06 mol·dm^{-3} ammonia. Neither did Arilahti et al. /2000/ during slow strain rate tests (SSRT) in deaerated synthetic saline and brackish Olkiluoto groundwater with between 1 and 100 mg/L ammonia (6 x 10^{-5} – 0.005 mol·dm^{-3}) at 80°C. Based mainly on the results of Sato and Nagata /1978/, Saario et al. /1999/ proposed a lower threshold ammonia concentration of ~0.5 mg/L. Rosborg /1998/ and Rosborg and Werme /2001/ reported no SCC of OFP Cu in a bentonite equilibrated synthetic groundwater containing 0.5 mg/L ammonia.

No systematic study has been performed on the effect of potential on the SCC of Cu in ammonia solutions. Based on the requirement to form a Cu_2O film, Saario et al. /1999/ argued that the minimum potential for cracking is given by the equilibrium potential for the reaction

$$2Cu + H_2O = Cu_2O + 2H^+ + 2e^- \qquad 7\text{-}6$$

which is equal to –0.002 V_{SHE} at pH 8 at 25°C and –0.11 V_{SHE} at the same pH at 80°C. These threshold potentials are consistent with the failure to observe SCC in ammonia-containing deaerated Olkiluoto groundwaters at 80°C, for which the E_{CORR} was in the range –0.35 to –0.46 V_{SHE} /Arilahti et al. 2000/. Pettersson and Oskarsson /2000/ failed to observe SCC in aerated 0.06 mol·dm^{-3} ammonia, even though the E_{CORR} value of ~0.15 V_{SHE} at room temperature was well above the threshold potential.

There is a limited amount of information in the literature on the SCC of Cu in OAc^- solutions (table 7-1(b)). Both tarnish-rupture and film-induced cleavage mechanisms have been proposed. There is no information available regarding the minimum [OAc^-] for cracking, although the threshold concentration, if there is one, must be below the concentration of 0.05 mol·dm^{-3} OAc^- (0.025 mol·dm^{-3} $Cu(OAc)_2$) used by Escalante and Kruger /1971/. The use of this solution implies that Cu(II) can act as an oxidant in support of cracking. Cassagne et al. /1990/ associated the onset of cracking with the formation of a Cu_2O film. As such, the pH and potential (E) dependence for SCC would be expected to follow that given above for reaction 7-6.

There is considerably more information available regarding the SCC of Cu in NO_2^- solutions (table 7-1(c)). Many of the reported studies in NO_2^- solutions have stemmed from the academic interest in the Cu/NO_2^- system and the mechanistic information it provides. In addition, a significant number of studies have been performed in connection with the use of Cu canisters. As in ammonia environments, however, there is no agreement on the mechanism of SCC.

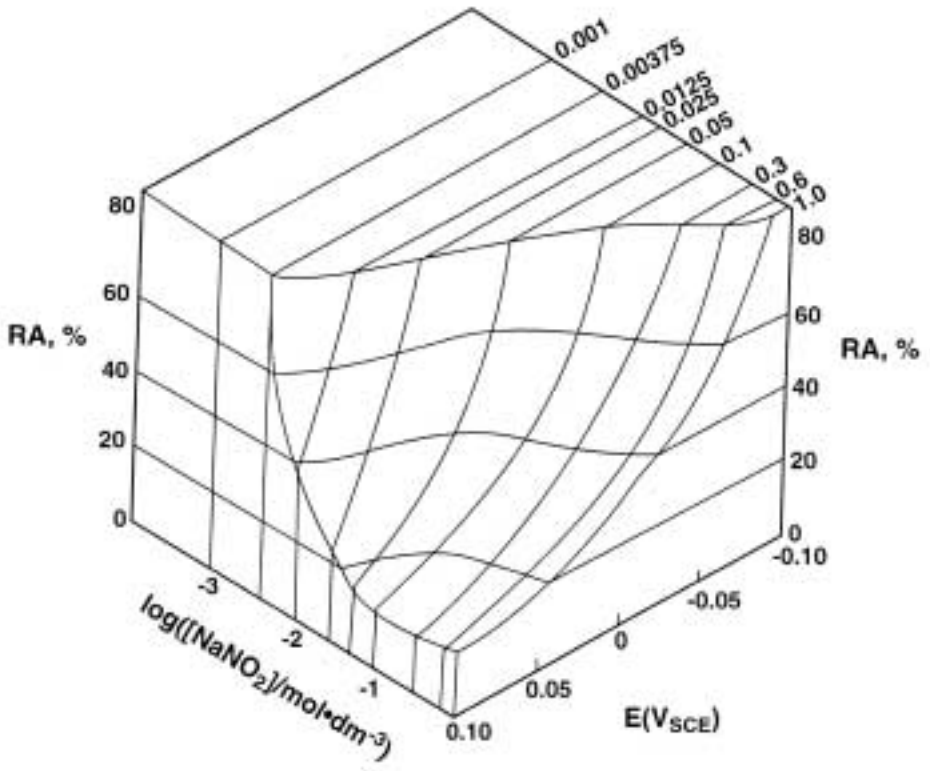

Figure 7-1. *Dependence of the percentage reduction in area (%RA) of smooth oxygen-free high-conductivity and phosphorus-deoxidized copper tensile specimens during slow strain testing in $NaNO_2$ solutions as a function of potential /Benjamin et al. 1988/. The data suggest a threshold nitrite concentration and a threshold potential below which SCC is not observed.*

The work of Benjamin et al. /1988/ and Yu and Parkins /1987/ identified threshold $[NO_2^-]$ and E below which SCC was not observed during short-term SSRT. Figure 7-1 shows the dependence of the ductility of oxygen-free high-conductivity (OFHC) and phosphorus-deoxidized (PDO) Cu in $NaNO_2$ solutions as a function of E and $[NO_2^-]$ at room temperature. The results suggest a threshold E of approximately –0.1 V_{SCE} and a threshold $[NO_2^-]$ of ~0.003 mol·dm^{-3} below which SCC was not observed. This threshold potential is supported by data from Yu and Parkins (figure 7-2), Rosborg and Svensson /1994/, Rosborg /1998/ and Rosborg and Werme /2001/. The E_{CORR} value in aerated solution is positive of this threshold potential, and SCC is observed under freely corroding conditions /Pednekar et al. 1979; Aaltonen et al. 1984; Cassagne et al. 1990/.

In Canada, studies have been performed under controlled current density conditions to simulate a given flux of oxidants to the canister surface /King and Litke 1997; King et al. 1999a,b,c; Ikeda and Litke 2000/. Constant extension rate (CERT) and constant load tests were performed on pre-cracked compact-tension specimens made from an oxygen-free Cu and from as-received and electron-beam welded OFP Cu. As expected, the crack growth rate decreased with decreasing current density, but not in a linear manner. Both annealed base metal and welded OFP Cu were susceptible to cracking. Cracking was inevitably observed under the aggressive CERT loading conditions, but was not observed in all constant-load tests. The potentials measured on the galvanostatically controlled samples were more positive than the threshold potential of –0.1 V_{SCE}.

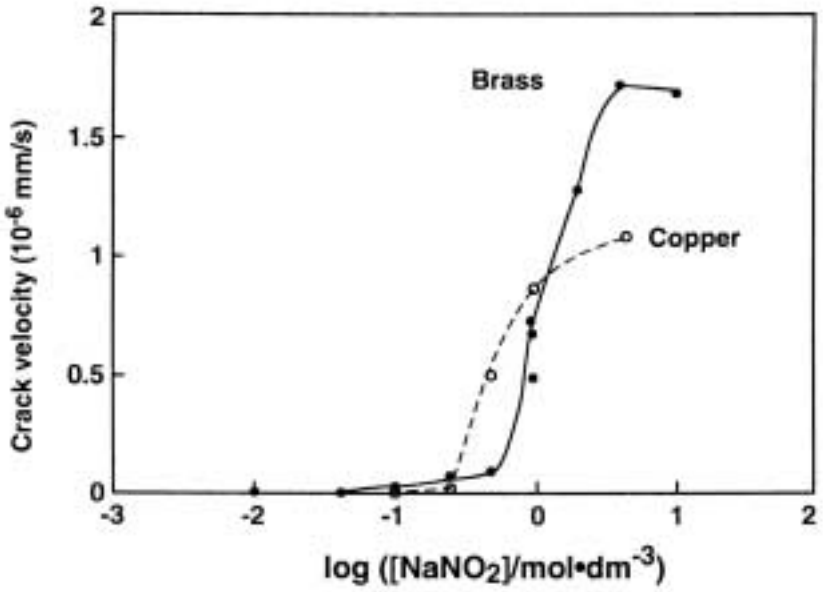

Figure 7-2(a). *Evidence for a threshold nitrite concentration. Potential of 0 V_{SCE} for Cu and –0.1 V_{SCE} for brass.*

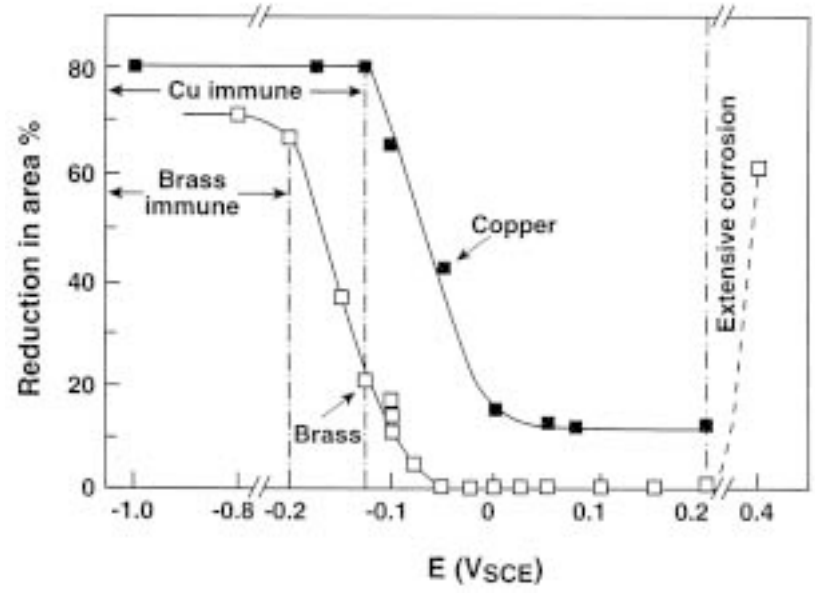

Figure 7-2(b). *Evidence for a threshold potential in pH 9, 1 mol· dm^{-3} $NaNO_2$.*

Figure 7-2. *Evidence for a threshold nitrite concentration and threshold potential for the stress corrosion cracking of copper and brass in $NaNO_2$ at room temperature /Yu and Parkins 1987/.*

Effect of chloride ions

Chloride ions diffusing into the repository from the groundwater will tend to promote general dissolution over localized corrosion of the canister. As a consequence, the possibility of SCC should diminish as the bentonite pore water in contact with the canister becomes more saline. The effects of Cl^- on the SCC behaviour of Cu have not been studied in detail, but some studies have been reported and information is also available from the effect of Cl^- on Cu_2O film stability and the competitive complexation of Cu(I) by Cl^- and NH_3.

Figure 7-3 shows the results of CERT tests with OFP Cu in 0.1 mol·dm^{-3} $NaNO_2$ with additions of varying amounts of Cl^- to the solution (data taken from King et al. /1999a/). The specimens were maintained at a constant current density (to simulate the flux of oxidant to the canister) and the corresponding potential recorded. The crack velocity was estimated from the extension of the fatigue pre-crack, but was not corrected for the extension due purely to ductile tearing (indicated in figure 7-3 by the horizontal line in air). The crack velocity decreases slightly with increasing [Cl^-] for chloride concentrations of up to 0.01 mol·dm^{-3}. At higher [Cl^-], the crack velocity falls to that in air (i.e., pure ductile tearing) and the measured potential drops by ~250 mV to more active values. Thus, the decrease in SCC susceptibility is a result of the shift from passive to active dissolution. Similar behaviour is observed with decreasing nitrite concentration in 0.01 mol·dm^{-3} chloride containing solution. In this case, the transition between passive and active potentials and from high to low crack growth rates occurs for a nitrite concentration between 0 mol·dm^{-3} and 10^{-3} mol·dm^{-3}. These results indicate that Cu canisters exposed to saline groundwaters will be less susceptible to SCC in nitrite solutions.

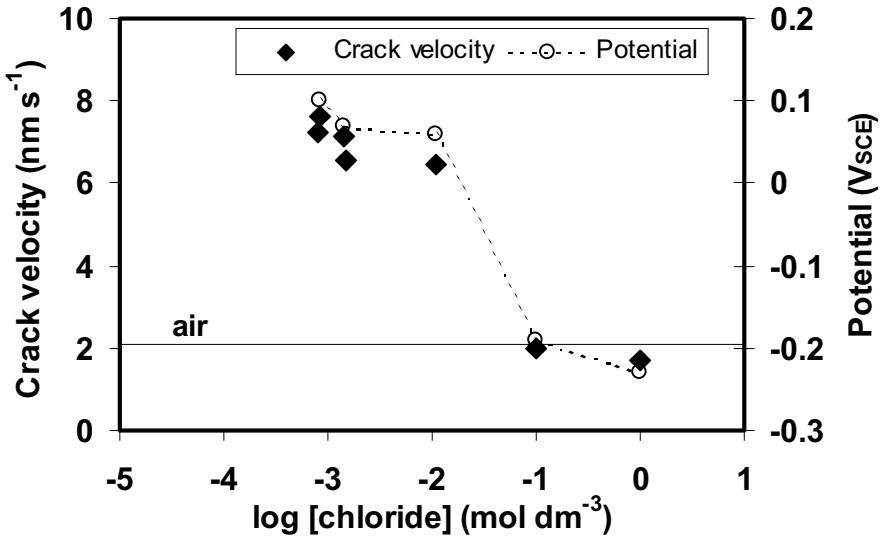

Figure 7-3. *Effect of chloride ion concentration on the crack velocity and potential of OFP copper specimens in 0.1 mol·dm^{-3} $NaNO_2$ at room temperature. The OFP specimens were maintained at a constant current density of 1 μA·cm^{-2} and the corresponding potential is shown in the figure. Crack velocities were estimated from surface crack extension rates, with the value determined in air corresponding to crack extension due to ductile tearing of the pre-cracked compact tension specimens.*

Similarly, Cl^- may be expected to inhibit the SCC of Cu in ammonia solutions. Arilahti et al. /2000/ observed no SCC of OFP Cu in deaerated Olkiluoto groundwaters at 100°C with between 1 and 100 mg/L ammonia, i.e., in excess of the threshold concentration of ~0.05 mg/L suggested by Saario et al. /1999/. The synthetic groundwaters contained either 3,700 mg/L (~0.1 mol·dm^{-3}) or 17,000 mg/L (~0.5 mol·dm^{-3}) Cl^-, and had a pH of ~7. Chloride ions will compete with NH_3 for the complexation of Cu(I) and will also inhibit Cu_2O film formation. King et al. /1999d/ report the effects of ammonia on the dissolution of Cu in Cl^- solutions and on Cu_2O film formation. At pH 7 at room temperature, Cl^- ions dominate the dissolution behaviour for ammonia concentrations <180 mg/L (<0.01 mol·dm^{-3}). The concentration at which the formation of $Cu(NH_3)_2^+$ becomes important decreases with increasing pH, because of the effect of pH on the speciation of dissolved ammonia (at room temperature, NH_3 predominates at pH values >9.25 /Tromans 1997/). At 100°C, the relative importance of Cl^- and NH_3 on the dissolution of Cu will depend on the temperature dependence of the stabilities of the respective complex ions and of the dissociation constant of NH_3/NH_4^+. Thus, the failure of Arilahti et al. /2000/ to observe cracking may have been a result of the competition between Cl^- and NH_3. In effect, at sufficiently high [Cl^-], the dissolution behaviour of Cu in Cl^-/ammonia mixtures is essentially the same as in Cl^--only solutions, in which SCC is not observed. This implies that the threshold ammonia concentration for SCC will be higher in saline groundwaters than in the ammonia solutions reported in the literature on which the threshold proposed by Saario et al. /1999/ was based.

Chloride ions may inhibit SCC of Cu in all three SCC environments (NO_2^-, OAc^-, and ammonia) because of the effect on the formation and stability of Cu_2O films. As discussed in more detail in section 6, Cl^- ions inhibit Cu_2O film formation by competing with OH^- ions for surface sites ($Cu(OH)_2$ is a precursor to Cu_2O formation). Furthermore, the incorporation of Cl^- ions into an existing Cu_2O layer (as may form on a canister surface prior to emplacement in the repository) increases the defect density of the oxide and tends to promote general dissolution over localized corrosion. A defected Cu_2O layer will be less protective, and, therefore, less likely to support SCC, than a Cu_2O film formed in Cl^--free environments. Although the effect of Cl^- ions on the stability of Cu_2O films has not been demonstrated for the SCC of pure Cu, there is substantial evidence that the inhibitive effect of Cl^- on the SCC of brass is due to an effect on the film stability /King 1996/.

Temperature

All available experimental evidence suggests that Cu becomes less susceptible to SCC with increasing temperature. Benjamin et al. /1988/ reported that the range of potentials over which SCC was observed for both OFHC and PDO Cu in aerated 0.6 mol·dm^{-3} $NaNO_2$ was narrower at 80°C than it was at 20°C. Under freely corroding conditions, this effect was most likely a result of the lower dissolved O_2 concentration in the open experimental vessel at the higher temperature. However, lower susceptibility was also observed at potentials away from the corrosion potential, suggesting a true effect of temperature on the SCC susceptibility. Beavers and Durr /1992/ also observed a beneficial effect of increased temperature on the SCC of oxygen-free Cu (UNS C10200) in $NaNO_2$ solutions. Transgranular cracking was observed at the open-circuit potential during slow strain rate testing in 0.005 mol·dm^{-3} and 1 mol·dm^{-3} nitrite solutions at 23°C, but not at 90°C.

In addition to lower susceptibility in nitrite solutions with increasing temperature, there is a large body of evidence to suggest that Cu is not susceptible to SCC in deep Fenno-Scandian groundwaters at elevated temperature. Aaltonen et al. /1984/, Benjamin et al. /1988/ and Rosborg and Svensson /1994/ all failed to observe SCC of Cu in natural and synthetic groundwaters at 80°C. Yunker /1990/ did not observe SCC of Cu alloys in irradiated J-13 water (a dilute synthetic groundwater based on conditions at the Yucca Mountain site in the U.S.) and moist air at either 95°C or 150°C. Beavers and Durr /1992/ failed to induce SCC in J-13 water or the vapour phase above it at 90°C. Comparable experiments at room temperature were not performed in either of these latter two studies.

The apparent decrease in SCC susceptibility with increasing temperature may be the result of several factors. First, in Cl^- solutions, increasing temperature promotes general dissolution of the surface resulting in negative shifts in E_{CORR}. A similar negative shift in E_{CORR} occurs in aerated nitrite solutions /Benjamin et al. 1988/. Second, there is some evidence to suggest that the range of potentials for SCC shifts to more positive values with increasing temperature. For example, in 0.6 $mol \cdot dm^{-3}$ $NaNO_2$, the threshold potential for SCC shifts from approximately –0.1 V_{SCE} at 20°C to ~+0.1 V_{SCE} at 80°C. This shift in threshold (and corrosion) potentials with temperature is sufficient to render OFHC and PDO Cu immune to SCC at E_{CORR} in aerated solution at 80°C, whereas cracking is observed at E_{CORR} at room temperature.

7.1.2.2 Effect of material properties

The material properties known to have an effect on the SCC of pure Cu are:
(i) phosphorus content and (ii) grain size. In addition, consideration must be given to possible differences between base metal and welded material.

There have been two systematic studies of the effect of P content of pure Cu on the SCC behaviour in ammonia environments /Thompson and Tracy 1949; Sato and Nagata 1978/. In both cases, tests were performed in moist atmospheres with ammonia vapour. Figure 7-4 shows the results from the two studies. Thompson and Tracy /1949/ report a ductility minimum at a P content of ~0.014 wt.% (140 ppm), with a measurable decrease in ductility for P contents as low as 40 ppm. These results are broadly in line with the later findings of Sato and Nagata /1978/, who found a threshold P content of between 50 and 80 ppm P. In contrast to these studies in ammonia environments, Benjamin et al. /1988/ found no difference between the behaviour of OFHC and PDO Cu (P content unknown) in a range of nitrite solutions and synthetic Swedish groundwater.

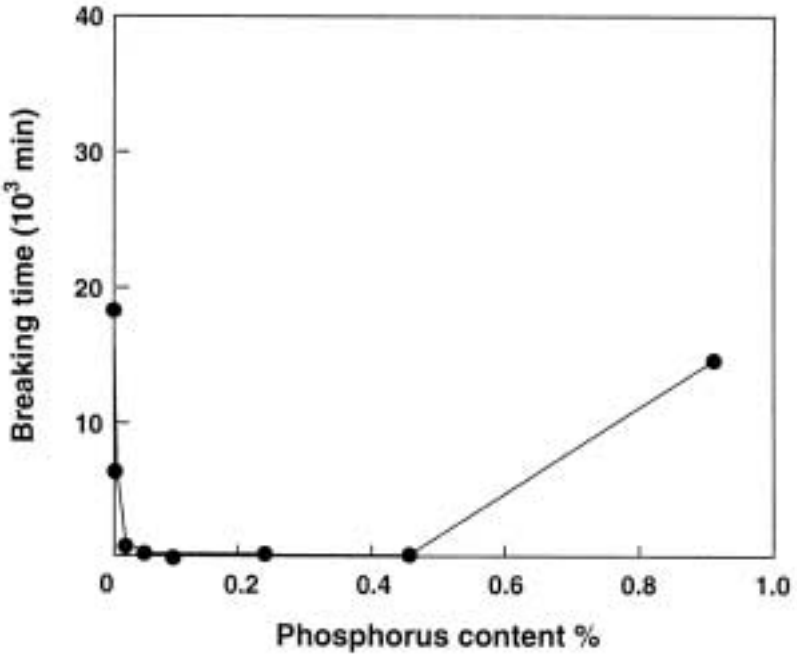

Figure 7-4(a). *Dependence of time-to-failure on P content /Thompson and Tracy 1949/.*

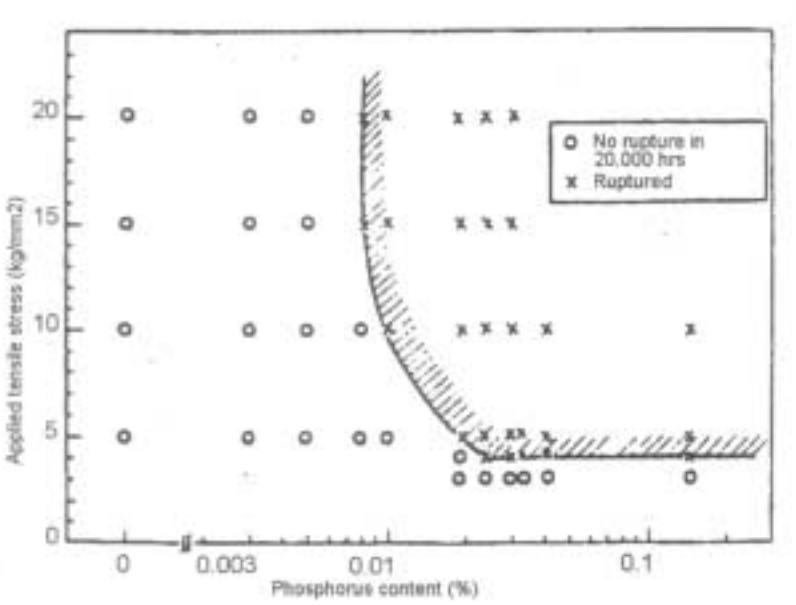

Figure 7-4(b). *Effect of P content and applied stress on SCC of Cu /Sato and Nagata 1978/.*

Figure 7-4. *Effect of phosphorus content on the SCC of copper in moist ammonia atmospheres.*

Grain size can affect both the initiation and propagation of SCC. In general, initiation of cracking is favoured by a smaller grain size /Yu et al. 1987/, whereas crack propagation is favoured by larger grains. Much of the evidence for the effect of grain size on the SCC of Cu alloys comes from studies on α-brass. The exception is the study of Sato and Nagata /1978/ in moist ammonia atmospheres. Figure 7-5(a) shows the dependence of failure time of Cu-300 ppm P tensile samples in a moist ammonia atmosphere for various applied stresses. The susceptibility increases with increasing grain size, suggesting that the effect of grain size on crack propagation outweighs the effect on crack initiation. Alloys with grain sizes of ~10 μm were relatively immune, but the susceptibility increased significantly for grain sizes of between 10 and 100 μm, and became relatively insensitive for larger grain sizes. A similar trend has been observed for α-brass (figure 7-5(b)), with a significant increase in susceptibility between grain sizes of 10 μm and 100 μm.

No study has yet shown a significant difference in the SCC behaviour of base metal and electron-beam (EB) welded OFP Cu. Arilahti et al. /2000/ did not observe cracking for either the base metal or EB-welded OFP Cu in deaerated synthetic Olkiluoto groundwaters with 1–100 mg/L ammonia at 100°C. The respective grain sizes of the base and welded materials were 190–260 μm and 260–430 μm. Thus, the grain size of both materials is within the range where no difference based on grain size would be expected (figure 7-5). Ikeda and Litke /2000/ report a lower stress intensity factor for crack growth (K_{ISCC}) for EB-welded OFP Cu than for the base metal, but reported similar crack growth rates for the two materials. Again, the grain size of the two materials were >250 μm.

Pettersson and Oskarsson /2000/ introduced various degrees of cold work to annealed OFP Cu samples and studied their SCC behaviour in nitrite solutions. The use of cold-worked material was partly for experimental convenience, as annealed samples suffered extensive plastic deformation. In SSRT experiments, samples with 20% cold work were marginally more susceptible than annealed specimens (13% elongation-to-failure for cold-worked material versus 15% for annealed), although the difference in the ductility in air was much greater (17% and 48% for the cold-worked and annealed material, respectively).

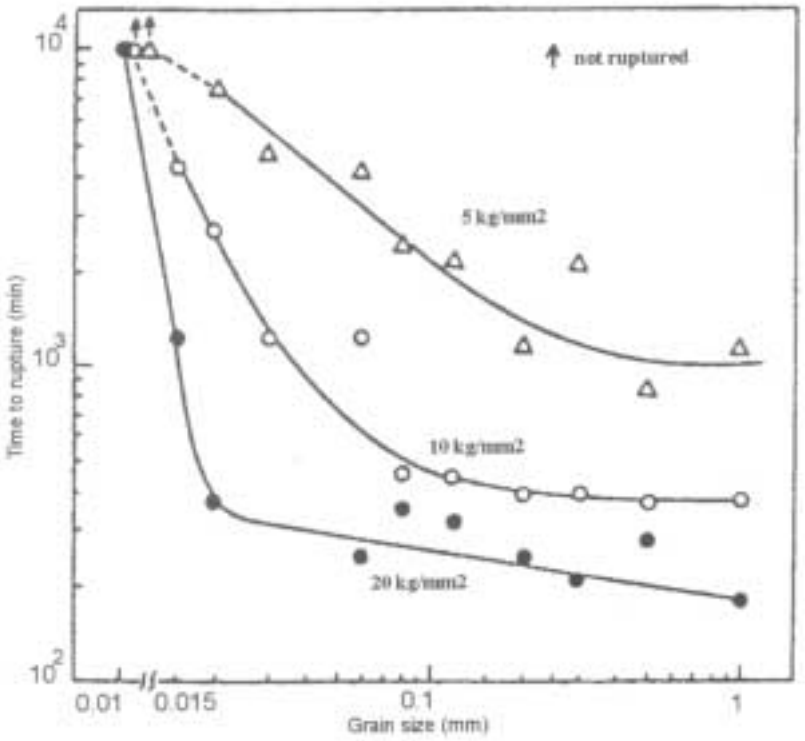

Figure 7-5(a). *Effect of grain size on the SCC of a Cu-300 ppm P alloy in moist air in contact with 49 mg/L ammonia /Sato and Nagata 1978/.*

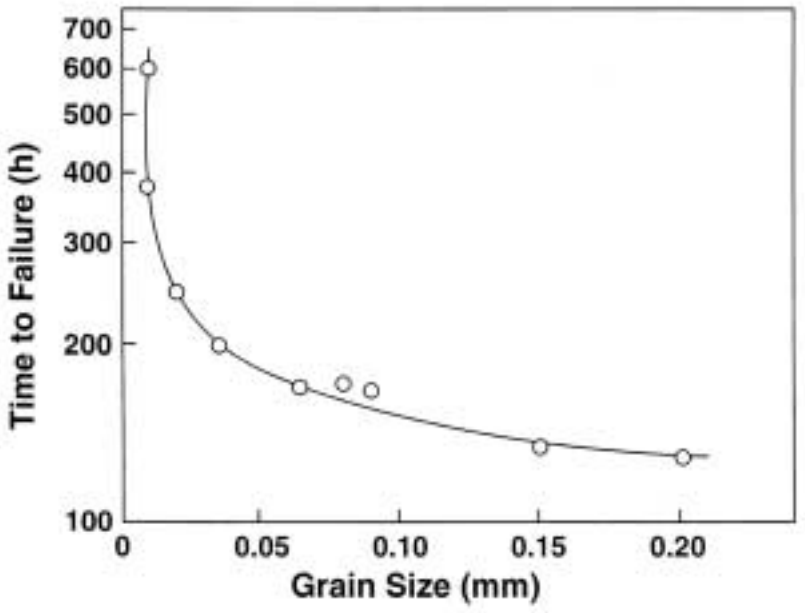

Figure 7-5(b). *Effect of grain size on the intergranular SCC of Cu-30Zn in moist ammonia atmospheres /Pugh et al. 1969/.*

Figure 7-5. *Effect of grain size on the SCC of copper alloys.*

7.1.2.3 Stress-related effects

Canisters will be subject to both applied stresses (from swelling of the buffer and from hydrostatic loading) and a residual stress (from the non-heat-treated final closure weld). Stress effects on SCC are usually reported in terms of the stress-dependence of crack initiation and crack growth or, for pre-cracked specimens, as a stress intensity factor. The applied stress, and the consequent strain, may affect both the cracking process(es) and/or result in creep of the material.

Pettersson and Oskarsson /2000/ reported the results of an on-going fracture-mechanics study of the SCC of OFP Cu. Figure 7-6(a) shows a schematic illustration of the dependence of crack velocity on stress intensity factor (K_I). In Region I, the crack velocity is a strong function of K_I. A threshold stress intensity factor (K_{Ith}) may exist, below which the crack velocity is truly zero. A more practical threshold value is the K_{ISCC}, which may be experimentally measurable. In Region II, crack growth is limited by non-mechanical factors (e.g., the environment), and in Region III mechanical overload occurs.

In Region I, the crack velocity (v) depends on K_I

$$v = C \cdot (K_I)^n \qquad 7\text{-}7$$

where C and n are constants. By fitting their data to this expression, Pettersson and Oskarsson /1997, 2000/ proposed that the crack growth rate in $NaNO_2$ solutions could be described by

$$v = 5.2 \times 10^{-24} (K_I)^{11} \qquad 7\text{-}8$$

where v is in $mm \cdot s^{-1}$ and K_I is in $MPa\sqrt{m}$. (Data from various sources, employing various nitrite concentrations and potentials were used to develop equation 7-8). Further studies have indicated an approximate K_{ISCC} value for cold-worked material of ~30 $MPa\sqrt{m}$ (figure 7-6(b)).

Conditional stress intensity factors for crack growth of annealed and EB-welded OFP Cu have been estimated in the Canadian programme. In this case, true stress intensities could not be calculated because the test-specimens were of sub-standard size, due primarily to the low yield strength of the material (as opposed to the cold-worked material used by Pettersson and Oskarsson /2000/). The parameter determined (K_Q) is the estimated stress intensity at which cracks started to grow during the constant extension rate tests of pre-cracked compact-tension specimens. For the base metal, an upper bound for K_{ISCC} was estimated of ~22 $MPa\sqrt{m}$. That of the EB-welded material was much lower, but this could have been an artifact due to the method used to estimate the load at which crack growth occurred and the much shorter elastic deformation range for the welded material /Ikeda and Litke 2000/. Reviewing the data of Hietanen et al. /1996/, King et al. /1999a/ and Pettersson and Oskarsson /2000/ in nitrite solutions, Rosborg and Werme /2001/ noted the difficulty in defining a K_{ISCC}, since the values reported in these various studies ranged from 16–30 $MPa\sqrt{\sqrt{m}}$.

On un-cracked specimens, the equivalent parameter is the threshold stress for crack initiation and/or growth. There have been relatively few reports of the threshold stress for the SCC of Cu and none in simulated repository conditions. Saario et al. /1999/ report a threshold stress of 120 MPa for Cu in 1 $mol \cdot dm^{-3}$ $NaNO_2$ at room temperature, and suggest a much smaller value (~40 MPa) in ammonia environments. This latter value comes from the study of Sato and Nagata /1978/, who studied the SCC of Cu-P alloys in moist ammonia atmospheres. For example, the results in figure 7-4(b) suggest a threshold load of ~3 $kg \cdot mm^{-2}$, equivalent to a stress of ~30 MPa.

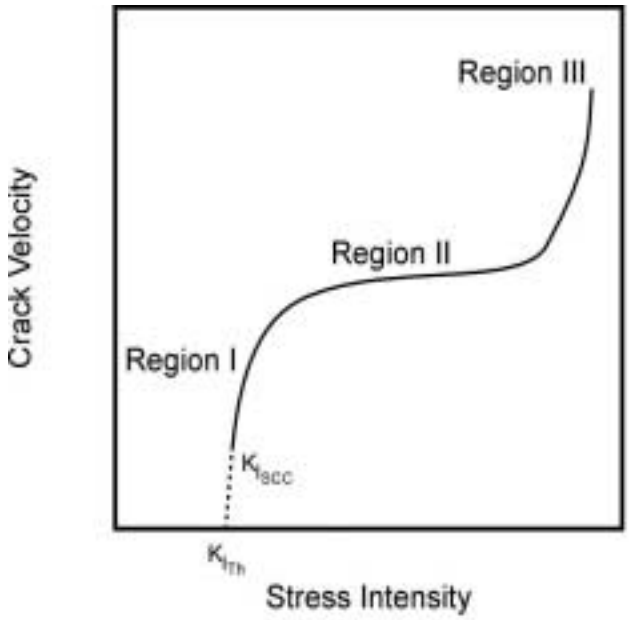

Figure 7-6(a). *Schematic illustration of the effect of stress intensity on crack growth.*

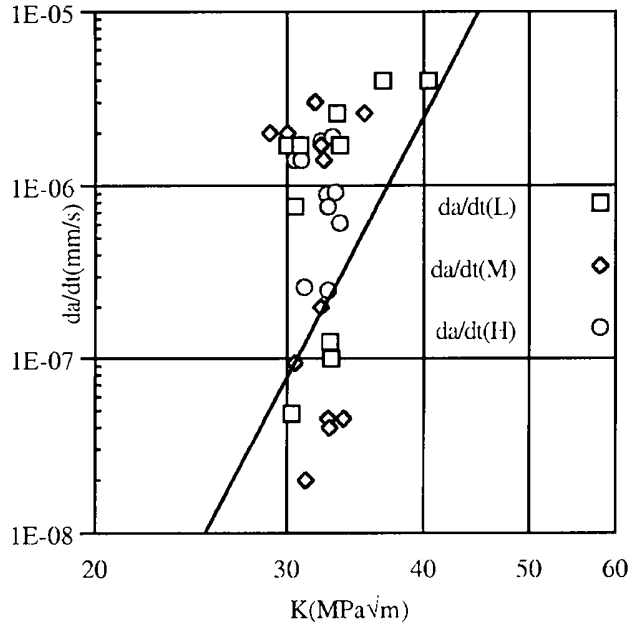

Figure 7-6(b). *Experimental measurements of the effect of stress intensity on crack growth for OFP copper in sodium nitrite solutions /Pettersson and Oskarsson 2000/.*

Figure 7-6. *Effect of stress intensity on SCC crack growth.*

The impact of the applied stress is to cause strain at the crack tip. This strain may have both detrimental and beneficial effects. Strain at the crack tip will rupture protective oxide films, or prevent their formation in the first place) (film-rupture/anodic dissolution and tarnish-rupture mechanisms, equations 7-2 and 7-3) or initiate cracks which then propagate into the underlying ductile material (the film-induced cleavage mechanism, equation 7-4). The theoretical crack growth expressions for each of these mechanisms suggest that the crack velocity will increase with crack-tip strain rate. This is indeed found to be the case, as reported by Benjamin et al. /1988/ and Yu and Parkins /1987/ for OFHC and PDO Cu in nitrite solutions, although Rosborg and Svensson /1994/ found cracking to be most evident at an intermediate strain rate in their tests in aerated 0.3 $mol \cdot dm^{-3}$ $NaNO_2$. This latter observation is consistent with a film-rupture/anodic-dissolution mechanism, for which the optimum balance between the crack-tip repassivation and film-rupture processes is established at an intermediate strain rate.

Strain at the crack tip may also be in the form of creep of the material. Although creep could rupture protective films at the crack tip, sustaining crack growth, it could also blunt cracks by relieving the stress at the crack tip. Stress relief through creep is more likely at higher temperatures. Creep of the Cu shell could be a significant factor, both in terms of the mechanical stability and the SCC behaviour of the canister. A number of creep studies have been performed on OFP Cu /Andersson et al. 1999; Henderson 1994; Henderson et al. 1992/, but no detailed analysis of the interaction of creep and SCC has been performed. There are indications, however, in the results of Pettersson and Oskarsson /2000/ that crack-tip creep will slow crack growth. In at least two of the reported tests, the crack growth rate under constant load conditions decreased with time, possibly as a result of creep at the crack tip.

7.1.2.4 Crack coalescence

Crack coalescence is a phenomenon in which multiple crack initiation occurs and the individual cracks join together once they have grown sufficiently that the tips of the surface cracks interact /Parkins and Singh 1990/. Crack coalescence usually leads to faster effective crack growth rates, since small individual cracks can join together to produce a larger, more significant, crack. However, multiple crack initiation can also be beneficial, since cracks will shield each other from the applied stress and, in an oxidant-limited environment, the growth of many small cracks is preferable to the growth of a small number of deep cracks.

There have been few studies of crack coalescence for Cu alloys. Multiple crack initiation has been observed for OFP Cu, as indicated by the characteristic change in direction of interacting crack tips /figure 7-7, King et al. 1999c/. Various stages of cracking can be seen in figure 7-7, ranging from coalesced multiple cracks, to individual cracks, to faint pre-cursor cracks at the crack tip, believed to be emergent slip planes, from which cracks initiate. Pettersson and Oskarsson /2000/ reported seeing “jumps” in the growth of the crack, which they attributed to crack tunneling ahead of the crack tip and rupture of the resultant ligament.

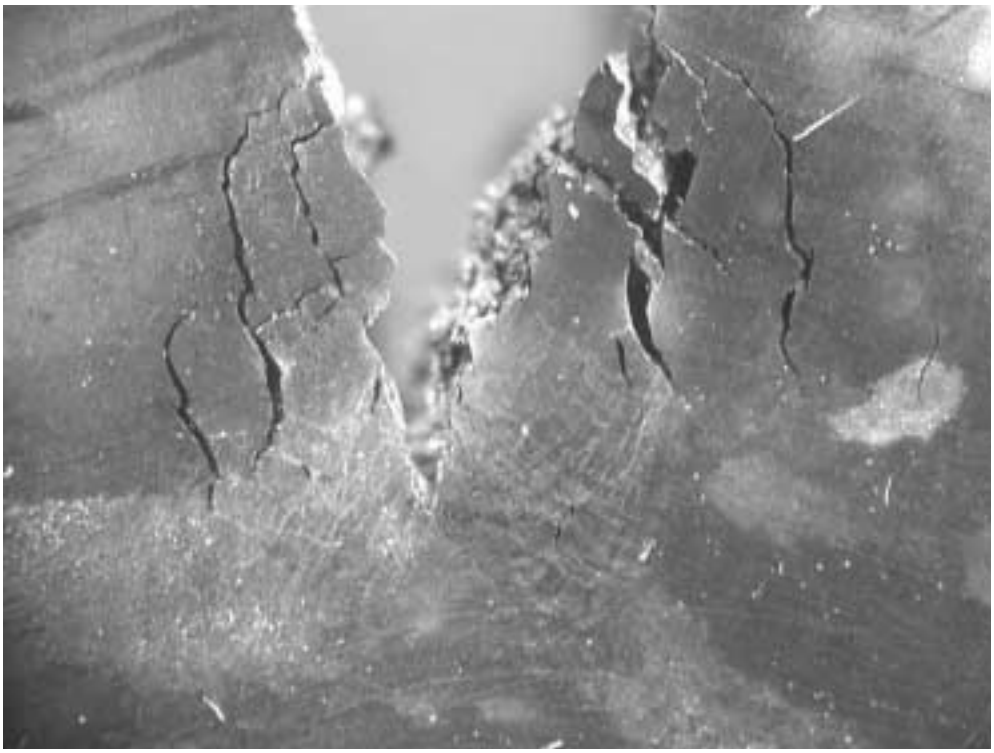

Figure *7-7. Evidence for multiple crack initiation and crack coalescence on OFP sample subject to constant extension rate testing in 0.1 mol·dm^{-3} $NaNO_2$ /King et al. 1999c/.*

7.2 Approaches to predicting the SCC behaviour of copper canisters

7.2.1 General approaches to predicting the SCC of copper canisters

Two broad approaches have been taken to predict the SCC behaviour of Cu canisters. The first is that there exist threshold values for various environmental, material and mechanical parameters, below which the crack growth rate is zero. The other approach has been to assume that the crack growth rate is always finite, but that it is so small that failure of the canister by SCC does not occur within the required lifetime. There are advantages and disadvantages to each approach.

An example of the threshold approach is that proposed by Saario et al. /1999/, in which various "boundary conditions" were defined for the SCC of Cu in nitrite and ammonia environments. For example, threshold potentials for SCC can be defined based either on experimental data or on thermodynamically calculated potentials for the formation of the requisite Cu_2O film. Threshold concentrations (particularly for nitrite) and stresses can also be defined. The true threshold stress intensity factor (K_{Ith}, figure 7-6(a)) can also be used to define conditions under which the crack growth rate is zero.

The advantage of the "threshold" approach is that it defines an absolute set of conditions under which SCC will not occur. The disadvantage of this approach is that the threshold values may need to be determined over a wide range of conditions, and it is difficult to guarantee that the crack growth rate is zero. For instance, it is currently impossible to measure crack velocities of less than ~10^{-9} mm·s^{-1}. However, a crack growing at this rate

would penetrate a 50-mm-thick canister in <1,600 years. Thus, if threshold values are to be used, they must be soundly based on mechanistic principles (e.g., the potential at which a Cu_2O film grows), and should be used with a suitable margin of safety (e.g., E_{CORR} should be a minimum of X volts below the threshold potential). Long-term exposure tests can be used to support lifetime predictions based on this approach.

In the alternative approach, the crack growth rate is measured under accelerated conditions, from which predictions are made about the crack growth rate for the canister using suitable extrapolation techniques. Pettersson and Oskarsson /2000/ have proposed such an approach, based on fracture-mechanics principles (figure 7-6(a)). A similar "limited-propagation" model has also been proposed in Canada /King and Litke 1997/, in which the crack growth rate is estimated as a function of the evolving conditions in the repository.

The advantages of the limited-propagation approach are that it (i) avoids the problems associated with defining threshold parameters and (ii) tends to provide a conservative assessment. The disadvantages are that long extrapolations may be required because tests must be greatly accelerated in order to measure crack growth rates, and that as a consequence, the predictions may be too conservative. Extrapolation of experimental data is aided by the use of mechanistic models which provide a basis for the extrapolation.

7.2.2 Specific approaches to predicting the SCC of copper canisters

Various approaches have been taken towards, or proposed for, the prediction of the long-term SCC behaviour of Cu canisters. Here, the various approaches are categorized according to the three pre-requisites for SCC: a suitable environment, a susceptible material, and an appropriate tensile stress.

7.2.2.1 Approaches based on the repository environment

Since more is known about the effect of environmental parameters on the SCC of Cu, the majority of attempts at predicting the long-term behaviour of copper canisters have been based on the environmental conditions in the repository. Of the two general approaches to predicting SCC discussed above, most of the assessments performed to date have involved the concept of one or more threshold environmental conditions.

An important consideration when making predictions of the long-term SCC behaviour is the evolution of environmental conditions in the repository. Since all SCC mechanisms involve some degree of oxidation of the metal (apart from the intrinsic susceptibility of the surface-mobility model), the probability of SCC will diminish with time as conditions become anoxic. Thus, as with other forms of localized and general corrosion (see section 6), SCC should be a relatively short-term phenomenon. As a consequence, what seems at first to be a formidable task of guaranteeing that a Cu canister will not fail by SCC over a period of at least 100,000 years simplifies into one of demonstrating that SCC will not cause canister failure over a much shorter time period of, perhaps, a few hundred years.

Saario et al. /1999/ are developing an SCC model based on the concept of threshold parameters (or boundary conditions /Saario et al. 1999/) for SCC. Thus, a threshold concentration and critical potential (E_{SCC}) are defined for each SCC agent (NO_2^-, OAc^-, and ammonia). Then, provided the concentration of these species at the canister surface and the canister corrosion potential are below the respective threshold values, SCC will

not occur. As discussed below, with currently available data, this approach has shown that SCC due to NO_2^- will not occur in a Finnish/Swedish repository, and that cracking by ammonia and acetate is unlikely (although more experimental data are being collected for these latter two species).

Threshold concentrations and E_{SCC} values have been estimated based on a survey of the available literature and theoretical considerations. Based primarily on the studies of Parkins and co-workers /Benjamin et al. 1988; Yu and Parkins 1987/, the threshold NO_2^- concentration for the SCC of pure Cu alloys is ~0.001 mol·dm^{-3} (equivalent to 46 mg/L NO_2^-). From the same studies, confirmed subsequently by others /Saario et al. 1999/, E_{SCC} in nitrite environments is ~0.1 V_{SHE} (–0.14 V_{SCE}). In comparison, the **maximum** nitrite concentration in deep Finnish groundwaters is ~0.01 mg/L. Since there is no other source of nitrite in the repository, it can be concluded that nitrite-induced SCC of Cu canisters will not occur. In addition, the long-term redox conditions in the groundwater (E_H of –0.2 to –0.3 V_{SHE} /Anttila et al. 1999a/) are more-negative than E_{SCC}. (The thermodynamic redox potential represents the maximum value of E_{CORR}).

The situation for acetate and ammonia is less definitive, and additional experimental studies are in progress to confirm that SCC of Cu canisters will not occur. For acetate, there are no literature data available to define a threshold concentration for SCC, although the requirement for the presence of a Cu_2O film /Cassagne et al. 1990/ suggests that E_{SCC} is equivalent to the equilibrium potential for Cu_2O formation (i.e., equation 7-6). For ammonia, the most thorough study of the effect of concentration on the SCC of Cu is the study of Sato and Nagata /1978/ in moist ammonia atmospheres. Although a threshold ammonia concentration of ~0.5 mg/L can be inferred from their study, the actual concentration in the thin moisture film on the Cu surfaces could have been much higher. In comparison, maximum ammonia concentrations of between 1 and 3 mg/L have been found in deep Finnish groundwaters /Anttila et al. 1999a,b/. Thus, it is not possible to exclude the possibility of ammonia-induced SCC based on the threshold value of ~0.5 mg/L from Sato and Nagata /1978/ (assuming, conservatively, that the surface concentration of ammonia in these experiments was the same as that in the ammonia solution used to saturate the atmosphere). Based on the assumption that a Cu_2O film is necessary for SCC in ammonia environments, E_{SCC} can be equated to the equilibrium potential for reaction 7-6, i.e., –0.002 V_{SHE} at pH 8 at room temperature and –0.11 V_{SCE} at 80°C and pH 8 /Saario et al. 1999/.

To determine whether SCC would occur in deep Finnish groundwaters, Arilahti et al. /2000/ performed a series of SSRT in synthetic Olkiluoto groundwaters at 100°C with additions of between 1 and 100 mg/L ammonia. Both base metal and EB-welded OFP (45 ppm P) were tested. The deaerated groundwaters contained either 3,700 mg/L or 17,000 mg/L Cl^- ions and ~1 mg/L sulphide (TDS of ~8,300 mg/L and ~30,000 mg/L, respectively). The estimated pH of the solution at the experimental temperature of 100°C was ~pH 7.

No SCC was observed in either groundwater for either material, regardless of the ammonia concentration. Based on the elongation-to-failure and fractography, the samples suffered purely ductile failure, with no evidence for brittle environmentally assisted cracking. The measured corrosion potentials were in the range –0.35 to –0.46 V_{SHE}, i.e., significantly more negative than the E_{SCC} value of approximately –0.03 V_{SHE} at pH 7 and 100°C, predicted from equation 7-6. These results provide strong support for the argument that Cu canisters will not be subject to SCC in ammonia-containing groundwaters under long-term anoxic conditions.

The approach being taken in Canada is to argue that the necessary environmental conditions for SCC will not persist for a sufficient period of time, if at all, to cause failure of the canister by SCC. The environmental parameters being considered are: (i) the concentration of SCC agent (NO_2^-, OAc^-, and ammonia) at the canister surface, (ii) redox conditions in the buffer material and the supply of oxidant, (iii) the influx of Cl^- ions from the groundwater, and (iv) the canister surface temperature. With the exception of the decrease in temperature, the evolution of environmental conditions will result in a decrease in the probability of SCC with time.

This approach can be used in conjunction with either the concept of threshold conditions for SCC or for the limited-propagation argument. In both cases, the time dependence of the various environmental parameters and of the E_{CORR} of the canister will be estimated. Then, comparison of the time-dependent E_{CORR} and/or of the interfacial concentration of SCC agents with the respective threshold values can be used to determine if SCC is possible. Alternatively, the predicted E_{CORR} and environmental parameters can be combined with a suitable extrapolation of crack growth rate measurements obtained under accelerated conditions to predict the maximum extent of crack growth for a canister.

To date, the only prediction made in Canada has been based on the limited-propagation approach. Crack growth rate measurements as a function of anodic current density (to simulate various oxidant fluxes) were combined with the predicted time-dependent corrosion current density for a canister in a repository /Johnson et al. 1996/, to predict the time dependence of the crack growth rate /King et al. 1999a,b,c/. The experimental crack growth measurements were made in 0.1 $mol \cdot dm^{-3}$ $NaNO_2$ (pH 9) at room temperature under constant extension rate conditions. A linear dependence of crack growth rate on the oxidant flux was assumed, which would be consistent with a film-rupture/anodic-dissolution, tarnish-rupture or film-induced cleavage mechanisms, although it is not necessary to know the SCC mechanism in order to make the extrapolation. Figure 7-8(a) shows a comparison between measured crack velocities and those calculated based on these three mechanisms (and for four different crack-tip:cathode surface area ratios for the film-rupture/anodic-dissolution mechanism). The theoretical dependence for the film-rupture/anodic-dissolution mechanism was then used to predict the time-dependent crack velocity for a Cu canister in a repository, based on the predicted time dependence of the corrosion current density (figure 7-8(b), also see section 6). Integrating the time-crack velocity curves in figure 7-8(b) gives predicted maximum crack depths of between 11 μm and 11 mm for anodic:cathodic surface area ratios of 1 (general corrosion) and 1,000, respectively /King et al. 1999a,b,c/. It is interesting to note that the crack velocity is predicted to decrease (but not to fall to zero) as the O_2 trapped in the buffer material surrounding the canister is consumed.

These predictions are considered to be very conservative. The prediction is based only on the rate of supply of oxidant (which is assumed to limit the rate of cracking), and implicitly assumes that the canister is exposed continuously to 0.1 $mol \cdot dm^{-3}$ $NaNO_2$ environment, and that the canister shell is being constantly strained (since the data in figure 7-8(a) were obtained from CERT). In addition, the inhibitive effects of Cl^- ions, apparent from the data in figure 7-3, were not taken into account. Furthermore, the predicted E_{CORR} (figure 6-13) is at least 50 mV more negative than the threshold potential for SCC in nitrite solutions proposed by Saario et al. /1999/ of –0.14 V_{SCE}. Thus, according to the threshold potential approach, the canister should not be susceptible to SCC at all (although the predicted E_{CORR} in figure 6-13 does not include the effect of nitrite, which would be expected to result in more positive E_{CORR} values).

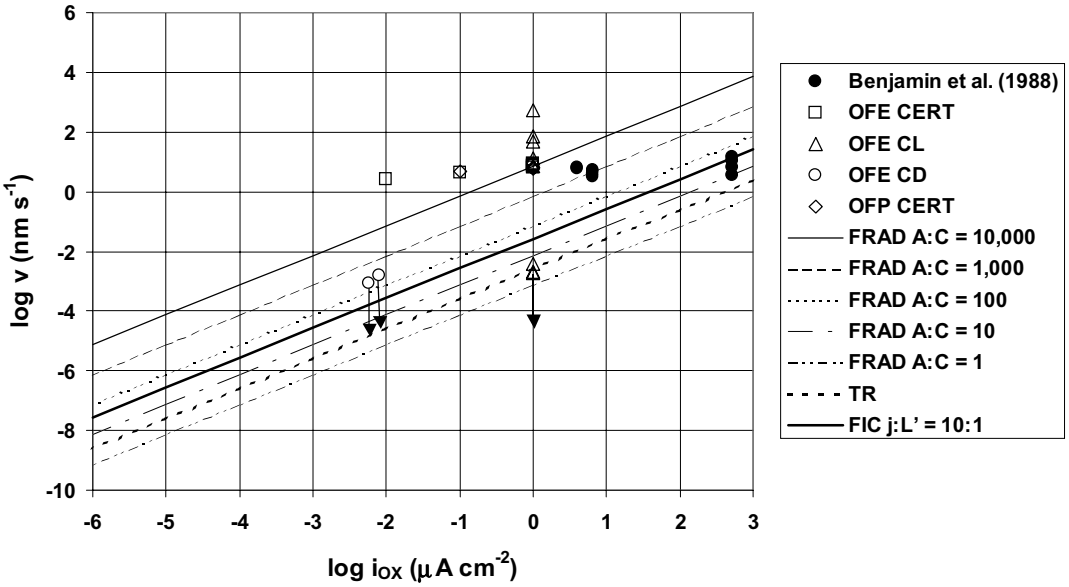

Figure 7-8(a). *Comparison of the dependence of measured and predicted crack velocities in $NaNO_2$ solution on current density for various SCC mechanisms.*

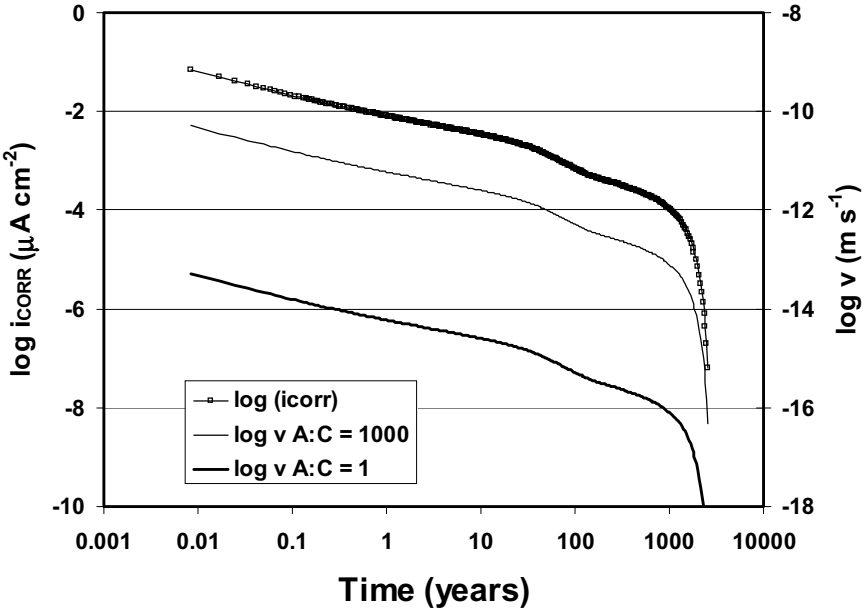

Figure 7-8(b). *Predicted time dependence of the crack velocity of a copper canister in a Canadian repository based on the predicted corrosion current density and assuming crack growth by a film-rupture/anodic-dissolution mechanism.*

Figure 7-8. *Prediction of the time dependence of the SCC crack velocity in a Canadian repository based only on oxidant transport limitation /King et al. 1999a,b,c/.*

Further developments of this approach are planned /King 2001/. Future versions of the model will include the prediction of the time-dependent concentration of NO_2^-, OAc^-, and ammonia in the repository as a result of construction activities, gas-phase radiolysis, and microbial activity (which is possible in a Canadian repository because of the use of a lower density sand:clay buffer material).

7.2.2.2 Approaches based on the canister material

There has been no attempt to argue that SCC of Cu canisters will either not occur or will be limited in extent based on the properties of the canister material. Based on the P content and grain size of the proposed alloy, it is difficult to claim that the canister would be immune to SCC. For example, the proposed P content of 30–80 ppm exceeds the threshold P contents for SCC in ammonia environments reported by both Thompson and Tracy /1949/ and Sato and Nagata /1978/ (figure 7-4). In addition, the possibility of large grain sizes in the annealed canister shell and as a consequence of EB welding also renders the material susceptible to SCC (figure 7-5).

7.2.2.3 Approaches based on the effect of stress

Several stress-related arguments can be made regarding the susceptibility of Cu canisters to SCC. These arguments include: (i) the existence of a threshold stress for SCC, (ii) crack exhaustion due to compressive stresses in the canister wall, (iii) the detection of sub-critical flaws based on fracture mechanics principles, (iv) the time dependence of the crack-tip strain rate, and (v) the effect of creep on stress relaxation.

There is relatively little information available regarding the threshold stress for SCC of Cu in relevant environments. Only two values were reported by Saario et al. /1999/ (140 MPa in 1 mol·dm^{-3} $NaNO_2$ at room temperature, and ~40 MPa in moist ammonia atmospheres). It is likely that the outer Cu shell will undergo some plastic deformation, making it difficult to claim that the sum of the applied and residual stresses will not exceed the threshold stress for SCC.

Saario et al. /1999/ have suggested that a propagating crack will stop growing because of compressive stresses in the Cu shell. Whilst it is true that the tensile and compressive stresses must be balanced through the canister wall, the actual distribution of stresses is difficult to predict and may change with time in response to deformation of the Cu shell. Therefore, no attempt has been made to argue that SCC will be limited by the presence of compressive stresses in the canister wall.

Based on their crack growth rate measurements as a function of stress intensity factor, Pettersson and Oskarsson /1997/ were able to predict the size of the deepest sub-critical defect that would lead to canister failure within a given period of time. These authors used the limited-propagation approach, rather than rely on a threshold stress intensity factor for SCC (K_{ISCC}), even though their own data could be used to estimate a K_{ISCC} value. Pettersson and Oskarsson used an "acceptable" crack growth rate of 3×10^{-12} mm·s^{-1} (equivalent to ~10 mm crack growth in 100,000 years) and equation 7-8 to estimate a stress intensity factor of 12 MPa$\sqrt{m}$ that could not be exceeded on the canister surface. For an assumed maximum tensile stress of 100 MPa, this stress intensity factor corresponds to a maximum allowable defect size of ~5 mm. It was argued that such a deep defect was readily detectable by inspection, so that the maximum crack depth after 100,000 years would be <10 mm.

Recently, Rosborg and Werme /2001/ have reviewed all the available data relating the crack velocity to K_I Given the wide range of K_{ISCC} values estimated from the various studies (16–30 MPa√m), they concluded that predicting the long-term SCC behaviour based on the existence of a threshold K_I for SCC would be difficult.

A stress-based argument proposed in the Canadian program, but not developed further to date, is that the period of crack-tip strain will be limited. Crack-tip strain (or stress, in the case of the surface mobility model) is a crucial factor in supporting crack growth for all SCC mechanisms (equations 7-2 to 7-5). If an inner steel or iron structural member is used to support the external load (as in the Swedish/Finnish canister design), strain of the outer Cu shell is only possible until such time that the initial 1.75 mm gap between the inner and outer canister components /Werme 2000/ is closed by deformation of the Cu shell. Once the gap has been closed, deformation of the Cu shell will only be possible by creep. Thus, the strain (deformation) rate of the Cu shell, and, hence, also at the tip of any crack in the shell, will be high initially as the hydrostatic load increases, but will then diminish considerably after the collapse of the shell onto the inner cast iron load-bearing member. It might be possible to argue, therefore, especially in conjunction with other limiting factors such as the supply of oxidant or SCC agent to the canister surface, that SCC will either not occur or will do so for such a short time that the canister will not fail. A model for predicting the time dependence of the crack-tip strain rate for a canister in a repository has not been developed.

The final stress-related argument against the SCC of a Cu canister is based on the creep behaviour of the Cu shell. Creep is a result of tensile stress and serves to relieve the stress through deformation of the material. One of the prime requirements for specification of the material for the outer Cu shell is that it should have suitable creep properties, both the creep rate and the creep failure strain. Much work has gone into the specification of a suitable alloy composition /Andersson et al. 1999; Henderson 1994; Henderson et al. 1992/. The crack growth rate under possible repository conditions will be so slow that creep processes will relieve crack-tip stresses before crack growth can occur. In this way, creep of the Cu shell will preclude any possible SCC.

7.3 Summary of the stress corrosion cracking of copper canisters

As stated at the beginning of this section, there is extensive experience with, and knowledge of, the SCC of Cu alloys. Considerable effort has gone into studying the mechanism of SCC of Cu alloys. For these reasons, it is unlikely that any species other than those already identified will cause the SCC of Cu canisters.

As with other forms of corrosion, the probability of SCC of a Cu canister will diminish with time as the repository environment evolves. Because of this, the difficult task of predicting the SCC behaviour of components with design lifetimes of the order of 100,000 years is reduced to a simpler task of predicting the SCC behaviour over the much shorter duration of aggressive conditions (perhaps of the order of tens to hundreds of years). Early in the evolution of the repository, conditions may be at their most suitable for SCC. Oxidant will be available in the form of trapped atmospheric O_2 and/or Cu(II) produced by corrosion of the canister. Ammonia, and possibly acetate ions, will be present in the groundwater and, possibly as a result of human activity during construction /Saario et al. 1999/, although it is highly unlikely that sufficient nitrite will be present to cause SCC. Furthermore, the beneficial effects of Cl^- ions will not be fully felt until the bentonite pore water has equilibrated with the groundwater. During this

early period, the outer Cu shell may also be subject to considerable strain as the hydrostatic load develops and the Cu shell is deformed onto the inner cast iron insert. As the available oxidant is consumed, as the pore water becomes more saline, and as the buffer material saturates and restricts the transport of SCC agents from the groundwater to the canister surface, the probability of SCC will diminish considerably. Only the decrease in repository temperature with time will tend to render the canister more susceptible to SCC. The period of highest SCC susceptibility is not known with certainty, but is likely to be of the order of tens or hundreds of years. Thus, valuable supporting evidence that the canister will not be subject to SCC can be obtained from long-term exposure tests under realistic repository conditions, as are currently under way at the Äspö Hard Rock Laboratory.

Further work on the SCC of copper canisters could include (section 10): measurement and prediction of E_{CORR} values in highly compacted bentonite and in a repository, and the effect of acetate and ammonia on the SCC of copper. Other studies that may also be valuable include: studies of the distribution of tensile stress on a canister, and information about the effect of welds on the SCC of OF Cu.

8 Corrosion induced by radiation effects

The corrosion environment will be determined by the groundwater chemistry at the disposal site and the chemical properties of the buffer and backfill. In addition to these factors, the near field environment will, for the first few hundred years after disposal, also be influenced by the γ-radiation field outside the canister. The radiation is dominated by the decay of ^{137}Cs, which has a half-life of 30 years. With the canister design proposed by SKB and Posiva, the surface dose rate immediately after encapsulation is about 0.5 Gy/h. With the half-life of 30 years, the dose rate will have dropped to negligible levels after a few hundred years.

The main effect of γ-radiation on the corrosion behaviour of the copper canister will be through radiolysis of the gases and the aqueous solutions that are present close to the canister surface. Radiolysis will produce oxidizing and reducing radicals and molecular species. In pure water, the oxidizing species are radicals like OH and molecular species like O_2, H_2O_2 and O_2^-. The reducing species will include H, e_{aq}^- and H_2. In a closed system, a steady state will develop rapidly and the net production of radiolytic species would cease. Calculations by Sunder and Christensen /1993/ show that steady state is reached after about 20 hours. The concentrations of oxidants are then in the range 10^{-12} to 10^{-10} mol/dm^3 for a dose rate of 1 Gy/h.

The canister near field in the repository cannot be regarded as closed. The hydrogen is mobile and will escape from the near field faster than the oxidizing species, resulting in a mildly oxidizing environment. The oxidants, on the other hand, may be consumed through oxidation processes, e.g., by oxidising Fe(II) in the bentonite or dissolved Fe^{2+} in the pore water or supporting corrosion of the canister. The result will then be a net production of reductants and the steady state will be shifted towards higher concentrations of the species that are not consumed. The actual concentrations will depend on the efficiency at which the oxidants are removed from the solution.

In groundwater, other species may also be produced depending on the composition of the solution. For example, in highly saline solutions, chloride species are produced (Cl_2^-, Cl_2, ClO^- etc.) and at high carbonate concentration the carbonate radical may form (CO_3). During radiolysis of moist air, nitrogen oxides (and as a consequence, nitric oxide) will be produced.

Experimental studies of the effects of γ-radiation on corrosion have been performed within the Yucca Mountain Project in the U.S. for corrosion in moist air (see e.g. Yunker and Glass /1986/ and Reed and Van Konynenburg /1991/). Corrosion in irradiated water has been performed by Nagra in Switzerland (Simpson/1984/) and by AECL in Canada (see e.g. King and Litke /1987/), and also within the Yucca Mountain Project (Yunker and Glass /1986/). AECL has also published an excellent review of the effects of γ-radiation on the corrosion of high level waste canister materials (Shoesmith and King /1999/).

8.1 Corrosion in air in the presence of γ-radiation

Yunker and Glass /1986/ reported results from exposing oxygen free copper to an air/water vapour mixture at 150°C and to vapour saturated air at 95°C in a γ-radiation field of 10^5 rad/h (approximately 10^3 Gy/h). This dose rate is more than a factor of 1,000 higher than the expected maximum surface dose rate on the canister. For exposures of about half a year, the corrosion rate at 150°C was about 1 μm per year and at 95°C, it was about 4 μm per year. The difference could be due to differences in relative humidity at the two temperatures.

Reed and Van Konynenburg /1991/ performed experiments in both dry air and at 40% relative humidity at almost the same temperatures as Yunker and Glass /1986/. The dose rates were 0.021 Mrad/h (210 Gy/h) at 94°C and between 0.011 and 0.015 Mrad/h (110–150 Gy/h) at 152°C. The experiments were run for about 75 days. The observed corrosion rates ranged from about 1 mm per year to 3 μm per year. The dominating corrosion product at the longer exposure times seems to have been cuprite (Cu_2O).

Apart from a possible increase in the corrosion rate due to strongly oxidizing species being formed through radiolysis of water, there is also the possibility for the radiolytic formation of nitrogen oxides and nitric acid. Reed et al. /1990/ confirm formation of nitrogen oxides in the gas phase at all temperatures (90°C, 120°C and 150°C) and for both dose rates that were used in the experiment (0.7 kGy/h and 2 kGy/h). They also identify basic cupric nitrate ($Cu_2NO_3(OH)_3$) as a lesser component in the corrosion products, but only at lower relative humidity (< 15 % RH). The dose rates used in the experiments are at least a factor of 100 higher than the maximum surface dose rate for the canister.

Marsh /1990/ shows a simple method to make a rough calculation of the quantity of nitric acid produced. The rate of formation is given by

$$\frac{d[HNO_3]}{dt} = \frac{G \cdot V \cdot \rho \cdot D_o}{A_v} \cdot e^{\frac{-0,693 \cdot t}{T}} \qquad 8\text{-}1$$

where G is the G value (in number of molecules/eV), V the irradiated air volume (dm^3), ρ the density of air (g/dm^3), D the initial dose rate (eV/g·year), A_v Avogado's number, t the time (years) and T the half-life (years) of the radiation source. If is assumed that the γ-radiation has a half-life of 30 years, G = 0.02 molecules/eV and an air gap of 5 cm around the canister (V = 825 dm^3), then the production rate for nitric acid in the repository will be 0.002 mol/year. This is a very small quantity, which will have a negligible effect on the life of the canister.

The corrosion rates that are measured in the presence of γ-radiation are not higher than what one would expect for corrosion of copper in unirradiated moist air (see section 4). The data, therefore, suggest that the influence of radiation will be negligible even at dose rates considerably higher than the maximum surface dose rate for the canister.

8.2 Corrosion in water in the presence of γ-radiation

Yunker and Glass /1986/ report copper corrosion rates in a fresh water of low ionic strength irradiated with 10^3 Gy/h for about 200 days. After an initially somewhat higher corrosion rate, the rate attains a nearly constant value of about 2 μm per years after a few months.

What appears to be the same data are also reported by Kass /1990/. Kass, however, also presents corrosion data from exposure without radiation showing that the radiation has a very small effect, if any, on the corrosion of pure copper. The rates measured without irradiation are, in fact, slightly higher than those obtained with irradiation. At much lower dose rates (13 Gy/h) Simpson /1984/ finds lower corrosion rates than without irradiation. This observation is corroborated by King and Litke /1987/. They used dose rates in the range 14 to 27 Gy/h for irradiation of copper in a saline solution (about 1 mol/dm^3 chloride) at 150°C. The experiments were performed in aerated and deaerated solutions and the corrosion rates were about a factor of four lower in the presence of radiation. King and Litke attributed this to the more protective nature of the surface film formed in irradiated solutions. Furthermore, they saw no effect of the radiation on the corrosion potential during the experiment. The corrosion rates (weight loss) were, however, very high, probably because of the high solution volume to surface area ratio in the tests. In deaerated solutions, however, King and Litke saw no difference in the corrosion rate in irradiated and unirradiated solutions.

Available information shows that there is no evidence for enhanced corrosion rates caused by γ-radiation. On the contrary, at least for dose rates in the range of 10–100 Gy/h, the experimental data seem to indicate a lower corrosion rate in the presence of radiation.

9 Implications for the canister service life

9.1 Introduction

Formal assessments of the long-term corrosion behaviour of Cu canisters and predicted canister lifetimes have been presented in four countries. Sweden was the first country to propose the use of copper canisters in 1978 /Swedish Corrosion Institute 1978/, since when various assessments have been published /SKB 1983; Swedish Corrosion Institute 1983; Werme et al. 1992; Wersin et al. 1994b; Raiko and Salo 1999/. In 1996, Canada presented a case study of the use of Cu canisters /Johnson et al. 1996/. Finally, Japan is also considering the use of Cu canisters for the disposal of vitrified waste /JNC 2000/.

Table 9-1 summarizes the various assessments of the long-term corrosion behaviour of Cu canisters and, where given, the predicted canister lifetimes. A more detailed discussion of the predictions is given below for each country.

9.2 Lifetime predictions from various international programmes

9.2.1 Sweden/Finland

The corrosion processes considered in the Swedish/Finnish studies include: general corrosion under oxic and anoxic conditions, localized corrosion (pitting), microbially influenced corrosion (MIC), and stress corrosion cracking (SCC). Of these processes, detailed analyses have been performed for general corrosion and pitting. Microbial effects are limited to the reduction of SO_4^{2-} to HS^-. Stress corrosion cracking is believed to be unlikely, either because the maximum concentration of SCC agents, and of the corrosion potential, lie below the respective threshold values for SCC, or because the creep rate will exceed the crack growth rate (section 7).

A combined mass-balance/mass-transport approach was taken in predicting the long-term corrosion behaviour in the original Swedish/Finnish canister lifetime assessments /SKB 1983; Swedish Corrosion Institute 1978; Swedish Corrosion Institute 1983; Werme et al. 1992/. The corrosion assessment was divided into an initial period of aerobic (oxic) corrosion, followed by a longer period of corrosion under anaerobic (anoxic) conditions. During both periods, general corrosion and pitting were assumed to be possible.

In the 1983 assessment /SKB 1983; Swedish Corrosion Institute 1983; and later revisited by Werme et al. 1992/, corrosion during the aerobic period was supported by all of the trapped O_2 in the buffer material and a small fraction (~1%) of that in the backfilled tunnels above the deposition holes, the remainder being consumed by reaction with Fe(II) minerals. Radiolytically produced oxidants were also considered. The combined general corrosion due to trapped O_2 and radiolytic oxidants was estimated to be 0.084 mm, virtually all of which occurred in the first 1,000 years. Pitting was assessed using a pitting factor (PF), with a realistic value of 2 and a conservative value of 5.

Thus, the maximum penetration due to general corrosion and pitting during the initial aerobic phase was estimated to be between 0.17 mm and 0.42 mm, for PF of 2 and 5, respectively.

During the long-term anaerobic phase, corrosion was supported by HS^- from a number of sources. Sulphide is present naturally in the MX-80 bentonite in the deposition hole and tunnel and in the groundwater. These sources of HS^- were assumed to be supplemented by the microbial reduction of SO_4^{2-} in the deposition hole, tunnel and groundwater. The corrosion rate was assumed to be limited by the rate of supply of HS^- to the canister surface. After 10^6 yrs, an additional 0.27 mm of general corrosion was predicted due to HS^-, of which ~40% was of microbial origin. As for the aerobic phase, a PF of 2 or 5 was applied, to produce a maximum additional depth of corrosion (general and pitting) of 0.53 mm (PF = 2) to 1.33 mm (PF = 5).

Adding the estimated depths of corrosion for the two periods produces an estimate of the total amount of corrosion on a Cu canister over a period of 10^6 yrs. For realistic (PF = 2) and conservative (PF = 5) assessments, the maximum predicted depth of general and localized corrosion is 0.70 mm and 1.75 mm, respectively (table 9-1). Such an amount is negligible compared with the proposed canister wall thickness of 50 mm, from which it can be concluded that the expected canister lifetime is $>10^6$ yrs /SKB 1983; Swedish Corrosion Institute 1983; Werme et al. 1992; Raiko and Salo 1999/.

A slightly different approach to predicting the corrosion rates of Cu canisters in a Swedish/Finnish repository was taken by Wersin et al. /1994b/. A steady-state mass transport-reaction model was used, in which the repository system was described by boxes representing the buffer, canister, and a box in which various fast and slow chemical and mass-transport processes were assumed to occur. As in the previous assessments, the evolution of repository conditions was divided into an aerobic and an anaerobic period. For each period, the rate of general corrosion was predicted based on a series of coupled chemical and mass-transport processes for various possible corrosion reactions.

In the aerobic period, the corrosion rate was predicted to be 7×10^{-6} mm·yr^{-1}. Through a series of sensitivity analyses, the rate-determining process was shown to be the diffusion of Cu(II) away from the canister surface. Thus, any parameter which lead to an increase in the rate of Cu(II) diffusion (such as changes to the CO_3^{2-} concentration and pH, which affect the solubility of precipitated $CuCO_3 \cdot Cu(OH)_2$) resulted in an increase in corrosion rate, whereas parameters which did not affect Cu(II) transport (such as the dissolved O_2 concentration) were predicted to have no effect. Because of the independence of the corrosion rate on $[O_2]$, the extent of corrosion during the aerobic period was estimated by multiplying the predicted corrosion rate by the length of the aerobic period, which was estimated separately. Pitting corrosion was again estimated using a pitting factor. Wersin et al. /1994b/ proposed a realistic estimate of the extent of general corrosion and pitting during the aerobic period of 0.003 mm, based on a 65-yr aerobic period and a PF of 5. A conservative estimate was also provided, based on a 10-times higher corrosion rate, a PF of 100, and a 280-yr-long aerobic period, giving a maximum corrosion depth of 2 mm.

During the anaerobic period, corrosion was assumed to be supported by either the reduction of Fe(III) (produced from the dissolution of $Fe(OH)_3$ impurities in the bentonite) or of H_2O/H^+ in the presence of HS^-. The predicted corrosion rates for corrosion supported by Fe(III) and HS^- were 5×10^{-8} mm·yr^{-1} and 4×10^{-6} mm·yr^{-1}, respectively. Pitting corrosion was believed to be less severe during the anaerobic phase, so realistic and conservative PF values of 2 and 5, respectively, were used. Consequently,

Table 9-1. Comparison of predictions of long-term corrosion behaviour and canister lifetimes.

Country	General Corrosion	Localized Corrosion	Microbially Influenced Corrosion	Stress Corrosion Cracking	Predicted Lifetime	Reference
Sweden/ Finland[1)]	0.05 mm in 10^6 yrs (realistic) 4 mm in 10^6 yrs (conservative)	0.05 mm in 10^6 yrs (realistic) 18 mm in 10^6 yrs (conservative)	–	–	>10^6 yrs	Wersin et al. /1994/
Sweden/ Finland[1)]	0.35 mm in 10^6 yrs	0.35 mm in 10^6 yrs (realistic) 1.4 mm in 10^6 yrs (conservative)	SRB assumed to reduce SO_4^{2-} to HS^-	Maximum possible nitrite concentration below threshold for SCC	>10^6 yrs	Werme et al. /1992/, Swedish Corrosion Institute /1983/, SKB /1983/
Sweden/ Finland[1)]	0.33 mm in 10^6 yrs	0.33 mm in 10^6 yrs (realistic) 1.3 mm in 10^6 yrs (conservative)	SRB assumed to reduce SO_4^{2-} to HS^- in tunnel and groundwater only	SCC does not occur based on threshold potential and concentrations of SCC agent, and because creep is faster than SCC	>10^6 yrs	This report
Canada[2)]	0.011 mm in 10^6 yrs	6 mm in 10^6 yrs	Limited impact. Maximum additional wall loss of 1 mm in 10^6 yrs	SCC not included because of limited period of stress, absence of SCC agents, general lack of oxidant and inhibitive effects of Cl^-	>10^6 yrs	Johnson et al. /1996/
Japan	9–13 mm in 10^3 yrs, depending on repository design	18–26 mm in 10^3 yrs based on pitting factor of 3, 2 mm in 10^3 yrs based on extreme-value analysis	SRB assumed to reduce all SO_4^{2-} to HS^-	Maximum concentrations of ammonia, nitrite and acetate less than threshold concentration	None given	JNC /2000/

[1)] Reference canister wall thickness of 50 mm.
[2)] Reference canister wall thickness of 25 mm.

over a period of 10^6 yrs, the minimum and maximum depths of general corrosion and pitting were estimated to be 0.1 mm (PF = 2, Fe(III)-supported corrosion) and 20 mm (PF = 5, HS^--supported corrosion), respectively.

Combining the estimated corrosion depths for the aerobic and anaerobic periods, Wersin et al. /1994b/ estimated realistic and conservative corrosion depths after 10^6 yrs of 0.1 mm and 22 mm, respectively. Compared with the reference wall thickness of 50 mm, it was concluded that the canister lifetime would be >10^6 yrs (table 9-1).

A new estimate of the canister lifetime can be made based on the information contained in this report. Using the analysis of Werme et al. /1992/ as the basis for the estimate, two new factors need to be taken into account. First, since microbial activity is unlikely in highly compacted bentonite (section 2.3), the microbially mediated reduction of SO_4^{2-}

to HS^- will not occur in the deposition hole. In the analysis of Werme et al. /1992/, microbially produced HS^- in the deposition hole resulted in 0.023 mm general corrosion in 10^6 yrs. Second, the thermodynamic and mass transport evaluation presented in section 6.2.4.1 suggests that corrosion of Cu supported by the reduction of H_2O may occur at high Cl^- concentrations. The mass-transport-limited corrosion rate depends on the HS^- and Fe(III) content of the bentonite, since these species are assumed to react with the corrosion products $CuCl_2^-$ and H_2, respectively, maintaining steep concentration gradients at the canister surface. However, for HS^- and Fe(III) concentrations of 1 mg and 3 mg per kg of bentonite, respectively, the predicted additional corrosion is <0.001 mm in 10^6 yrs (figure 6-13).

This new analysis predicts less general and localized corrosion than the previous analysis of Werme et al. /1992/. The decrease in the extent of general corrosion during the anoxic period due to the absence of microbial reduction of SO_4^{2-} in the deposition hole is much greater than the here predicted incremental corrosion due to the dissolution of Cu as $CuCl_2^-$ supported by the reduction of H_2O. Therefore, using the previous analysis of Werme et al. /1992/ to estimate the depth of general corrosion due to the initially trapped O_2, radiolysis products, and HS^- (in the bentonite in the deposition hole and tunnel, in the groundwater itself and produced by microbial activity in the tunnel and groundwater only), the maximum depth of general corrosion in the new analysis is 0.33 mm after 10^6 yrs, compared with 0.35 mm in the previous assessment. As a consequence of using pitting factors to assess the depth of localized corrosion (realistic PF = 2, conservative PF = 5), the predicted depth of localized corrosion is also lower for this new assessment. The overall canister lifetime is predicted to be >10^6 yrs (table 9-1).

9.2.2 Canada

As in the Swedish/Finnish assessments, general corrosion and pitting were assumed to be the two major processes leading to corrosion of the canister in a Canadian repository /Johnson et al. 1996/. Microbial effects were considered to be possible, but were thought to contribute no more than 1 mm additional corrosion, and were not part of the detailed assessment. Reasoned arguments were used to claim that the canisters would not be subject to SCC, because of (i) limited strain of the canister wall, (ii) the lack of SCC agents in the repository, (iii) the general lack of oxidants, and (iv) the inhibitive effects of Cl^- ions.

Whilst it was recognized that the repository environment would evolve over time, the aerobic and anaerobic phases were not distinguished as in the Swedish/Finnish assessments. The extent of general corrosion was predicted using the 1-dimensional coupled reaction-diffusion model described in section 6.2.4.2. This model is based on the reaction scheme shown in figure 6-14. The repository was described by a series of layers representing buffer, backfill, excavation-disturbed rock, and a layer of sparsely fractured rock. The model geometry was bounded by the canister surface and a major groundwater-bearing fracture. By using electrochemical expressions for the mathematical boundary conditions at the canister surface, it was possible to predict the effect of the evolving repository environment on the corrosion potential (E_{CORR}) and corrosion current density (i_{CORR}) of the canister (figure 6-15). General corrosion of the canister was predicted to stop once all of the initially trapped O_2 had been consumed, since there is no sulphide in either the Avonlea bentonite specified for a Canadian repository or in deep Canadian Shield groundwaters. The absence of sulphide minerals in the clay resulted in a longer aerobic phase, predicted to be a maximum of 2,000–3,000 yrs in duration. Most of the trapped O_2, however, was predicted to be consumed by reaction with Fe(II) minerals, so that the maximum depth of general corrosion was predicted to be only 0.011 mm /Johnson et al. 1996/.

Pitting corrosion was assumed to be possible at all times during the evolution of the repository environment. The depth of the deepest pit on any of the 60,000 canisters in the repository was estimated using an extreme-value statistical analysis of literature pit-depth data (section 6.3.2). The data included in the analysis were from long-term burial studies and from a study of Bronze Age archaeological artifacts /Bresle et al. 1983/. The maximum estimated pit depth was 6 mm after 10^6 yrs. This estimate of maximum pit depth was considered to be conservative because pitting was assumed to continue indefinitely, despite the fact that the aerobic period lasted only a few thousand years.

In a Canadian repository, therefore, the maximum depth of general corrosion and pitting was predicted to be 6.0 mm after 10^6 yrs. Since the reference wall thickness was 25 mm, canisters were predicted to have a lifetime of $>10^6$ yrs (table 9-1).

9.2.3 Japan

Although no formal lifetime prediction has been made for a Cu canister in a Japanese repository, the maximum depth of corrosion has been assessed /JNC 2000/. As in the Swedish/Finnish and Canadian programmes, the two corrosion processes considered were general corrosion and pitting. Although it was believed that microbial activity would be limited by nutrient availability, it was implicitly included in the assessment through the production of HS^- from the reduction of SO_4^{2-}. Stress corrosion cracking was not considered because the maximum concentrations of ammonia, nitrite and acetate ions in the repository were believed to be below the threshold values for cracking. The Japanese assessment was similar to that used in Sweden and Finland, although using very much more conservative assumptions. Various repository designs were considered, employing various amounts of buffer and backfill materials. These different designs resulted in a range of values for the predicted corrosion damage.

General corrosion was assumed to be caused by O_2 trapped in the buffer and backfill materials, and by HS^- in the buffer and groundwater. It was conservatively assumed that all of the O_2 in the deposition holes and tunnels would lead to corrosion of the canister. Depending upon the repository design, this resulted in between 0.6 mm and 3.6 mm of general corrosion. For HS^--induced corrosion, it was assumed that all of the SO_4^{2-} in the buffer and backfill was reduced to HS^- by sulphate-reducing bacteria, and that the groundwater itself contained 0.03 mol·dm^{-3} HS^-. The rate of corrosion was assumed to be limited by the rate of diffusion of HS^- to the canister surface. Over a 1,000-yr period, the additional corrosion due to HS^- was 0.2–1.1 mm from the SO_4^{2-} in the buffer material and 8.1 mm due to HS^- in the groundwater. Thus, after 1,000 yrs, the maximum depth of general corrosion due to both O_2 and HS^- was predicted to be 9–13 mm, depending upon the repository design (table 9-1).

The extent of pitting corrosion was assessed using both a pitting factor and the extreme-value analysis approach described above. For the pitting factor approach, a PF of 3 was used. For the extreme-value analysis, the maximum pit depth after 1,000 yrs was predicted to be 2.2 mm.

The overall extent of general corrosion and pitting after 1,000 yrs was predicted to be 27–39 mm from the PF approach and 11–15 mm based on the extreme-value pitting analysis. These estimates are believed to be highly conservative, due mainly to the very high groundwater HS^- concentration used in the assessment.

9.3 Conclusions

There are certain similarities and certain distinct differences between the two detailed assessments of the lifetimes of Cu canisters. In both the Swedish/Finnish and Canadian assessments, general corrosion and pitting are believed to be the processes most likely to result in corrosion of the canister. In a Swedish/Finnish repository, HS^- (or, rather, H_2O/H^+ in the presence of HS^-) is the most prevalent oxidant. In a Canadian repository, trapped O_2 is the major oxidant. Different approaches have been used to assess the extent of general corrosion and pitting. Both mass-balance and detailed kinetic modelling have been used to model general corrosion. For pitting, empirical pitting factors and statistical analyses have been used. Despite these differences in repository conditions, and in the approaches taken to make long-term predictions, the predicted canister lifetimes exceed 10^6 yrs in both cases.

Based on these analyses, it is apparent that corrosion is not the limiting factor in determining the canister design wall thickness.

10 Areas for further research

Studies of copper corrosion under repository conditions have been going on since 1977 and a large amount of information has been gathered during this period. A number of lifetime assessments have been performed over the years, as discussed in detail in section 9. The conclusion from these assessments is that copper canisters will have a very long lifetime in the repository environment and that corrosion is highly unlikely to be a limiting factor for lifetimes exceeding 100,000 years. The canister is an important barrier in the overall multi-barrier system, and also, in case of local failure, as a barrier against the dispersion of radionuclides to the near field. It is important, therefore, that research into the corrosion behaviour of copper should continue in order to maintain a high level of certainty about the expected excellent long-term corrosion performance of the canister. Those areas that may benefit from further studies include (in no particular order of priority):

Measurement and prediction of the evolution of environmental conditions

The length of the initial oxic period in the evolution of the repository environment is still uncertain. Whilst the extent of corrosion during this period is limited, because of the small amount of trapped oxygen, it is of interest to predict how long this period may last because the probability of localized corrosion is highest under oxic conditions. Various estimates have been made of the length of the oxic period, but none have included all of the chemical, electrochemical, and microbiological processes that are likely to occur. Additional data will be produced from laboratory experiments and experiments at Äspö Hard Rock Laboratory, and further modelling could be performed in an attempt to simulate the observed behaviour.

Measurement and prediction of corrosion potentials in highly compacted bentonite

An important factor determining the corrosion behaviour of the canister is the corrosion potential (E_{CORR}). The E_{CORR} is likely to undergo a large transition during the evolution of the repository environment, from relatively positive values during the oxic period to relatively negative values when corrosion is dominated by the presence of sulphide. Comparison of E_{CORR} to threshold values for localized corrosion and SCC can be used to assess the probability of these forms of corrosion. Although a threshold potential argument has been proposed in the Finnish programme as a means of predicting the long-term SCC behaviour, no measured or predicted E_{CORR} values under simulated repository conditions have been reported. Data from laboratory experiments, experiments at Äspö Hard Rock Laboratory, and modelling studies will provide the necessary information for predicting the development of E_{CORR} under repository conditions.

Possible microbial activity in highly compacted bentonite

Sulphate reducing bacteria (SRB) are likely to be present in deep groundwater and active at the repository level after the oxygen has disappeared. The activity of these bacteria will not constitute a threat to the integrity of the canister unless they can populate the immediate vicinity of the canister or form a biofilm on the canister surface. The studies

so far have shown that the environment in the highly compacted bentonite is too extreme (i.e., the water activity is too low and the pore size of the clay at full compaction is too small) for SRB from the groundwater to survive and to actively produce sulphide. These studies will continue both as laboratory experiments and as field experiments at Äspö Hard Rock Laboratory, so that the conditions for SRB survival and activity in a deep geologic repository can be better defined.

Stress corrosion cracking

Stress corrosion cracking requires the presence of a tensile stress on the surface of the canister. Modelling and, possibly, experimental verification of the distribution of tensile stress on a canister subjected to external loads would assist in identifying regions most at risk of SCC. In addition, more experimental data on the sensitivity of copper to SCC under repository conditions will be acquired, for example, in the presence of ammonia and/or acetate ions. Such experiments could include both laboratory studies and field experiments at Äspö Hard Rock Laboratory. Information is also required about the SCC behaviour of welded OF Cu, since residual stresses and differences in microstructure may make the weld area more susceptible to cracking.

Corrosion during water saturation

Based on information available in the literature, little corrosion is expected during the saturation phase. However, the duration of the saturation phase is not known with certainty and will, in any case, vary from location to location within the repository. Some corrosion testing in unsaturated highly compacted bentonite would be useful in confirming the expectation that corrosion will be limited during this period.

Copper corrosion in highly saline groundwaters

Higher salinity groundwaters are being encountered at depth in the Fenno-Scandian Shield. On the basis of currently available experimental and thermodynamic data, it is not possible to totally exclude the possibility that copper will corrode in the absence of oxygen in saline groundwaters, supported by the electrochemical reduction of water. Additional studies are required to quantify the extent of corrosion under these conditions. Possible approaches include thermodynamic and/or electrochemical kinetic modelling, and corrosion rate measurements under strictly controlled anoxic conditions.

Effect of near-surface-breaking defects

A question has been raised as to whether near-surface defects (e.g., weld pores) could act as sites of enhanced localized corrosion. Although not believed to pose an increased risk of localized corrosion, an experimental and/or theoretical assessment of the dangers posed by such defects is required.

Properties of Cu_2O films

SKI (Swedish Nuclear Power Inspectorate) have raised the issue of the possible wide range of properties of Cu_2O films formed on the canister surface. The properties of such films may be important in determining the localized and SCC behaviour of the canister. The effects of pore-water species, such as chloride and sulphide ions, on the properties of such films should be evaluated.

Corrosion in saline solutions at high pH

If concrete is used extensively in the repository, an alkaline plume could reach the canister surface. The relative rates of diffusion of the alkaline plume and the saline groundwater to the canister surface are unknown. The impact on the canister may depend on whether the alkaline plume or the saline groundwater contacts the surface first. If the canister is first passivated in a high-pH environment, it could become more susceptible to localized corrosion, especially in saline groundwaters. An experimental and/or theoretical assessment of the effect of the alkaline plume is required.

Corrosion due to differential bentonite properties

The bentonite surrounding the canister is unlikely to swell evenly. Therefore, there could be a period of time during which chemical gradients are established on the canister surface due, for example, to differential pH or oxygen concentrations. These chemical gradients are likely to disappear with time as the bentonite swells, but the period for this to happen and the extent of localized corrosion that could occur during this period are unknown. Some theoretical and/or experimental studies of this phenomenon are advisable.

References

Aaltonen P, Hänninen H, Kemppainen M, 1984. Stress corrosion testing of pure OFHC-copper in simulated groundwater conditions. YJT-84-21. Nuclear Waste Commission of Finnish Power Companies Report.

Aaltonen P, Varis P, 1993. Long term corrosion tests of OFHC-coppers in simulated repository conditions – final report. YJT-93-05. Nuclear Waste Commission of Finnish Power Companies Report.

Ageskog L, Jansson P, 1999. Heat propagation in and around the deep repository. Thermal calculations applied to three hypothetical sites: Aberg, Beberg and Ceberg. SKB TR-99-02. Svensk Kärnbränslehantering AB.

Ahonen L, 1995. Chemical stability of copper canisters in deep repository. Report YJT-95-19. Helsinki, Nuclear Waste Commission of Finnish Power Companies.

Ahonen L, 1999. Effect of saline water on metallic copper. Posiva Working Report 99-58. Posiva Oy.

Ahonen L, 2001. Appendix II in this report.

Alhajji J N, Reda M R, 1994. The conflicting roles of complexing agents on the corrosion of copper-nickel alloys in sulfide polluted seawater. J. Electrochem. Soc. 141, 1432-1439.

Andersson J, 1999. Data and data uncertainties. Compilation of data and data uncertainties for radionuclide transport calculations. SKB TR-99-09, Svensk Kärnbränslehantering AB.

Andersson H, Seitisleam F, Sandström R, 1999. Influence of phosphorous and sulphur as well as grain size on creep in pure copper. SKB TR-99-39. Svensk Kärnbränslehantering AB.

Anttila P, Ahokas H, Front K, Hinkkanen H, Johansson E, Paulamäki S, Riekkola R, Saari J, Saksa P, Snellman M, Wikström L, Öhberg A, 1999a. Final disposal of spent nuclear fuel in Finnish bedrock – Olkiluoto site report. POSIVA 99-10. Posiva Oy.

Anttila P, Ahokas H, Front K, Hinkkanen H, Johansson E, Paulamäki S, Riekkola R, Saari J, Saksa P, Snellman M, Wikström L, Öhberg A, 1999b. Final disposal of spent nuclear fuel in Finnish bedrock – Hästholmen site report. POSIVA 99-08. Posiva Oy.

Appelo C A J, Postma D, 1993. Geochemistry, groundwater and pollution. A.A. Balkema, Rotterdam, Netherlands.

Apps J A, van de Kamp P C, 1993. Energy gases of abiogenic origin in the Earth's crust. In The Future of Energy Gases, Howell G. (ed.), pp. 81–132. U.S. Geological Survey Professional Papers. United States Government Printing Office, Washington.

Arilahti E, Bojinov M, Mäkelä K, Laitinen T, Saario T, 2000. Stress corrosion cracking investigation of copper in groundwater with ammonium ions. POSIVA Working Report 2000-46. Posiva Oy.

Baes C F, Mesmer R E, 1976. The hydrolysis of cations. John Wiley.

Banwart S, 1995. The Äspö redox investigations in block scale. Project summary and implications for repository performance assessment. SKB TR 95-26. Svensk Kärnbränslehantering AB.

Banwart S, Tullborg E-L, Pedersen K, Gustafsson E, Laaksoharju M, Nilsson A-C, Wallin B, Wikberg P, 1996. Organic carbon oxidation induced by largescale shallow water intrusion into a vertical fracture zone at the Äspö Hard Rock Laboratory (Sweden). J. Contam. Hydrol. 21, 115–125.

Barton P B, Bethke P M, 1960. Thermodynamic properties of some synthetic zinc and copper minerals. Am. J. Sci. 258A, 21–34.

Bath A, Milodowski A, Ruotsalainen P, Tullborg E-L, Cortés Ruiz A, Aranyossy J-F, 2000. Evidence from mineralogy and geochemistry for the evolution of groundwater systems during the Quaternary for use in radioactive waste repository safety assessment (EQUIP project). Luxembourg, European Commission: Nuclear Science and Technology, Report EUR 19613 EN.

Beavers J A, Durr C L, 1992. Stress-corrosion cracking studies on candidate container alloys for the tuff repository. U.S. Nuclear Regulatory Commission Report, NUREG/CR-5710.

Benjamin L A, Hardie D, Parkins R N, 1988. Stress corrosion resistance of pure coppers in ground waters and sodium nitrite solutions. Br. Corros. J. 23, 89–95.

Beverskog B, Puigdomenech I, 1998. Pourbaix diagrams for the system copper-chlorine at 5–100°C. SKI Report 98:19, Swedish Nuclear Power Inspectorate.

Bianchi G, Fiori G, Longhi P, Mazza F, 1978. "Horse shoe" corrosion of copper alloys in flowing sea water: mechanism, and possibility of cathodic protection of condenser tubes in power stations. Corrosion 34, 396–406.

Blomqvist R, Ruskeeniemi T, Kaija J, Ahonen L, Paananen M, Smellie J, Grundfelt B, Bruno J, Pérez del Villar, Rasilainen K, Pitkänen P, Suksi J, Casanova J, Read D, Frape S, 2000. The Palmottu natural analogue project Phase II: Transport of radionuclides in a natural flow system at Palmottu. Report EUR 19611 EN. European Commission: Nuclear Science and Technology.

Bresle A, Saers J, Arrhenius B, 1983. Studies in pitting corrosion on archaeological bronzes: Copper. SKBF-KBS-TR-83-05. Svensk Kärnbränsleförsörjning AB.

Brossard L, 1983. Anodic dissolution of copper in concentrated LiCl solution at pH between 3 and 7. J. Electrochem. Soc. 130, 403–405.

Bruno J, Acros D, Duro L, 1999. Processes and features affecting the near field hydrochemistry. Groundwater-bentonite interaction. SKB TR-99-29. Svensk Kärnbränslehantering AB.

Buhler K, 1993. Impurity constituents of flue gas condensates and their significance for the corrosion of heat exchangers. Werkst. Korros. 44, 289–294.

Börgesson L, Hernelind J, 1999. Coupled thermo-hydro-mechanical calculations of the water saturation phase of a KBS-3 deposition hole. Influence of hydraulic rock properties on the water saturation phase, SKB TR-99-4. Svensk Kärnbränslehantering AB.

Campbell H S, 1974. A review: pitting corrosion of copper and its alloys. In Localized Corrosion, Editors, R.W. Staehle, B.F. Brown, J. Kruger and A. Agrawal, pp. 625–638. NACE International.

Cassagne T B, Kruger J, Pugh E N, 1990. Role of the oxide film in the transgranular stress corrosion cracking of copper. In Environmentally Assisted Cracking: Science and Engineering, ASTM-STP-1049, W.B. Lisagor, T.W. Crooker and B.N. Leis, Editors, pp. 59–75. American Society for Testing and Materials.

Ciavatta L, 1980. The specific interaction theory in evaluating ionic equilibria. Ann. Chim. 70, 551–567.

Coates J D, Ellis D J, Blunt-Harris E L, Gaw C V, Roden E E, Lovley D R, 1998. Recovery of humic-reducing bacteria from a diversity of environments. Appl. Environ. Microbiol. 64, 1504–1509.

Collin M, Rasmuson A, 1988. A comparison of gas diffusivity models for unsaturated porous media. Soil Sci. Soc. Am. J. 52, 1559–1565.

Corbett R A, Elliot P, 2000. Ant-nest corrosion – digging the tunnels. CORROSION/2000, NACE International, Houston, TX, Paper No. 646.

Crawford M B, Wilmot R D, 1998. Normal evolution of a spent fuel repository at the candidate sites in Finland. Helsinki, Finland. POSIVA-98-15. Posiva Oy.

de Chialvo M R G, Arvia A J, 1985. The electrochemical behaviour of copper in alkaline solutions containing sodium sulphide. J. Appl. Electrochem. 15, 685–696.

de Chialvo M R G, Salvarezza R C, Vasquez Moll D, Arvia A J, 1985. Kinetics of passivation and pitting corrosion of polycrystalline copper in borate buffer solutions containing sodium chloride. Electrochim. Acta 30, 1501–1511.

Drogowska M, Brossard L, Ménard H, 1992. Copper dissolution in $NaHCO_3$ and $NaHCO_3$ + NaCl aqueous solutions at pH 8. J. Electrochem. Soc. 139, 39–47.

Drogowska M, Brossard L, Ménard H, 1994. Comparative study of copper behaviour in bicarbonate and phosphate aqueous solutions and effect of chloride ions. J. Appl. Electrochem. 24, 344–349.

Ekendahl S, Pedersen K, 1994. Carbon transformations by attached bacterial populations in granitic ground water from deep crystalline bed-rock of the Stripa research mine. Microbiology 140, 1565–1573.

Escalante E, Kruger J, 1971. Stress corrosion cracking of pure copper. J. Electrochem. Soc. 118, 1062–1066.

Escobar I S, Silva E, Silva C, Ubal A, 1999. Study of the effect of sulfide ions on the corrosion resistance of copper for use in containers for high-level waste. Proc. Fourth International Conference Copper 99-Cobre 99, G.A. Eltringham, N.L. Piret and M. Sahoo (eds.), Vol. I, 371–386.

Farmer J C, Van Konynenburg R A, McCright R D, Gdowski G E, 1988. Survey of degradation modes of candidate materials for high-level radioactive-waste disposal containers. Volume 4. Stress corrosion cracking of copper-based alloys. Lawrence Livermore National Laboratory Report, UCID-21362 Vol. 4.

Fennell P A H, Graham A J, Smart N R, Sofield C J, 2001. Grain boundary corrosion of copper canister material. AEA Technology Report, AEAT/R/PS-0041. AEA Technology plc.

Fischer W, Hänßel I, Paradies H H, 1988. First results of microbial induced corrosion of copper pipes. In Microbial Corrosion-1, (Editors, C.A.C. Sequeira and A.K. Tiller), Elsevier, London, UK, p. 300–327.

Fredrickson J K, Onstott T C, 1996. Microbes deep inside the earth. Sci. Am. 275, 42–47.

Fujii T, Kodama T, Baba H, 1984. The effect of water quality on pitting corrosion of copper tube in hot soft water. Corros. Sci. 24, 901–912.

Galvele J R, 1987. A stress corrosion cracking mechanism based on surface mobility. Corros. Sci. 24, 1–33.

Grenthe I, Wanner H, Östhols E, 2000. Guidelines for the extrapolation to zero ionic strength. OECD/NEA Thermochemical Data Base Project, TDB-2. Le Seine-St. Germain, France. (http://www.nea.fr/html/dbtdb/cgi-bin/tdbdocproc.cgi).

Hallberg R O, Ostlund P, Wadsten T, 1988. Inferences from a corrosion study of a bronze cannon, applied to high level nuclear waste disposal. Appl. Geochem. 3, 273–280.

Harned H S, Owen B B, 1958. The physical chemistry of electrolytic solutions. Reinhold, New York.

Haveman S H, Pedersen K, Routsalainen P, 1999. Distribution and metabolic diversity of microorganisms in deep igneous rock aquifers of Finland. Geomicrobiol. J. 16, 277–294.

Helgeson H C, Kirkham D H, Flowers G C, 1981. Prediction of the thermodynamic properties of electrolytes at high pressures and temperatures. In Chemistry and geochemistry of solutions at high temperatures and pressures. Eds. D.T. Rickard and F. E. Wickman. Pergamon Press.

Henderson P J, Osterberg J-O, Ivarsson B, 1992. Low temperature creep of copper intended for nuclear waste containers. Swedish Nuclear Fuel and Waste Management Company Technical Report, SKB-92-04.

Henderson P J, 1994. Creep of copper. In International Seminar on Design and Manufacture of Copper Canisters for Nuclear Waste, Sollentuna, April 1994. Paper IM-3112. Swedish Institute for Metals Research.

Herbert R A, 1990. Methods for enumerating microorganisms and determining biomass in natural environments. In Methods in Microbiology, Grigorova R., Norris J.R. (eds.), vol. 22. Academic Press, London. pp 1–39.

Hietanen S, Ehrnstén U, Saario T, 1996. Environmentally assisted cracking behaviour of copper in simulated ground water. STUK-YTO-TR 105. Finnish Centre for Radiation and Nuclear Safety Report.

Hindrichs K-U, Hayes J M, Sylva S P, Brewer P G, DeLong E F, 1999. Methane-consuming archaebacteria in marine sediments. Nature 398, 802–805.

Huertas F, Fuentes-Cantillana J L, Jullien F, Rivas P, Linares J, Fariña P, Ghoreyychi M, Jockwer N, Kickmaier W, Martínez M A, Samper J, Alonso E, Elorza F J, 2000. Full-scale engineering barriers experiment for a deep geological repository for high-level radioactive waste in crystalline host rock (FEBEX project). EUR 19147 EN, Commission of European Communities.

Ikeda B M, Litke C D, 2000. The effect of oxidant flux, nitrite concentration and chloride concentration on the stress corrosion cracking behaviour of non-welded and electron-beam welded copper. Report 06819-REP-01200-10049-R00. Ontario Power Generation, Nuclear Waste Management Division.

Ikeda B M, King F, 2001. State of knowledge on stress corrosion cracking of copper for used-fuel disposal containers. Report 06819-REP-01200-10058-R00. Ontario Power Generation, Nuclear Waste Management Division.

Imai H, Fukuda T, Akashi M, 1996. Effects of anionic species on the polarization behavior of copper for waste package material in artificial ground water. Mat. Res. Soc. Symp. Proc. 412, 589–596. Materials Research Society.

JNC, 2000. H12: project to establish the scientific and technical basis for HLW disposal in Japan. Supporting Report 2. Repository design and engineering technology. Japan Nuclear Cycle Development Institute Report, JNC TN1410 2000-003.

Johnson L H, LeNeveu D M, King F, Shoesmith D W, Kolář M, Oscarson D W, Sunder S, Onofrei C, Crosthwaite J L, 1996. The disposal of Canada's nuclear fuel waste: a study of postclosure safety of in-room emplacement of used CANDU fuel in copper containers in permeable plutonic rock: volume 2: vault model. AECL-11494-2, COG-96-552-2. Atomic Energy of Canada Limited Report.

Karnland O, 1995. Salt redistribution and enrichment in compacted bentonite expsoed to a thermal gradient – results from laboratory tests. SKB AR 95-31, Svensk Kärnbränslehantering AB.

Karnland O, Sandén T, 2000. Long term test of buffer material at Aspo Hard Rock Laboratory, Sweden, Mat. Res. Soc. Symp. Proc. Vol. 608, 173–178, Materials Research Society.

Karnland O, Sandén T, Johannesson L-E, Eriksen T E, Jansson M, Wold S, Pedersen K, Motamedi M, Rosborg B, 2000. Long term test of buffer material. Final report on the pilot parcels. SKB TR-00-22, Svensk Kärnbränslehantering AB.

Kasahara K, Komukai S, 1987. Case studies of pitting corrosion of copper tubes in central hot-water supply systems. Corros. Eng. 36, 453–459.

Kasahara K, Komukai S, Fujiwara T, 1988. Preventing copper-pipe pitting in central hot water supply by residual-chlorine UV photolysis. Corros. Eng. 37, 361–370.

Kass J, 1990. Evaluation of copper, aluminum bronze, and copper-nickel container material for the Yucca Mountain Project. In Corrosion of nuclear fuel containers: Proceedings of a Workshop (D.W. Shoesmith, editor) AECL-10121, 87–108. Atomic Energy of Canada Ltd.

Kato C, Ateya B G, Castle J E, Pickering H W, 1980a. On the mechanism of corrosion of Cu-9.4Ni-1.7Fe alloy in air saturated aqueous NaCl solution. I. Kinetic investigations. J. Electrochem. Soc. 127, 1890–1896.

Kato C, Castle J E, Ateya B G, Pickering H W, 1980b. On the mechanism of corrosion of Cu-9.4Ni-1.7Fe alloy in air saturated aqueous NaCl solution. II. Composition of the protective surface layer. J. Electrochem. Soc. 127, 1897–1903.

King F, Litke C D, 1987. The corrosion of copper in synthetic groundwater at 150°C. Part I. The results of short term electrochemical tests. Technical Record TR-428. Atomic Energy of Canada Ltd.

King F, LeNeveu D, 1992. Prediction of the lifetimes of copper nuclear waste containers. In Proceedings of Conference on Nuclear Waste Packaging, FOCUS '91, (American Nuclear Society, La Grange Park, IL), 253–261.

King F, Litke C D, Ryan S R, 1992. A mechanistic study of the uniform corrosion of copper in compacted Na-montmorillonite/sand mixtures, Corros. Sci. 33, pp. 1979–1995.

King F, Litke C, Ryan S, LeNeveu D, 1994. Predicting the long-term corrosion behaviour of copper nuclear fuel waste containers. In Life Prediction of Corrodible Structures, Editor, R.N. Parkins, p. 497–512. NACE International.

King F, 1995. A natural analogue for the long-term corrosion of copper nuclear waste containers – reanalysis of a study of a bronze cannon. Appl. Geochem. 10, 477–487.

King F, Kolář M, 1995. Prediction of the lifetimes of copper nuclear waste containers under restrictive mass-transport and evolving redox conditions. CORROSION/95, NACE International, Houston, TX, Paper #425.

King F, Stroes-Gascoyne S, 1995. Microbially influenced corrosion of nuclear fuel waste disposal containers. In Proc. 1995 Int. Conf. on Microbially Influenced Corrosion, NACE International and American Welding Society, 35/1–35/14.

King F, Litke C D, Quinn M J, LeNeveu D M, 1995a. The measurement and prediction of the corrosion potential of copper in chloride solutions as a function of oxygen concentration and mass-transfer coefficient. Corros. Sci. 37, 833–851.

King F, Quinn M J, Litke C D, 1995b. Oxygen reduction on copper in neutral NaCl solution. J. Electroanal. Chem. 385, 45–55.

King F, Litke C D, Tang Y, 1995c. Effect of interfacial pH on the reduction of oxygen on copper in neutral $NaClO_4$ solution. Journal Electroanalytical Chemistry 384, 105–113.

King F, Tang Y, Quinn M J, Litke C D, 1995d. The effects of dissolved oxygen concentration and mass-transport conditions on the dissolution behaviour of copper nuclear waste containers. CORROSION/95, NACE International, Paper #424.

King F, 1996. The potential for stress corrosion cracking of copper containers in a Canadian nuclear fuel waste disposal vault. AECL-11550, COG-96-94. Atomic Energy of Canada Limited Report.

King F, 1996a. Microbially influenced corrosion of copper nuclear fuel waste containers in a Canadian disposal vault. AECL-11471, COG-94-519. Atomic Energy of Canada Limited.

King F, 1996b. A copper container corrosion model for the in-room emplacement of used CANDU fuel. AECL-11552, COG-96-105. Atomic Energy of Canada Limited.

King F, Kolář M, 1996a. A numerical model for the corrosion of copper nuclear fuel waste containers. Mat. Res. Soc. Symp. Proc. 412, 555–562. Materials Research Society.

King F, Kolář M, 1996b. Mechanistic modelling of the corrosion behaviour of copper nuclear fuel waste containers. In Proceedings of International Conference on Deep Geological Disposal of Radioactive Waste, p. 5-39 to 5-50. Canadian Nuclear Society.

King F, Litke C D, 1997. Stress corrosion cracking of copper – report on experimental methodologies and preliminary results, 06819-REP-01200-0010 R00. Ontario Hydro.

King F, Kolář M, 1997a. Corrosion of copper containers prior to saturation of a nuclear fuel waste disposal vault. AECL-11718, COG-96-566-I. Atomic Energy of Canada Limited.

King F, Kolář M, 1997b. The effect of geosphere conditions on the lifetimes of copper containers. AECL-11717, COG-96-565-I. Atomic Energy of Canada Limited.

King F, Ryan S R, Litke C D, 1997a. The corrosion of copper in compacted clay. AECL-11831, COG-97-319-I. Atomic Energy of Canada Limited.

King F, Greidanus G, Jobe D J, 1997b. Dissolution of copper in chloride/ammonia mixtures and the implications for the stress corrosion cracking of copper containers. AECL-11865, COG-97-412-I. Atomic Energy of Canada Limited.

King F, Tang Y, 1998. The anodic dissolution of copper in chloride-sulphate groundwaters. 06819-REP-01200-0058 R00. Ontario Hydro Nuclear Waste Management Division.

King F, Litke C D, Ikeda B M, 1999a. The effect of oxidant supply and chloride ions on the stress corrosion cracking of copper. 06819-REP-01200-10013-R00. Ontario Power Generation, Nuclear Waste Management Division.

King F, Litke C D, Ikeda B M, 1999b. The stress corrosion cracking of copper containers for the disposal of high-level nuclear waste. In CORROSION/99, NACE International, Houston, TX, Paper #482.

King F, Litke C D, Ikeda B M, 1999c. Mat. Res. Soc. Proc. 556, 887–894, Materials Research Society.

King F, Greidanus G, Jobe D J, 1999d. Dissolution of copper in chloride/ammonia mixtures and the implications for the stress corrosion cracking of copper containers. AECL-11865, COG-97-412-I. Atomic Energy of Canada Limited.

King F, Kolář M, 2000. The copper container corrosion model used in AECL's second case study. 06819-REP-01200-10041-R00. Ontario Power Generation, Nuclear Waste Management Division.

King F, 2001. The development of a predictive model for the SCC of copper containers in a Canadian geologic repository including the influence of microbially influenced corrosion. Report 06819-REP-01300-10024 R00. Ontario Power Generation, Nuclear Waste Management Division.

Kiss L, Farkas J, Korosi A, 1971. Ionization of metals and the neutralization of the metal ions on the rotating ring disk electrode. VII. Dependence of the anodic dissolution of copper on the concentration of the chloride ions. Acta Chim. Hung. 68, 359–370.

Kolář M, King F, 1996. Modelling the consumption of oxygen by container corrosion and reaction with Fe(II). Mat. Res. Soc. Symp. Proc. 412, p. 547–554. Materials Research Society.

Kostra J E, Wu J, Nealson H, Stucki J W, 1999. The impact of structural Fe(III) reduction by bacteria on the surface chemistry of smectite clay minerals, Geochim et Cosmochim. Acta, 63, 3705–3713.

Kotelnikova S, Pedersen K, 1998. Distribution and activity of methanogens and homoacetogens in deep granitic aquifers at Äspö Hard Rock Laboratory, Sweden. FEMS Microbiol. Ecol. 26, 121–134.

Kotelnikova S, Pedersen K, 1999. The microbe-REX project: Microbial O_2 consumption in the Äspö tunnel. SKB TR-99-17. Svensk Kärnbränslehantering AB.

Kotelnikova S, Pedersen K, 2000. Microbial oxygen reduction during the REX field experiment. SKB International Progress Report 00-19. Svensk Kärnbränslehantering AB.

Kubaschewski O, Alcock C B, Spencer P J, 1993. Materials Thermochemistry. Pergamon Press, Oxford, 363 p. 6 edition.

Laaksoharju M (ed.), 1995. Sulphate reduction in the Äspö HRL tunnel. SKB TR-95-25, Svensk Kärnbränslehantering AB.

Langmuir D, 1997. Aqueous Environmental Geochemistry. Prentice Hall, Upper Saddle River.

Laz M M, Souto R M, González S, Salvarezza R C, Arvia A J, 1992. Pitting corrosion of polycrystalline annealed copper in alkaline sodium perchlorate solutions containing benzotriazole. J. Appl. Electrochem. 22, 1129–1134.

Lee H P, Nobe K, 1986. Kinetics and mechanisms of Cu electrodissolution in chloride media. J. Electrochem. Soc. 133, 2035–2043.

Leygraf C, 1995. Atmospheric Corrosion, in: Corrosion Mechanisms in Theory and Practice, Eds.: P. Marcus and J. Oudar, Marcel Dekker, New York, NY.

Litke C D, Ryan S R, King F, 1992. A mechanistic study of the uniform corrosion of copper in compacted clay-sand soil, AECL-10397, COG-91-304. Atomic Energy of Canada Limited.

Lobo V M, 1989. Handbook of electrolyte solutions, Elsevier, Amsterdam.

Lucey V F, 1967. Mechanism of pitting corrosion of copper in supply waters. Br. Corros. J. 2, 175–185.

Luukkonen A, 2001. Groundwater mixing and geochemical reactions – An inverse-modelling approach. (Task5 modelling exercise, draft).

Lyle F F, 1993. Experimental evaluation of copper corrosion by constituents of natural gas. Final report, September 1988 – March 1993. PB93-193621/XAB. Southwest Research Institute.

Löfman J, 1999. Site scale groundwater flow in Olkiluoto. Report Posiva 99-03. Posiva Oy.

Löfman J, 2000. Site scale groundwater flow in Olkiluoto – Complementary simulations. Report Posiva 2000-07. Posiva Oy.

Macdonald D D, Syrett B C, Wing S S, 1979. The corrosion of Cu-Ni alloys 706 and 715 in flowing sea water. II-Effect of dissolved sulfide. Corrosion 35, 367–378.

Mansfeld F, Liu G, Xiao H, Tsai C H, Little B J, 1994. The corrosion behavior of copper alloys, stainless steels and titanium in seawater. Corros. Sci. 36, 2063–2095.

Marsh G P, 1990. A preliminary assessment of the advanced cold process canister. Harwell Laboratory, Report AEA-InTec-0011. AEA Industrial Technology.

Mattsson E, 1997. Utvändig korrosion hos kopparkapslar i avvaktan på slutförvar och under slutförvarets inledningsskede, SKB Projekt Inkapsling Projekt PM 97-3420-22, Stockholm.

Mattsson E, 1980. Corrosion of copper and brass: practical experience in relation to basic data. Br. Corros. J. 15, 6–13.

Miley H A, Evans U R, 1948. Oxidation of copper in air. I Metallic corrosion, passivity and protection, Edward Arnold.

Mor E D, Beccaria A M, 1975. Behaviour of copper in artificial sea water containing sulphides. Br. Corros. J. 10, 33–38.

Mor E D, Beccaria A M, 1979. Effects of temperature on the corrosion of copper in seawater at different hydrostatic pressures. Werkst. Korros. 30, 551–558.

Motamedi M, Karland O, Pedersen K, 1996. Survial of sulfate reducing bacteria at different water activities in compacted bentonite. FEMS Microbiol Lett 141, 83–87.

Muurinen A, Lehikoinen J, 1999. Porewater chemistry in compacted bentonite. Posiva 99-20. Posiva Oy.

NBS 82 according to HSC Chemistry ver 3.0, Outokumpu Research Oy.

Neretnieks I, Skagius C, 1978. Diffusivitetsmätningar av metan och väte i våt lera, KBS TR-86, Svensk Kärnbränslehantering AB.

Nilsson A-C, 1995. Compilation of groundwater chemistry data from Äspö 1990–1994. SKB MRL Progress Report 25-95-02, Svensk Kärnbränslehantering AB.

Nishikata A, Itagaki M, Tsuru T, Haruyama S, 1990. Passivation and its stability on copper in alkaline solutions containing carbonate and chloride ions. Corros. Sci. 31, 287–292.

Parkins R N, Singh A, 1990. Stress corrosion crack coalescence. Corrosion 46, 485–499.

Pedersen K, Ekendahl S, 1992. Incorporation of CO_2 and introduced organic compounds by bacterial populations in groundwater from the deep crystalline bedrock of the Stripa mine. J Gen Microbiol 138, 369–376.

Pedersen K, 1993. The deep subterranean biosphere. Earth-Science Rev. 34, 243–260.

Pedersen K, Karlsson F, 1995. Investigations of subterranean microorganisms – their importance for performance assessment of radioactive waste disposal. SKB TR-95-10, Svensk Kärnbränslehantering AB.

Pedersen K, Arlinger J, Ekendahl S, Hallbeck L, 1996. 16S rRNA gene diversity of attached and unattached groundwater bacteria along the access tunnel to the Äspö Hard Rock Laboratory, Sweden. FEMS Microbiol. Ecol. 19, 249–262.

Pedersen K, 1997. Microbial life in granitic rock. FEMS Microbiol Rev 20, 399–414.

Pedersen K, Hallbeck L, Arlinger J, Erlandson A-C, Jahromi N, 1997. Investigation of the potential for microbial contamination of deep granitic aquifers during drilling using 16S rRNA gene sequencing and culturing methods. J. Microbiol. Meth. 30, 179–192.

Pedersen K, 2000. Microbial processes in radioactive waste disposal. SBK TR-00-04. Svensk Kärnbränslehantering AB.

Pedersen K, Motamedi M, Karnland O, Sandén T, 2000a. Cultivability of microorganisms introduced into a compacted bentonite clay buffer under high-level radioactive waste repository conditions. Engin. Geol. 58, 149–161.

Pedersen K, Motamedi M, Karnland O, Sandén T, 2000b. Mixing and sulphate-reducing activity of bacteria in swelling compacted bentonite clay under high-level radioactive waste repository conditions. J. Appl. Microbiol. 89, 1038–1047.

Pedersen K, 2001. Diversity and activity of microorganisms in deep igneous rock aquifers of the Fennoscandian Shield. In Subsurface Microbiology and Biogeochemistry, Fredrickson J.K., Fletcher M. (eds). pp 97–139. Wiley-Liss Inc., New York.

Pednekar S P, Agrawal A K, Chaung H E, Staehle R W, 1979. Transgranular cracking of copper in 1M $NaNO_2$ solution. J. Electrochem. Soc. 126, 701–702.

Pérez Sánchez M, Barrera M, González S, Souto R M, Salvarezza R C, Arvia A J, 1990. Electrochemical behaviour of copper in aqueous moderate alkaline media containing sodium carbonate and bicarbonate and sodium perchlorate. Electrochim. Acta 35, 1337–1343.

Pérez Sánchez M, Souto R M, Barrera M, González S, Salvarezza R C, Arvia A J, 1993. A mechanistic approach to the electroformation of anodic layers on copper and their electroreduction in aqueous solutions containing $NaHCO_3$ and Na_2CO_3. Electrochim. Acta 38, 703–715.

Perry D L, Taylor J A, 1986. X-ray photoelectron and Auger spectroscopic studies of Cu_2S and CuS. J. Mat. Sci. Lett. 5, 384–386.

Peters D G, Cruser S A, 1965. Cathodic chronopotentiometry of copper(I) and copper(II) in chloride media. J. Electroanal. Chem. 9, 27–40.

Pettersson K, Oskarsson M, 1997. A study of stress corrosion crack growth in copper for nuclear waste canister application. TRITA-MAC-0611, Materials Research Center, Royal Institute of Technology.

Pettersson K, Oskarsson M, 2000. Stress corrosion crack growth in copper for waste canister applications. Mat. Res. Soc. Symp. Proc. 608, 95–101, Materials Research Society.

Pinnel M R, Tompkins H G, Heath D E, 1979. Oxidation of copper in controlled clean air and standard laboratory air at 50°C and 150°C, Appl. Surf. Sci. 2, pp. 558–577.

Pitkänen P, Snellman M, Vuorinen U, 1996. On the origin and chemical evolution of groundwater at the Olkiluoto site. Report POSIVA-96-04. Posiva Oy.

Pitkänen P, Luukkonen A, Ruotsalainen P, Leino-Forsman H, Vuorinen U, 1999. Geochemical modelling of groundwater evolution and residence time at the Olkiluoto site. Report POSIVA-98-10. Posiva Oy.

Pitzer K S, 1991. Ion interaction approach – theory and data correlation. In Activity coefficients in electrolyte solutions, K. S. Pitzer editor: 2. ed. Boca Raton: CRC Press.

Pitzer K S, 1995. Thermodynamics. McGraw-Hill, New York.

Plyasunova N V, Wang M, Zhang Y, Muhammed M, 1997. Critical evaluation of thermodynamics of complex formation of metal ions in aqueous solutions II. Hydrolysis and hydroxo-complexes of Cu^{2+} at 298.15 K. Hydrometallurgy 45, 37–51.

Pourbaix M, Pourbaix A, 1992. Potential-pH diagrams for the system S-H_2O from 25 to 150°C: Influence of access of oxygen in sulphide solutions. Geochim. Cosmochim. Acta 56, 3157–3178.

Power G P, Ritchie IM, 1981. Mixed potential measurements in the elucidation of corrosion mechanisms – 1. Introductory theory. Electrochim. Acta 26, 1073–1078.

Press W H, Teukolsky S A, Vetterling W T, Flannary B P, 1992. Numerical Recipes in C", 2nd ed, Cambridge University Press, Cambridge.

Pugh E N, Montague W G, Westwood A R C, 1966. Stress-corrosion cracking of copper. Corros. Sci. 6, 345–346.

Pugh E N, Craig J V, Sedriks A J, 1969. The stress-corrosion cracking of copper, silver and gold alloys. In Fundamental Aspects of Stress Corrosion Cracking (R.W. Staehle, A.J. Fory and D. van Rooyen, Editors) pp. 118–158. NACE.

Pugh E N, 1979. The stress-corrosion cracking of copper alloys. In Stress Corrosion Research, (H. Arup and R.N. Parkins, Editors), pp. 177–208. Sijthoff and Noordhoff.

Puigdomenech I, Rard J A, Plyasunov A V, Grenthe I, 1997. Temperature corrections to thermodynamic data and enthalpy calculations. In Modelling in Aquatic Chemistry (eds. I. Grenthe and I. Puigdomenech), pp. 427–493. OECD Nuclear Energy Agency.

Puigdomenech I, Taxén C, 2000. Thermodynamic data for copper. Implications for the corrosion of copper under repository conditions. SKB TR-00-13. Svensk Kärnbränslehantering AB.

Puigdomenech I, Taxén C, 2001. Thermodynamic data for copper from SKB TR-00-13. Appendix I in this report.

Puigdomenech I, Ambrosi J-P, Eisenlohr L, Lartigue J-E, Banwart S A, Bateman K, Milodowski A E, West J M, Griffault L, Gustafsson E, Hama K, Yoshida H, Kotelnikova S, Pedersen K, Michaud V, Trotignon L, Rivas Perez J, Tullborg E-L, 2001. O_2 depletion in granitic media. The REX project. SKB TR-01-05. Svensk Kärnbränslehantering AB.

Pusch R, Karnland O, Hökmark H, Sandén T, Börgesson L, 1991. Final report of the Rock Sealing Project – sealing properties and longevity of smectite clay grouts. Stripa Project Report TR 91-30. Svensk Kärnbränslehantering AB.

Qafsaoui W, Mankowski G, Dabosi F, 1993. The pitting corrosion of pure and low alloyed copper in chloride-containing borate buffered solutions. Corros. Sci. 34, 17–25.

Raiko H, Salo, J-P, 1999. Design report of the disposal canister for twelve fuel assemblies. Report POSIVA-99-18. Posiva Oy.

Reed D T, Swayambunathan V, Tani B S, Van Konynenburg R A, 1990. Corrosion product identification and relative rates of corrosion of candidate metals in an irradiated air-steam environment. Mat. Res. Soc. Symp. Proc. Vol. 176, pp. 517–524, Materials Research Society.

Reed D T, Van Konynenburg R A, 1991. Effect of ionizing radiation on moist air systems. Mat. Res. Soc. Symp. Proc. Vol. 212, pp. 317–325, Materials Research Society.

Rice D W, Peterson P, Rigby E B, Phipps P B P, Cappel R J, Tremoureux R, 1981. Atmospheric corrosion of copper and silver, J. Electrochem. Soc. 128, pp. 275–284.

Robie R A, Hemingway B S, 1995. Thermodynamic properties of minerals and related substances at 298.15 K and 1 bar (10^5 Pascals) pressure and at higher temperatures, USGS Bull. 2131, p. 461. U.S. Geological Survey.

Robinson R A, Stokes R H, 1959. Electrolyte Solutions, 2nd ed. Butterworths.

Romanoff M, 1989. Underground Corrosion. NACE International.

Rosborg B, Svensson B-M, 1994. Stress corrosion testing of copper in synthetic groundwater. STUDSVIK/M-94/73. Studsvik Material AB.

Rosborg B, 1998. The resistance of the copper canister to stress corrosion cracking. STUDSVIK/M-98/100. Studsvik Material AB.

Rosborg B, Werme L, 2001. The resistance of pure copper to stress corrosion cracking in repository environments. Presentation at 2001 MRS Spring Meeting. In SKB TR-01-25, Svensk Kärnbränslehantering AB.

Roy S K, Sircar S C, 1981. A critical appraisal of the logarithmic rate law in the thin film formation during oxidation of copper and its alloys, Oxid. Metals 15, pp. 9–20.

Ryan S R, King F, 1994. The adsorption of Cu(II) on sodium bentonite in a synthetic saline groundwater. AECL-11062, COG-I-94-125. Atomic Energy of Canada Limited.

Ryan S R, Clarke C F, Ikeda B M, King F, Litke C D, McKay P, Mitton D B, 1994. An investigation of the long-term corrosion behaviour of selected nuclear fuel waste container materials under possible disposal vault conditions. Technical Record, TR-489, COG-94-55. Atomic Energy of Canada Limited.

Saario T, Laitinen T, Mäkelä K, Bojinov M, 1999. Literature survey on stress corrosion cracking of Cu in presence of nitrites, ammonia, carbonates and acetates. Posiva Working Report 99-57. Posiva Oy.

Sato S, Nagata K, 1978. Stress corrosion cracking of phosphorus deoxidised copper. J. Jpn. Copper Brass Res. Assoc. 17, 202–214.

Schüssler A, Exner H E, 1993. The corrosion of nickel-aluminium bronzes in seawater-I. Protective layer formation and the passivation mechanism. Corros. Sci. 34, 1793–1802.

Sharma V K, Millero F J, 1988. The oxidation of Cu(I) in electrolyte solutions. J. Sol. Chem. 17, 581–599.

Shoesmith D W, Lee W, 1977. The dissolution of cupric hydroxide films from copper surfaces. Electrochim. Acta 22, 1411.

Shoesmith D W, King F, 1999. The effects of gamma radiation on the corrosion of candidate materials for the fabrication of nuclear waste packages. AECL-11999. Atomic Energy of Canada Ltd.

Sieradzki K, Sabatini R L, Newman R C, 1984. Stress-corrosion cracking of copper single crystals. Metall. Trans. A 15A, 1941-1946.

Sieradzki K, Kim J S, 1992. Etch pitting and stress-corrosion cracking of copper. Acta Metall. Mater. 40, 625-635.

Simpson J P, 1984. Experiments on container materials for Swiss high-level waste disposal projects Part II. Nagra Technical Report 84-01. Nagra.

Sirkiä P, Saario T, Mäkelä K, Laitinen T, Bojinov M, 1999. Electric and electrochemical properties of surface films formed on copper in the presence of bicarbonate anions. STUK Report, STUK-YTO-TR 157.

SITE 94, 1996. SKI Site 94 deep repository performance assessment projects. SKI Report 96:36. Swedish Nuclear Power Inspectorate.

SKB, 1983. Final storage of spent nuclear fuel – KBS-3. Volumes I-IV. Svensk Kärnbränsleförsörjning AB.

SKB, 1992. Background report to RD & D Programme 92. Treatment and final disposal of nuclear waste. Detailed R&D Programme 1993–1998. Svensk Kärnbränslehantering AB.

SKB, 1995. SR 95 – Template for safety reports with descriptive example. SKB TR 92-05. Svensk Kärnbränslehantering AB.

SKB, 1999a. Deep repository for spent nuclear fuel. SR 97 – Post closure safety. SKB TR-99-06, part I. Svensk Kärnbränslehantering AB.

SKB, 1999b. Deep repository for spent nuclear fuel. SR 97 – Post closure safety. SKB TR-99-06, part II. Svensk Kärnbränslehantering AB.

SKB, 1999c. Deep repository for spent nuclear fuel. SR 97 – Post-closure safety. Main Report, Volume I. SKB TR-99-06. Svensk Kärnbränslehantering AB.

SKB, 1999d. Deep repository for spent nuclear fuel. SR 97 – Post-closure safety. Main Report, Summary. SKB TR-99-06. Svensk Kärnbränslehantering AB.

SKB, 2000. Äspö Hard Rock Laboratory, Annual Report 1999. SKB TR-00-10. Svensk Kärnbränslehantering AB.

Smith R M, Martell A E, 1989. Critical stability constants. Volume 6: Second supplement. Plenum Press.

Smith R M, Martell A E, Motekaitis R J, 1998. NIST Critically selected stability constants of metal complexes database. Version 5. National Institute of Standards and Technology (NIST). Standard Reference Data Program, Gaithersburg. (http://www.nist.gov/srd).

Snellman M, Uotila H, Rantanen J, 1987. Laboratory and modelling studies of sodium bentonite groundwater interaction. Mat. Res. Soc. Symp. Proc. 84, 781–790, Materials Research Society.

Sridhar N, Cragnolino G A, 1993. Effects of environment on localized corrosion of copper-based, high-level waste container materials. Corrosion 49, 967–976.

Stumm W, Morgan J J, 1995. Aquatic Chemistry: Chemical Equilibria and Rates in Natural Waters, 3rd ed. Wiley.

Sunder S, Christensen H, 1993. Gamma radiolysis of water solutions relevant to the nuclear fuel waste management program, Nucl. Technol. 104, pp. 403–417.

Suzuki Y, Hisamatsu Y, 1981. Stress corrosion cracking of pure copper in dilute ammoniacal solution. Corros. Sci. 21, 353–368.

Suzuki I, Ishikawa Y, HisamatsuY, 1983. The pitting corrosion of copper tubes in hot water. Corros. Sci. 23, 1095–1106.

Swedish Corrosion Institute, 1978. Copper as a canister material for unreprocessed nuclear waste – evaluation with respect to corrosion. KBS-TR-90. Svensk Kärnbränsleförsörjning AB.

Swedish Corrosion Institute, 1983. The corrosion resistance of a copper canister for spent nuclear fuel – follow up. SKBF-KBS-TR-83-24. Svensk Kärnbränsleförsörjning AB.

Syrett B C, 1981. The mechanism of accelerated corrosion of copper-nickel alloys in sulphide-polluted seawater. Corros. Sci. 21, 187–209.

Taxén C, 1991. Pitting corrosion of copper with sulphide as the reaction of determining reactant. Report 53 698/3. Swedish Corrosion Institute.

Taxén C, 1996. In Proc. 13th International Corrosion Conference, Nov 25–29, 1996, Melbourne Australia. Proceedings, Paper #141.

Taxén C, 2000. Pitting corrosion of copper. Equilibrium – mass transport limitations. Mat. Res. Soc. Symp. Proc. 608, 103–108, Materials Research Society.

Thomas J G N, Tiller A K, 1972a. Formation and breakdown of surface films on copper in sodium hydrogen carbonate and sodium chloride solutions. I. Effects of anion concentrations. Br. Corros. J. 7, 256–262.

Thomas J G N, Tiller A K, 1972b. Formation and breakdown of surface films on copper in sodium hydrogen carbonate and sodium chloride solutions. II. Effects of temperature and pH. Br. Corros. J. 7, 263–267.

Thompson D H, Tracy A W, 1949. Influence of composition on the stress-corrosion cracking of some copper-base alloys. Metall. Trans. 1949, 100–109.

Tromans D, 1997. Copper and zinc equilibria in concentrated ammonia solutions: relevance to stress corrosion cracking of alpha-brass. Corros. Sci. 39, 1307–1319.

Uchida H, Inoue S, Koyama M, Morii M, Koterazawa K, 1991. Susceptibility to stress corrosion cracking of pure copper in $NaNO_2$ solutions. Soc. Mat. Sci. Jpn. 40, 1073–1078.

Var'yash L N, 1989. Equilibria in the Cu - Cu_2O - H_2O system at 150–450°C. Geochem. Int. 26 (10), 80–90.

Vasquez Moll D, de Chialvo M R G, Salvarezza R C, Arvia A J, 1985. Electrochim. Acta, 30, 1011–1016.

Vazquez M V, de Sanchez S R, Calvo E J, Schiffrin D J, 1994a. The electrochemical reduction of oxygen on polycrystalline copper in borax buffer. J. Electroanal. Chem. 374, 189–197.

Vazquez M V, de Sanchez S R, Calvo E J, Schiffrin D J, 1994b. The electrochemical reduction of hydrogen peroxide on polycrystalline copper in borax buffer. J. Electroanal. Chem. 374, 179–187.

Vieno T, 2000. Groundwater salinity at Olkiluoto and its effects on a spent fuel repository. POSIVA 2000-11. Posiva Oy.

Wagman D D, Evans W H, Parker V B, Schumm R H, Halow I, Bailey S M, Churney K L, Nuttall R L, 1982. The NBS tables of chemical thermodynamic properties. Selected values for inorganic and C1 and C2 organic substances in SI units. J. Phys. Chem. Ref. Data 11.

Walter R J, Matejczyk D E, Gunderloy F C, Morinishi R, 1989. Methane-fuel corrosion in regeneratively cooled rocket-engine combustors. Corrosion 45, 685–688.

Wang M, Zhang Y, Muhammed M, 1997. Critical evaluation of thermodynamics of complex formation of metal ions in aqueous solutions III. The system Cu(I,II) - Cl^- - e at 298.15 K. Hydrometallurgy 45, 53–72.

Wanner H, Wersin P, Sierro N, 1992. Thermodynamic modelling of bentonite-groundwater interaction and implications for near field chemistry in a repository for spent fuel. Swedish Nuclear Fuel and Waste Management Co, Stockholm, SKB TR 92-37.

Wanner H, Östhols E, 2000. Guidelines for the assignment of uncertainties. OECD/NEA Thermochemical Data Base Project, TDB-3. Le Seine-St. Germain, France. (http://www.nea.fr/html/dbtdb/cgi-bin/tdbdocproc.cgi).

Wehrli B, 1990. Redox reactions of metal ions at mineral surfaces. In Aquatic Chemical Kinetics (Editor, W. Stumm), Wiley-Interscience.

Werme L, Sellin P, Kjellbert N, 1992. Copper canisters for nuclear high level waste disposal. SKB TR 92-26, Svensk Kärnbränslehantering AB.

Werme L, 2000. Fabrication and testing of copper canister for long term isolation of spent fuel.

Wersin P, Spahiu K, Bruno J, 1994. Time evolution of dissolved oxygen and redox conditions in a HLW repository. SKB TR 94-02, Svensk Kärnbränslehantering AB.

Wersin P, Spahiu K, Bruno J, 1994b. Kinetic modelling of bentonite-canister interaction. Long-term predictions of copper canister corrosion under oxic and anoxic conditions. SKB TR 94-25, Svensk Kärnbränslehantering AB.

Wieland E, Wanner H, Albinsson Y, Wersin P, Karnland O, 1994. A surface chemcal model of the bentonite-water interface and its implications for modelling the near field chemistry in a repository for spent fuel. SKB TR 94-26, Svensk Kärnbränslehantering AB.

Xiao Z, Gammons C H, Williams-Jones A E, 1998. Experimental study of copper(I) chloride complexing in hydrothermal solutions at 40 to 300°C and saturated water vapor pressure. Geochim. Cosmochim. Acta 62(17), 2949–2964.

Yu J, Parkins R N, 1987. Stress corrosion crack propagation in a-brass and copper exposed to sodium nitrite solutions. Corros. Sci. 27, 159–182.

Yu J, Parkins R N, Xu Y, Thompson G, Wood G C, 1987. Stress corrosion crack initiation in a-brass exposed to sodium nitrite solutions. Corros. Sci. 27, 141–157.

Yunker W H, Glass R S, 1986. Long-term corrosion behavior of copper-base materials in a gamma-irradiated environment. Mat. Res. Soc. Symp. Proc. Vol. 84, 579–590, Materials Research Society.

Yunker W H, 1990. Corrosion behavior of copper-base materials in a gamma-irradiated environment. Final report. WHC-EP-0188. Westinghouse Hanford Company.

Appendix I

Thermodynamic data from SKB-TR 00-13

Table I-1. Thermodynamic data at 25°C for copper, copper compounds and aqueous species.

Species	$\Delta G_f°$ (kJ/mol)	$S°$ (J·K^{-1}·mol^{-1})	$C_p°(T)/(J·K^{-1}·mol^{-1}) = a + bT + cT^{-2}$		
			a†	b x 10^3	c x 10^{-6}
Cu(cr)	0.	33.15	20.531	8.611	0.155
Cu^+	48.87	40.6	57.3		
CuOH(aq)	−122.32	226	−280		
$Cu(OH)_2^-$	−333.05	−135	562		
Cu_2O(cr)	−147.90	92.36	58.199	23.974	−0.159
Cu^{2+}	65.04	−98.0	−23.8		
$CuOH^+$	−126.66	−61	382		
$Cu(OH)_2$(aq)	−316.54	26	214		
$Cu(OH)_3^-$	−493.98	−14	105		
$Cu(OH)_4^{2-}$	−657.48	−175	800		
$Cu_2(OH)_2^{2+}$	−285.1	−4	190		
$Cu_3(OH)_4^{2+}$	−633.0	−59	404		
CuO(cr)	−128.29	42.6	48.597	7.427	−0.761
$Cu(OH)_2$(cr)	−359.92	87.0	86.99	23.26	−0.54
CuF(cr)	−192.22	65.26	47.9		
CuF^+	−225.5	−38	99		
CuF_2(cr)	−501.5	73.0	72.01	19.96	−1.138
$CuF_2×2H_2O$(cr)	−998.21	152.75	152.3		
CuCl(aq)	−101.2	173.	−215		
$CuCl_2^-$	−245.6	202.	−20		
$CuCl_3^{2-}$	−372.48	217.	98		
$Cu_2Cl_4^{2-}$	−487.42	325	80		
$Cu_3Cl_6^{3-}$	−731.99	349	70		
CuCl(cr)	−120.	87.	38.28	34.98	
$CuCl^+$	−69.81	−3.25	88		
$CuCl_2$(aq)	−198.75	73.4	158		
$CuCl_3^-$	−321.25	121.6	187		
$CuCl_4^{2-}$	−437.05	145.9	174		
$CuCl_2$(cr)	−176.07	116.7	67.03	17.57	
$CuCl_2×3Cu(OH)_2$(cr)	−1339.9	335.57	312.621	134.86	−3.10959
$Cu_{37}Cl_8(SO_4)_2(OH)_{62}×8H_2O$(cr)	−15635.12	3409.	3525.3		
$CuClO_3^+$	55.14	36.3	161		
CuHS(aq)	−13.2	206	−209		
$Cu(HS)_2^-$	−22.98	239	32		
$Cu_2S(HS)_2^{2-}$	−32.59	80	−270		
Cu_2S(cr)	−84.11	116.2	52.84	78.74	
$Cu_{1.934}S$(cr)	−82.4	109.6	73.0		

† For aqueous ions and complexes "a" corresponds to the standard partial molar heat capacity at 25°C, and its temperature dependence has been calculated with the revised Helgeson-Kirkham-Flowers model as described in the text.

Table I-1. (Continued)

Species	$\Delta G_f°$ (kJ/mol)	$S°$ (J·K^{-1}·mol^{-1})	$C_p°(T)/$(J·K^{-1}·mol^{-1}) $= a + bT + cT^{-2}$		
			a†	b x 10^3	c x 10^{-6}
$Cu_{1.75}S$(cr)	−76.4	98.3	68.4		
CuS(cr)	−48.65	64.4	44.35	11.05	
$CuS_2O_3^-$	−531.36	130	−35		
Cu_2SO_4(cr)	−657.4	201	126.8		
$CuSO_4$(aq)	−692.154	−18.15	−96		
$CuSO_4$(cr)	−662.2	109.2	152.84	−12.30	−7.159
$CuSO_4 \times 5H_2O$(cr)	−1880.0	301.2	70.88	−18.58	
$Cu_4SO_4(OH)_6$(cr)	−1818.0	339.7	258.57	387.23	−4.4649
$Cu_4SO_4(OH)_6 \times H_2O$(cr)	−2044.0	335.	403.5		
$Cu_3SO_4(OH)_4$(cr)	−1446.6	266.4	362.7		
$CuO \times CuSO_4$(cr)	−792.26	157.3	170.83	45.355	−3.925
$Cu(NH_3)_2^+$	−64.5	272	207		
$CuNH_3^{2+}$	15.0	12.1	51		
$Cu(NH_3)_2^{2+}$	−31.2	112	126		
$Cu(NH_3)_3^{2+}$	−73.9	197	201		
$Cu(NH_3)_4^{2+}$	−112.1	272	276		
$CuNH_3OH^+$	−183.4	68	126		
$Cu(NH_3)_2(OH)_2$(aq)	−399.8	191	276		
$Cu(NH_3)_3OH^+$	−257.9	210	275		
$CuNO_2^+$	21.64	43.5	115		
$Cu(NO_2)_2$(aq)	−14.01	166.	170		
$CuNO_3^+$	−48.61	34.	130		
$Cu(NO_3)_2$(aq)	−154.26	185	−160		
$Cu(NO_3)_2 \times 3Cu(OH)_2$(cr)	−1278.67	399.2	415.0		
CuH_2PO_4(aq)	−1093.25	150	0		
$Cu(H_2PO_4)_2^-$	−2235.71	230	0		
$Cu(HPO_4)(H_2PO_4)^{2-}$	−2208.31	170	0		
$CuHPO_4$(aq)	−1054.35	−20	−70		
$Cu(HPO_4)_2^{2-}$	−2168.94	−170	−200		
$Cu(HPO_4)(H_2PO_4)^-$	−2198.64	−40	−200		
$CuH_2PO_4^+$	−1078.62	0	200		
$Cu(H_2PO_4)_2$(aq)	−2220.34	100	0		
$Cu_3(PO_4)_2$(cr)	−2066.20	370	229		
$Cu_3(PO_4)_2 \times 3H_2O$(cr)	−2767.75	504	351		
$CuCO_3$(aq)	−501.50	−19	−117		
$Cu(CO_3)_2^{2-}$	−1048.98	122	−410		
$CuHCO_3^+$	−532.08	65.4	170		
$CuCO_3$(cr)	−528.20	87.9	92.05	38.91	−1.799
$Cu_2CO_3(OH)_2$(cr)	−902.35	166.3	49.57	328.36	−0.616
$Cu_3(CO_3)_2(OH)_2$(cr)	−1431.43	254.4	137.89	387.46	−2.205

Table I-2. Thermodynamic data at 25°C for auxiliary species.

Species	$\Delta G_f°$ (kJ·mol^{-1})	$S°$ (J·K^{-1}·mol^{-1})	$C_p°$ (J·K^{-1}·mol^{-1})
H_2(g)	0.	130.68	‡
H^+	0.	0.	0.
OH^-	−157.22	−10.9	−125.
F^-	−281.5	−13.8	−113.9
HF(g)	−275.4	173.78	29.14
HF(aq)	−299.675	88.	−58.6
HF_2^-	−583.709	92.68	−138.9
Cl^-	−131.20	56.6	−123.2
ClO_3^-	−7.903	162.3	−51.5
S(cr)	0.	32.05	‡
H_2S(g)	−33.4	205.81	‡
H_2S(aq)	−27.648	126.0	178.7
HS^-	12.243	67.0	−93.
S^{2-}	120.7	−14.6	−300.
S_5^{2-}	66.96	187.	−180.
HS_5^-	32.14	269.	27.
H_2S_5(aq)	9.88	328.	297.
S_4^{2-}	66.22	165.	−210.
HS_4^-	27.98	247.	267.
H_2S_4(aq)	4.0	306.	273.
S_3^{2-}	78.2	95.	−240.
S_2^{2-}	97.17	5.	−210.
S_2^-	58.18	144.	−105.
$S_2O_3^{2-}$	−522.58	66.94	−240.
$HS_2O_3^-$	−532.21	127.6	14.6
$H_2S_2O_3$(aq)	−535.55	188.3	115.1
SO_3^{2-}	−487.47	−29.	−318.
HSO_3^-	−528.69	139.7	−6.
H_2SO_3(aq)	−539.19	231.9	270.
SO_4^{2-}	−744.00	18.5	−269.
HSO_4^-	−755.32	131.7	−18.
H_2SO_4(aq)	−748.47	83.5	250.
NO_3^-	−110.79	146.7	−69.
NO_2^-	−32.22	123.0	−97.5
HNO_2(aq)	−50.63	135.56	28.
NH_3(g)	−16.41	192.77	‡
NH_3(aq)	−26.67	109.04	74.9
NH_4^+	−79.40	111.17	65.9
PH_3(g)	13.4	210.23	‡
PH_3(aq)	25.36	120.1	188.

‡ Heat capacity functions:

H_2(g) $C_p°(T)/(J·K^{-1}·mol^{-1}) = 7.442 + 0.011707\ T - 1.3899'10^{-6}\ T^2 - 5.1041'10^5\ T^{-2} + 410.17\ T^{-0.5}$

S(cr) $C_p°(T)/(J·K^{-1}·mol^{-1}) = 14.795 + 0.024075\ T + 7.1'10^4\ T^{-2}$

H_2S(g) $C_p°(T)/(J·K^{-1}·mol^{-1}) = 26.356 + 0.026497\ T - 6.0244'10^{-6}\ T^2 + 2.6599'10^5\ T^{-2} - 43.559\ T^{-0.5}$

NH_3(g) $C_p°(T)/(J·K^{-1}·mol^{-1}) = 51.39 + 0.0266\ T - 4.90'10^{-6}\ T^2 + 7.584'10^5\ T^{-2} - 548.0\ T^{-0.5}$

PH_3(g) $C_p°(T)/(J·K^{-1}·mol^{-1}) = 26.3 + 0.04048\ T - 1.14'10^5\ T^{-2}$

Table I-2. (Continued)

Species	$\Delta G_f°$ (kJ·mol^{-1})	$S°$ (J·K^{-1}·mol^{-1})	$C_p°$ (J·K^{-1}·mol^{-1})
H_3PO_4(aq)	−1149.367	161.91	98.7
$H_2PO_4^-$	−1137.15	92.5	−29.3
HPO_4^{2-}	−1095.99	−33.5	−243.9
PO_4^{3-}	−1025.49	−220.97	−480.7
CO_2(g)	−394.37	213.79	‡
"CO_2(aq)"	−385.97	119.36	243.1
HCO_3^-	−586.845	98.4	−35.4
CO_3^{2-}	−527.899	−50.0	−290.8
C(cr)	0.	5.74	‡
CH_4(g)	−50.7	186.26	‡
CH_4(aq)	−34.451	87.82	277.4
Na^+	−262.00	58.45	37.9
NaOH(aq)	−417.98	44.8	−13.4
NaF(aq)	−537.94	50.2	46.9
NaCl(aq)	−388.74	117.2	35.6
$NaSO_4^-$	−1010.12	95.	−16.1
$NaCO_3^-$	−792.99	−43.9	−37.9
$NaHCO_3$(aq)	−847.89	120.9	89.5
$NaPO_4^{2-}$	−1295.61	−100.5	−192.8
$NaHPO_4^-$	−1360.79	−27.4	9.0
Ca^{2+}	−552.8	−56.2	−31.5
$CaOH^+$	−716.72	28.0	5.9
$Ca(OH)_2$(cr)	−898.0	83.4	‡
CaF^+	−838.43	−37.7	125.9
CaF_2(cr)	−1175.3	68.9	‡
$CaCl^+$	−682.41	18.8	73.1
$CaCl_2$(aq)	−811.70	25.1	129.5
$CaSO_4$(aq)	−1309.3	20.9	−104.6
$CaSO_4$(cr)	−1321.8	107.4	‡
$CaSO_4 \times 2H_2O$(cr)	−1797.0	193.8	183.
$CaCO_3$(aq)	−1099.76	10.5	−123.9
$CaHCO_3^+$	−1145.99	101.1	163.1
$CaCO_3$(cr)	−1129.10	91.71	‡
$CaPO_4^-$	−1615.17	−110.0	−212.2
$CaHPO_4$(aq)	−1664.43	9.1	−78.4
$CaH_2PO_4^+$	−1698.01	111.02	89.2
$Ca_5(PO_4)_3OH$(cr)	−6337.1	390.4	‡
$Ca_5(PO_4)_3F$(cr)	−6489.7	387.9	‡

‡: Heat capacity functions:

CO_2(g) $C_p°(T)/(J{\cdot}K^{-1}{\cdot}mol^{-1}) = 87.82 - 0.0026442\ T + 7.064'10^5\ T^{-2} - 99.886\ T^{-0.5}$

C(cr) $C_p°(T)/(J{\cdot}K^{-1}{\cdot}mol^{-1}) = 60.86 - 0.01024\ T + 1.669'10^{-6}\ T^2 + 7.139'10^5\ T^{-2} - 99.22\ T^{-0.5}$

CH_4(g) $C_p°(T)/(J{\cdot}K^{-1}{\cdot}mol^{-1}) = 119.4 + 0.02055\ T - 5.0'10^{-6}\ T^2 + 2.814'10^6\ T^{-2} - 2090\ T^{-0.5}$

$Ca(OH)_2$(cr) $C_p°(T)/(J{\cdot}K^{-1}{\cdot}mol^{-1}) = 186.7 - 0.02191\ T - 1600\ T^{-0.5}$

CaF_2(cr) $C_p°(T)/(J{\cdot}K^{-1}{\cdot}mol^{-1}) = 2033 - 1.436\ T + 5.04'10^{-4}\ T^2 + 2.988'10^7\ T^{-2} - 33120\ T^{-0.5}$

$CaSO_4$(cr) $C_p°(T)/(J{\cdot}K^{-1}{\cdot}mol^{-1}) = 372.8 - 0.1574\ T + 7.99'10^{-5}\ T^2 + 1.695'10^6\ T^{-2} - 4330.8\ T^{-0.5}$

$CaCO_3$(cr) $C_p°(T)/(J{\cdot}K^{-1}{\cdot}mol^{-1}) = 99.546 + 0.027137\ T - 2.1481'10^6\ T^{-2}$

$Ca_5(PO_4)_3OH$(cr) $C_p°(T)/(J{\cdot}K^{-1}{\cdot}mol^{-1}) = 387.8 + 0.1186\ T - 1.27'10^7\ T^{-2} + 1811\ T^{-0.5}$

$Ca_5(PO_4)_3F$(cr) $C_p°(T)/(J{\cdot}K^{-1}{\cdot}mol^{-1}) = 754.3 - 0.03026\ T - 9.084'10^5\ T^{-2} - 6201\ T^{-0.5}$

Appendix II

Discussion and selection of thermodynamic data (L. Ahonen)

Cu^{+} – Cu^{2+} equilibrium

A revised, internally consistent thermodynamic data set for different oxidation states of copper is given in table II-1. Compared to the corresponding data set of Ahonen /1995/, certain changes have been made, and are explained below.

Wang et al. /1997/ re-interpreted the data of several earlier studies on copper disproportionation (equation 1 in table II-1). Their results indicated that the stability constant of this reaction, when extrapolated from several experiments to an ionic strength of I = 0, fall 0.2–0.3 units below 6.0 (figure II-1). The final values given were logK° = –5.76±0.06, ΔH° = 87.8 ± 5.0). Other recent studies support this result /Ciavatta 1980/.

Using the CODATA key values for Cu^{2+}, Wang et al. /1997/ calculated a ΔG°-value of 48.99±0.24 kJ/mol for aqueous Cu^{+}, compared with the value given by Robie and Hemingway /1995/ is 50.0 kJ/mol. Due to the discrepancy between these values, as well as the need to maintain internal consistency of the database, the logK-value for copper disproportionation was rounded to 5.8. Consequently, the value of the standard free energy of formation of Cu^{+}(aq) increases to 49.1, which is clearly within the given range of uncertainty.

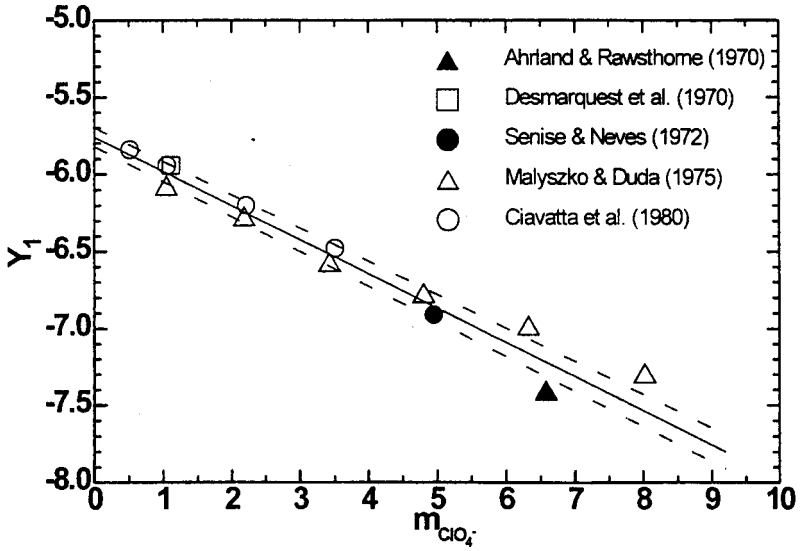

***Figure II-1**. Extrapolation of the stability constant for the copper disproportionation reaction to I = 0 /from Wang et al. 1997/.*

Table II-1: Thermodynamic data for the system $Cu^{\circ}(cr)$–$Cu^{+}(aq)$–$Cu^{2+}(aq)$. CODATA key values are indicated by bold text.

	ΔG° kJ/mol	ΔH° kJ/mol	C_p° J/K·mol	$logK_{25}$	$logK_{100}$	Eqn. #
$2Cu^{+} = Cu^{2+} + Cu^{\circ}$	−33.1	−87.8	−118	5.8	2.6	1
$Cu^{\circ} = Cu^{2+} + 2e-$	**65.1**	**64.9**	−44	−11.4	−9.2	2
$Cu^{\circ} = Cu^{+} + e-$	49.1	76.35	+37	−8.6	−5.9	3
$Cu^{+} = Cu^{2+} + e-$	16.0	−11.45	−81	−2.8	−3.3	4

Copper-chloride complexes

Since 1995 /Ahonen 1995/, new research papers on the thermodynamics of the system Cu-Cl have been published: Wang et al. /1997/ re-extrapolated the data of several previous studies to infinite dilution (I = 0) using the specific interaction theory (SIT), and Xiao et al. /1998/ reported an experimental study on the copper(I)-chloride complexes for the temperature range 40°–300° C. As a rule, the new information is in accordance with the earlier data on the thermodynamics of the system. However, certain relationships between Cu-Cl complexes are now defined more precisely. The revised thermodynamic data are presented in table II-2.

Stability-constant determinations of copper(I) chloride complexes are mainly based on solubility experiments of solid cuprous chloride (nantokite, CuCl(cr)). At different chloride concentrations, different complexes prevail:

$$CuCl(cr) + (x-1)Cl^{-} = CuCl_x^{(1-x)} \quad (x = 1 \text{ or higher}) \qquad \text{II-1}$$

Data on the stability constant of the uncharged complex ($CuCl^{\circ}$) are scarce in low-temperature studies, probably because of the predominance of the higher complexes. However, formation of this complex has been frequently reported in experiments carried out at higher temperatures, and the data can be reliably extrapolated to 25° C /e.g., Xiao et al. 1998/.

The most important copper(I)-chloride complexes are $CuCl_2^{-}$ and $CuCl_3^{2-}$. With respect to these complexes, the results of Wang et al. /1997/ and Xiao et al. /1998/ are in agreement; at chloride concentrations from 10 mM to 5 M, $CuCl_2^{-}$ is the predominant form.

Copper(II)-chloride complexes are much less stable than those of Cu(I). In numerous studies, the stability constant values are reported to be around zero. Data presented in table II-2 are taken from Wang et al. 1997, whenever possible. In order to maintain consistency between all standard free energy data and logK's, some values are not exactly the same as in the original paper, but always clearly within the given limits of uncertainty. Consistency with CODATA recommended key values were also checked.

Table II-2. Thermodynamic data for the aqueous system Cu^{+}–Cu^{2+} – Cl^{-}.

	$\Delta G°$ kJ/mol	$\Delta H°$ kJ/mol	$\Delta C_r°$ J/K·mol	$\log K_{25}$	$\log K_{100}$	Eqn.#
$CuCl(cr) = Cu^{+} + Cl^{-}$	39.1	47.35	−104	−6.9	−5.4	5
$Cu^{+} + Cl^{-} = CuCl(aq)$	−18.8	+2	−149	3.3	+3.2	6
$Cu^{+} + 2Cl^{-} = CuCl_2^{-}$	−32.6	−20	+169	5.7	+5.2	7
$Cu^{+} + 3Cl^{-} = CuCl_3^{2-}$	−28.5	−33	+410	5.0	+4.3	8
$Cu^{2+} + Cl^{-} = CuCl^{+}$	−3.7	8.7	+235	0.64	+1.2	9
$Cu^{2+} + 2Cl^{-} = CuCl_2°$	−3.5	23	+428	0.6	+1.9	10
$Cu^{2+} + 3Cl^{-} = CuCl_3^{-}$	5.7	20	+580	−1	+0.4	11
$CuCl_2(cr) = Cu^{2+} + 2Cl^{-}$	21.6	37	−337	−3.8	−2.9	12
$CuCl_2 \times 3Cu(OH)_2(cr) + 6H^{+}$ $= 4Cu^{2+} + 2Cl^{-} + 6H_2O$	−85	−130	−202	14.9	+10.1	13
$Cu^{+} + Cl^{-} + H_2O = CuClOH^{-} + H^{+}$	24.5	+13	0	−4.3	−3.8	14

Data for the two solid cupric chloride phases in table II-2 are taken from Wagman et al. 1982 and from Barton and Bethke /1960/. Different polynuclear copper(I) chloride complexes may exist in concentrated chloride solutions (>3–5 M) and high copper concentrations (>1M) /Wang et al. 1997/. Due to the large uncertainty involved and due to their negligible role for chloride concentrations below 1 M, the complexes $CuCl_4^{2-}$, $Cu_2Cl_4^{2-}$ and $Cu_3Cl_6^{3-}$ are not included in the present database. A mixed hydroxide-chloride complex, CuClOH was included in the database of Ahonen /1995/. The existence of this complex may be considered questionable, because of the scarcity of data. However, because this complex may be important in basic conditions (pH ~8 and higher) in warm (80–100°C) water /Ahonen 1995/, it is also included into the present database.

Hydrolysis of copper

Formation of hydroxo-complexes are important reactions for copper(II) in natural waters. Thermodynamic properties of the copper-hydroxide complexes have been extensively studied (a list of references up to 1995 was given by Ahonen /1995/). Plyasunova et al. /1997/ published a critical evaluation of several recent publications, and re-extrapolated the data using the SIT method. The data are summarized in table II-3.

Copper(I) is far less hydrolyzable than Cu(II). There are very few experimental data on the stability constants of Cu(I) hydroxide complexes. Beverskog and Puigdomenech /1998/ reported the standard free energies of formation of complexes Cu(OH)° and $Cu(OH)_2^{-}$, being based on the data of Var'yash /1989/. Standard enthalpy values for equations 23 and 24 (table II-3) are estimated to match the temperature dependence of the free energy change between 25°C and 200°C reported by Var'yash /1989/.

Table II-3. Thermodynamic data for the system Cu^{+}–Cu^{2+} – H_2O.

	$\Delta G°$ kJ/mol	$\Delta H°$ kJ/mol	$\Delta C_r°$ J/K·mol	$\log K_{25}$	$\log K_{100}$	Eqn.#
$CuO(cr) + 2H^+ = Cu^{2+} + H_2O$	−43.6	−64.9	3	7.64	5.4	15
$Cu^{2+} + H_2O = Cu(OH)^+ + H^+$	45.5	36	331	−7.97	−6.3	16
$Cu^{2+} + 2H_2O = Cu(OH)_2° + 2H^+$	92.7	92.8	87	−16.2	−12.8	17
$Cu^{2+} + 3H_2O = Cu(OH)_3^- + 3H^+$	152	–	−97	26.6	+26.4	18
$Cu^{2+} + 4H_2O = Cu(OH)_4^{2-} + 4H^+$	227	178	+523	39.7	+46.6	19
$2Cu^{2+} + 2H_2O = Cu_2(OH)_2^{2+} + 2H^+$	60.2	75	+87	−10.5	−7.8	20
$3Cu^{2+} + 4H_2O = Cu_3(OH)_4^{2+} + 4H^+$	120	110	+174	−21.0	−16.9	21
$Cu_2O(cr) + 2H^+ = 2Cu^+ + H_2O$	8.86	37.5	+131	−1.55	−0.1	22
$Cu^+ + H_2O = Cu(OH)° + H^+$	66	75	−413	−11.6	−9.5	23
$Cu^+ + 2H_2O = Cu(OH)_2^- + 2H^+$	92	15	+354	−16.1	−15.1	24

Complexes of Cu with N-compounds

Copper(II)-ammonia complexes have been extensively studied over the last few decades. Stability constants reported in recent studies agree well with each other. The data listed in table II-4 are derived from Puigdomenech and Taxén /2000/, being in accordance with the most recent compilations of thermodynamic properties of these complexes. The main uncertainty is in the enthalpy values of the mixed hydroxo-ammonia complexes, which have been estimated as the sum of enthalpies for the single-ligand complex reactions.

The existence and stability of Cu(I)-ammonia complexes is far less well-established than that of the corresponding Cu(II) complexes. There are only a few studies in the literature reporting the existence of $CuNH_3^+$ or $Cu(NH_3)_2^+$. However, in deeply reducing conditions, Cu(I) and (NH_4^+) are expected to be the predominant oxidation states of copper and nitrogen, respectively. Consequently, the possible existence of these complexes must be taken into consideration.

Nitrite is not a thermodynamically stable oxidation state of nitrogen, but it may exist in small amounts in natural groundwaters. Only Cu(II) complexes with NO_2^- have been reported. Stability constants reported in table II-4 for these complexes are those given by Puigdomenech and Taxén /2000/, being in accordance with other sources. Enthalpy data for the formation of these complexes are not available. Formation of corresponding complexes of silver ($AgNO_2°$ and $Ag(NO_2)_2^-$) and cadmium have negative enthalpies /Smith and Martell 1989/, indicating that the stability of the complexes decreases with increasing temperature. In order to get qualitative information on the temperature dependence of the copper-nitrite complexes, enthalpy data of the silver complexes was used for copper in table II-4.

Copper(II) forms two weak complexes with nitrate (NO_3^-), their stability constants listed in Smith et al. /1998/ are given in table II-4. No data on the temperature-dependence of the formation of these complexes are available, but the temperature dependence is assumed to be negligible between 25° and 100° C /Puigdomenech and Taxén 2000/, and the enthalpy value was set to zero in table II-4.

Table II-4. Thermodynamic data for the copper-nitrogen complexes.

	ΔG° kJ/mol	ΔH° kJ/mol	$\Delta C_r°$ J/K·mol	$\log K_{25}$	$\log K_{100}$	Eqn. #
$NH_4^+ = NH_3(aq) + H^+$	52.7	52.1	−2	−9.2	−7.4	25
$Cu^{2+} + NH_4^+ = CuNH_3^{2+} + H^+$	29.9	28.1	−36	−5.2	−4.3	26
$Cu^{2+} + 2NH_4^+ = Cu(NH_3)_2^{2+} + 2H^+$	62.5	59.2	−76	−11	−9.0	27
$Cu^{2+} + 3NH_4^+ = Cu(NH_3)_3^{2+} + 3H^+$	99.2	88	−109	−17.4	−14.4	28
$Cu^{2+} + 4NH_4^+ = Cu(NH_3)_4^{2+} + 3H^+$	140	118	−145	−24.6	−20.6	29
$Cu^{2+} + NH_4^+ + H_2O = CuNH_3OH^+ + 2H^+$	68	64	−37	−11.9	−9.7	30
$Cu^{2+} + 2NH_4^+ + 2H_2O = Cu(NH_3)_2(OH)_2 + 4H^+$	170	145	−73	−30	−25	31
$Cu^{2+} + 3NH_4^+ + H_2O = Cu(NH_3)_3OH^+ + 4H^+$	154	120	−110	−27	−22.9	32
$Cu^+ + 2NH_4^+ = Cu(NH_3)_2^+ + 2H^+$	46	48	−73	−8	−6.4	33
$Cu^{2+} + NO_2^- = CuNO_2^+$	−11	−30	236	2	+1.2	34
$Cu^{2+} + 2NO_2^- = Cu(NO_2)_2$	−15	−45	389	2.6	+1.5	35
$Cu^{2+} + NO_3^- = CuNO_3^+$	−3	0	223	0.5	+0.8	36
$Cu^{2+} + 2NO_3^- = Cu(NO_3)_2$	2	0	2	−0.4	−0.4	37

Copper-carbonate complexes

Bicarbonate is a common constituent of natural waters, and copper (II) has a strong tendency to form complexes with CO_3^{2-} and HCO_3^-. Puigdomenech and Taxén /2000/ reviewed the recent literature, and recommended the data set presented in table II-5. Compared to Ahonen /1995/, the main difference is in the stability constant of the bicarbonate complex; the value of log K = 1.8 (equation 41) has been used instead of the earlier value 4.27 of Ahonen /1995/. The main implication of this correction is that the predominance field of the Cu(II)-bicarbonate complex vanishes at pH values below 6.

Table II-5. Thermodynamic data for the copper-carbonate complexes and solids.

	ΔG° kJ/mol	ΔH° kJ/mol	$\Delta C_r°$ J/K·mol	$\log K_{25}$	$\log K_{100}$	Eqn. #
$CuCO_3(s) = Cu^{2+} + CO_3^{2-}$	+65.4		−407	−11.5	−12.0	38
$Cu^{2+} + HCO_3^- = CuCO_3(aq) + H^+$	+20.2	+25	−58	−3.5	−2.7	39
$Cu^{2+} + 2HCO_3^- = Cu(CO_3)_2^{2-} + 2H^+$	+59.6	?	−15	−10.4	−10.4	40
$Cu^{2+} + HCO_3^- = CuHCO_3^+$	−10.2	?	+229	+1.8	+2.1	41
$Cu_2CO_3(OH)_2(s) + 3H^+ = 2Cu^{2+} + HCO_3^- + 2H_2O$	−28.3	?		+5		42
$Cu_3(CO_3)_2(OH)_2(s) + 4H^+ = 3Cu^{2+} + 2HCO_3^- + 2H_2O$						43

Appendix III

Modelling of general corrosion under oxygen-free conditions, bentonite as barrier

1 Introduction

Chloride at high concentrations in combination with low pH and high temperature could be unfavourable for the general corrosion of copper (section 6.2.2). Sulphide and some modifications of Fe(III) are, in principle, corrosive for copper. The influence of sulphide and Fe(III) on the corrosion of a copper canister under repository conditions is strongly limited by their low solubilities and by the low rates of mass transport in the bentonite. In this study we explore the effects of stationary, non-dissolving sulphide and Fe(III) in the bentonite on the anaerobic corrosion of copper in bentonite containing dissolved chloride. The influence of solid sulphide and Fe(III) that is not in contact with copper is limited to interference with dissolved corrosion products. Sulphide may precipitate dissolved copper species and Fe(III) may consume dissolved molecular hydrogen.

2 Reactions

In saline waters copper can corrode to aqueous copper complexes under liberation of dissolved molecular hydrogen, according to the reaction:

$$Cu(s) + H^+ + n\ Cl^- \leftrightarrow \tfrac{1}{2}\ H_2(aq) + CuCl_n^{(1-n)} \quad (1)$$

As the double arrow indicates, reaction (1) can go in both directions. The corrosion reaction, to the right, is possible only when the species $H_2(aq)$ and $CuCl_n^{(1-n)}$ are present at concentrations lower than the equilibrium concentrations. In a closed system, corrosion would stop once the equilibrium concentrations of the aqueous corrosion products were attained. In a semi-closed system such as the repository, a maximum rate for reaction (1) is given by the rate with which the corrosion products diffuse away from the copper surface. The rate of corrosion may, therefore, be influenced by the length of the diffusion path. The diffusion path is the distance from the copper canister to a site where the concentration of the corrosion products may be regarded as being zero. If the bentonite is considered to be totally inert, the length of the diffusion path may be set to be the bentonite wall thickness.

But bentonite contains sulphide minerals that may react with the cuprous chloride complexes according to reaction (2). Because of ion-exchange of metal ions (Me(II)) with the bentonite, according to reaction (3), the equilibrium concentration of cuprous copper may be very low in the presence of other metal sulphides.

$$2CuCl_n^{(1-n)} + MeS(s) \rightarrow Cu_2S(s) + Me(II) + 2\ n\ Cl^- \quad (2)$$

$$Me(aq) + 2\ Na^+\ (bentonite) \rightarrow Me\ (bentonite) + 2\ Na^+ \quad (3)$$

Bentonite also contains variable amounts of Fe(III) that may react with the molecular hydrogen liberated by the corrosion process.

$$\tfrac{1}{2}\ H_2(aq) + Fe(III)(s,\ bentonite) \rightarrow H^+ + Fe(II)(s,\ bentonite) \quad (4)$$

3 Transport-reaction equations

Assuming that the reactions (2) and (4) behave irreversibly, we can write a transport-reaction equation for Cu(I) and a corresponding equation for H_2(aq):

$$\frac{\partial C_{Cu(I)}}{\partial t} = D_{Cu(I)} \frac{\partial^2 C_{Cu(I)}}{\partial x^2} + k_1 \cdot a_{Cu(s)} \cdot C_H \cdot C_{Cl}^n - k_{-1} \cdot C_{H_2}^{1/2} \cdot C_{Cu(I)} - 2 \cdot k_2 \cdot C_{MeS} \cdot C_{Cu(I)} \quad (5)$$

$$\frac{\partial C_{H_2}}{\partial t} = D_{H_2} \frac{\partial^2 C_{H_2}}{\partial x^2} + \frac{k_1}{2} \cdot a_{Cu(s)} \cdot C_H \cdot C_{Cl}^n - \frac{k_{-1}}{2} \cdot C_{H_2}^{1/2} \cdot C_{Cu(I)} - \frac{k_4}{2} \cdot C_{H_2}^{1/2} \cdot C_{Fe(III)} \quad (6)$$

where k_1 is a rate constant for reaction (1) in the forward direction and k_{-1} is a rate constant for the reversed reaction, k_2 and k_4 are rate constants for reactions (2) and (4), respectively. For chloride, only the first term on the right hand side needs to be considered. Insignificant fractions of the chloride are bound in the cuprous chloride complexes.

Equations (5) and (6) imply knowledge of the reaction mechanisms that we do not have and we will not use the values of the rate constants as such. In order to obtain the maximum rate of the corrosion reaction we use values of k_1 and k_{-1} such that electrochemical equilibrium is maintained at the copper surface, k_2 such that metal sulphides efficiently consume aqueous copper and k_4 such that Fe(III) efficiently consumes H_2(aq). Equations (5) and (6) are written for linear diffusion, while the real problem mostly resembles cylindrical diffusion.

For high contents of sulphide and Fe(III) in the bentonite, the time dependent diffusion equations become impractical to use. The mass transport of copper and hydrogen is then better described through a series of stationary concentration profiles. The highest concentration is at the canister wall and the lowest, zero, is set to a radius in the bentonite where the metal sulphide has not yet been converted to Cu_2S(s). Similarly for hydrogen, the highest concentration is at the canister wall and the lowest, zero, is set to a radius in the bentonite where the Fe(III) has not yet been converted to Fe(II). The flux of dissolved copper per unit length of the canister, away from the canister, j_{Cu}, is described by the equation:

$$j_{Cu} = 2\Pi \cdot D_{Cu} \frac{C_{Cu}}{\ln(\frac{r_i}{r_S})} \quad [moles/s, cm] \quad (7)$$

where r_i is the inner radius of the bentonite=52.5 cm, r_S is the radius at the site where the sulphide is not yet converted to Cu_2S(s). C_{Cu} is the concentration of dissolved copper, in the form of $CuCl_2^-$, at the canister wall.

The corresponding flux of molecular hydrogen, j_{H2}, is described by the equation:

$$j_{H_2} = 2\Pi \cdot D_{H_2} \frac{C_{H_2}}{\ln(\frac{r_i}{r_{Fe}})} \quad [moles/s, cm] \quad (8)$$

where r_{Fe} is the radius where there is Fe(III) that can oxidise the molecular hydrogen. C_{H2} is the concentration of dissolved copper at the canister wall. Groundwater is assumed to maintain zero concentration of H_2(aq) outside the bentonite. The two fluxes are related so that the flux of copper is twice the flux of molecular hydrogen.

$$j_{Cu} = 2 \cdot j_{H_2} \tag{9}$$

Furthermore, the concentrations of dissolved copper and molecular hydrogen at the canister wall are related through electrochemical equilibrium, according to equation (1), with protons, chloride and copper metal:

$$C_{Cu} \cdot \sqrt{C_{H_2}} = k_k \tag{10}$$

k_k is a conditional equilibrium constant =$1.2 \cdot 10^{-11}$ at pH 7 and 1.0 mol/kg NaCl at 50°C. This value is obtained using thermodynamic data for $CuCl_2^-$, Cu(s), Cl^-, H^+ from SKB TR-00-13 /Puigdomenech and Taxén 2000/ (also in appendix I in this report) and thermodynamic data for H_2(aq) from /NBS 82/. The transition from activities to concentrations was made using Davies' approximation for the charged species. The activity of the dissolved molecular hydrogen was assumed to be equal to its concentration (γ=1). Copper metal was assumed to be present at unit activity.

The flux of dissolved copper to the radius r_S causes an increase, *dr*, in r_S since sulphide is converted to Cu_2S(s).

$$jCu \cdot dt = 2 \cdot C_S \cdot 2 \cdot \Pi \cdot r_S \cdot dr \quad [mol/cm] \tag{11}$$

C_S is the contents of sulphide in the bentonite expressed as mol/cm^3.

Fe(III) is consumed in proportion to sulphide which gives a relation between r_{Fe} and r_S:

$$r_{Fe} = \sqrt{\frac{2 \cdot C_S}{C_{Fe}}(r_S^2 - r_i^2) + r_i^2} \tag{12}$$

C_{Fe} is the concentration of reducible Fe(III) in the bentonite.

A rather complicated differential equation arises when equations (7) through (12) are put together. The quantity *dr/dt* as function of r_S is, however, evaluated numerically with relative ease using iterative methods.

4 Availability of reactants

Bentonite (MX-80) may contain sulphide in the order of 0.1%. Pyrite, FeS_2, is a major form of this sulphide. The total content of iron is in the order of 4%. The major part of this iron is in the form of Fe(III). A fraction of this Fe(III) is found in the montmorillonite structure at sites occupied by aluminium in the 'ideal' structure. The stable state of iron in the presence of molecular hydrogen at low concentrations is expected to be magnetite, Fe_3O_4. Magnetite can formally be written as a mixture between ferrous and ferric oxide, $FeO{\cdot}Fe_2O_3$. Thus, the stable state of iron contains Fe(III) as the major constituent. It has been shown that the structural Fe(III) may be reduced to Fe(II) by bacterial action /Kostra et al. 1999/. In the absence of other information we assume that up to 1.0% of the bentonite is Fe(III) that can be converted to Fe(II)(in magnetite) by reduction with molecular hydrogen at low concentration.

5 The numerical model

Cylindrical diffusion in the radial direction is considered. The bentonite is segmented into 70 cylindrical shells. The inner one has a radius of 0.525 m and the outer one has a radius of 0.8745 m.

Diffusion in porous media is complicated and as an approximation we consider aqueous diffusion and use the observation by Neretnieks and Skagius /1978/, as quoted by Wersin et al. /1994/, that the diffusion rate in bentonite is approximately 100 times lower. The calculations are performed for diffusion in water but the results are reported for diffusion in bentonite by multiplying the time for aqueous diffusion with a constant factor of 100. The canister surface is assumed to have a temperature of 50°C and the bentonite is assumed to have a uniform temperature of 25°C. Only the dichloride complex of Cu^+ is considered; $CuCl_2^-$ is the dominating cuprous species for the chloride concentrations considered. The bentonite is assumed to be saturated with 0.1 molal NaCl and encounter 1.0 molal NaCl at time zero. For sodium chloride solutions up to 1 mol/kg , the maximum difference between moles per liter and moles per kilogram water is in the order of three percent at 50°C and the two units of measure are treated as interchangeable. Fe(III) and sulphide are here treated as non-dissolving solids. The amounts in the bentonite are varied. The differential equations are integrated using the fourth order Runge-Kutta method /Press et al. 1992/.

Tables III-1 and III-2 show the parameter values used in this study.

Table III-1. Diffusion coefficients in bentonite.

Chloride	10^{-11}	m^2/s
Cu(I)	10^{-11}	m^2/s
$H_2(aq)$	$4.5{\cdot}10^{-11}$	m^2/s

Table III-2. Bentonite dimensions.

Inner radius	0.525 m
Outer radius	0.875 m

6 Results

Figure III-1 illustrates some consequences of the equilibrium condition for reaction (1) expressed in equation (10). The diagram shows the equilibrium concentration of $H_2(aq)$ as a function of $[CuCl_2^-]$ in 1.0 mol/kg NaCl at 50°C. At pH 7.0, corrosion according to reaction (1) is possible only if the point representing $[H_2(aq)]$ and $[CuCl_2^-]$ is located to the left of the solid thick line in figure III-1. At pH 6.0, corrosion is possible only to the left of the dashed thick line.

Consequences of the diffusion condition in equation (9) are also illustrated in figure III-1. The thin solid line shows the concentration of $H_2(aq)$ required to satisfy equation (9) for the case where the diffusion paths are equal for $H_2(aq)$ and $CuCl_2^-$. The location of the equilibrium line is determined by thermodynamic data, pH and chloride concentration. The location of the diffusion line is determined by the diffusion coefficients and the relative lengths of the diffusion paths for $H_2(aq)$ and $CuCl_2$. The intersection between the equilibrium line and the diffusion line show the conditions at the copper surface during steady state, pH 7 solid circle and pH 6 dashed circle.

The chloride concentration at the copper canister is found reach 90% of the 1.0 mol/kg NaCl concentration after about 300 years. The resulting corrosion and corrosion rate are shown in figure III-2. After an initial increase in response to the increasing chloride concentration, the corrosion rate shows a steady decrease as the diffusion paths for copper and for molecular hydrogen increase. Only fractions of the reactive sulphide and the reactive Fe(III) are consumed within the time scale of the diagram.

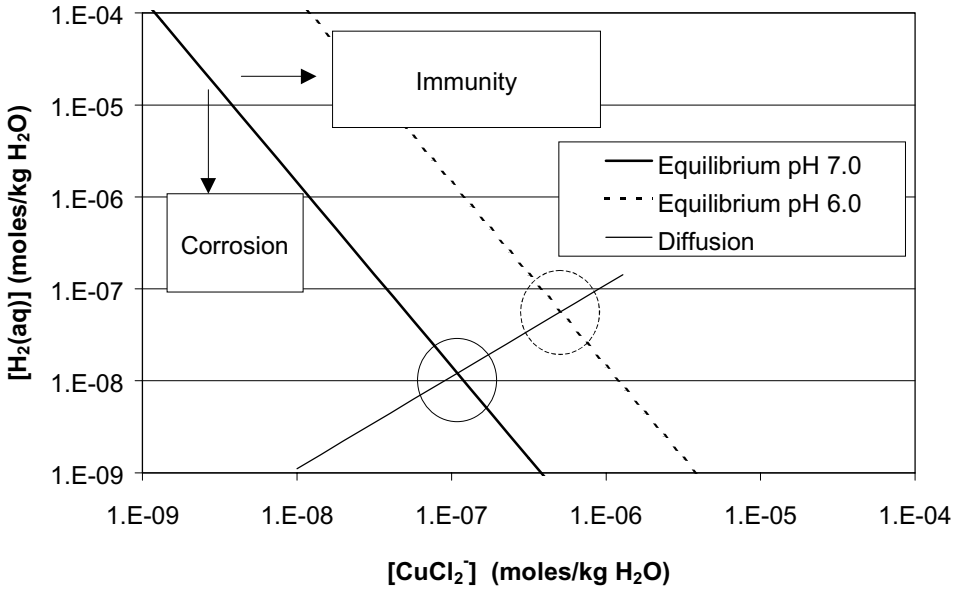

Figure III-1. *Equilibrium concentration of $H_2(aq)$ as a function of $[CuCl_2^-]$ in 1.0 mol/kg NaCl at 50°C. Solid line pH 7.0, dashed line pH 6.0. Diffusion relation imposed by equation (9) for the case of equal diffusion paths for $H_2(aq)$ and $CuCl_2^-$. The intersection between the equilibrium line and the diffusion line show the conditions at the copper surface during steady state, pH 7 solid circle and pH 6 dashed circle.*

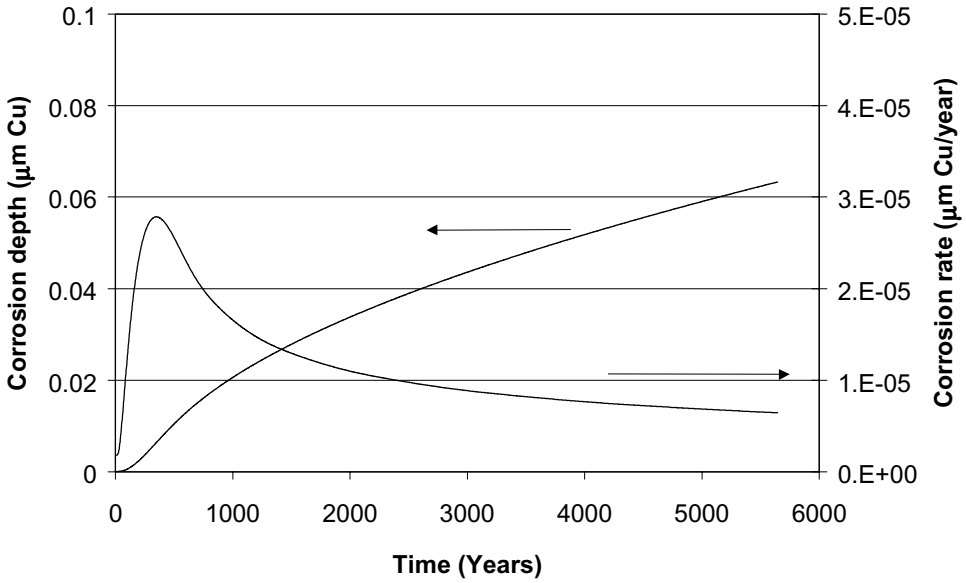

Figure III-2. *Corrosion and corrosion rate as function of time. pH 7.0 50°C, 1.0 mg reactive sulphide and 3 mg reactive Fe(III) per kilogram bentonite.*

The predicted corrosion for much higher contents of reactive sulphide and reactive Fe(III) is shown in figure III-3. All sulphide in the bentonite in figure III-3 is not consumed during the time scale of the diagram. For the higher sulphide concentrations, only a few millimetres of bentonite are depleted of reactive sulphides in 10,000 years. Lower contents of Fe(III) would decrease the corrosion rate. With the Fe(III) concentrations considered in figure III-3, only a few millimetres of bentonite are depleted of reactive Fe(III) in 10,000 years.

The short diffusion paths for aqueous copper and for molecular hydrogen, respectively, allow increased corrosion rates temporarily. As ferric iron and sulphides are consumed, the lengths of the diffusion paths increase and the corrosion rate decreases. Significantly higher corrosion rates are possible only during a phase when the diffusion path for both aqueous copper and for molecular hydrogen are short. The results indicate that the corrosion caused by the processes considered here is insignificant. For the highest sulphide contents in figure III-3, an average corrosion depth in the order of 10 µm is predicted for 100,000 years.

This type of corrosion, which is limited by local equilibrium and diffusion rates of corrosion products, is expected to favour general corrosion. The preference for general corrosion is so strong that this mode of corrosion may have a smoothing effect on a previously unevenly corroded surface. However, the rate limitation is such that the average corrosion rate is controlled by diffusion. A consequence of this is that if a part of the copper surface, because of local inertia, fails to attain local equilibrium, nearby sites may have a corrosion rate higher than average.

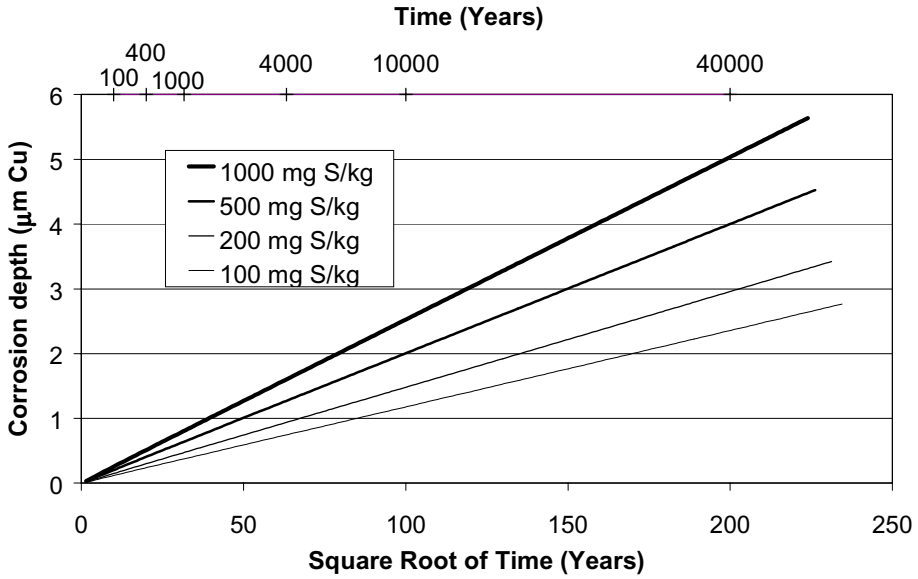

Figure III-3. *Predicted corrosion of a copper canister as function of time. Bentonite saturated with 1.0 mol/kg NaCl at 50°C and pH 7.0. 1.0% (10,000 mg/kg) reactive Fe(III) in the bentonite. The contents of reactive sulphide in the bentonite varied.*

7 Sensitivity to pH and chloride concentration

The conditional equilibrium constant, defined in equation (10), is proportional to the hydrogen ion activity and to the chloride concentration squared. The concentrations of corrosion products, $H_2(aq)$ and $CuCl_2^-$, at the copper surface are approximately proportional to the value of the conditional constant to the power of 2/3.

Diffusion rates are proportional to the surface concentrations of $H_2(aq)$ and $CuCl_2^-$. The time to reach a certain corrosion depth is therefore approximately inversely proportional to the hydrogen ion activity to the power of 2/3 and to the chloride concentration to the power of 4/3. If the values of the diffusion coefficients for $H_2(aq)$ and $CuCl_2^-$ are increased by a common factor, the time to reach a certain corrosion depth would decrease by that factor.

As figure III-3 shows, the corrosion depth increases linearly with the square root of time. The corrosion depth thus increases with the hydrogen ion activity to the power of 1/3 and with the chloride concentration to the power of 2/3. This means, for example, that for pH 6 (at 50ºC) and a chloride concentration of 1.5 mol/kg, the predicted corrosion depths in figures III-2 and III-3 should be multiplied by a factor of about three.

8 About the assumptions and uncertainties

Reactions between dissolved corrosion products and solids in the bentonite, reactions (2) and (4), do not seem unreasonable. The theoretical equilibrium concentration of $CuCl_2^-$ in contact with a solid metal sulphide comes out as very low, particularly if the released metal is polyvalent, e.g. Fe^{2+}, and can undergo ion-exchange reactions with the bentonite. The fact that one of the reactants is a solid and the other is strongly stabilised by chloride ions may result in a low rate of reaction. However, whether a reaction rate is low or not must be related to the rates of mass transport and the rates of diffusion in bentonite are also low, compared to aqueous diffusion.

The reduction of Fe(III) by molecular hydrogen is strongly dependent on the nature of the Fe(III) ions. The Fe(III) formally present in magnetite is considered stable. For the structural Fe(III) there probably exists a lower limit for the hydrogen concentration below which reduction is not possible.

The treatment of the diffusion in bentonite is very simplified. The interaction of different species with the bentonite depends on the charge and size of the species. The factor 100 between the rates of diffusion in water and in bentonite was found for small neutral molecules. Chloride ions and the dichloro-complex with Cu(I) are both negatively charged and repelled by the stationary charges on bentonite (ion exclusion) /Andersson 1999/. Lower values of the diffusion coefficients are, therefore, likely for these species. However, this may not be driven to the extreme because fractions of the dissolved copper ions are present as Cu^+ and CuCl(aq) for which the factor of 100 is reasonable.

The estimates of the corrosion of copper given here may be regarded as conservative. More narrow estimates of the may be obtained by:

- A more sophisticated diffusion model, i.e. pore diffusion, species-specific parameters for pore diffusion and differentiation between the various Cu(I)-chloride complexes.
- Establishing of a lower limit for the hydrogen concentration required to reduce Fe(III).
- Considering the temperature of the canister as a function of time. Higher temperatures give higher corrosion rates and lower temperatures give lower corrosion rates. In actuality, the canister temperature will have dropped far below 50ºC during the time span covered by the diagrams III-2 and III-3.

ISSN 1404-0344

CM Digitaltryck AB, Bromma, 2001